NASA CR-135307
EDR 9339

AERODYNAMIC PERFORMANCE OF CONVENTIONAL AND ADVANCED DESIGN LABYRINTH SEALS WITH SOLID-SMOOTH, ABRADABLE, AND HONEYCOMB LANDS

BY

H. L. STOCKER, D. M. COX, AND G. F. HOLLE

DETROIT DIESEL ALLISON

DIVISION OF GENERAL MOTORS CORPORATION

INDIANAPOLIS, INDIANA

NOVEMBER, 1977

PREPARED FOR

NATIONAL AERONAUTICS AND SPACE ADMINISTRATION

NASA LEWIS RESEARCH CENTER

CONTRACT NAS 3-20056

1 Report No.	2 Government Accession No	3 Recipient's Catalog No
CR-135307		

4 Title and Subtitle	5 Report Date
Aerodynamic Performance of Conventional and Advanced Design Labyrinth Seals with Solid-Smooth, Abradable, and Honeycomb Lands.	November 1977
	6. Performing Organization Code
7 Author(s)	8. Performing Organization Report No
H. L. Stocker, D. M. Cox, and G. F. Holle	EDR 9339
	10. Work Unit No.
9. Performing Organization Name and Address Detroit Diesel Allison P. O. Box 894 Indianapolis, Indiana 46206	11. Contract or Grant No NAS3-20056
	13. Type of Report and Period Covered Final 21 July 1976 21 Nov. 1977
12. Sponsoring Agency Name and Address NASA Lewis Research Center 21000 Brookpark Road Cleveland, Ohio 44135	14. Sponsoring Agency Code

15 Supplementary Notes

Project Manager: L. P. Ludwig
NASA Lewis Research Center
Cleveland, Ohio 44135

16. Abstract

An experimental evaluation was conducted to determine labyrinth air seal static and dynamic performance using solid, abradable, and honeycomb lands with standard and advanced seal designs. This investigation studied the effects on leakage of land surface roughness, abradable land porosity, rub grooves in abradable lands, and honeycomb land cell size and depth using a standard labyrinth seal. The effects of rotation on the optimum seal knife pitch were also investigated. Selected geometric and aerodynamic parameters for an advanced seal design were evaluated to derive an optimized performance configuration. The rotational energy requirements were also measured to determine the inherent friction and pumping energy absorbed by the various seal knife and land configurations tested in order to properly assess the net seal system performance level.

The results obtained in this program show:

- o Seal leakage can be significantly affected with honeycomb or abradable lands.
- o Rotational energy absorption does not vary significantly with the use of a solid-smooth, an abradable, or a honeycomb land.
- o Optimization of an advanced lab seal design produced a configuration that had leakage 25% below a conventional stepped seal.

17. Key Words (Suggested by Author(s))	18 Distribution Statement
Labyrinth Seals Rotating Seals Gas Path Seals Air Leakage in Gas Turbines Interstage Seals	UNLIMITED

19. Security Classif. (of this report)	20. Security Classif. (of this page)	21. No of Pages	22 Price*
Unclassified	Unclassified		

* For sale by the National Technical Information Service, Springfield, Virginia 22161

NASA-C 168 (Rev 10-75)

FOREWORD

This program was funded by the Engine Component Improvement (ECI) Project Office of the NASA Aircraft Energy Efficiency (ACEE) Program.

The NASA Project Manager was Mr. L. P. Ludwig of the Fluid Systems Components Division. The ECI Program Coordinator for this project was Mr. T. N. Strom. Both of these gentlemen contributed timely comments and valuable suggestions during the course of the program.

The initial NASA Project Manager for this program was Dr. J. Zuk. The program structure, organization, and planning incoporated many of Dr. Zuk's suggestions.

The Detroit Diesel Allison Program Manager was Mr. H. L. Stocker. The Technical Director was Mr. D. M. Cox. Substantial testing and analysis were provided by Mr. G. F. Holle.

TABLE OF CONTENTS

LIST OF ILLUSTRATIONS

LIST OF TABLES

SUMMARY

The objectives of this program were to obtain additional knowledge regarding the parameters that affect the performance of conventional labyrinth seal configurations and to optimize the performance of an advanced labyrinth seal.

Rig testing was conducted to determine labyrinth air seal static and dynamic leakage performance for solid-smooth, abradable, and honeycomb lands using a conventional four knife straight-through seal and an advanced seal design. The effects of land surface roughness, abradable land porosity, rub grooves, honeycomb cell size and depth, and rotation on seal performance were determined using the conventional straight-through seal. The effects of rotation on optimum seal knife pitch were also investigated. Selected geometric and aerodynamic parameters for an advanced seal design were evaluated to derive an optimized performance configuration.

Seal rotational energy requirements were also measured to determine the inherent friction and pumping energy absorbed by the various seal knife and land configurations tested in order to properly assess the net seal system performance level.

The major results obtained in this program include the following:

- An advanced labyrinth seal design was developed that reduced leakage 26.9% compared to a conventional stepped seal.

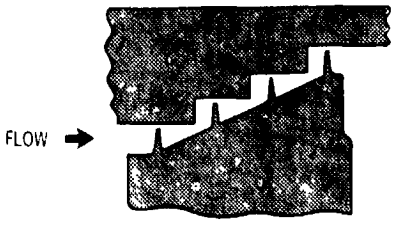

CONVENTIONAL STEPPED LABYRINTH SEAL

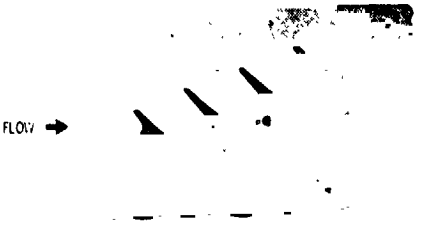

ADVANCED DESIGN LABYRINTH SEAL

- Using a honeycomb land with the advanced seal <u>increased</u> leakage 68.6% compared to the solid-smooth land.

- Honeycomb lands were found to reduce leakage up to 24% for conventional straight-through labyrinth seals.

- Medium surface roughness was found to reduce straight-through seal leakage approximately 23% relative to a smooth land at .013 cm (.005 in.) clearance and 5.0% at .051 cm (.020 in.) clearance. Greater roughness increased leakage.

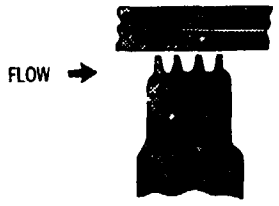

CONVENTIONAL STRAIGHT-THROUGH LABYRINTH SEAL

- Some abradable lands were found to leak substantially more than a solid-smooth land.

- Grooving a porous abradable seal land significantly reduced leakage <u>through</u> the material.

- Rotation reduced straight-through seal leakage up to 10% for smooth and abradable lands, but it had negligible effect with the honeycomb land.

- Rotation decreased the advanced seal leakage approximately 6% for the solid-smooth and abradable lands. However, the honeycomb land experienced a 6.4% leakage increase with rotation compared to the static performance.

- The rotational power absorption for solid-smooth, abradable, and honeycomb lands using a conventional four knife straight-through seal showed small differences. The honeycomb land had the maximum value which was 5.7% higher than the power absorption level of the smooth land.

- The advanced seal rotational power absorption for the solid-smooth land is approximately the same as the four knife straight-through seal.

- Rotational effects do not influence the selection of the seal knife optimum pitch for a straight-through seal.

INTRODUCTION

Technological advancements to achieve higher thermal and propulsive efficiencies for current and advanced aircraft gas turbine engines have been characterized by significant increases in the operating cycle pressure ratio and turbine inlet temperature. These trends typically cause internal air seal leakage to increase. A higher operating temperature causes greater differential growth, frequently resulting in larger seal clearances. A higher cycle pressure ratio tends to increase seal leakage, even at the same seal clearance level. This flow increase can be predicted from the compressible flow relationship,

$$w = \frac{p_U A}{\sqrt{T_U}} \phi .$$

As engine pressure ratio increases, pressure (p_U) increases more rapidly than temperature (T_U). The airflow parameter (ϕ) increases or remains constant if the seal is choked. Therefore, seal leakage increases on an approximately proportional basis with increases in seal inlet pressure. Applying this relationship to a labyrinth seal in a gas turbine, assuming constant engine airflow, as compressor pressure ratio is increased, the seal leakage increases as presented in Figure 1.

Incorporating a variable cycle engine approach to future designs may also increase seal leakage. Normally, seal clearances are set to run as tight as possible at the engine maximum time operating point. The resulting clearances at other conditions are accepted since they usually represent a small percentage of the operating time. However, the variable cycle engine, through differential growth of hardware caused by temperature and material differences, will cause the average seal clearance to be greater and thus, increase leakage.

Compensating for the current state of sealing technology by attempting to improve aerodynamic component efficiencies has normally resulted in limited payoffs relative to time, cost, and effort expended. For an advanced high bypass ratio gas turbine engine, Figure 2 shows examples of the improvements in compressor and turbine component efficiencies required to achieve the same increase in engine performance as a reduction in turbine seal component leakage of 1% of the engine airflow. A reduction in the compressor rotor exit seal leakage amounting to 1% of engine airflow would produce the same results as a compressor efficiency increase of 0.91%.

The benefits of improved sealing effectiveness are equally significant for fuel conservation oriented engines. Figure 2 illustrates the percent change in engine specific fuel consumption for a 1% (of gas generator inlet flow) reduction in seal leakage.

There are also development cost savings. The cost trade-off for improving seal performance compared to improving the compressor or turbine component aerodynamic efficiency is of significant consideration. Extracting the same performance improvement with compressor or turbine efficiency improvements, as compared to seal leakage improvements, is several times more expensive. Typical examples of these cost trade-offs are shown in Figure 3.

The foregoing trends and payoffs have, therefore, added increased emphasis to the immediate need for accelerated development and continued improvement of gas turbine sealing technology in order to reduce costly seal leakage to a minimum. This development will also provide better and more reliable control over sophisticated cooling circuits and prevent high seal leakage flows from entering critical locations in the turbine gas path which can result in considerable penalty from thermal and momentum losses.

The objectives of improved gas turbine performance and fuel savings can be achieved by reducing the leakage in current seals with design modifications and by developing high efficiency labyrinth seal concepts. However, there are technology voids in the design, analysis, and "in service" performance of labyrinth seals that required detailed investigation and understanding. This information is required to provide direction for design improvements. Detroit Diesel Allison (DDA) has been investigating various aspects of labyrinth seal performance under in-house funding and through two contracts with the Naval Air Propulsion Test Center. Through the results of these studies, design concepts have been tested that significantly reduce seal leakage as compared to a conventional seal. The program that is the subject of this report is an extension and expansion of experimental work accomplished at DDA over the past several years.

A diagram illustrating the efforts of this program is presented in Figure 4. The program was divided into two basic technical tasks. The work involved in Task I included experimentally determining labyrinth seal performance for a conventional four knife straight-through seal using abradable and honeycomb lands. Task II was directed toward optimizing an advanced labyrinth seal design and exploring the effect of non-constant geometry to reduce leakage in an advanced seal.

In Task I, four commercially available abradable land materials and three honeycomb cell size lands were evaluated for aerodynamic performance on the 2D test rig. The effects of surface roughness on solid lands, porosity leakage on the abradable lands, and cell depth on the honeycomb lands were also determined using the 2D rig. One of the porous material abradable lands was grooved to simulate a rub condition and retested to determine the effect on leakage. All 2D rig testing in this task was accomplished at three clearance levels: 0.013 cm (.005 in.), 0.025 cm (.010 in.), and 0.051 cm (.020 in.).

Based on the results of the 2D rig tests, selected abradable and honeycomb lands were fabricated and tested in the 3D rig up to 239 m/s (785 ft/sec) to investigate the effect of rotation on seal leakage and to determine the rotational power absorption differences of solid-smooth, abradable, and honeycomb lands. The rotational power difference combined with seal leakage difference gave the net seal system performance change.

The abradable land for the 3D rig was grooved 102° to simulate a light rub. Then the rub grooves were extended to 360° and retested. Tests were conducted statically and dynamically with the rotor knives forward, over, and behind the grooves to determine the leakage performance.

Also, in Task I, the effect of rotation on the optimum design pitch of a straight-through seal was investigated with solid-smooth, abradable, and honeycomb lands. Three values of pitch were tested: .203 cm (0.080 in.), .279 cm (0.110 in.), and .356 cm (0.140 in.). Radial clearances of 0.025 cm (0.010 in.) and 0.051 cm (0.020 in.) were used. Testing was done statically and at three levels of rotational velocity: 80 m/s (261 ft/sec), 159 m/s (523 ft/sec), and 239 m/s (785 ft/sec).

In Task II, the major geometric seal parameters (knife pitch, knife height, knife angle, and step height) were explored to optimize an advanced seal design in terms of minimum leakage. Also, the use of non-constant knife pitch was investigated as a technique to maximize the internal seal cavity turbulence between knives. The optimization of individual knife discharge coefficients will result in minimum seal leakage. The 2D air seal test rig was employed as an expedient and economical means of conducting the advanced seal design optimization work and non-constant pitch studies. The optimum advanced seal configuration identified by the 2D rig tests was fabricated for the 3D rig and tested statically and up to 239 m/s (785 ft/sec) rotational velocity. The advanced seal configuration was tested with solid-smooth, abradable, and honeycomb lands at 0.051 cm (0.020 in.) radial clearance. Rotational power absorption was also measured for the advanced seal 3D rig tests.

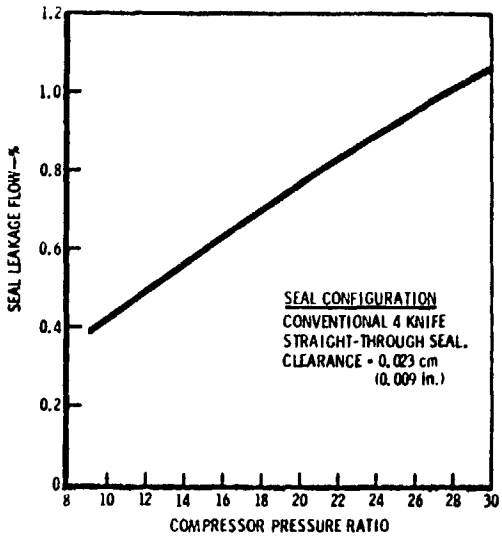

FIGURE 1. EFFECT OF COMPRESSOR PRESSURE RATIO ON LABYRINTH SEAL LEAKAGE

ADVANCED TRANSPORT ENGINE		TRADE-OFF IN COMPONENT EFFICIENCY
REDUCTION OF 1% SEAL LEAKAGE = 0.0% THRUST		+0.91% η HP COMPRESSOR
(WITH REMATCHING)		OR
BPR = 5.25	= -0.40% SFC	+0.51% η HP TURBINE

FIGURE 2. PERFORMANCE PAYOFFS FOR REDUCING HIGH PRESSURE TURBINE SEAL LEAKAGE 1% OF ENGINE AIRFLOW

LABYRINTH SEAL PERFORMANCE IMPROVEMENTS

Seal Development Costs are Significantly Lower Than Other Component Development

- Minimum Compressor Redesign—4 Times Higher
- Complete Compressor Redesign—6 Times Higher
- Turbine Redesign—5-20 Times Higher

FIGURE 3. LABYRINTH SEAL AND GAS TURBINE COMPONENT DEVELOPMENT COST TRADE-OFFS

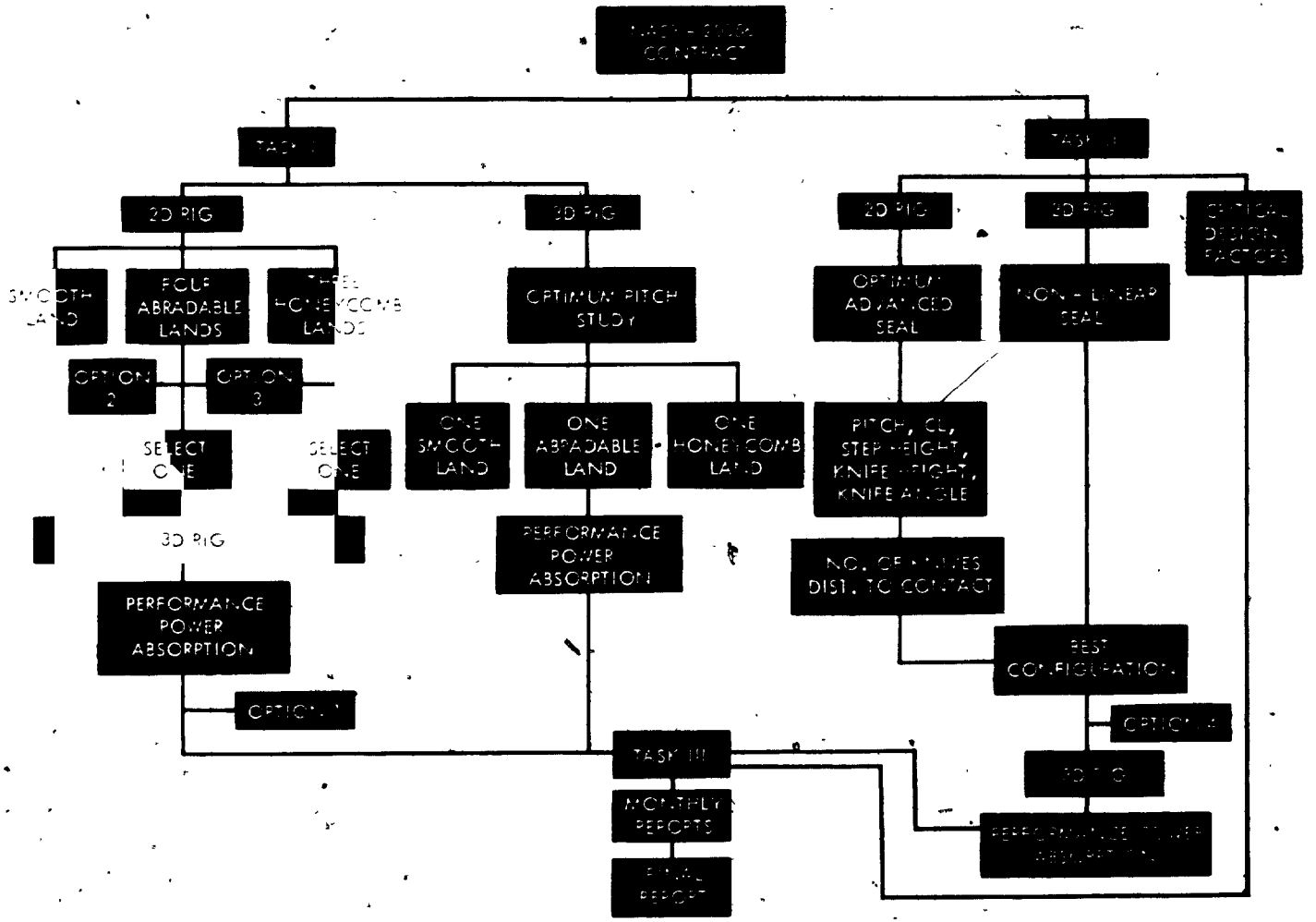

FIGURE 4. DIAGRAM OF SEAL PROGRAM EFFORTS

TEST RIGS AND PROCEDURES

Two complementary test rigs were used for this program. A "two-dimensional" (2D), static rig was used to investigate the primary effects of land material. The influence of geometric variations on the leakage performance of an advanced seal was also surveyed, optimized, and mapped with the 2D rig in preparation for the design and fabrication of an optimum advanced seal for dynamic testing. A "three-dimensional" (3D), dynamic rig was used to obtain the effects of annular geometry and rotation on the seal leakage and power absorption. An abradable land material and a honeycomb land material were compared to a solid-smooth land using straight seals and an optimized advanced seal.

2D Rig

The terminology, "two-dimensional" static test rig, is based on the seal models which are installed in the rectangular test section. These models do not simulate the effects of seal curvature or rotation and involve small end-wall effects. However, the high aspect ratio test section, 16.0 cm (6.28 in.) wide, minimizes these end effects.

Building block, adjustable seal hardware is used to obtain versatility and multiple use of components. Individually adjustable knife and land sections can produce continuous changes in the primary geometric variables of straight, stepped, and advanced seals in a cost effective manner. The features incorporated in the rig design, Figure 5, allow one set of knife hardware (knife angle) to cover the conventional range of variation in:

- knife clearance
- knife pitch
- knife height
- number of knives
- step height
- distance-to-contact (axial clearance)

The maximum seal length test envelope of 5.1 cm (2.0 in.) will allow a considerable number of straight seal knives (depending on pitch) and up to four stepped seal knives to be tested over a complete range of clearance encountered in small and large high temperature aircraft engines.

Figure 6 shows a close-up view of the two-dimensional test section with the four knife stepped seal installed. Each knife and each land are an individual horizontal piece and can be adjusted in an axial direction relative to adjacent pieces to make arbitrary changes in the pitch. Step height can be varied by inserting shims (not shown) between

adjacent knife and land sections. The knife-to-land axial seal clearance can be easily changed with the adjustment screw as shown in Figure 6. Vertical clearances between the corresponding lands and knives can be varied by clearance shims as noted. Changes in knife height are accomplished by filling the knife cavities with low temperature pattern wax. The number of knives can be changed by removing corresponding knife and land sections. For vertical knife seals, the flow direction through the seal can be changed by reversing the knife and land foundations. Changes in knife angle and land contour do require different hardware.

Figure 7 shows a close-up view of a two-dimensional four knife straight seal installed in the test section. The straight seal assembly is similar to, but simpler than, that for the stepped seal since one land section is required. Spacers between knives, with specific height and thickness dimensions, are used to adjust knife pitch and height in the straight seal.

The 2D rig installation permits aerodynamic evaluation of seal performance to a seal inlet pressure of eight atmospheres at room ambient temperature. Alternately, clear arcrylic side plates will allow flow visualization testing to a seal inlet pressure of 2.5 atmospheres. The rig normally discharges outside the test cell through a 14.6 cm (5.76 in.) I.D. pipe which creates less than 0.5 cm (0.2 in.) Hg pressure loss.

The plane walls forming the square test section of the 2D rig experience small structural deflections which can result in clearance changes under high air pressure loading. A micrometer dial gauge (see Figure 8) with .00005 cm (.00002 in.) readability is mounted on the top plate to monitor the relative movement of the seal knife hardware, which is indicated by the vertical travel of the follower pin.

The 2D rig allowed the extensive survey of seal geometry and material effects on performance to be accomplished expeditiously at minimal costs in hardware fabrication, manpower, and schedule.

3D Rig

The terminology, "three-dimensional" dynamic test rig, is based on the circular geometry of the seal models. The test seals typically have a maximum diameter of 15.24 cm (6.00 in.) and can be run at rotational speeds to 30,000 rpm for the simulation of actual engine applications. The 3D rig rotor is driven by an impulse turbine with speed control that is independent of the seal inlet pressure. Therefore, static performance (at 0 rpm) and the influence of knife tip speeds up to 239 m/s (785 ft/sec) can be evaluated over a range of seal pressure ratio from 1.0 to approximately $0.51/\sqrt{CL}$, cm, (or $0.32/\sqrt{CL}$, in.). Figure 9 shows the 3D rig installed in the test cell. The rig lubrication system is prominent on the shelf beneath the test section and drive turbine section.

The seal knife geometry is normally tested on the rotor which is a single combination of knife angle, number of knives, pitch, and knife height for a given flow direction and step height in the case of stepped seals. The matching stator is designed for a single clearance and can be reversed for the large-to-small diameter (LTSD) and the small-to-large diameter (STLD) flow direction testing in the case of stepped seals. The distance-to-contact (DTC) for stepped seals or knife position over the land, as in the case of rub groove testing on straight seals, can be varied by inserting shims behind the stator. Additional use of the seal rotors has been achieved by removing some of the knives to obtain data for shorter seals.

Instrumentation

Comparable air temperature and static pressure instrumentation were used to determine the seal leakage performance in both the 2D static rig and the 3D dynamic rig. The 3D rig employed additional temperature and static pressure instrumentation to define the turbine power produced during dynamic operation. Dynamic testing also required some electronics to record rotor speed and to monitor two-degrees-of-freedom vibration levels at the seal test and turbine drive sections.

2D Rig Instrumentation. The instrumentation locations for the 2D rig are shown schematically in Figure 10. Airflow through the seal model was determined with a standard ASME square edge orifice, 0.760 cm (0.299 in.) diameter, installed in a 4.925 cm (1.939 in.) I.D. flow tube with static pipe taps. This flow tube was utilized for all 2D rig tests except the porosity leakage evaluation of the porous abradable lands.

During the porosity testing of the abradable land materials, the leakage was exhausted to laboratory ambient through a 5.0 cm (2.0 in.) I.D. flow tube with a 1.270 cm (0.500 in.) diameter flow measurement orifice. This test section exit instrumentation permitted accurate measurement of the very low airflows which were throttled through the porous materials.

Static pressures upstream and downstream of the airflow orifice and at the seal inlet plenum were normally measured on 0 to 950 cm (0 to 375 in.) HgA Heise absolute pressure gauges. Meriam 0 to 200 cm (0 to 80 in.) water manometers were used to measure p_{SOU} and p_{SOD} during the porosity tests.

The seal downstream plenum static pressure was measured on a Meriam -25 to 175 cm (-10 to 70 in.) mercury manometer during all 2D rig tests.

Air temperatures upstream of the airflow measuring orifice and upstream of the seal model were measured with shielded iron-constantan (I.C.) thermocouples. The temperatures were displayed in degrees Fahrenheit on a direct reading Brown potentiometer scale.

3D Rig Instrumentation. The instrumentation locations for the 3D rig are shown schematically in Figure 11. The airflow conditions required to define the seal leakage performance in the 3D rig are the same as those required in the 2D rig.

The same 4.925 cm (1.939 in.) I.D. flow tube with pipe taps delivers air from the high pressure source to the inlet diffuser of the 3D rig. However, a standard ASME square edge orifice, 1.270 cm (0.500 in.) diameter, was installed in the flow tube to accommodate the increased seal airflow rate. The 3D rig will pass three times the airflow rate of comparable 2D rig seal configuration.

$$\frac{\text{3D seal circumference}}{\text{2D seal length}} = \frac{6.0\pi}{6.28} = 3.002.$$

Additional data for the airflow conditions in the turbine section of the 3D rig were necessary to define the power delivered to the rotor during dynamic testing. The turbine airflow was measured in the supply line using a standard ASME flow tube with a thin plate, square edge orifice, which was calibrated against a secondary standard.

Several operating parameters were monitored to ensure proper and safe dynamic testing in the 3D rig:

- o rotor thrust balance cavity static pressure
- o lubrication system supply pressure
- o four temperatures within the lubrication system,
  1) pump discharge
  2) bearing sump
  3) rig discharge
  4) reservoir

The rotor thrust balance cavity pressure was measured on a 0 to 305 cm (0 to 120 in.) HgA Heise pressure gauge and manually recorded.

All of the seal and turbine performance data taken during 3D rig testing was displayed and recorded by an automatic data acquisition system which was installed at the beginning of the 3D dynamic air seal rig test phase to accommodate the increased data sampling requirements and to reduce data handling during processing. This system, shown on Figure 12, consists of commercially available components and was assembled as a self-contained integrated unit by DDA's Electronics and Test Equipment Department.

The system, as shown schematically in Figure 13, consists of a data input sequencer which selects a predetermined number of Scanivalve channels for pressure sampling. The 24 channel Scanivalve unit

accommodated the four seal pressures and the six turbine pressures utilized to calculate seal leakage and power absorption, respectively. The pressure was sensed by 0 to 689 kPa G (0 to 100 psig) Druck strain gauge transducer with ±.15% accuracy (full range). At each Scanivalve channel setting a Fluke Model 2200A data logger-multiplexer processed the analog output from the transducer and four iron-constantan (I.C.) thermocouples, which measured seal and turbine air temperatures. In addition, the data logger also recorded binary coded data (BCD) input at each channel setting from a Fluke 1900A digital counter that was utilized to monitor turbine rotational speed. The processed digital output was printed on paper tape by the data logger and, also, fed to a Facit 4070 paper tape perforator which was programmed for ASCI II punch coding. The total data sampling and recording time for one seal operating condition was approximately 25 seconds.

Data Reduction and Calculation Methods

The leakage performance of a labyrinth seal correlates on the airflow parameter,

$$\phi = \frac{w\sqrt{T_U}}{p_U A} ,$$

as a function of the seal pressure ratio, p_U/p_D, in the absence of Reynolds number or heat transfer effects. When the discharge pressure is approximately constant, the test Reynolds number is invariant at a given pressure ratio for the ambient temperature air source. The heat transfer influences are also minimized by the ambient temperature test fluid.

2D Rig Data Reduction. The 2D rig instrumentation was manually read and recorded on data sheets. The data were transposed from the sheets to computer cards and submitted as input to a program in an IBM 370-158 digital computer.

For each test condition, the 2D rig seal performance program converts the instrumentation readings to the desired units and computes seal airflow rate from the orifice tube calibration curves. The seal airflow is then expressed as an airflow parameter for each knife, based on the average operating knife clearance. The average clearance area of all the seal knives is used to determine the overall airflow parameter at the seal pressure ratio, p_U/p_D. These clearance values are corrected from the build-up measurements for the rig case deflection.

Examples of the computer program output data for the 2D rig performance can be found in Appendix F. The primary variables ($w\sqrt{T_U}/p_U A$ versus p_U/p_D) are automatically plotted by a Calcomp machine plotter from the overall airflow parameter and pressure ratio data. These plots can be found in Appendix A.

3D Rig Data Reduction. The punched paper tape generated by the automatic data acquisition system was read by a Modcomp minicomputer and the data then submitted to a permanent magnetic disc file for reduction by the IBM 370 computer system. The seal leakage performance is reduced by the same procedure employed for the 2D rig data.

Dynamic conditions at 10,000, 20,000, and 30,000 rpm were recorded in addition to the static performance. The 3D rig program calculates the rotor growth based on the dynamic conditions to determine the rotational seal clearance.

A sample calculation from the 3D rig data reduction program is presented in Appendix F. The Calcomp plotter automatically graphs the overall airflow parameter (ordinate) against the seal pressure ratio (abcissa) for lines of constant actual rotor speed (including static). These plots can be found in Appendix B.

3D Rig Power Absorption Analysis

The rotational power requirements for the 3D seal test configurations were evaluated at the same rotational speed and seal pressure ratio by measuring the rig drive turbine inlet and exit conditions.

The air impulse drive turbine on the DDA dynamic seal rig was utilized as the power sensitive device since, as the power requirements of various seals change, the energy levels into the drive turbine change in order to maintain the same rotational speed. Changes in turbine performance (efficiency) relative to turbine loading (or speed) were then used to calculate the turbine power output for various seal configurations.

The DDA dynamic seal rig turbine performance was determined by utilizing a discrete mapping procedure due to the impulse design of the turbine blading. In the case of a pure impulse turbine, the torque coefficient, as a function of blade-jet speed ratio (U/C*), is linear. Therefore the torque at stall (speed = 0) and the maximum blade-jet speed ratio at free running speed (torque = 0) were measured to determine the end points of the torque characteristic. Figure 14(a) illustrates the torque characteristic of the drive turbine and indicates the stall and ultimate speed conditions measured. The stall torque coefficient and ultimate speed ratio are notably low, based on state-of-the-art design. This is due to the low cost, simple blading of the drive turbine and the inherent power requirements of the integral balance seal, bearings, and drive shaft system attached to the turbine.

The turbine efficiency was then calculated as a function of blade-jet speed ratio (U/C*) knowing the torque coefficient (τ) where efficiency is $\eta_T = 4\ \tau\ U/C^*$.

Figure 14(b) illustrates the resulting efficiency characteristic calculated. A relatively low efficiency level is noted which, again, is

due to the blading and turbine shaft system. This low efficiency level, however, made the turbine more sensitive to small power requirement changes, thus making it a good differential power measurement system.

To determine the relative seal energy requirement for a given seal, the rotational speed and seal pressure ratio were maintained constant while the turbine inlet temperature, pressure, flow rate, and turbine exit pressure were monitored. From these quantities, the jet speed (spouting velocity) was calculated. Knowing the turbine speed, the blade-jet speed ratio was then computed and the turbine efficiency determined from Figure 14(b). The resulting horsepower was then calculated based on the expression:

$$P = \frac{w_T \quad c_p \quad \eta_T \quad T_{TOU}}{.7069} \left[1 - \left(\frac{p_{TD}}{p_{TU}} \right)^{\frac{\gamma-1}{\gamma}} \right]$$

This calculated horsepower value represents the total pumping and windage losses of the seal rotor, including the sides of the rotor. However, since all the rotors tested had essentially the same side wall geometry, the difference in power requirements could be attributed to the knife and land interface alone.

Initial 3D rig testing with the four knife straight seal rotor disclosed significant scatter in the measured seal rotor power absorption data when plotted versus seal pressure ratio. The thrust balancing of the seal rotor-turbine drive system was suspected as the influencing factor for this data scatter. The normal thrust balance procedure, to maintain a constant axial bearing load, was to change the thrust balance piston supply pressure as a function of the seal upstream pressure (p_U) only. However, after several tests it was noted that the seal donwstream pressure was varying considerably, depending upon the clearance and type of land tested. This was due to the range of seal leakage exiting through the rig exhaust system, which created a significant variation in seal downstream back pressure, thus influencing the thrust bearing load.

To determine if the turbine aerodynamics could detect these suspected changes in bearing load, a test was performed in which the thrust balance pressure was varied to purposely change the thrust load. Figure 15 illustrates the effect of varying the bearing load for a given seal configuration from 670 N (150 lb_f) to 1550 N (348 lb_f) at 20,000 rpm and at a seal pressure ratio of 1.7. As noted, a .142 kw (.19 hp) change was indicated over the thrust load range tested, thus substantiating that the power absorption technique, utilizing the turbine as a measurement device, could in fact differentiate relatively small changes in power absorption.

As a result of this sensitivity, all subsequent 3D test calibration points were made with a constant 670 N (150 lb_f) bearing load where possible. This was accomplished by monitoring the seal downstream

pressure and including its effect in determining the required thrust balance piston pressure to maintain constant bearing load.

The results of the seal power evaluations and comparisons are described in the section on "Rotational Power Absorption".

Description of Test Conditions

Test conditions for the 2D rig and 3D rig were selected to provide a good distribution for data plotting within the pressure range of the facility. Pressures were the only conditions arbitrarily controlled. Air supply temperatures varied only ±4 C (7°F) from a nominal 23 C (73°F).

2D Static Rig. The operational simplicity and low data sampling requirements of the 2D rig permitted the recording of fifteen seal pressure ratio conditions for each test configuration. Test conditions at seal inlet pressures up to a maximum of eight atmospheres were recorded for some seal configurations. The following table lists the standard seal inlet pressures set in increasing order during a typical 2D rig test.

TABLE 1. Typical 2D Rig Test Conditions

Sequence Number	p_U/p_D (Approximate)	p_U - Seal Upstream Pressure cm Hg A	in. Hg A
1	1.12	. .	33.
2	1.22	91.	36.
3	1.42	107.	42.
4	1.63	122.	48.
5	1.83	137.	54.
6	2.03	152.	60.
7	2.44	183.	72.
8	2.85	213.	84.
9	3.25	244.	96.
10	3.66	274.	108.
11	4.27	320.	126.
12	4.88	366.	144.
13	5.49	411.	162.
14	6.10	457.	180.
15	6.78	508.	200.

3D Dynamic Rig. Static testing on the 3D rig was similar to that on the 2D rig. However, the higher airflow rates and more restricted seal discharge area limited the pressure ratio range to about one-third that of the 2D rig. The following table lists the standard seal inlet pressures set in increasing order during a typical 3D rig test.

TABLE 2. Typical 3D Rig Test Conditions

Sequence Number	p_U/p_D (Approximate)	p_U - Seal Upstream Pressure cm Hg G	in. Hg G
1	1.12	9.4	3.7
2	1.21	17.0	6.7
3	1.40	32.3	12.7
4	1.58	47.5	18.7
5	1.76	62.7	24.7
6	1.94	78.0	30.7
7	2.28	108.	42.7
8	2.61	139.	54.7
9	2.93	169.	66.7
10	3.24	200.	78.7

Each 3D rig test was initiated by taking a static (zero rotor rpm) leakage flow calibration. The static calibration was followed by rotational calibrations at seal rotor speeds of 10,000, 20,000, and 30,000 rpm. At each point, a full scan of the automatic data acquisition system was recorded on punch paper tape printout. During the dynamic testing, thrust balance air was supplied at the pressure required by seal inlet pressure and seal discharge pressure to maintain a constant 670 N (150 lb_f) aft load on the rotor thrust bearing.

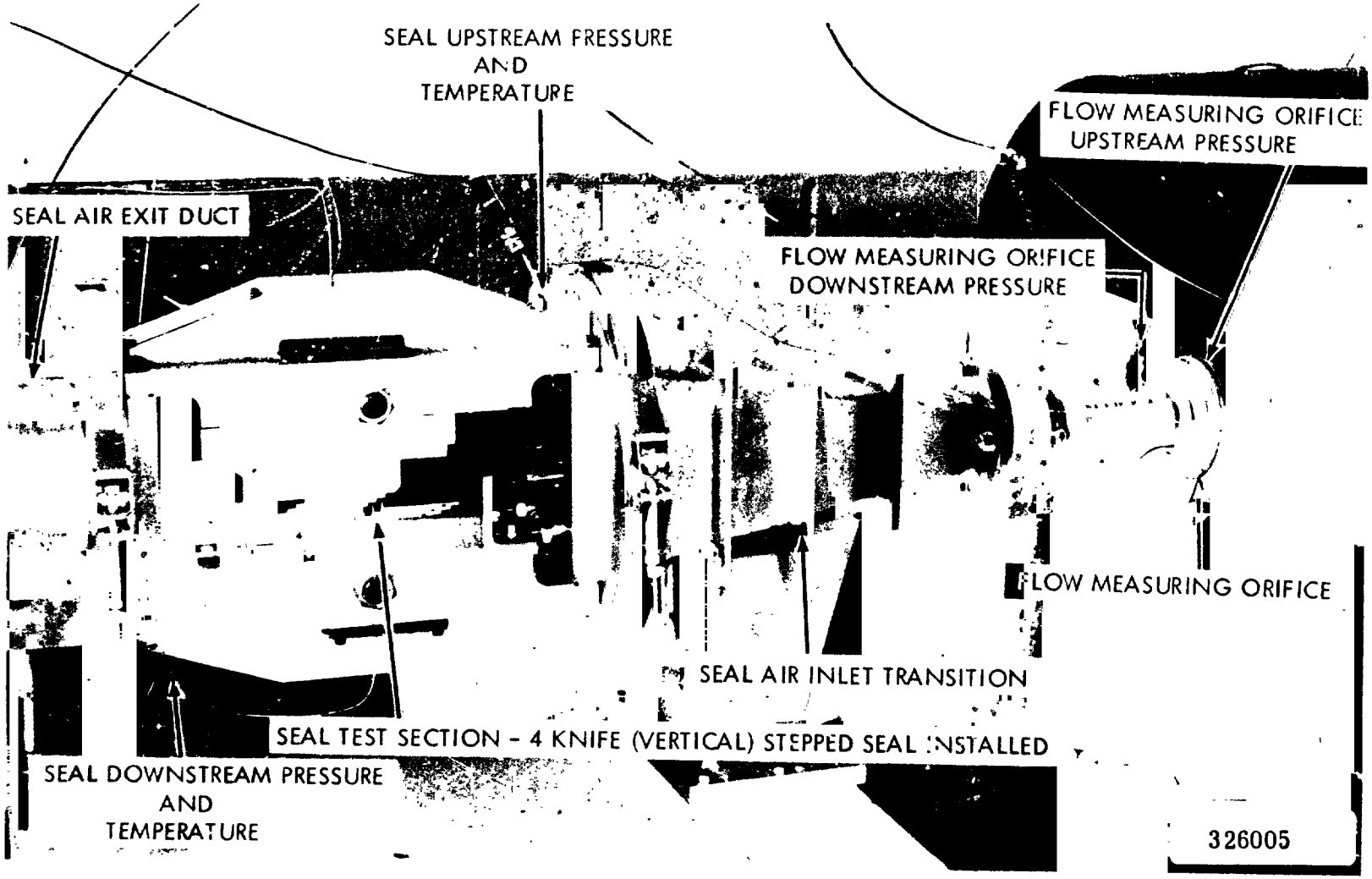

FIGURE 5. TWO-DIMENSIONAL LABYRINTH SEAL AIR TEST RIG INSTALLATION

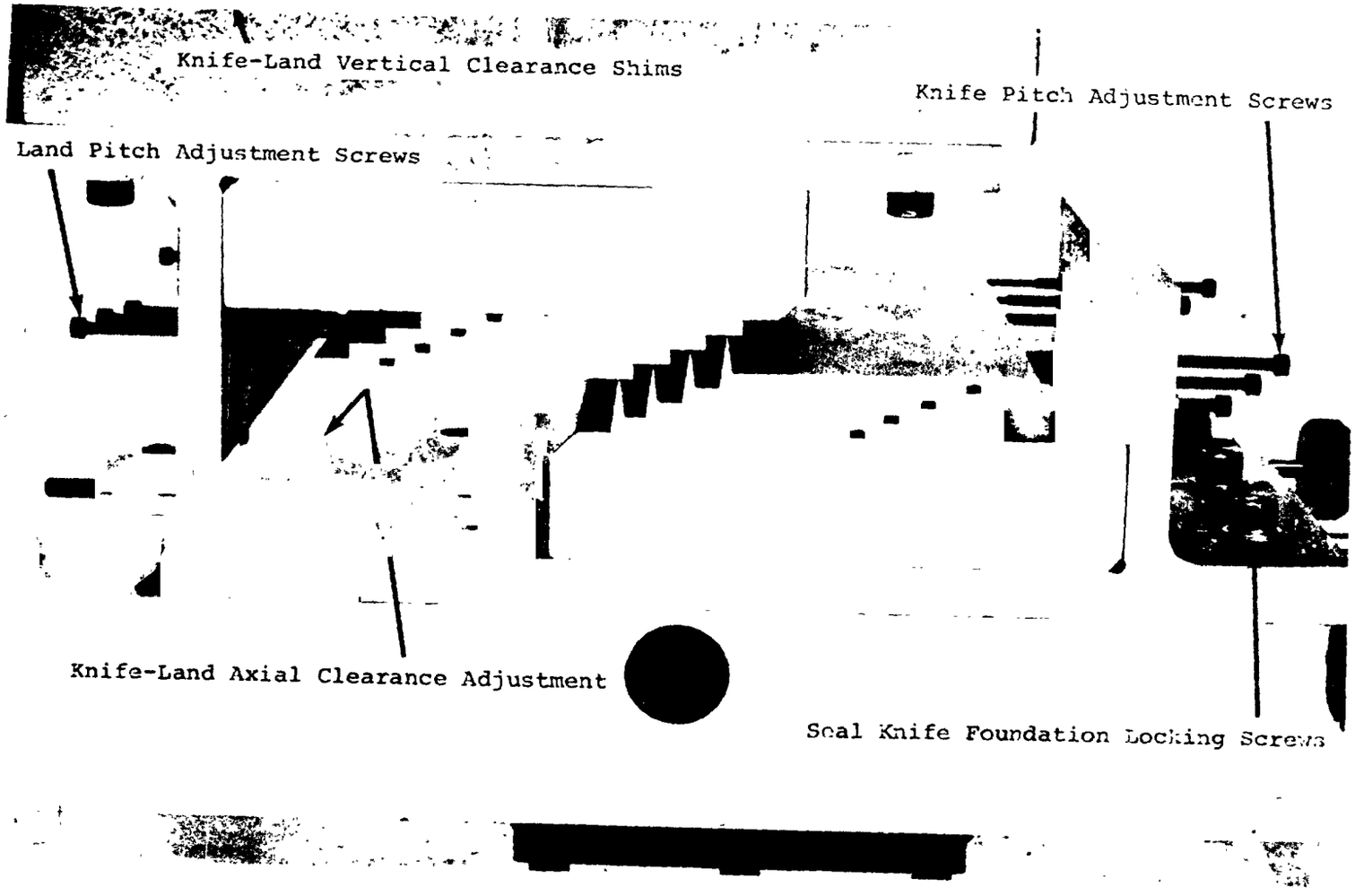

FIGURE 6. TWO-DIMENSIONAL LABYRINTH SEAL RIG WITH STEPPED SEAL INSTALLED

FIGURE 7. TWO-DIMENSIONAL LABYRINTH SEAL RIG WITH STRAIGHT-THROUGH SEAL INSTALLED

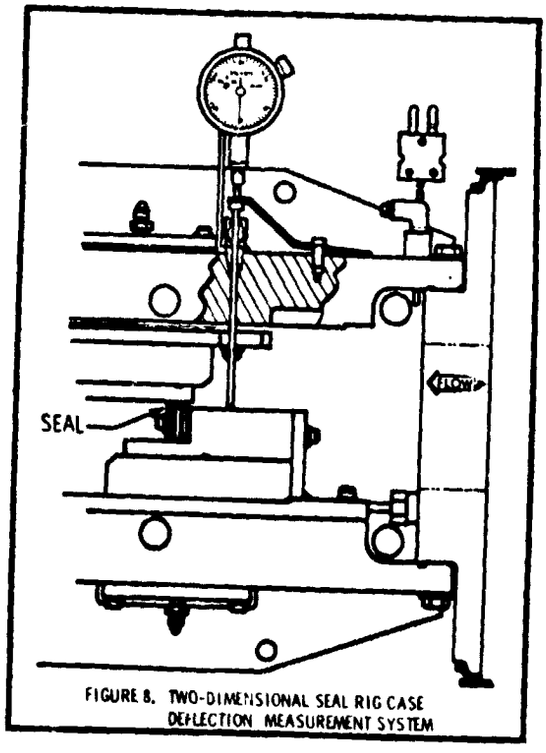

FIGURE 8. TWO-DIMENSIONAL SEAL RIG CASE DEFLECTION MEASUREMENT SYSTEM

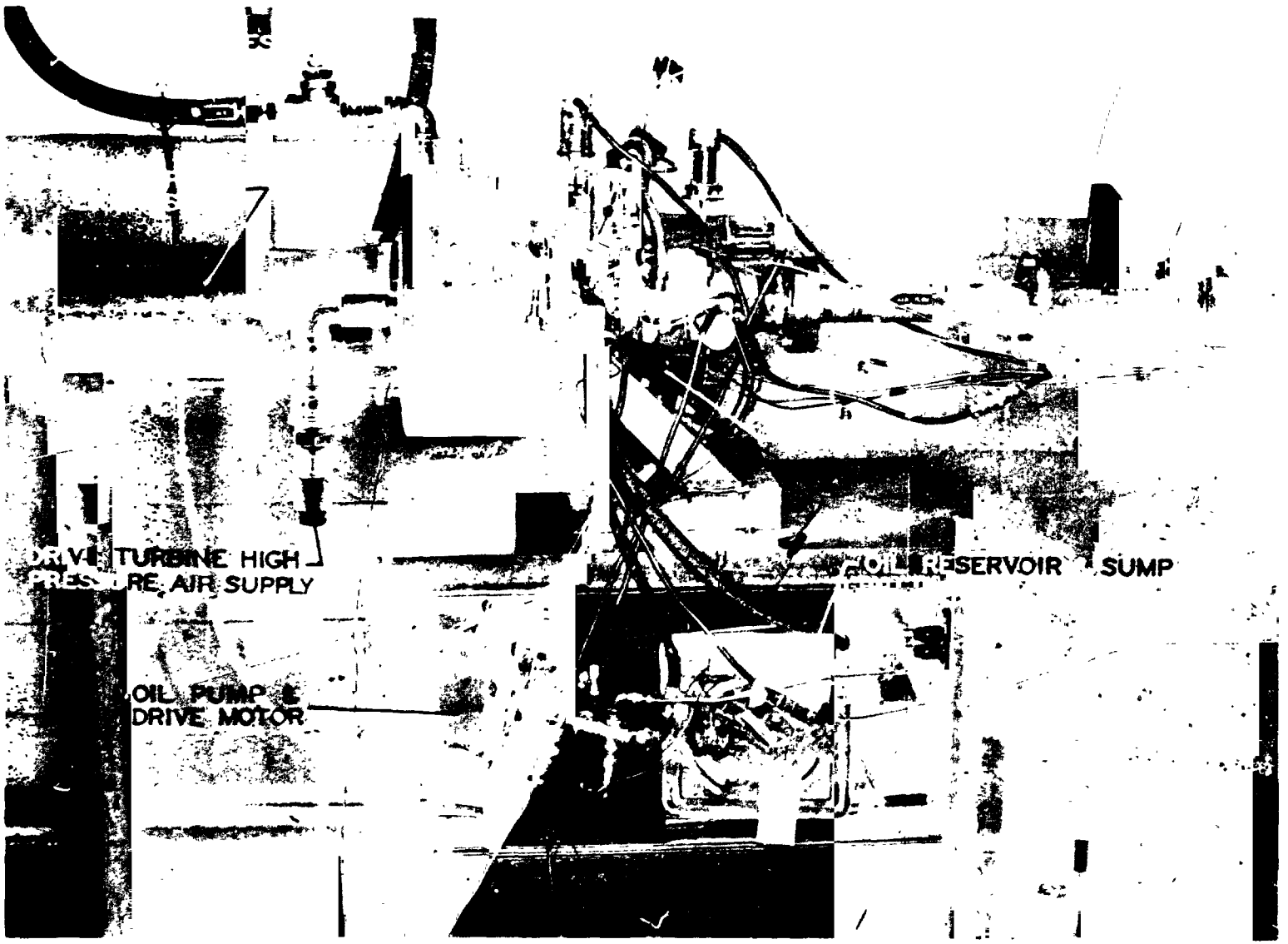

FIGURE 9. DYNAMIC LABYRINTH SEAL AIR TEST RIG INSTALLATION

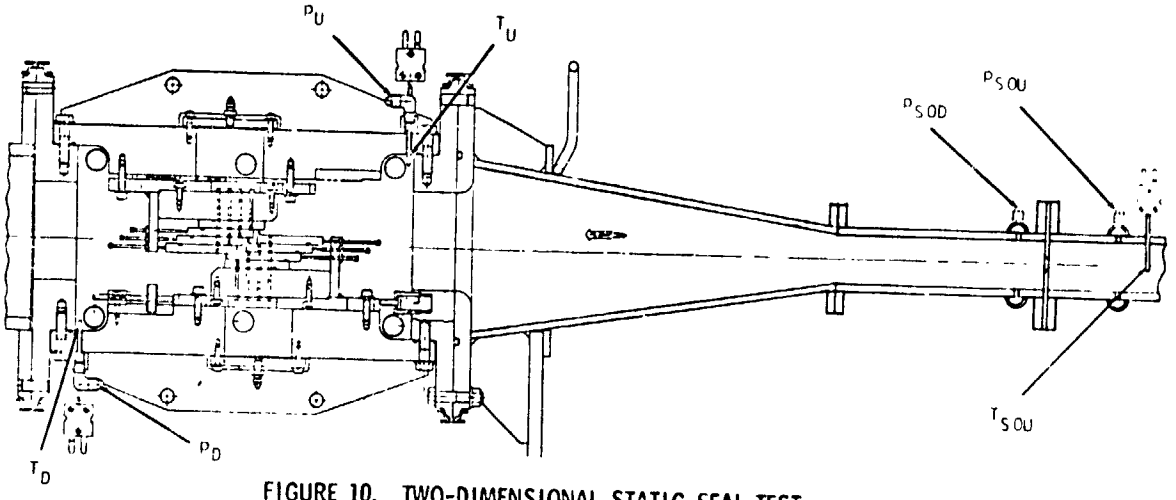

FIGURE 10. TWO-DIMENSIONAL STATIC SEAL TEST RIG INSTRUMENTATION SCHEMATIC

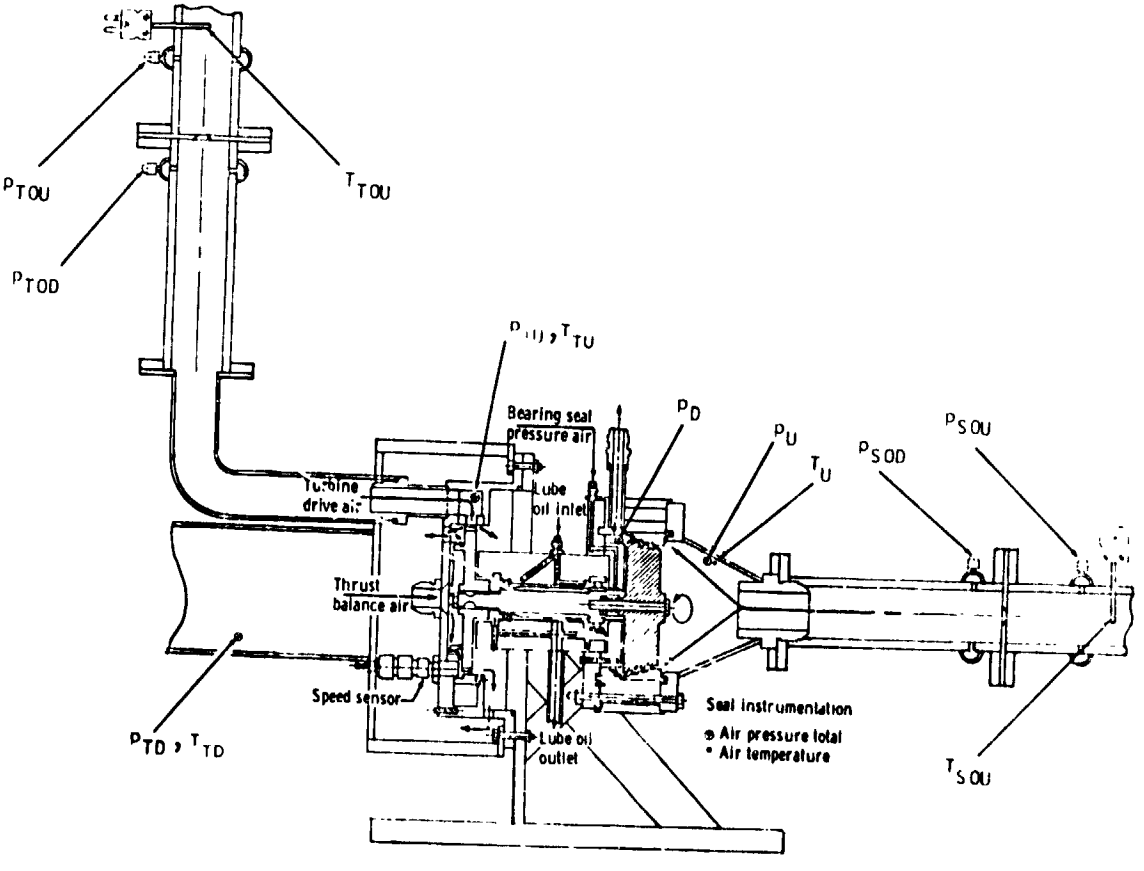

FIGURE 11. THREE-DIMENSIONAL DYNAMIC SEAL TEST RIG INSTRUMENTATION SCHEMATIC

FIGURE 12. AUTOMATIC DATA ACQUISITION SYSTEM FOR DDA LABYRINTH SEAL RIG

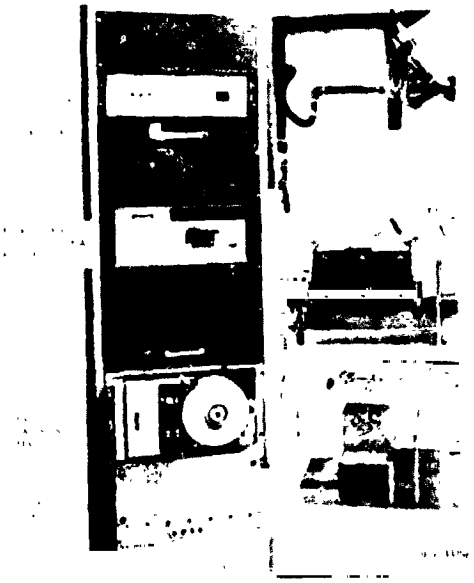

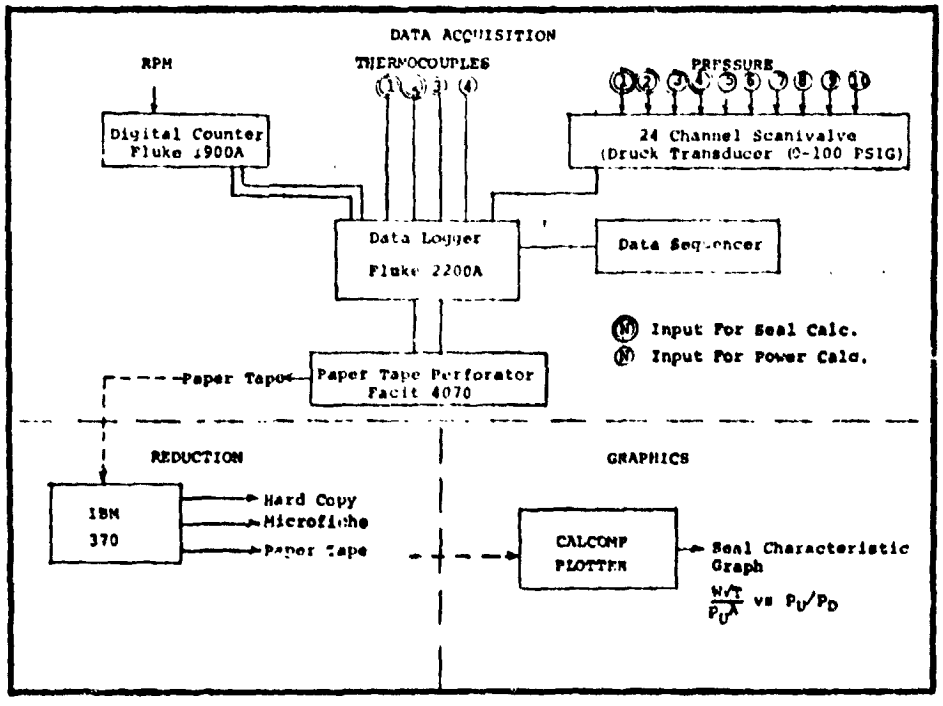

FIGURE 13. DESCRIPTIVE LAYOUT OF DDA SEAL DATA ACQUISITION, DATA PROCESSING, AND GRAPHICS

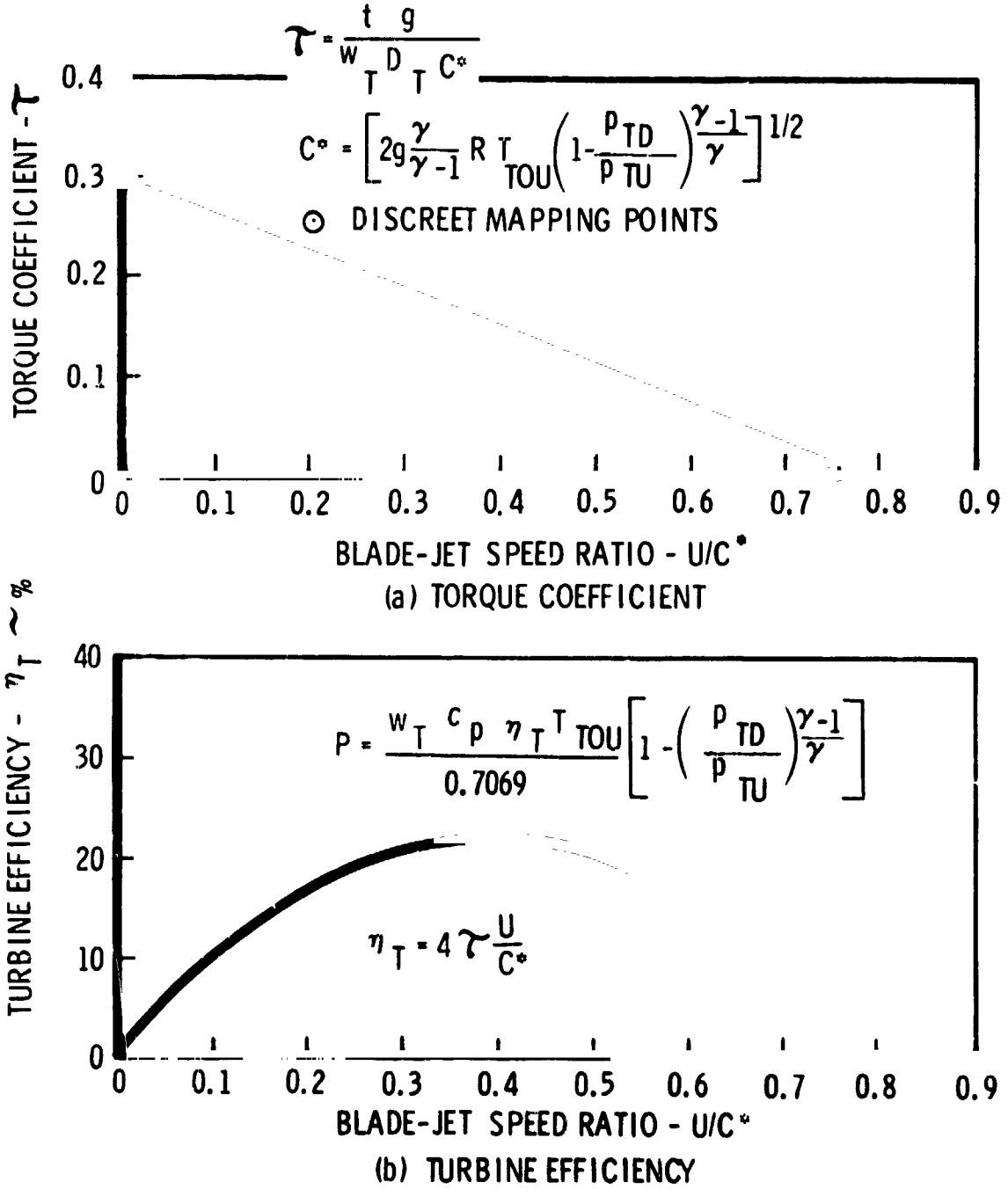

FIGURE 14. DDA DYNAMIC SEAL RIG DRIVE TURBINE PERFORMANCE AS A FUNCTION OF BLADE-JET SPEED RATIO

FIGURE 15. SENSITIVITY OF 3D RIG DRIVE TURBINE BEARING LOAD ON MEASURED POWER ABSORPTION

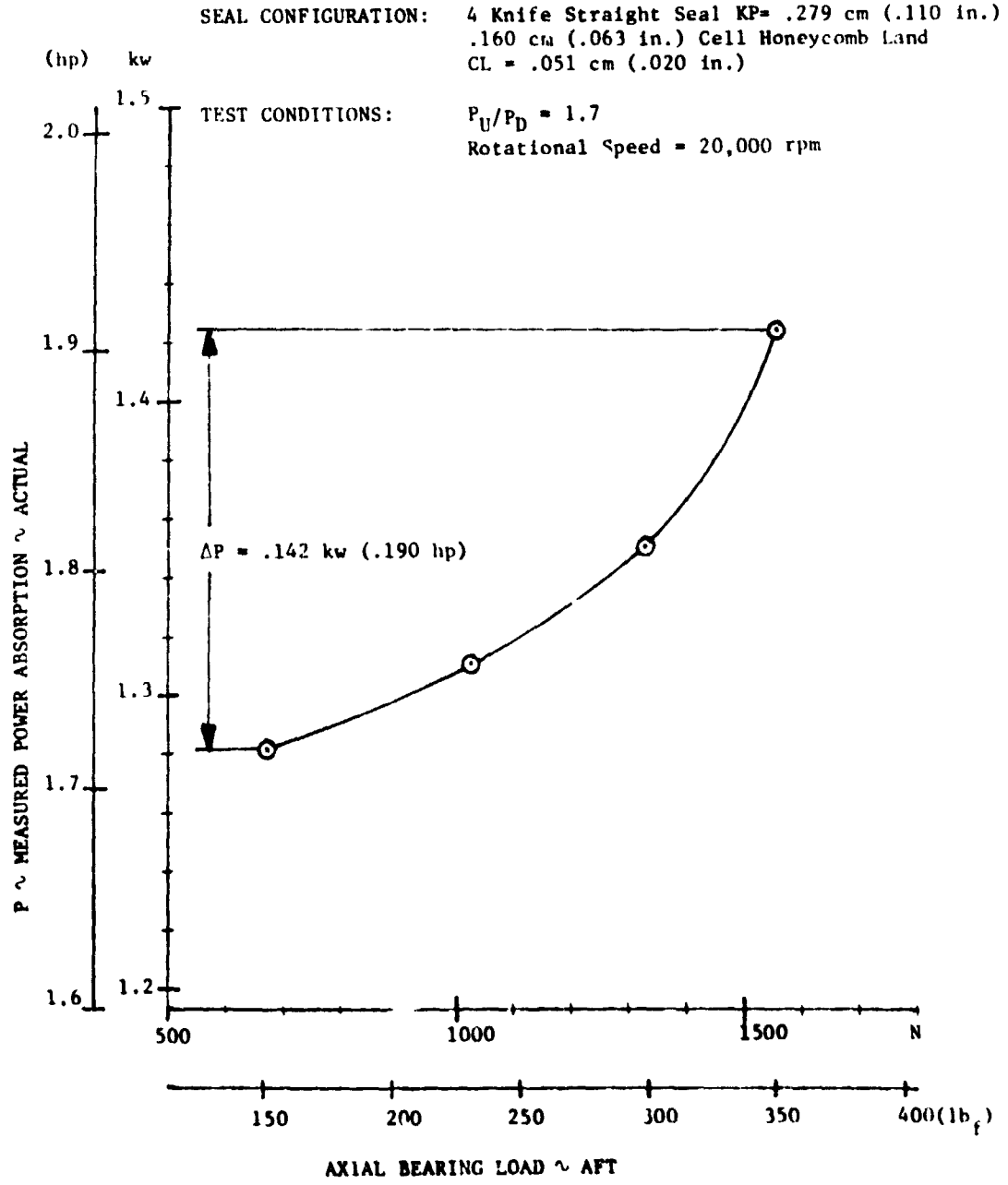

TEST RESULTS AND DISCUSSION

The aerodynamic performance of conventional and advanced labyrinth seals was investigated during the course of this program. These investigations were conducted for conventional straight-through seals using solid-smooth, abradable, and honeycomb lands. Evaluation tests were conducted in the two-dimensional (2D) and the rotating three-dimensional (3D) air seal test rigs.* An advanced labyrinth seal was also developed using these rigs. The previously unexplored subject of the inherent friction and pumping energy absorbed by a rotating seal was investigated during the 3D rig testing.

The information presented in this section has been divided into the following subsections:

- o Aerodynamic Test Results for Straight-Through Labyrinth Seals
- o Aerodynamic Test Results for an Advanced Labyrinth Seal
- o Rotational Power Absorption

Aerodynamic Test Results for Straight-Through Labyrinth Seals

The 2D air seal test rig (shown in Figure 5) was used extensively to evaluate the effect that abradable and honeycomb lands have on straight-through labyrinth seal leakage. The four knife conventional straight-through seal used for this series of 2D rig tests is shown in Figure 16. A solid-smooth land was tested in conjunction with the abradable and honeycomb lands to provide a baseline for comparison. A photograph of the solid-smooth land, the four abradable lands, and the three honeycomb lands tested is presented in Figure 17.

A porous abradable material land and a .159 cm (.062 in.) cell honeycomb land were tested in the 3D dynamic air seal test rig (shown in Figure 9) to determine the effect of rotational geometry and dynamic operation on seal leakage. The four knife straight-through seal used for this evaluation is similar to the 2D rig seal tested. A solid-smooth land was also evaluated statically and dynamically in the 3D rig for comparison. Two additional rotors with knife pitches of .203 cm (.080 in.) and .356 cm (.140 in.) were also run to permit the determination of the effects of rotation and land material on the selection of optimum knife pitch.

A convenient means of relating the leakage performance of special land materials to solid-smooth land performance, and an approach that will be

*An evaluation of the correlation of seal performance measured in the 2D rig with that obtained from the 3D rig is made in Appendix D.

used throughout this report, is to compare the flow parameter values, ϕ, at a constant pressure ratio for the various lands tested.*

Several of the seal land configurations were tested at pressure ratios approaching 8:1 in the 2D rig to determine the choked seal flow characteristics. A typical example of these tests is presented in Figure A-6, Appendix A, for the four knife straight-through seal using the nickel-graphite land. These tests verify that the flow parameter, ϕ, approaches a zero slope at the critical pressure ratio and remains approximately constant in the choked flow regime.

Abradable Lands Evaluation. The four abradable lands tested include two non-porous materials, nickel-graphite and aluminum-polyester with a material thickness of .076 cm (.030 in.), and two commercially available porous abradable materials, "Abradable A" and "Abradable B" with a material thickness of .229 cm (.090 in.).** The seal flow parameter characteristics derived from the aerodynamic test performance data are presented in Figures 18, 19 and 20 for .013 cm (.005 in.), .025 cm (.010 in.), and .051 cm (.020 in.) clearances, respectively. The baseline solid-smooth land flow parameter has also been included on these figures for comparison purposes. The abradable lands with porous materials "A" and "B" indicated leakage levels approximately 13% higher than the smooth solid land at .051 cm (.020 in.) clearance. At the two lower clearances investigated, however, the porous abradable lands showed substantially higher leakage levels. This is attributed to the increasing ratio of porosity flow (leakage through the material) relative to the leakage across the knife gap at the lower clearances.

Table 3 presents a comparison of the seal flow parameter values for the solid-smooth and abradable lands at a 2.0 and a 3.0 seal pressure ratio for the clearances tested. The percent variation in leakage from the solid-smooth land has also been calculated from the flow parameters. These results show that the porous land materials, "Abradable A" and "Abradable B", produced 10% to 60% increase in leakage at a 2.0 pressure ratio compared to the solid-smooth land. The nickel-graphite and aluminum-polyester lands gave a -8% to +7% leakage change from the solid-smooth land at 2.0 pressure ratio. Figure 21, which graphically presents the Table 3 results, clearly shows the higher leakage characteristic for the porous material abradable lands, particularly at small clearance levels. The apparent leakage through the porous abradable lands "A" and "B" diminishes as a percent of the total flow as clearance is increased.

*The complex interactions of seal geometry and clearance with the upstream fluid conditions and pressure ratio limits the discussion of absolute seal leakage in terms of massflow to specific flow conditions. For generality, comparisons of "seal leakage" in this report will imply the relationships among flow parameters, ϕ.

**The commercial names and manufcturers of the "Abradable A" and "Abradable B" materials can be obtained from the NASA Project Manager.

leakage than the smooth land, respectively. The nickel-graphite land had a rougher surface finish, 9 μm (350 μin.), than the solid-smooth land, 0.8 μm (30 μ in.). These results prompted an investigation to determine the individual effects that surface roughness and porosity had on the leakage performance of the seal.

The individual seal flow parameter curves for the smooth and abradable land tests in the 2D seal test rig are included in Appendix A.

Surface Roughness Effect on a Solid Land. A solid land with a medium rough surface 8.3 μm (325 μin.) and a solid land with a rough surface, 22.9 μm (900 μin.), were tested with the four knife straight-through seal at .013 cm (.005 in.), .025 cm (.010 in.), and .051 cm (.020 in.) clearances. The surface roughness flow parameters are presented in Figures 22, 23, and 24 for the three clearances tested. The solid-smooth land flow characteristics have also been included in these figures. A similar set of tests was performed using a single straightthrough knife. These results are presented in Figures 25, 26, and 27. A summary of the leakage results at a 2.0 and a 3.0 seal pressure ratio is presented in Table 4 for the four knife straight-through seal and in Table 5 for the single knife straight-through seal. The percent change in leakage performance from the smooth land to the medium rough surface and the rough surface lands is plotted in Figures 28 and 29 for the four knife and single knife configurations, respectively. Over the range of clearances tested, a medium rough land reduced the leakage of the four knife seal by as much as 28%. The relative reduction in leakage was greatest at .013 cm (.005 in.) clearance and least at .051 cm (.020 in.) clearance. The rough land actually increased leakage compared with the leakage for the smooth land at the clearances tested. The single knife performance results show that leakage was the same or higher than that for a smooth land.

The leakage reduction achieved with the medium rough land is believed to be the result of increased friction losses and higher surface turbulence which tends to disrupt the flow field through the seal. The increased level of leakage experienced with the rough land appears to be caused by a larger equivalent clearance. The seal clearance was measured from the knife tip to the maximum height of the roughness elements on the land surface. The bigger roughness elements may produce a larger path for leakage between the clearance reference surface and the solid subsurface. The benefit gained from increased friction and turbulence might be more than offset by the increased leakage area for the rough land configuration. The little change found in the single knife seal leakage for the medium rough land points out the significant contribution of the boundary layer and the seal intercavity turbulence in reducing leakage through multi-knife seals.

Combined Porosity and Surface Roughness Effects on the Abradable Lands. The porosity leakage tests were conducted using abradable materials "A" and "B". These tests were accomplished by clamping a rubber gasket, that duplicated the length of the four knife test seal, onto the surface of the abradable material. A sketch of the arrangement is presented in Figure 30. This approach was intended to be a rapid, first-order evaluation of the leakage rate through the abradable land material, however, this technique gave excellent results as evidenced in the following discussion.

Experimental results for solid lands with surface roughnesses similar to the "Abradable A" land and the "Abradable "B" land were combined with the porosity test results and compared to the measured performance of these porous abradable lands. The flow data are presented in the form $w\sqrt{T_{tj}}/p_{tj}$ which makes the parameter a function of clearance area. This approach was required to circumvent flow parameter, ϕ, indeterminancy since the clearance area was zero for the porosity tests. Table 6 presents the individual porosity (1) and surface roughness (2) leakage characteristics for the "Abradable A" land. The sum of these two leakage components (3) is compared to the actual "Abradable A" land results (4) at seal pressure ratios of 2.0 and 3.0. The sum of the individual components.investigated is generally within 5% of the "Abradable A" land results (see line 5). In one case only, the deviation reaches 8%. This level of agreement is significantly better than anticipated for a first-order evaluation. Figure 31 quantifies the fraction of the total four knife straight seal leakage represented by the porosity flow through an "Abradable A" land. Although the actual porosity flow does not appear to be a strong function of clearance, it does decrease steeply as a percent of the total leakage flow as clearance increases.

The "Abradable B" porosity and surface roughness components are summarized in Table 7. The analysis of the porosity and roughness components is similar to that for "Abradable A" in Table 6. The results for "Abradable B" show more deviation between the sum of the individual leakage components and the measured land performance than they did for the "Abradable A" land. The leakage component sum (3) was consistently greater than the measured land leakage (4). A possible explanation for this characteristic may be found in terms of the effective surface roughness present in the "Abradable B" land test. The porosity leakage, which is re-entering the mainstream path along the length of the seal, is effectively filling some portion of the roughness voids. This flow deflection action would have the effect of reducing the open area between surface roughness elements and subsequently reducing the associated surface roughness leakage. A plot of the porosity flow component relative to the total seal leakage is presented in Figure 32.

Since the porosity leakage fraction is approximately the same for the two abradables, it can be concluded that the "Abradable B" land leakage would

be reduced to the level of the "Abradable A" land if the surface roughnesses were the same. The results of these surface roughness tests reveal why the "Abradable B" land leaks more than the "Abradable A" land when the other seal parameters are equal.

Rotational Effect on the Abradable Land. An "Abradable A" material land was selected for testing with the straight-through seal rotor of Figure 33 (b) to determine the effects of rotation on leakage performance. A solid-smooth land was used as a performance baseline. Both configurations were tested at two radial clearance values, .025 cm (.010 in.) and .051 cm (.020 in.).

The static and dynamic aerodynamic test results from the 3D rig for the solid-smooth land are presented in Figures B-3 and B-4, Appendix B, for .025 cm (.010 in.) and .051 cm (.020 in.) radial clearances, respectively. Similar curves are presented in Figures B-9 and B-10 for the "Abradable A" material land.

Table 8 summarizes the solid-smooth and abradable land leakage performance at a 2.0 seal pressure ratio for the static and dynamic tests. The effects of rotation on the "Abradable A" land are very similar to the solid-smooth land results. At the maximum rotational speed test condition, 239 m/s (785 ft/sec), the leakage of both lands was reduced about 10% compared to the static leakage.

The 3D rig static test results showed approximately equal seal leakage for the solid-smooth land and "Abradable A" land. Comparison with the 2D rig tests shows the "Abradable A" land leaking 10% more than the solid-smooth land, suggesting a possible difference in "Abradable A" land porosity between the 2D and 3D rig tests. Also, the surface of the "Abradable A" land for the 3D rig, 4 μm (160 μin.), was somewhat smoother than the land for the 2D rig, 9 μm (350 μin.). The 2D rig investigations of surface roughness showed that a 9 μm (350 μin.) surface roughness would reduce leakage compared to a smooth surface. Specific leakage performance information for a surface roughness of 4 μm (160 μin.) is not available, but, based on the 2D rig surface roughness test results, it is expected to give less leakage than a smooth land. Since the 3D rig "Abradable A" land leakage was comparable to the solid-smooth land, it appears that the surface roughness may have offset an already low porosity leakage.

The smooth and abradable land flow parameter curves for the 3D rig tests are included in Appendix B.

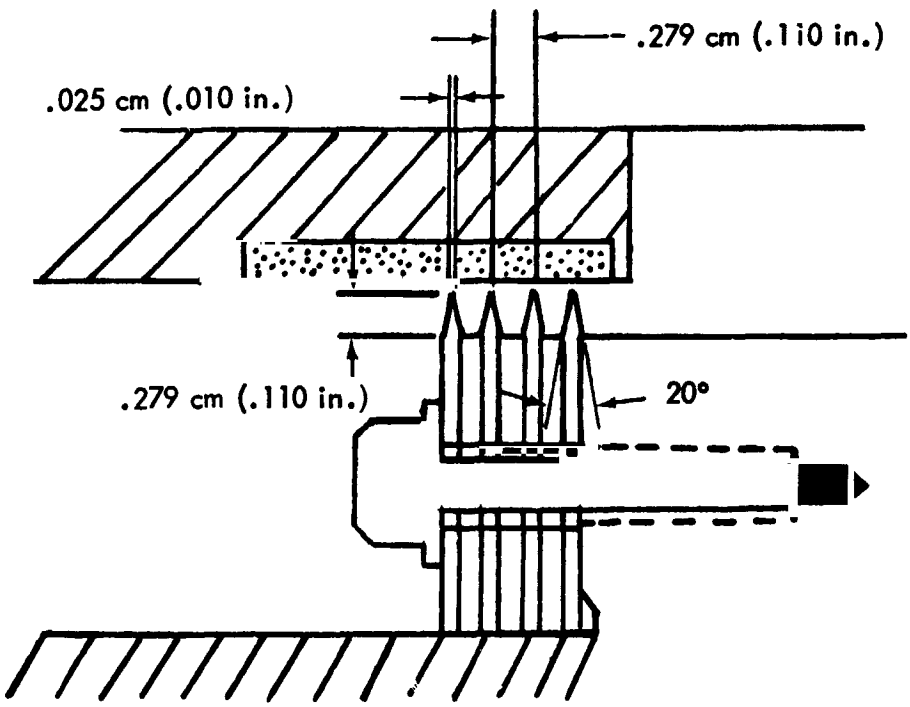

FIGURE 16. CONVENTIONAL STRAIGHT-THROUGH SEAL USED IN SEAL LAND PERFORMANCE EVALUATION

FIGURE 17. TWO-DIMENSIONAL TEST RIG STRAIGHT SEAL LANDS

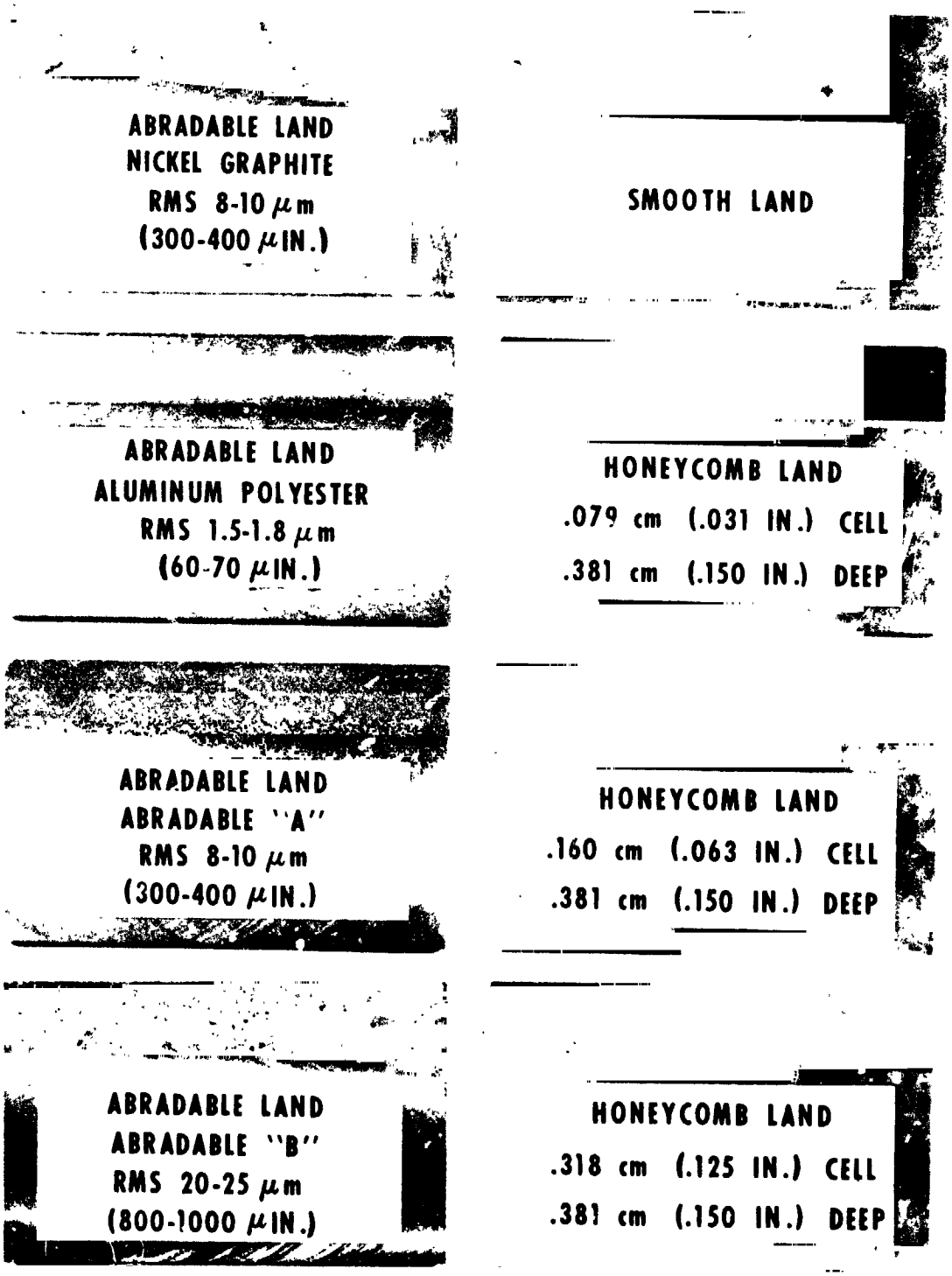

FIGURE 18. 2D RIG FOUR KNIFE STRAIGHT SEALS WITH SMOOTH AND ABRADABLE LANDS

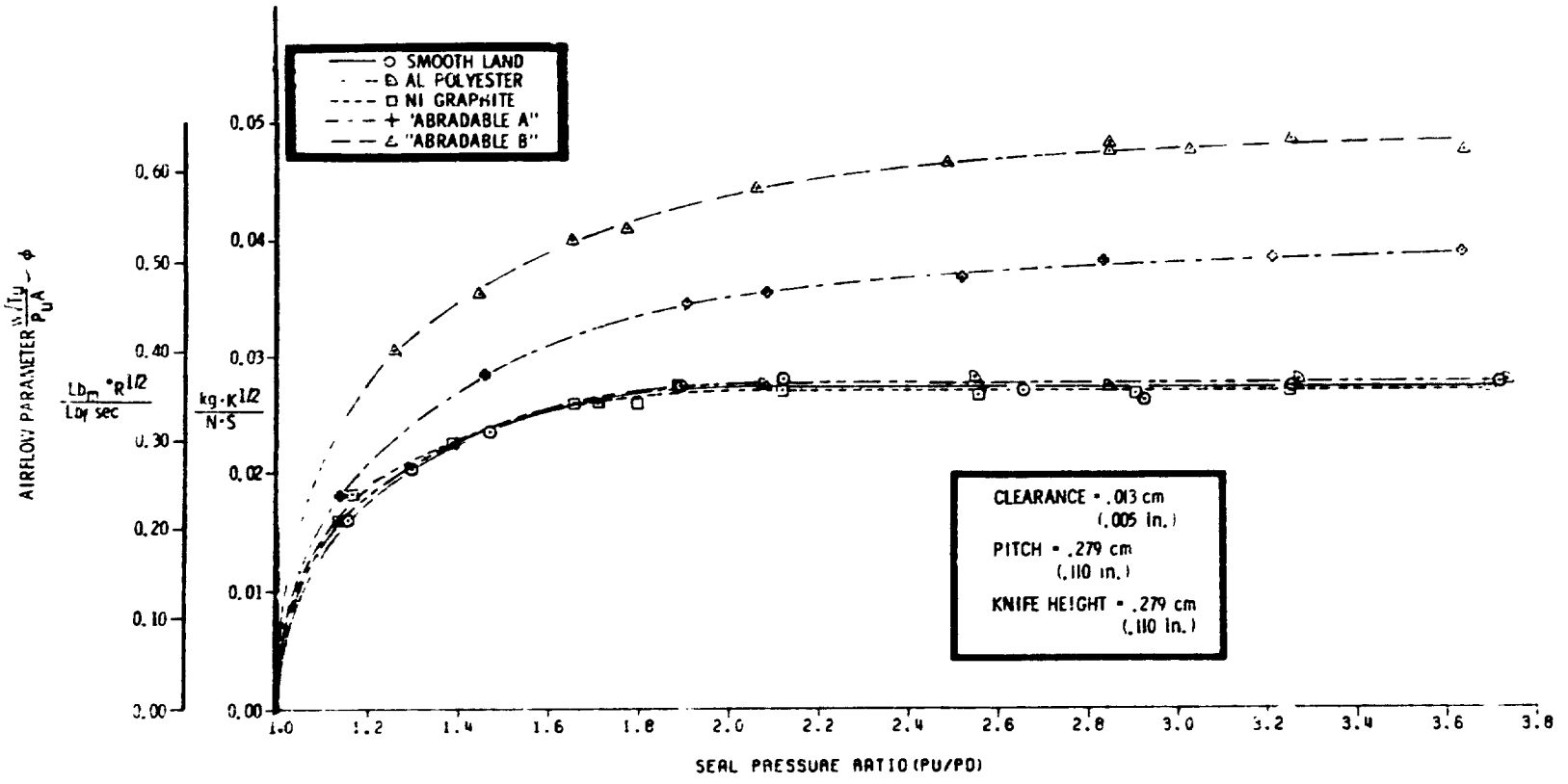

FIGURE 19. 2D RIG FOUR KNIFE STRAIGHT SEALS WITH SMOOTH AND ABRADABLE LANDS

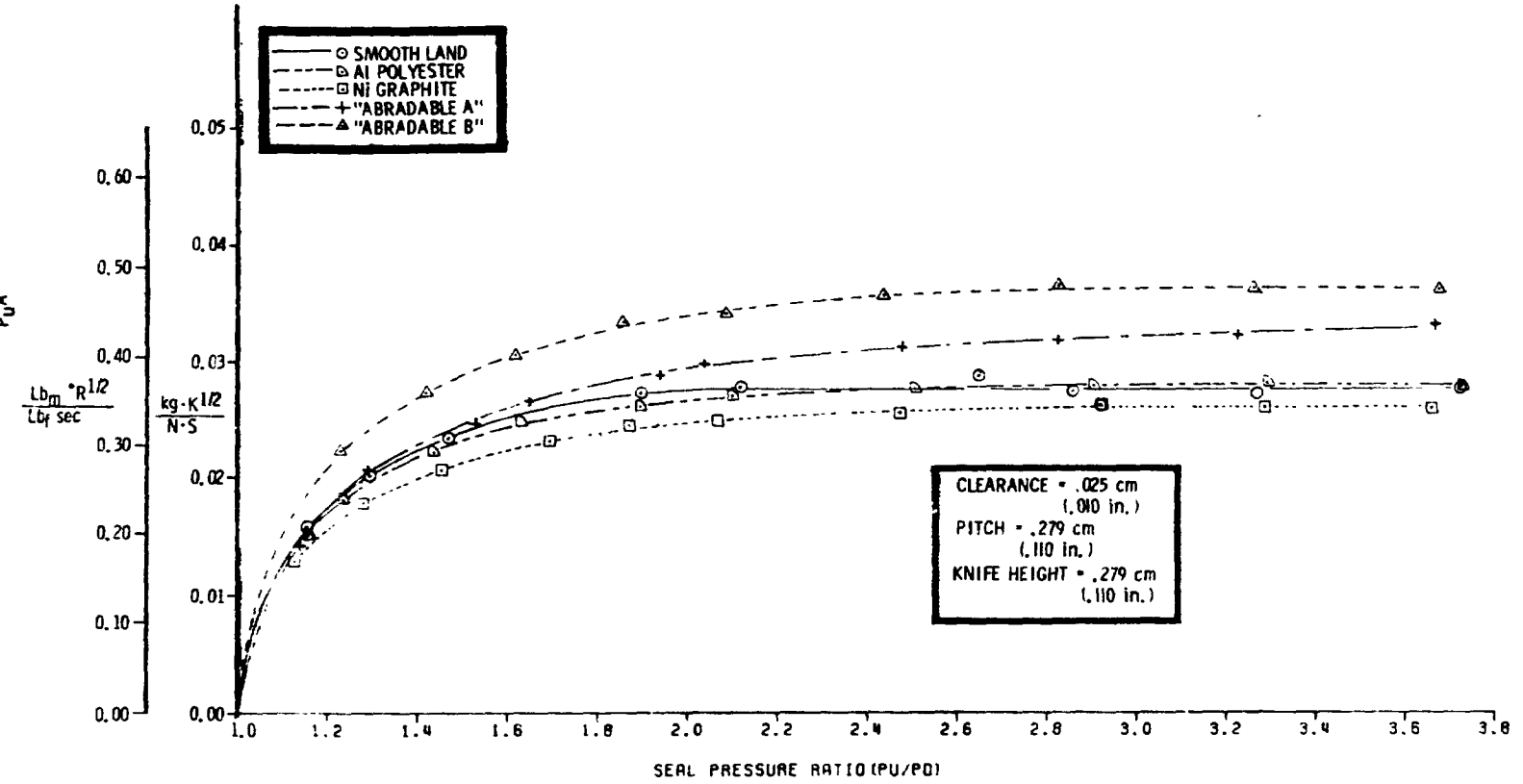

FIGURE 20. 2D RIG FOUR KNIFE STRAIGHT SEALS WITH SMOOTH AND ABRADABLE LANDS

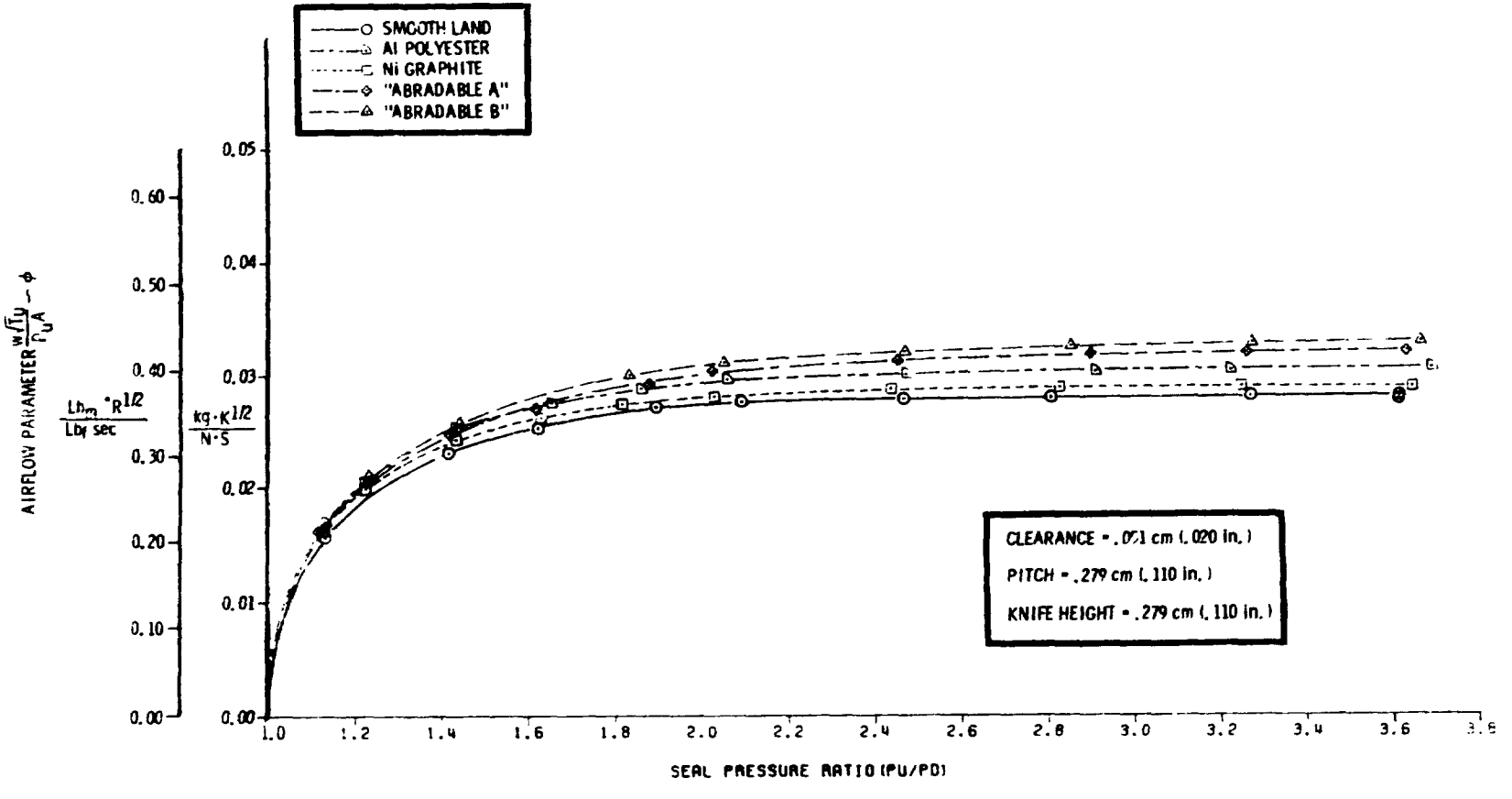

FIGURE 21. COMPARISON OF ABRADABLE LANDS PERFORMANCE AT PRESSURE RATIOS = 2.0 RELATIVE TO A SMOOTH LAND

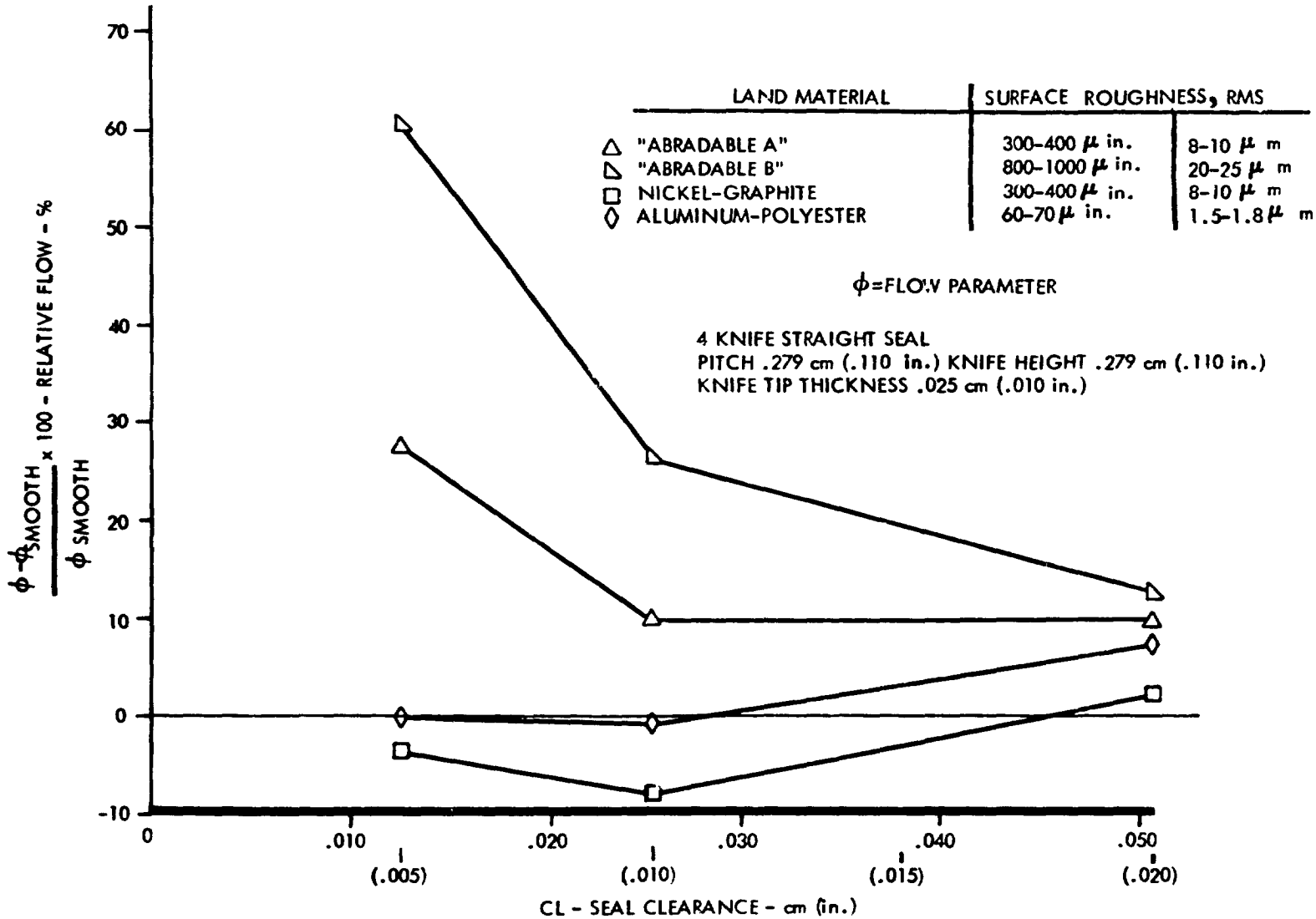

FIGURE 22. EFFECT OF SURFACE ROUGHNESS ON A FOUR KNIFE STRAIGHT SEAL

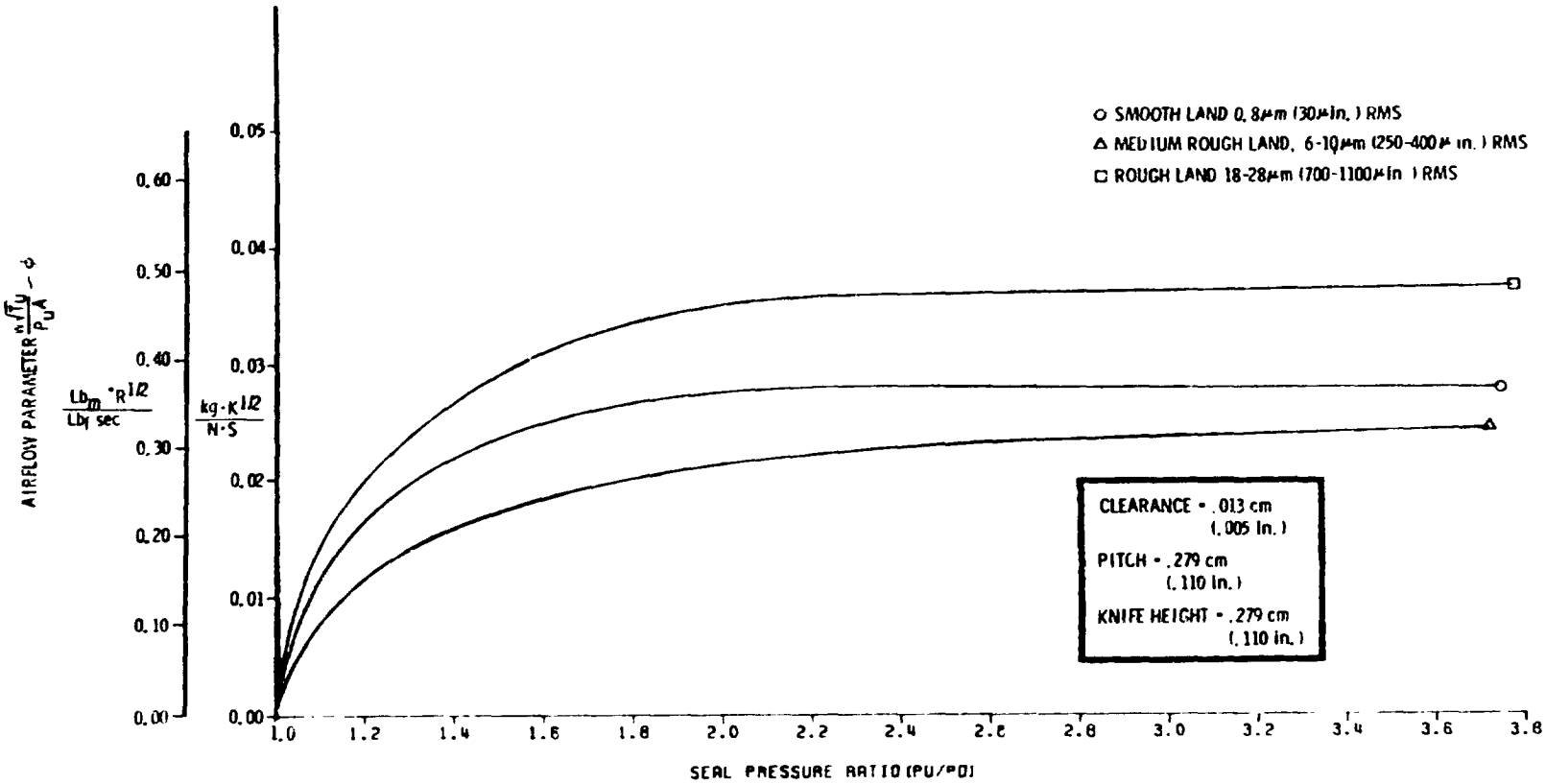

FIGURE 23. EFFECT OF SURFACE ROUGHNESS ON A FOUR KNIFE STRAIGHT SEAL

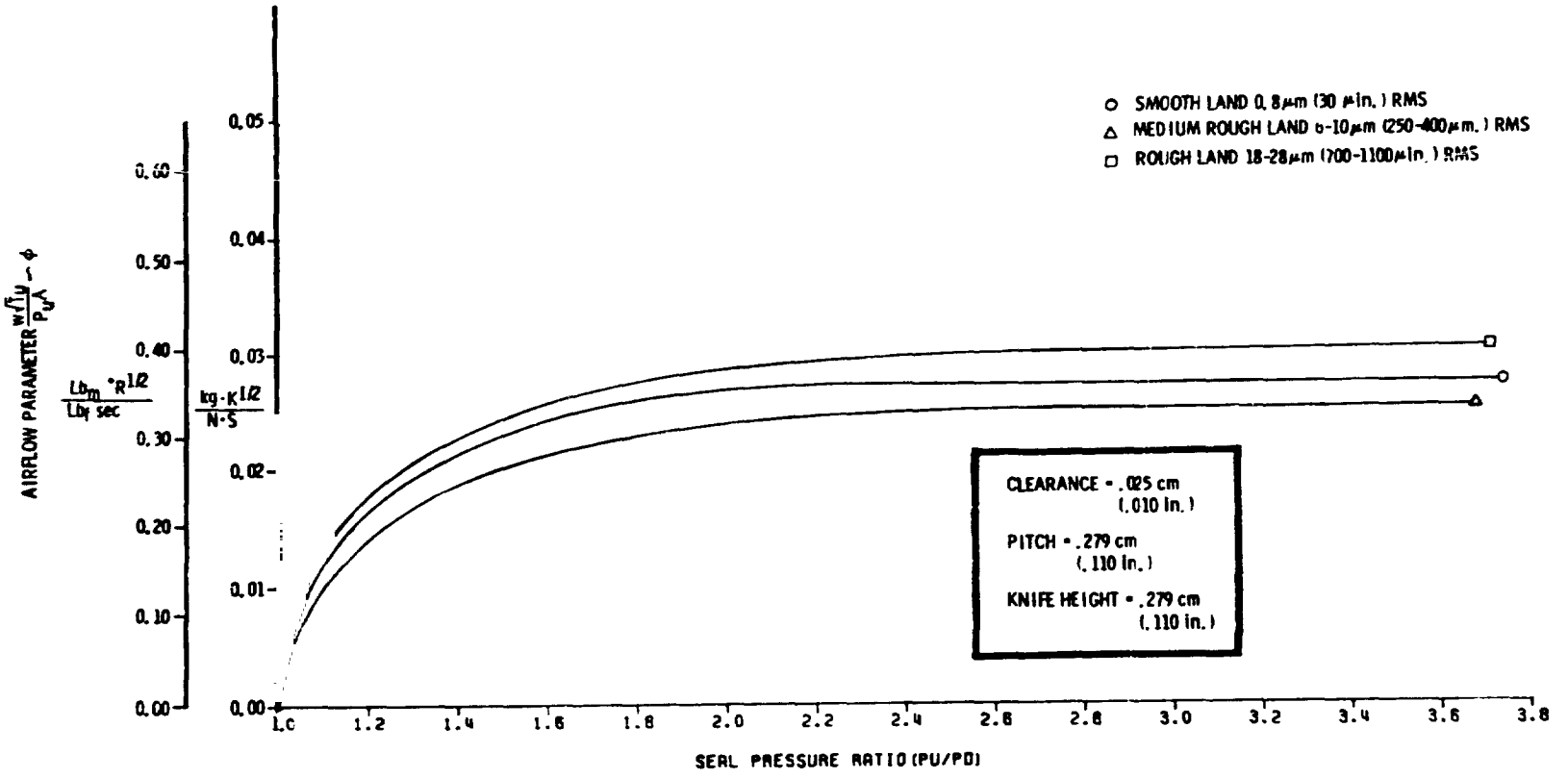

FIGURE 24. EFFECT OF SURFACE ROUGHNESS ON A FOUR KNIFE STRAIGHT SEAL

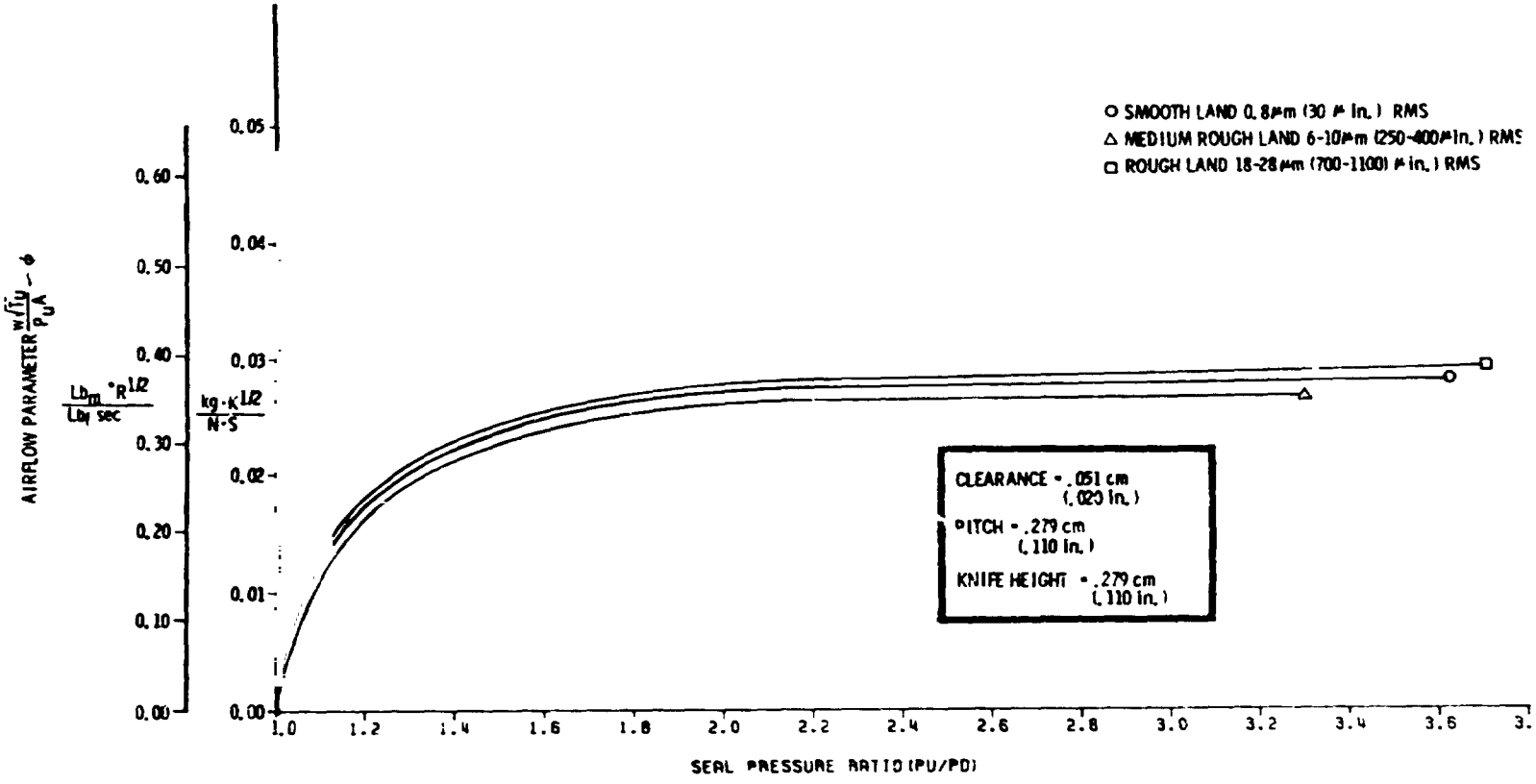

FIGURE 25. EFFECT OF SURFACE ROUGHNESS ON A SINGLE KNIFE SEAL

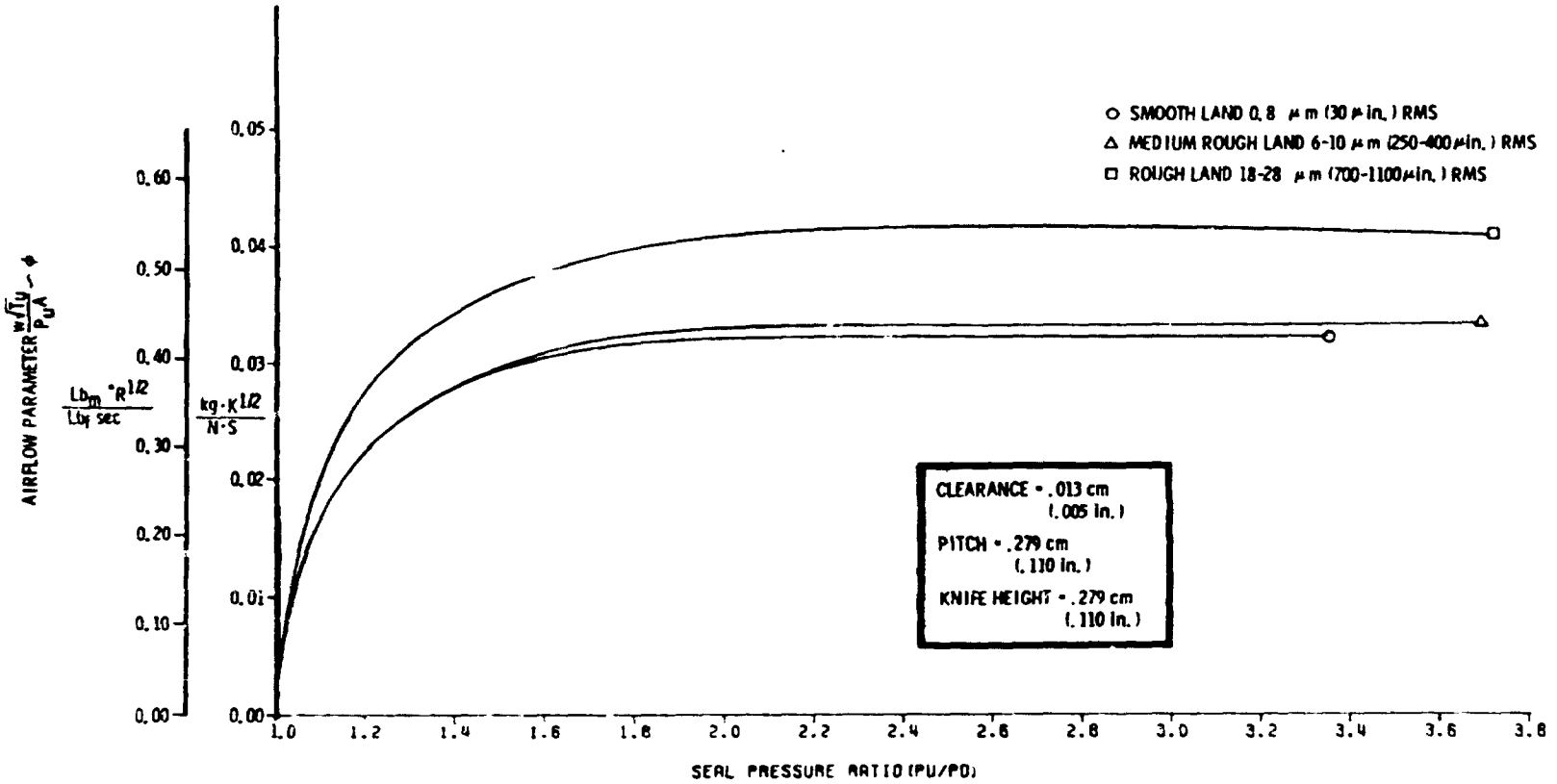

FIGURE 26. EFFECT OF SURFACE ROUGHNESS ON A SINGLE KNIFE SEAL

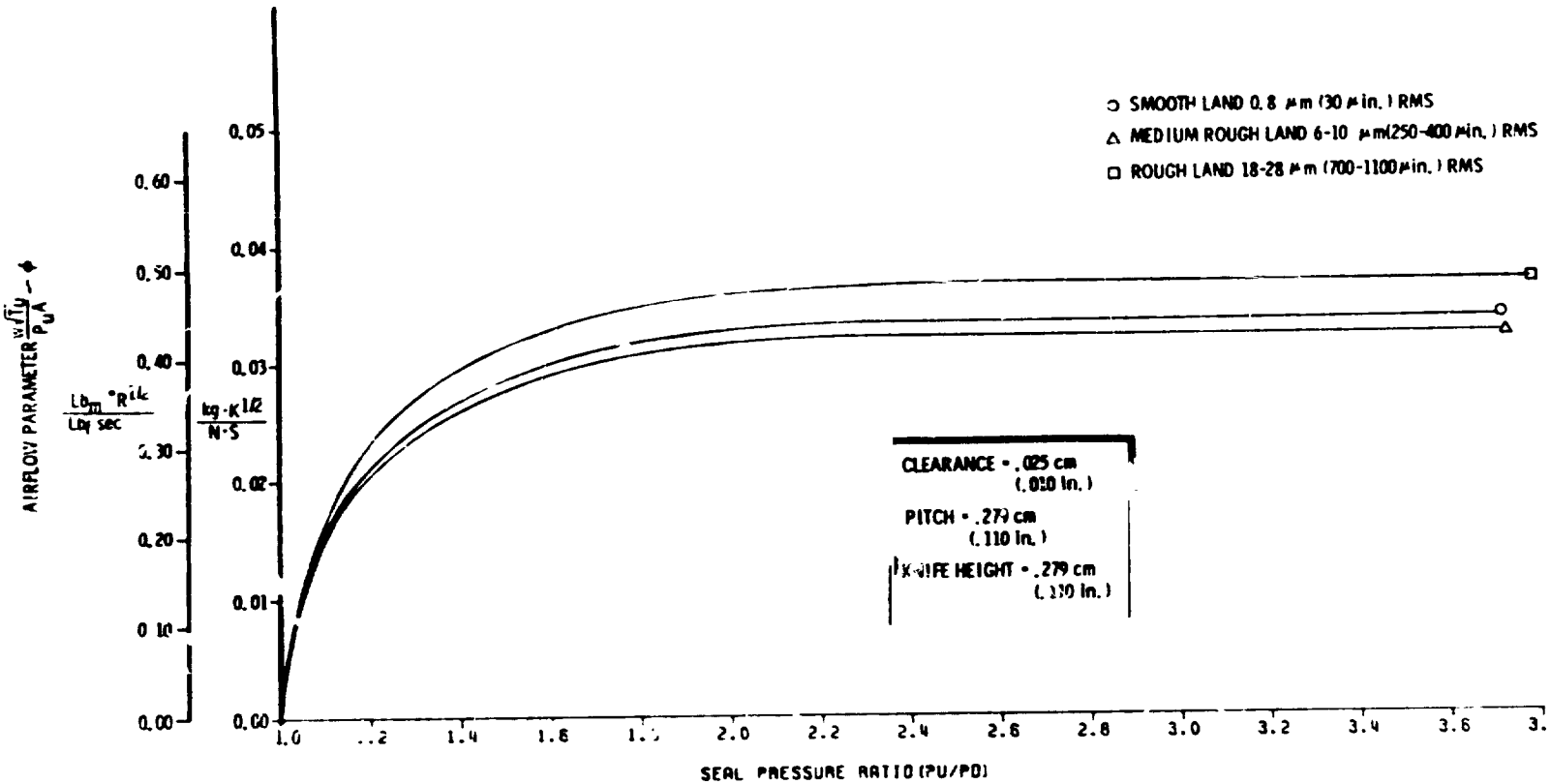

FIGURE 27. EFFECT OF SURFACE ROUGHNESS ON A SINGLE KNIFE SEAL

FIGURE 28. EFFECT OF SURFACE ROUGHNESS ON SEAL LEAKAGE COMPARED TO A SMOOTH LAND FOUR KNIFE STRAIGHT SEAL

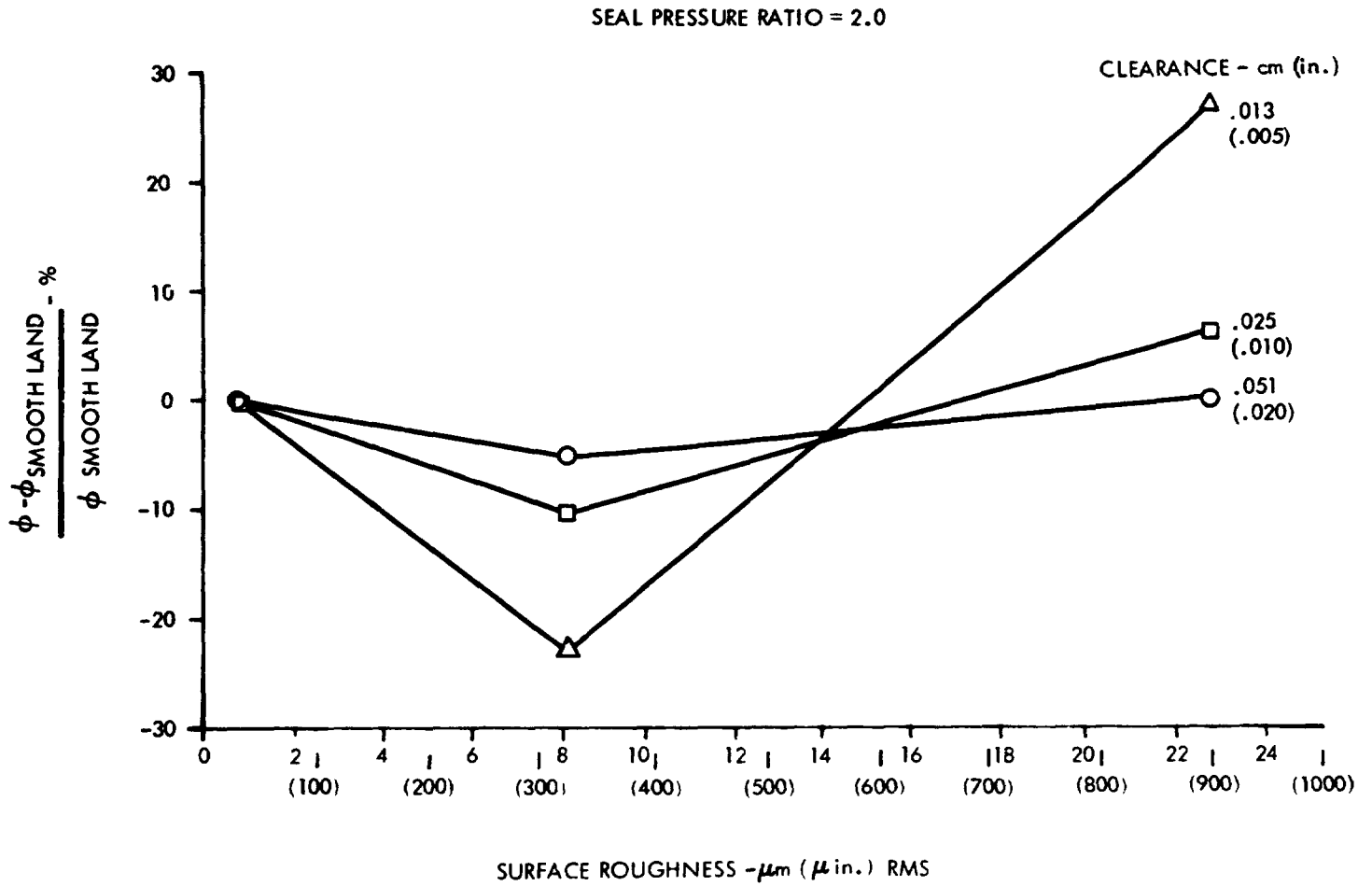

FIGURE 29. EFFECT OF SURFACE ROUGHNESS ON SEAL LEAKAGE COMPARED TO A SMOOTH LAND SINGLE KNIFE STRAIGHT SEAL

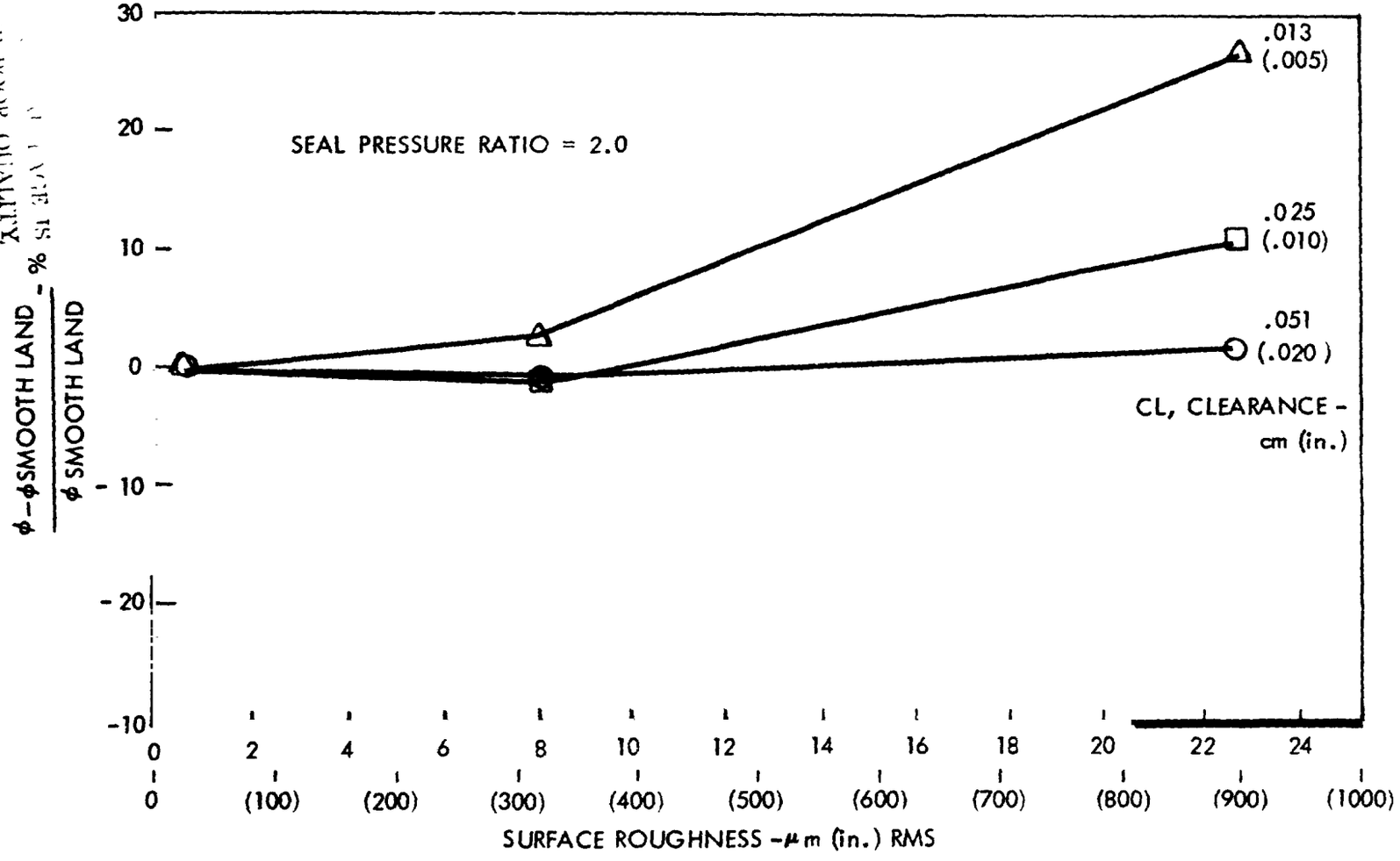

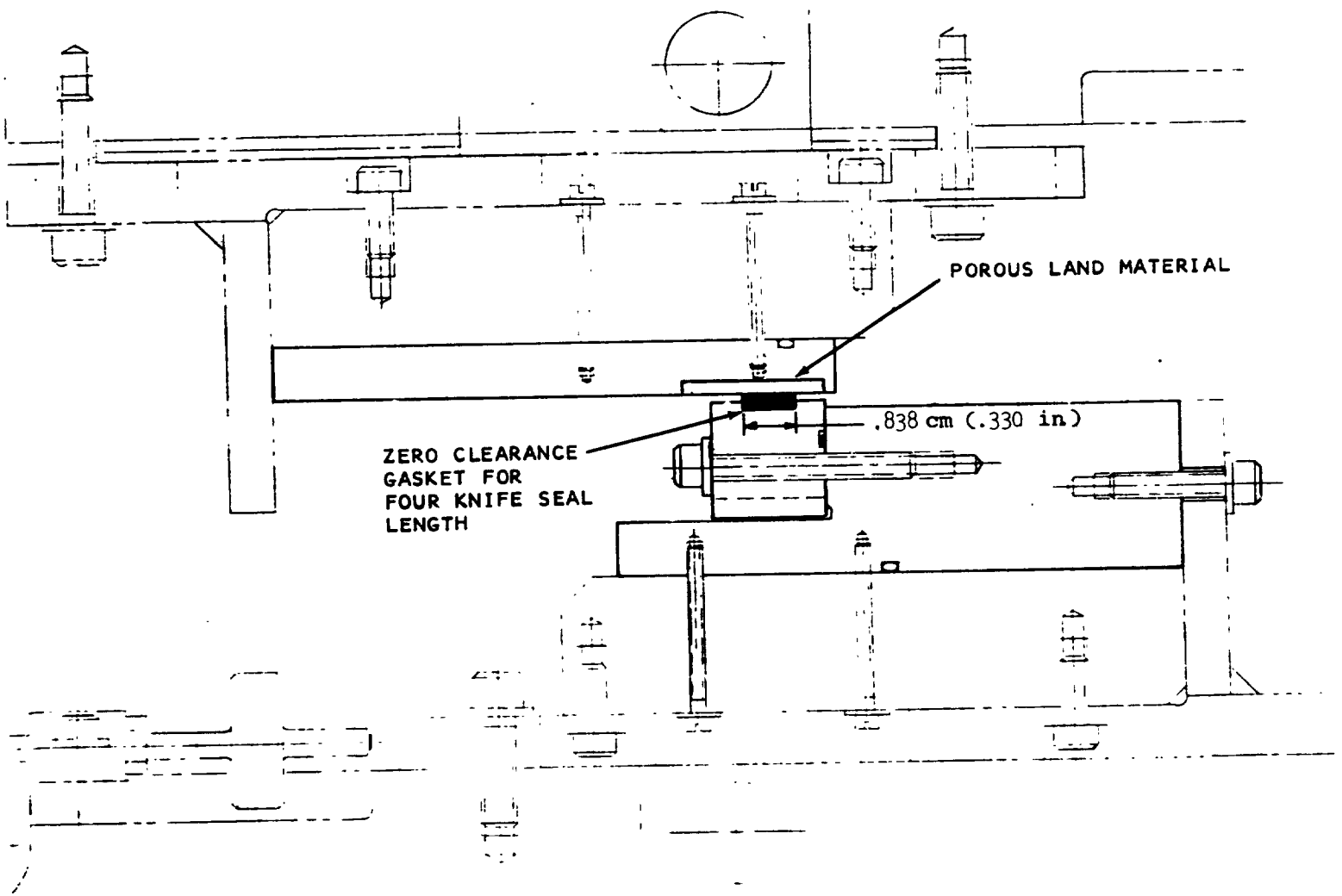

FIGURE 30. SKETCH OF POROSITY LEAKAGE TEST METHOD FOR FOUR KNIFE STRAIGHT-THROUGH SEAL

FIGURE 31. EFFECT OF "ABRADABLE A" POROSITY ON LEAKAGE THROUGH A 4 KNIFE STRAIGHT SEAL

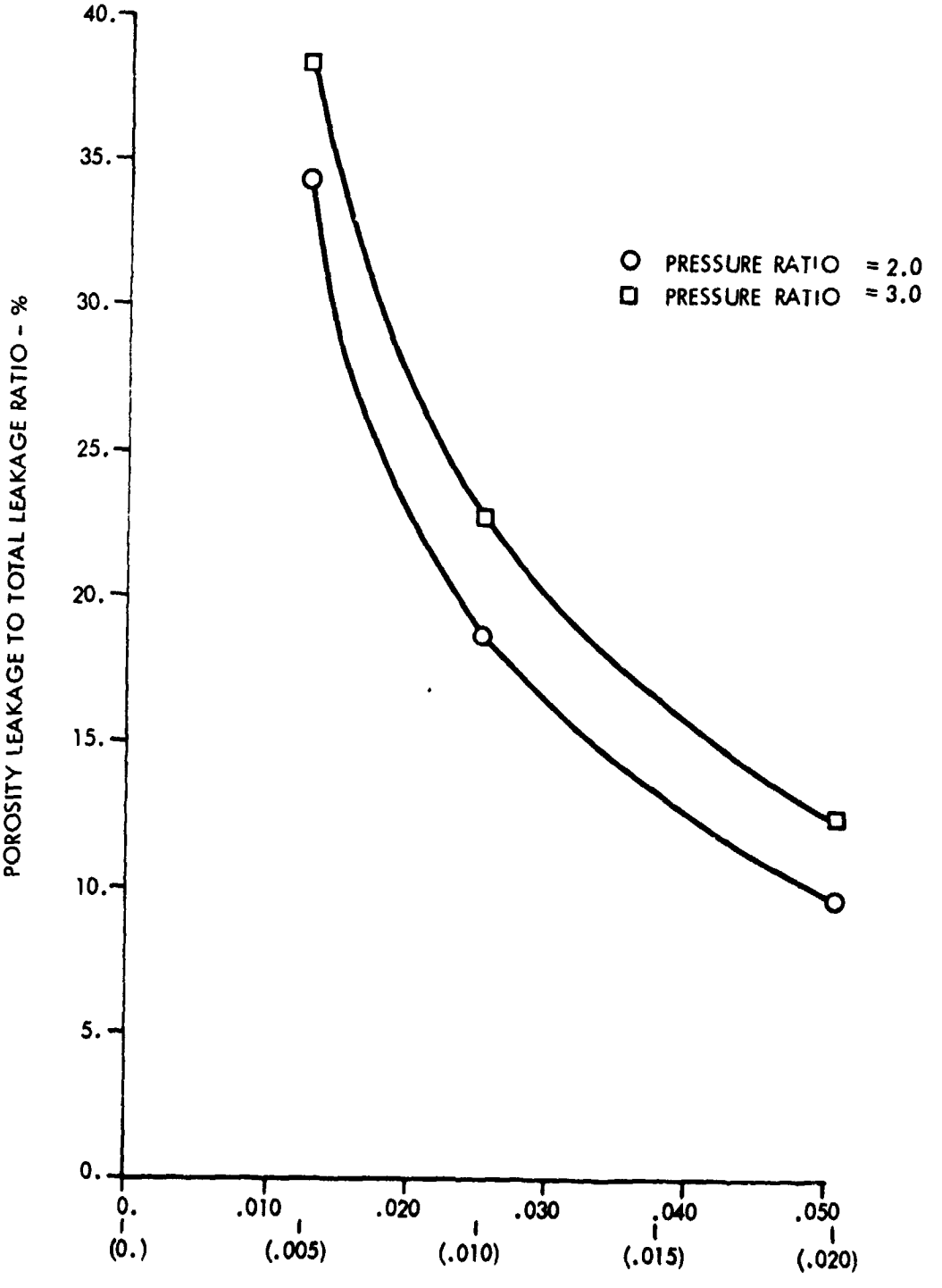

ORIGINAL PAGE IS
OF POOR QUALITY

FIGURE 32. EFFECT OF "ABRADABLE B" POROSITY ON LEAKAGE THROUGH A 4 KNIFE STRAIGHT SEAL

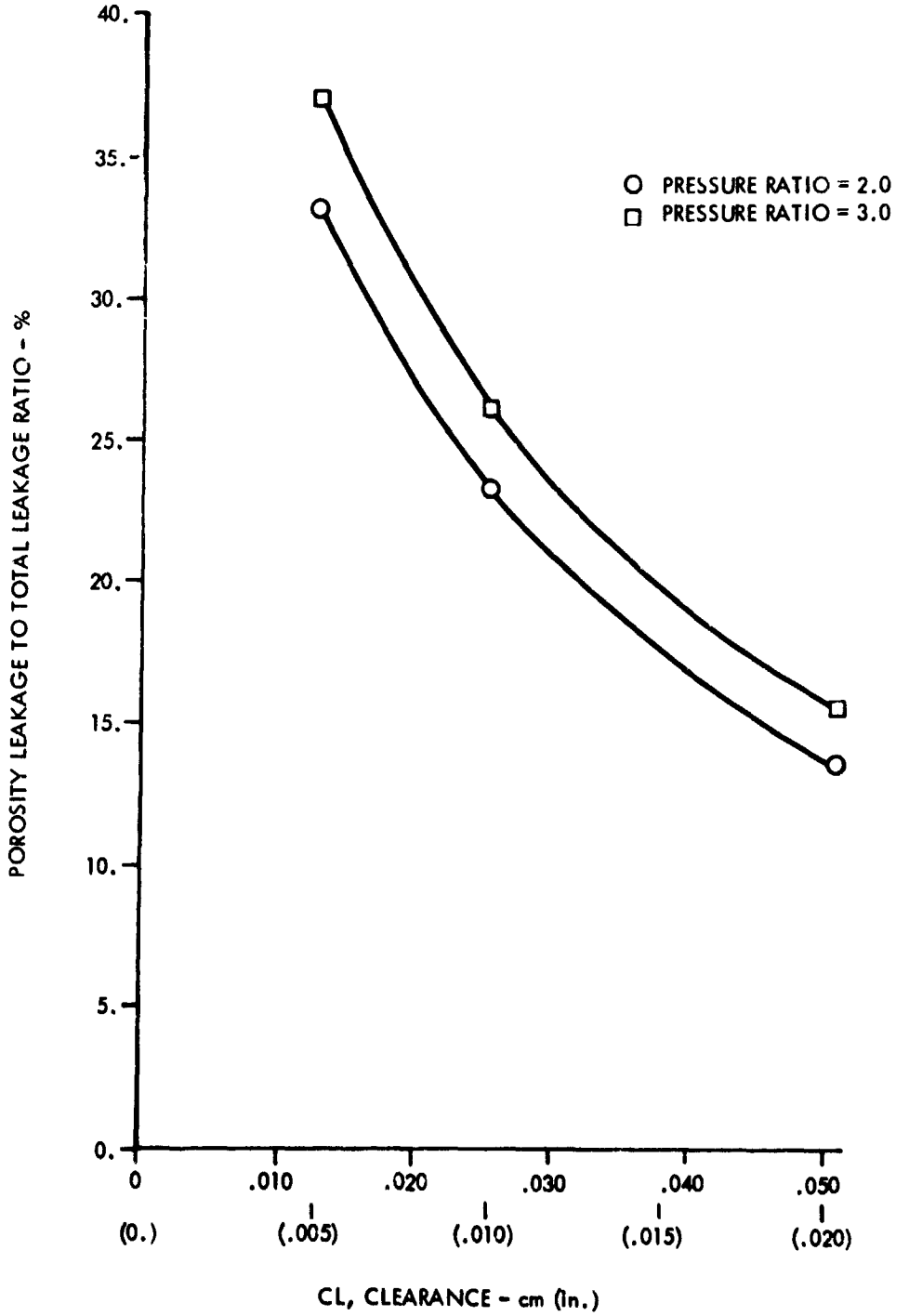

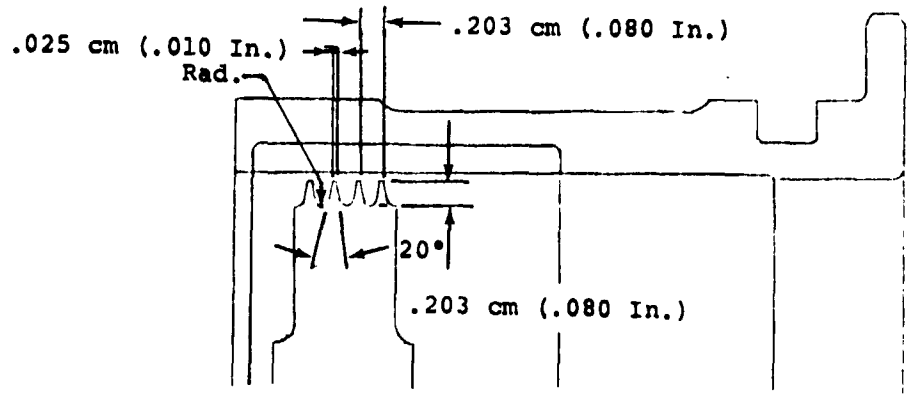

(a) Knife Pitch = .203 cm (.080 In.)

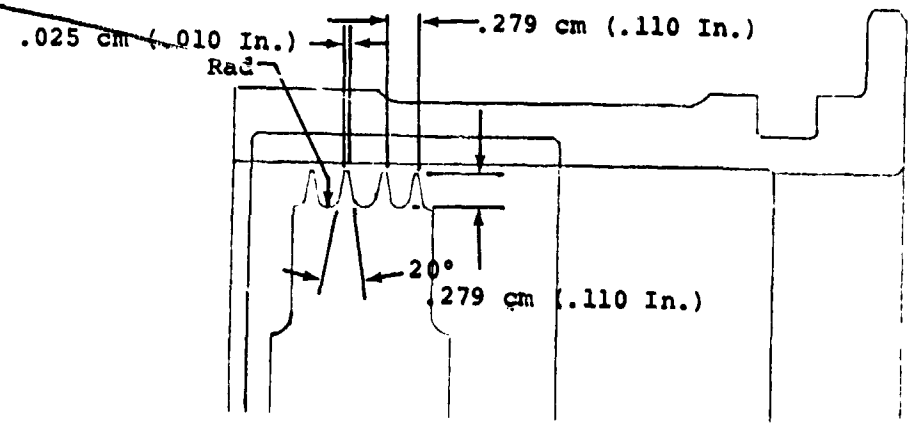

(b) Knife Pitch = .279 cm (.110 In.)

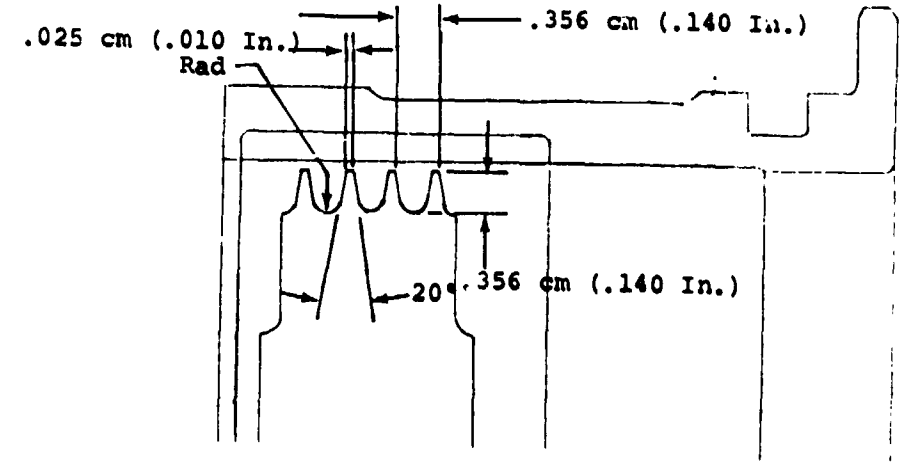

(c) Knife Pitch = .356 cm (.140 In.)

FIGURE 33. SKETCHES OF FOUR KNIFE ROTORS USED TO EVALUATE THE EFFECT OF ROTATION

TABLE 3. COMPARISON OF SMOOTH AND ABRADABLE LANDS PERFORMANCE AT VARIOUS OPERATING CONDITIONS

Seal configuration:

Four vertical knives,
pitch = .279 cm (.110 i.)
knife height = .279 cm (.110 in)
knife edge thickness = .025 ∿ .038 cm (.010 ∿ .015 in)

NOTE: + indicates leakage greater than smooth land at comparable clearance
- indicates leakage less than smooth land at comparable clearance

LAND TYPE	CL, CLEARANCE cm	CL, CLEARANCE in.	P_U/P_D PRESSURE RATIO	ϕ, FLOW PARAMETER $\frac{kg \cdot K^{\frac{1}{2}}}{N \cdot s}$	ϕ, FLOW PARAMETER $\frac{lb_m \cdot R^{\frac{1}{2}}}{lb_f \cdot sec}$	$\Delta\phi/\phi$ FROM SMOOTH LAND %	P_U/P_D PRESSURE RATIO	ϕ, FLOW PARAMETER $\frac{kg \cdot K^{\frac{1}{2}}}{N \cdot s}$	ϕ, FLOW PARAMETER $\frac{lb_m \cdot R^{\frac{1}{2}}}{lb_f \cdot sec}$	$\Delta\downarrow, \downarrow$ FROM SMOOTH LAND %
SOLID-SMOOTH	.013	.005	2.0	.0277	.365		3.0	.0279	.368	
	.025	.010		.0272	.358			.0279	.368	
	.051	.020		.0277	.365			.0285	.375	
"ABRADABLE A"	.013	.005		.0353	.465	+27.4		.0384	.505	+37.4
	.025	.010		.0299	.393	+ 9.8		.0325	.428	+16.5
	.051	.020		.0305	.401	+ 9.9		.0323	.425	+13.3
"ABRADABLE B"	.013	.005		.0445	.585	+60.3		.0484	.637	+73.3
	.025	.010		.0344	.452	+26.3		.0367	.483	+31.4
	.051	.020		.0312	.411	+12.6		.0331	.435	+16.0
Ni Graphite	.013	.005		.0268	.352	- 3.6		.0274	.361	- 1.8
	.025	.010		.0251	.330	- 7.8		.0264	.348	- 5.4
	.051	.020		.0284	.374	+ 2.3		.0295	.388	+ 3.3
Al Polyester	.013	.005		.0277	.365	0.0		.0285	.375	+ 2.0
	.025	.010		.0271	.356	- 0.6		.0284	.374	+ 1.8
	.051	.020		.0298	.392	+ 7.4		.0308	.405	+ 8.0

TABLE 4. EFFECT OF LAND ROUGHNESS ON FOUR KNIFE STRAIGHT-THROUGH LABYRINTH SEAL PERFORMANCE

LAND ROUGHNESS	CL, CLEARANCE cm	CL, CLEARANCE in.	P_U/P_D PRESSURE RATIO	ϕ, FLOW PARAMETER $\frac{kg \cdot K^{\frac{1}{2}}}{N \cdot s}$	ϕ, FLOW PARAMETER $\frac{lb_m \cdot R^{\frac{1}{2}}}{lb_f \cdot sec}$	$\Delta\phi/\phi$ FROM SMOOTH LAND %	P_U/P_D PRESSURE RATIO	ϕ, FLOW PARAMETER $\frac{kg \cdot K^{\frac{1}{2}}}{N \cdot s}$	ϕ, FLOW PARAMETER $\frac{lb_m \cdot R^{\frac{1}{2}}}{lb_f \cdot sec}$	$\Delta\downarrow/\phi$ FROM SMOOTH LAND %
Smooth (Baseline) 0.8 µm (30 µin.) RMS	.013	.005	2.0	.0277	.365		3.0	.0280	.368	
	.025	.010		.0272	.358			.0280	.368	
	.051	.020		.0277	.365			.0285	.375	
Medium Rough 6-10 µm (250-400 µin.) RMS	.013	.005		.0214	.281	-23.0		.0243	.320	13.0
	.025	.010		.0244	.321	-10.3		.0258	.339	- 7.9
	.051	.020		.0263	.346	- 5.2		.0270	.355	- 5.3
Rough 18-28 µm (700-1100 µin.) RMS	.013	.005		.0353	.464	+27.1		.0369	.485	+31.8
	.025	.010		.0290	.381	+ 6.4		.0306	.403	+ 9.5
	.051	.020		.0279	.367	+ 0.5		.0293	.386	+ 2.9

TABLE 5. EFFECT OF LAND ROUGHNESS ON SINGLE KNIFE STRAIGHT-THROUGH LABYRINTH SEAL PERFORMANCE.

LAND ROUGHNESS	CL, CLEARANCE cm	CL, CLEARANCE in.	P_U/P_D PRESSURE RATIO	Φ, FLOW PARAMETER $\frac{kg \cdot K^{\frac{1}{2}}}{N \cdot s}$	Φ, FLOW PARAMETER $\frac{lb_m \cdot °R^{\frac{1}{2}}}{lb_f \cdot sec}$	$\Delta\Phi/\Phi$ FROM SMOOTH LAND %	P_U/P_D PRESSURE RATIO	Φ, FLOW PARAMETER $\frac{kg \cdot K^{\frac{1}{2}}}{N \cdot s}$	Φ, FLOW PARAMETER $\frac{lb_m \cdot °R^{\frac{1}{2}}}{lb_f \cdot sec}$	$\Delta\Phi/\Phi$ FROM SMOOTH LAND %
Smooth (Baseline)	.013	.005	2.0	.0323	.425		3.0	.0327	.430	
	.025	.010		.0325	.427			.0341	.448	
0.8 µm (30 µin.) RMS	.051	.020		.0315	.415			.0337	.444	
Medium Rough	.013	.005		.0367	.483	+13.6		.0372	.490	+14.0
6-10 µm	.025	.010		.0319	.420	- 1.6		.0328	.431	- 3.8
(250-400 µin.) RMS	.051	.020		.0314	.413	- 0.5		.0338	.445	+ 0.2
Rough	.013	.005		.0414	.545	+28.?		.0422	.555	+29.1
18-28 µm	.025	.010		.0364	.479	+12.2		.0376	.495	+10.5
(700-1100 µin.) RMS	.051	.020		.0325	.427	+ 2.9		.0345	.454	+ 2.3

TABLE 6. "ABRADABLE A" POROSITY AND SURFACE ROUGHNESS RESULTS

CL, CLEARANCE	.013 cm(.005 in.)		.025 cm(.010 in.)		.051 cm(.020 in.)	
PRESSURE RATIO	2.0	3.0	2.0	3.0	2.0	3.0
(1) ΦA, Porosity	.000226 (.00460)	.000306 (.00625)	.000226 (.00460)	.000306 (.00625)	.000226 (.00460)	.000306 (.00625)
(2) ΦA, Surface Roughness	.000432 (.00882)	.000493 (.01005)	.000989 (.02016)	.001044 (.02129)	.002131 (.04346)	.002186 (.04459)
(3) ΦA, Porosity + Surface Roughness	.000658 (.01342)	.000799 (.01630)	.001214 (.02476)	.001350 (.02754)	.002357 (.04806)	.002493 (.05084)
(4) ΦA, Measured "Abradable A" Land	.000716 (.0146)	.000780 (.0159)	.00121 (.0247)	.00132 (.0269)	.00247 (.0504)	.00262 (.0534)
(5) $\frac{\Delta\Phi A}{\Phi A}$, From the Measured Land	-8.1%	+2.5%	+0.2%	+2.4%	-4.6%	-4.8%

$$\Phi A = \frac{w\sqrt{T_U}}{P_U}, \text{ Flow Factor} - \frac{kg \cdot K^{\frac{1}{2}}}{s \cdot kPa_a}\left(\frac{lb_m \cdot °R^{\frac{1}{2}}}{sec\ psia}\right)$$

(1) ΦA measured on "Abradable A" land at CL = 0.0

(2) ΦA measured with artificially rough, solid land, 9µm (350µ in.) RMS.

(3) Sum of the individual flow factors for porosity leakage and surface roughness leakage, $\Phi A_{(1)} + \Phi A_{(2)}$.

(4) Flow factor, ΦA, measured for the "Abradable A" land.

(5) $\frac{\Delta\Phi A}{\Phi A} = \frac{\Phi A_{(3)} - \Phi A_{(4)}}{\Phi A_{(4)}}$

TABLE 7. "ABRADABLE B" POROSITY AND SURFACE ROUGHNESS RESULTS

CL, CLEARANCE	.013 cm(.005 in.)		.025 cm(.010 in.)		.051 cm(.020 in.)	
PRESSURE RATIO	2.0	3.0	2.0	3.0	2.0	3.0
(1) ϕA, Porosity	.000356 (.00725)	.000434 (.00886)	.000356 (.00725)	.000434 (.00886)	.000356 (.00725)	.000434 (.00886)
(2) ϕA, Surface Roughness	.000714 (.01457)	.000747 (.01523)	.001173 (.02393)	.001241 (.02531)	.002261 (.04610)	.002377 (.04848)
(3) ϕA, Porosity + Surface Roughnes	.001070 (.02182)	.001181 (.02409)	.001529 (.03118)	.001676 (.03417)	.002616 (.05335)	.002812 (.05734)
(4) ϕA, Measured "Abradable B" Land	.000901 (.01837)	.000981 (.02000)	.001392 (.02839)	.001487 (.03033)	.002531 (.05162)	.002679 (.05464)
(5) $\frac{\Delta\phi A}{\phi A}$, From the Measured Land	+18.8%	+20.5%	+9.8%	+12.7%	+3.4%	+4.9%

$\phi A = \frac{w\sqrt{T_U}}{P_U}$, Flow Factor, $\frac{kg \cdot K^{\frac{1}{2}}}{s \cdot kPa} \left(\frac{lb_m \ ^\circ R^{\frac{1}{2}}}{sec \ psia} \right)$

(1) ϕA measured on "Abradable B" land at CL = 0.0

(2) ϕA measured with artificially rough, solid land, 22.9μm (900μ in.) RMS.

(3) Sum of the individual flow factors for porosity leakage and surface roughness leakage, $\phi A_{(1)} + \phi A_{(2)}$.

(4) Flow factor, ϕA, measured for the "Abradable B" land.

(5) $\frac{\Delta\phi A}{\phi A} = \frac{\phi A_{(3)} - \phi A_{(4)}}{\phi A_{(4)}}$

TABLE 8. EFFECT OF ROTATION ON THE PERFORMANCE OF FOUR KNIFE STRAIGHT SEALS AT A PRESSURE RATIO = 2.0 WITH A SMOOTH LAND AND AN ABRADABLE LAND.

LAND	KP, Knife Pitch		CL, Clearance		ϕ Flow Parameter		$\Delta\phi/\phi$ From Static Performance At Knife Tip Speed		
	cm	in.	cm	in.	$\frac{kg \cdot K^{\frac{1}{2}}}{N \cdot s}$	$\frac{lb_m \ ^\circ R^{\frac{1}{2}}}{lb_f \ sec}$			
					Static Knife Tip		V=80 m/s (261 ft/sec)	V=159 m/s (523 ft/sec)	V=239 m/s (785 ft/sec)
SOLID-SMOOTH	.279	.110	.025	.010	.0266	.350	-2.6	-6.0	-8.9
			.051	.020	.0283	.372	+1.3	-1.9	-6.7
"ABRADABLE A"	.279	.110	.025	.010	.0275	.362	-1.6	-5.5	-9.9
			.051	.020	.0280	.368	-0.8	-4.6	-10.3

Rub Grooved Abradable Land Evaluation. At the completion of the 2D rig abradable land testing, the "Abradable A" porous material land was grooved to simulate an "in service" interference rub from the four knife straight-through seal. The grooves were cut .025 cm (.010 in.) deep and .051 cm (.020 in.) wide. A sketch, illustrating the grooving procedure is presented in Figure 34, and a photograph of the grooved land is presented in Figure 35. The baseline four knife straight-through seal, pitch = .279 cm (.110 in.), was used for testing the grooved land. The test evaluation was conducted for clearances of .013 cm (.005 in.), .025 cm (.020 in.), and .051 cm (.020 in.) with the axial position of the seal knife relative to the groove at:

(1) .025 cm (.010 in.) and .013 cm (.005 in.) forward of the groove,

(2) over the groove,

(3) .013 cm (.005 in.) and .025 cm (.010 in.) aft of the groove,

(4) midway between grooves at .140 cm (.055 in.).

The results from the 2D rig grooved abradable land leakage tests are presented in Figures 36, 37, and 38 for the clearances tested. The non-grooved land and the solid-smooth land performance has been included for comparison.

The test data indicate that grooving the abradable land significantly reduces the leakage flow. The leakage at .025 cm (.010 in.) and .051 cm (.020 in.) clearances was reduced to, or slightly below, the levels of the solid-smooth land. This result implies that the grooves act to block the leakage through the material. The increased leakage caused by the material porosity that is associated with many abradables may be avoided by properly grooving the land surface.

Tables 9, 10, and 11 compare the solid-smooth, non-grooved abradable, and grooved abradable lands performance quantitatively. The tabulated results show that the grooved "Abradable A" land leakage is frequently reduced to less than the solid-smooth land, especially when the knife is operating axially displaced from the groove. It appears that the roughness of this land could have contributed about 7% reduction in leakage based on surface roughness tests with smooth to rough land counterparts.

The "Abradable A" material was also evaluated at .025 cm (.010 in.) clearance in a 3D rig land for the static and dynamic effects of interference rub grooving. The land was initially grooved 102° circumferentially to simulate a partial interference rub. This land was tested in the 3D seal test rig using the baseline four knife straight-through seal rotor, pitch = .279 cm (.110 in.), with the seal knives located at:

(1) .025 cm (.010 in.) aft of the grooves,

(2) over the grooves,

(3) .025 cm (.010 in.) ahead of the grooves.

The partial grooves were then extended around the full 360° circumference, and the land was retested as described for the 102° grooving. Photographs of the 102° grooves and the 360° grooves are presented in Figures 39, 40, and 41. The grooves were cut into the 3D rig abradable land with a rotating single-knife cutting wheel in a manner similar to that used on the 2D land. To ensure accurate spacing of the rub grooves in the land relative to the rotor knives, the knife spacing on the test rotor was measured on a 10X size digital output shadowgraph which gave measurements within $\pm$ .00064 cm ($\pm$ .00025 in.).

Table 12 summarizes the grooved abradable land leakage performance at a pressure ratio of 2.0 for the 102° and 360° rub grooves. The rub groove leakage performance change from the non-grooved land performance is also included. A plot illustrating the grooved land performance change from the non-grooved land is shown in Figure 42. The 102° rub grooves caused the leakage to increase slightly when the knives were located .025 cm (.010 in.) aft of the grooves. The leakage then decreased as the knives were moved over the rub grooves and, finally, ahead of the grooves. The minimum leakage, at static and dynamic rotor conditions, was produced with the knives ahead of the groove. The 360° rub grooved land performance indicates little change in leakage (statically and dynamically) for the knives located aft of the grooves. Leakage was reduced to a minimum (-7%) with the knives located over the grooves and increased slightly for the seal knives located forward of the grooves. The performance variation with axial position of the seal knives is similar to the 2D rig results, except for the knives located aft of the grooves.

One possible cause for the relatively higher leakage with the knives aft of the grooves is the increased potential for porosity leakage through the backface of the land (see Figures 39 and 41) as the flowpath through the abradable material is shortened. This leakage path can be eliminated by providing a solid wall enclosing the backface of the abradable land. The hardware design for the 2D rig used this approach. Test data from the 2D rig showed that grooving reduced leakage and that leakage was insensitive to the axial position of the knife when it was out of the groove.

The grooved abradable land individual flow parameter curves for the 2D and 3D rig tests are included in Appendix C.

FIGURE 34. 2D RIG ABRADABLE LAND GROOVING PROCEDURE

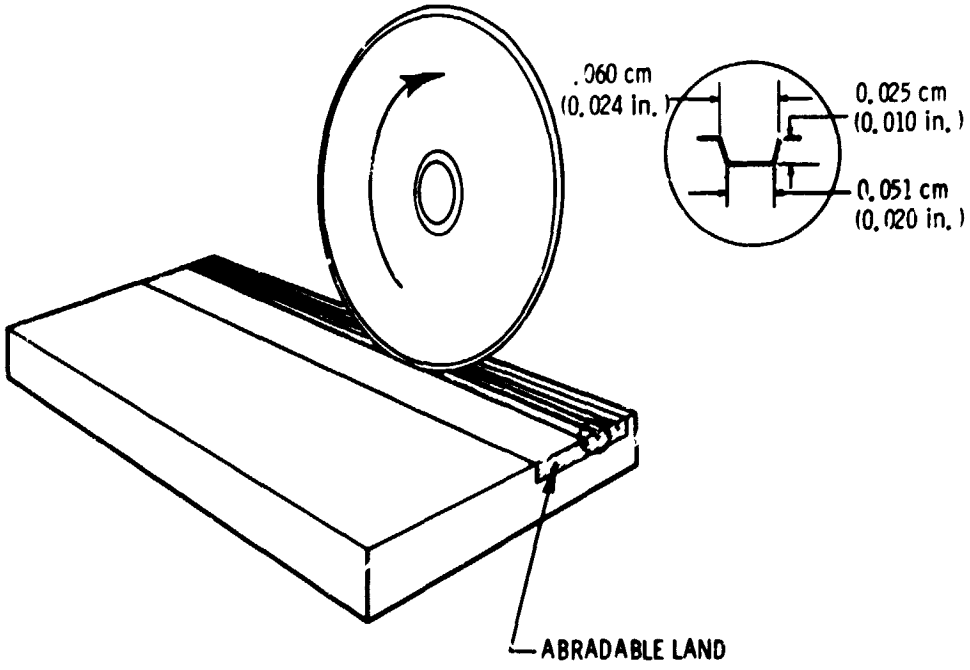

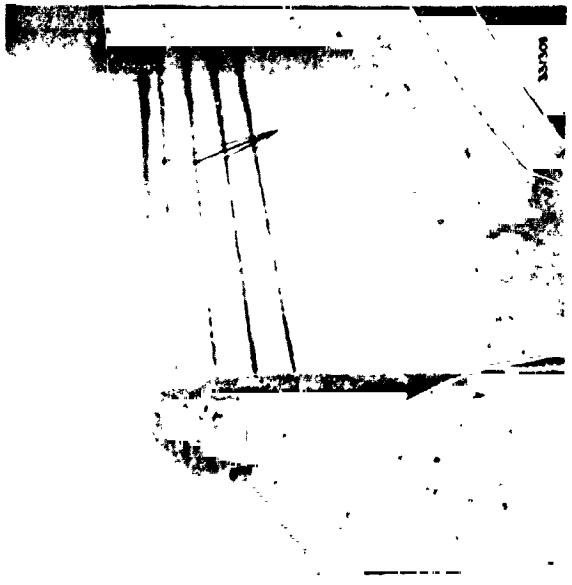

FIGURE 35. "ABRADABLE A" LAND WITH SIMULATED RUB GROOVES

FIGURE 36. EFFECT OF KNIFE AXIAL POSITION WITH RESPECT TO RUB GROOVES IN A 2D TEST RIG "ABRADABLE A" LAND AT A CLEARANCE = .013 cm (.005 in.)

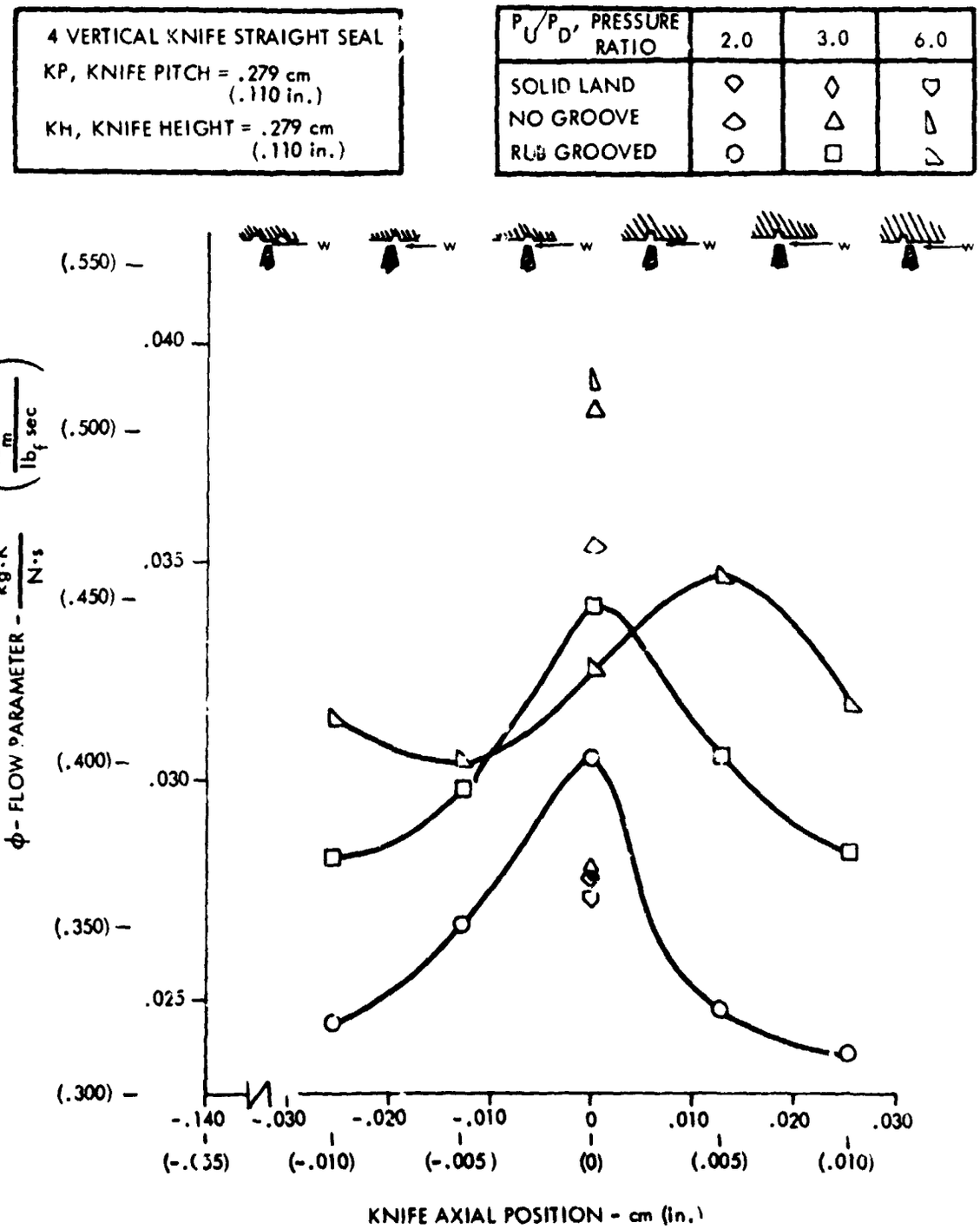

FIGURE 37. EFFECT OF KNIFE AXIAL POSITION WITH RESPECT TO RUB GROOVES IN A 2D TEST RIG "ABRADABLE A" LAND AT A CLEARANCE = .025 cm (.010 in.)

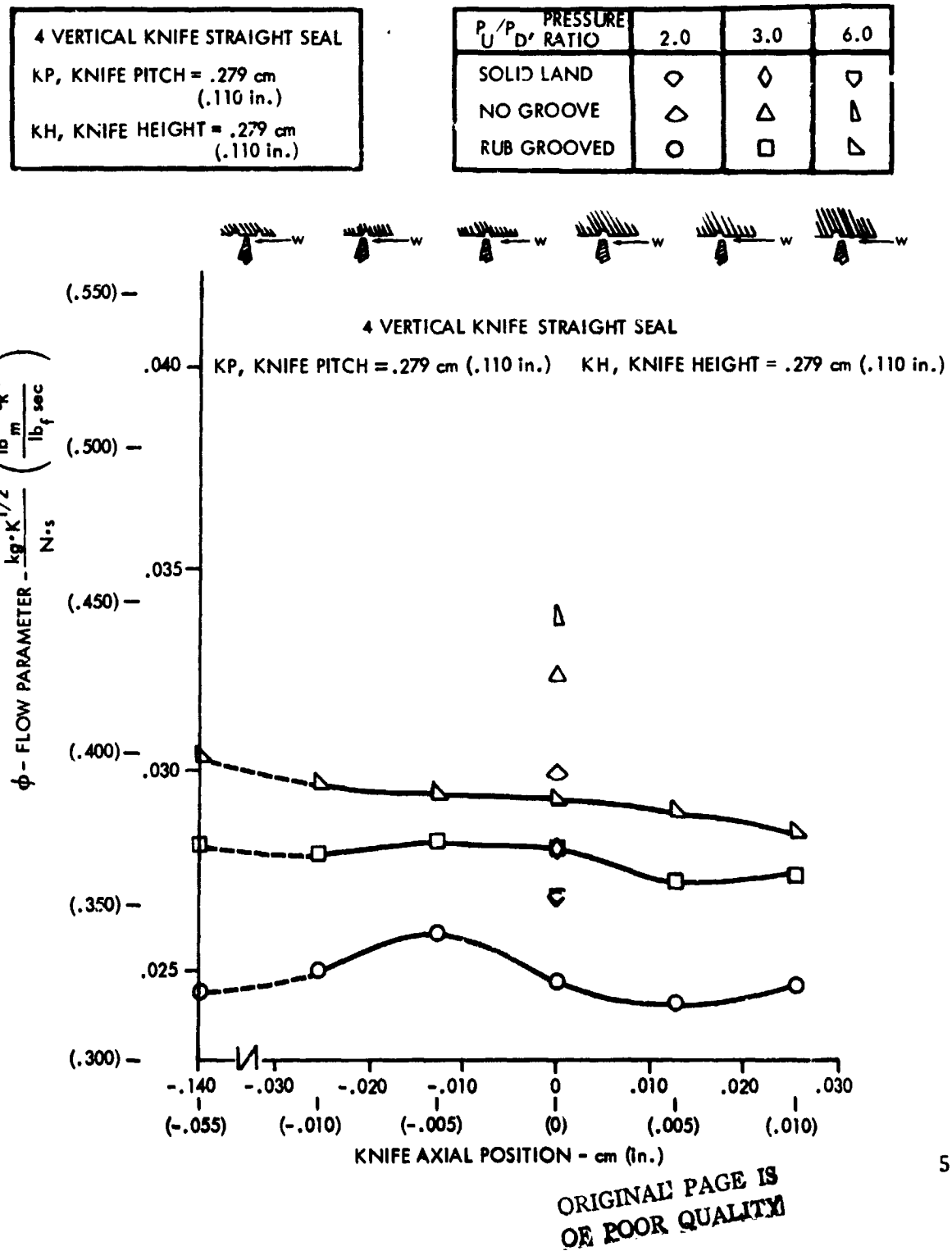

FIGURE 38. EFFECT OF KNIFE AXIAL POSITION WITH RESPECT TO RUB GROOVES IN A 2D TEST RIG "ABRADABLE A" LAND AT A CLEARANCE = .051 cm (.020 in.)

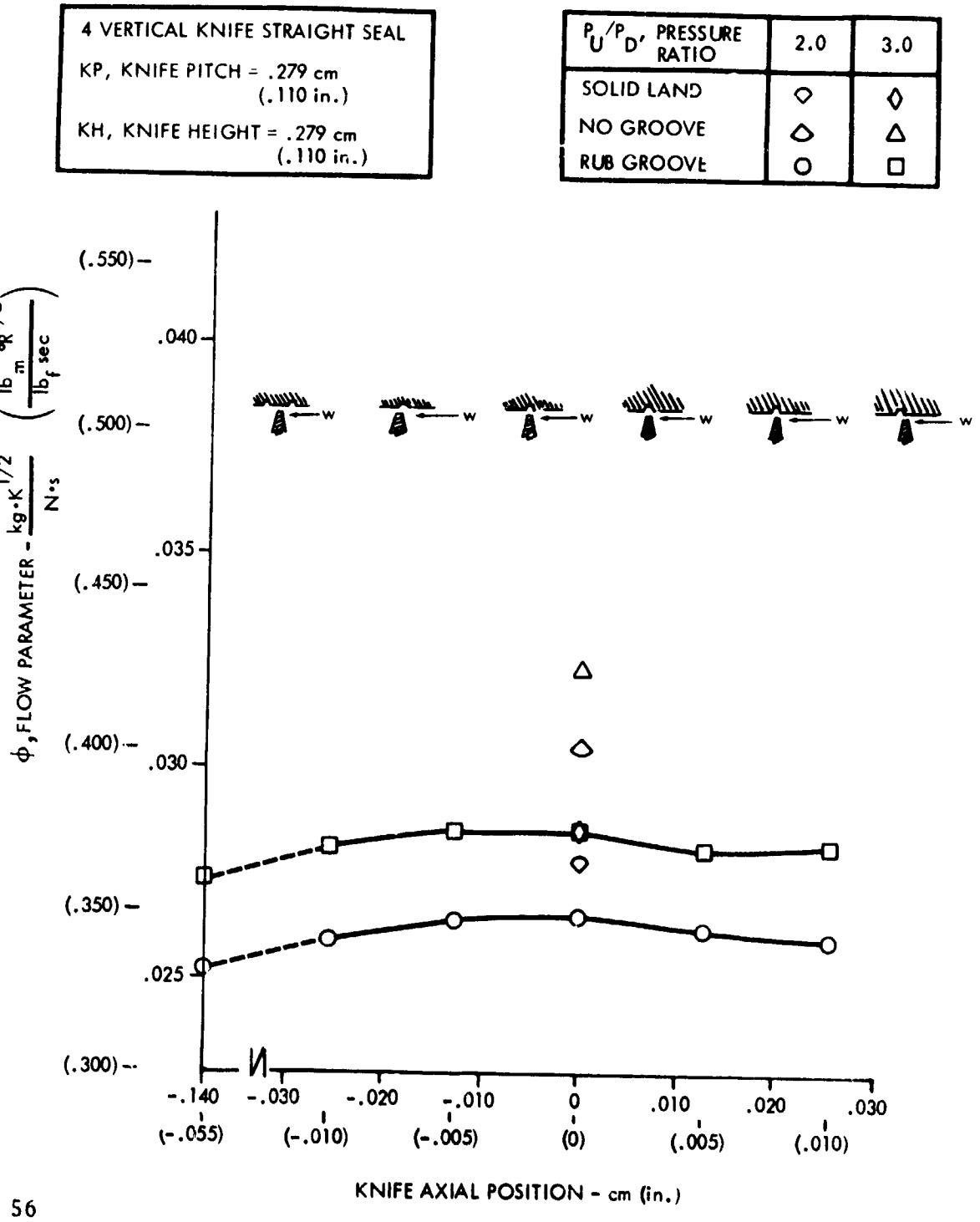

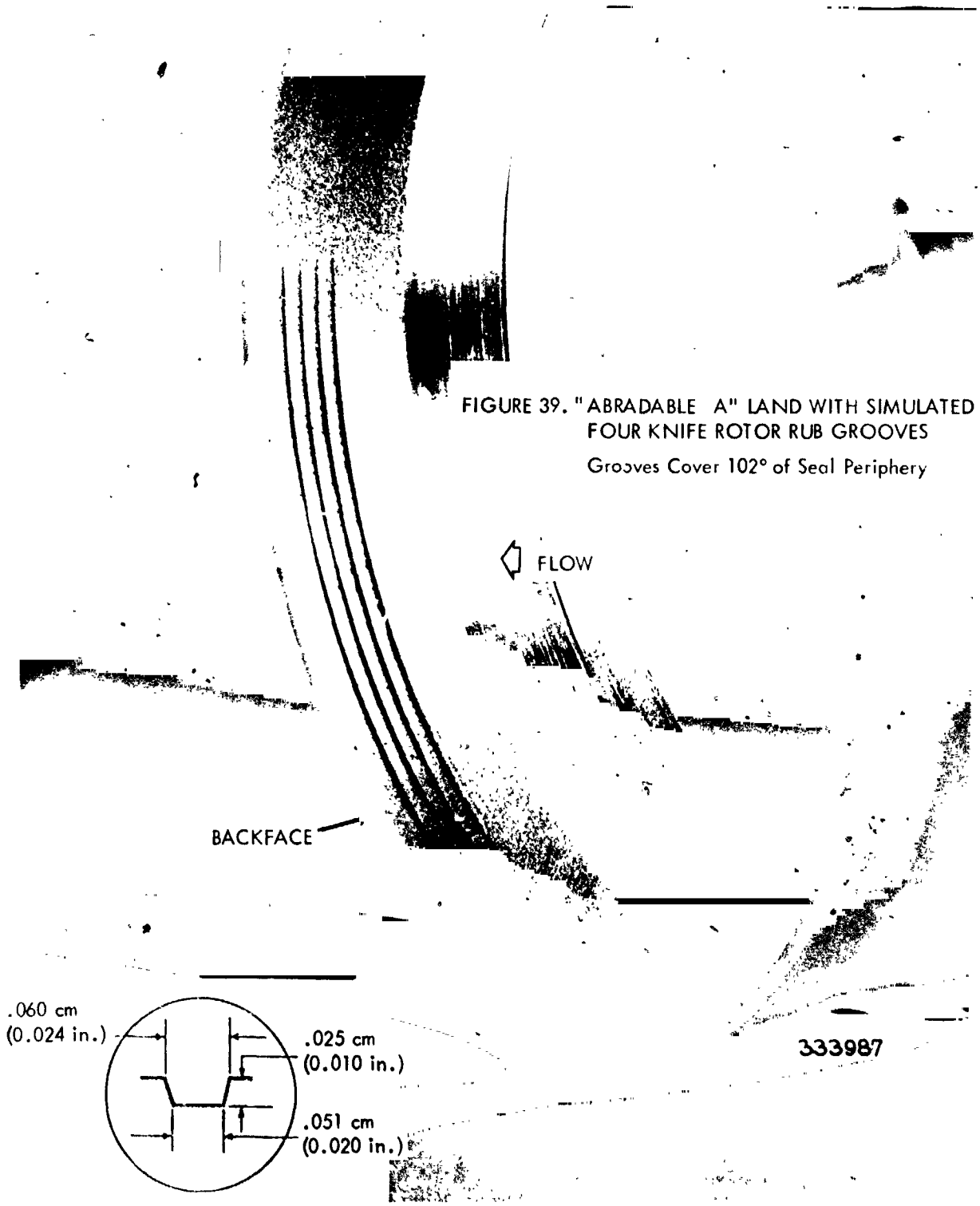

FIGURE 39. "ABRADABLE A" LAND WITH SIMULATED FOUR KNIFE ROTOR RUB GROOVES

Grooves Cover 102° of Seal Periphery

FIGURE 40." ABRADABLE A" LAND WITH SIMULATED FOUR KNIFE ROTOR RUB GROOVES

Grooves Cover 102° of Seal Periphery

FIGURE 41. "ABRADABLE A" LAND WITH SIMULATED FOUR KNIFE ROTOR RUB GROOVES

Grooves Cover 360° of Seal Periphery

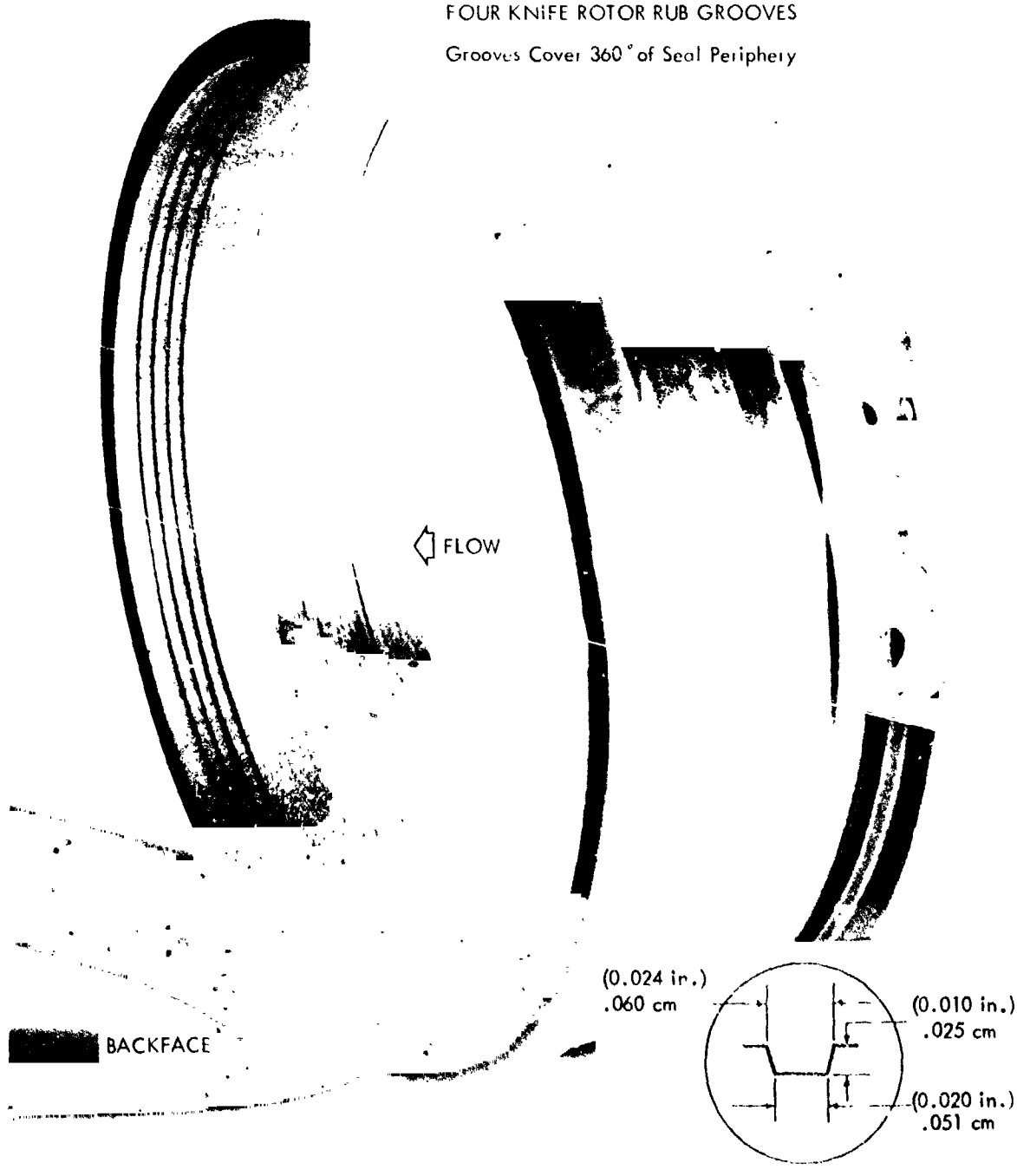

FIGURE 42. EFFECT OF RUB GROOVING ON THE LEAKAGE OF A FOUR KNIFE STRAIGHT SEAL WITH AN "ABRADABLE A" LAND AT A CLEARANCE OF .025 cm(.010 in.)

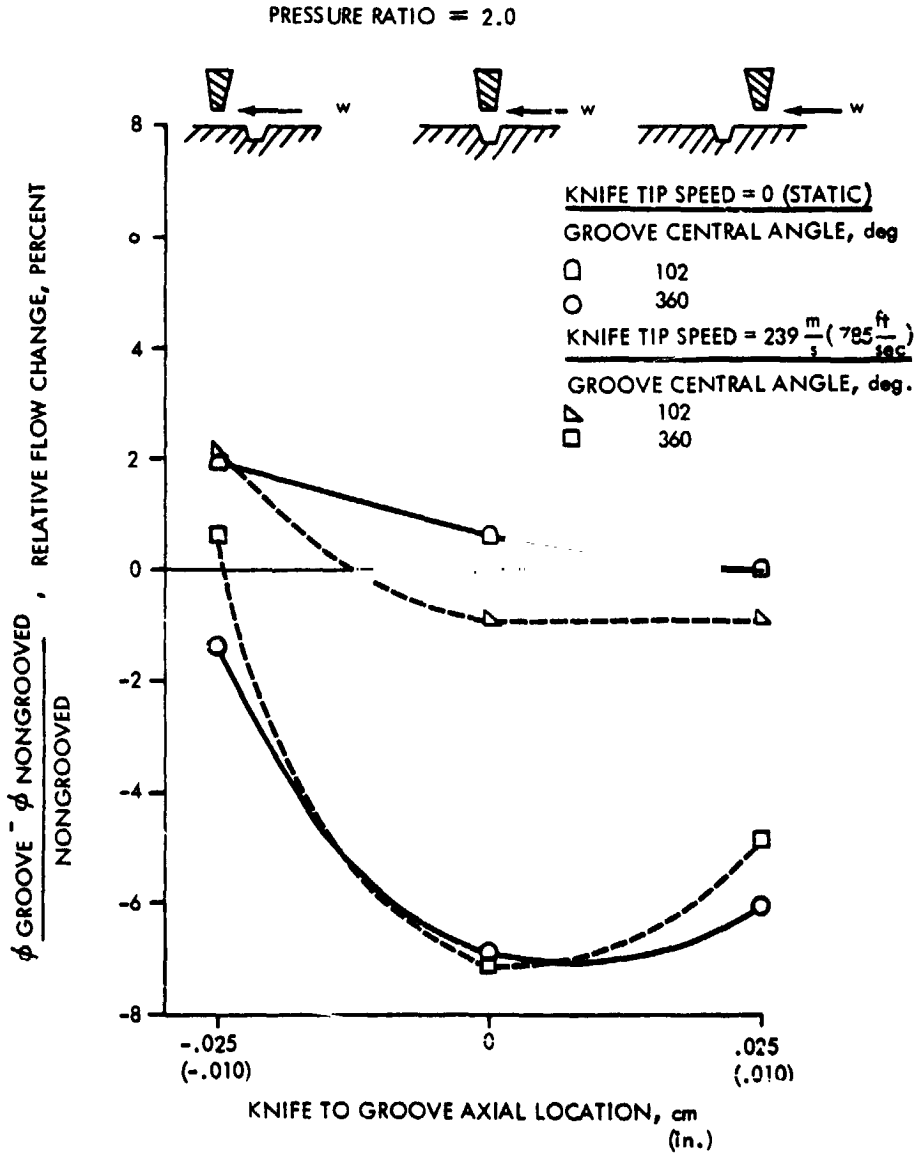

TABLE 9. COMPARISON OF SOLID-SMOOTH, NON-GROOVED ABRADABLE, AND GROOVED ABRADABLE LAND PERFORMANCE AT .013 CM (005 IN) CLEARANCE IN THE 2D TEST RIG

LAND TYPE	KNIFE-TO-GROOVE AXIAL POSITION* cm (in.)	PRESSURE RATIO	ϕ, FLOW PARAMETER $\frac{kg \cdot K^{1/2}}{N \cdot s}$ $\left(\frac{lbm \cdot R^{1/2}}{lbf\ sec}\right)$	$\Delta\phi/\phi$ FROM A SOLID-SMOOTH LAND %
Solid-Smooth		2.0	.0277 (.365)	
		3.0	.0279 (.368)	
Non-Grooved "Abradable A"		2.0	.0353 (.465)	+27.4
		3.0	.0384 (.505)	+37.4
Grooved "Abradable A"	-.025 (-.010)	2.0	.0244 (.321)	-12.1
	-.013 (-.005)		.0267 (.351)	- 3.8
	0.0		.0305 (.401)	+ 9.9
	+.013 (+.005)		.0247 (.325)	-11.0
	+.025 (+.010)		.0237 (.312)	-14.5
	-.025 (-.010)	3.0	.0282 (.371)	+ 1.0
	-.013 (-.005)		.0298 (.392)	+ 6.7
	0.0		.0340 (.447)	+21.6
	+.013 (+.005)		.0306 (.402)	+ 9.4
	+.025 (+.010)		.0283 (.373)	+ 1.5

* The zero reference for knife-to-groove axial position is taken where the knife tip is over the rub groove. Positive (+) axial position denotes the knife tip upstream from the land rub groove, and the negative (-) axial position denotes the knife tip downstream from the land rub groove.

TABLE 10. COMPARISON OF SOLID-SMOOTH, NON-GROOVED ABRADABLE, AND GROOVED ABRADABLE LAND PERFORMANCE AT .025 CM (.010 IN.) CLEARANCE IN THE 2D TEST RIG

LAND TYPE	KNIFE-TO-GROOVE AXIAL POSITION* cm (in.)	PRESSURE RATIO	ϕ, FLOW PARAMETER $\frac{kg \cdot K^{1/2}}{N \cdot s}$ $\left(\frac{lbm \cdot R^{1/2}}{lbf\ sec}\right)$	$\Delta\phi/\phi$ FROM A SOLID-SMOOTH LAND %
Solid-Smooth		2.0	.0272 (.358)	
		3.0	.0279 (.368)	
Non-Grooved "Abradable A"		2.0	.0299 (.393)	+ 9.8
		3.0	.0325 (.428)	+16.5
Grooved "Abradable A"	-.025 (-.010)	2.0	.0250 (.329)	- 8.1
	-.013 (-.005)		.0259 (.341)	- 4.8
	0.0		.0247 (.325)	- 9.2
	+.013 (+.005)		.0242 (.318)	-11.2
	+.025 (+.010)		.0246 (.324)	- 9.5
	-.025 (-.010)	3.0	.0279 (.367)	- 0.1
	-.013 (-.005)		.0282 (.371)	+ 1.0
	0.0		.0280 (.369)	+ 0.4
	+.013 (+.005)		.0272 (.358)	- 2.6
	+.025 (+.010)		.0274 (.360)	

* The zero reference for knife-to-groove axial position is taken where the knife tip is over the rub groove. Positive (+) axial position denotes the knife tip upstream from the land rub groove, and the negative (-) axial position denotes the knife tip downstream from the land rub groove.

TABLE 11. COMPARISON OF SOLID-SMOOTH, NON-GROOVED ABRADABLE, AND GROOVED ABRADABLE LAND PERFORMANCE AT .051 CM (.020 IN.) CLEARANCE IN THE 2D TEST RIG

LAND TYPE	KNIFE-TO-GROOVE AXIAL POSITION* cm (in.)	PRESSURE RATIO	ϕ, FLOW PARAMETER $\frac{kg \cdot K^{1/2}}{N \cdot s}$ $\left(\frac{lb_m \cdot R^{1/2}}{lb_f \cdot sec}\right)$	$\Delta\phi/\phi$ FROM A SOLID-SMOOTH LAND %
Solid-Smooth		2.0	.0277 (.365)	
		3.0	.0285 (.375)	
Non-Grooved "Abradable A"		2.0	.0305 (.401)	+ 9.9
		3.0	.0323 (.425)	+13.3
Grooved "Abradable A"	-.025 (-.010)	2.0	.0259 (.341)	- 6.6
	-.013 (-.005)		.0264 (.347)	- 4.9
	0.0		.0264 (.348)	- 4.7
	+.013 (+.005)		.0261 (.344)	- 5.8
	+.025 (+.010)		.0259 (.341)	- 6.6
	-.025 (-.010)	3.0	.0281 (.370)	- 1.3
	-.013 (-.005)		.0286 (.376)	+ 0.3
	0.0		.0285 (.375)	0.0
	+.013 (+.005)		.0280 (.369)	- 1.6
	+.025 (+.010)		.0281 (.370)	- 1 3

* The zero reference for knife-to-groove axial position is taken where the knife tip is over the rub groove. Positive (+) axial position denotes the knife tip upstream from the land rub groove, and the negative (-) axial position denotes the knife tip downstream from the land rub groove.

TABLE 12. EFFECT OF RUB GROOVING ON LEAKAGE USING A FOUR KNIFE STRAIGHT SEAL WITH "ABRADABLE A" LAND

Pitch = .279 cm (.110 in.) Knife Height = .279 cm (.110 in.
Clearance = .025 cm (.010 in.) Pressure Ratio = 2.0

Rub Groove Central Angle, degrees	Knife-To-Groove Axial Location*, cm (in.)	V, Knife Tip Speed, m/s (ft/sec)							
		0.0 - Static		80 (261)		159 (523)		239 (785)	
		ϕ, Airflow Parameter, $\frac{kg \cdot K^{1/2}}{N \cdot s}$ $\left(\frac{lb_m \cdot R^{1/2}}{lb_f \cdot sec}\right)$							
0.0	(Nongrooved)	.0275	(.362)	.0271	(.356)	.0263	(.342)	.0249	(.326)
102	+.025 (+.010)	.0275	(.362)	.0271	(.356)	.0258	(.340)	.0245	(.323)
	0.0	.0277	(.364)	.0271	(.357)	.0258	(.340)	.0245	(.323)
	-.025 (-.010)	.0280	(.369)	.0275	(.362)	.0264	(.347)	.0253	(.333)
360	+.025 (+.010)	.0258	(.340)	.0253	(.333)	.0244	(.321)	.0236	(.310)
	0.0	.0256	(.337)	.0250	(.329)	.0242	(.318)	.0230	(.303)
	-.025 (-.010)	.0271	(.357)	.0267	(.351)	.0259	(.341)	.0249	(.328)
		$(\phi_{Grooved} - \phi_{Nongrooved})/\phi_{Nongrooved}$, Relative Flow Change, %							
102	+.025 (+.010)	0.0		0.0		-0.6		-0.9	
	0.0	+0.6		+0.3		-0.6		-0.9	
	-.025 (-.010)	+1.9		+1.7		+1.5		+2.1	
360	+.025 (+.010)	-6.1		-6.5		-6.1		-4.9	
	0.0	-6.9		-7.6		-7.0		-7.1	
	-.025 (-.010)	-1.4		-1.4		-0.3		+0.6	

*The zero reference for knife-to-groove axial position is taken where the knife tip is over the rub groove. Positive (+) axial position denotes the knife tip upstream from the land rub groove, and the negative (-) axial position denotes the knife tip downstream from the land rub groove.

Honeycomb Lands Evaluation. Three honeycomb lands with cell sizes of .079 cm (.031 in.), .159 cm (.062 in.), and .318 cm (.125 in.) were evaluated for leakage in the 2D seal test rig. The cell depth and wall thickness were .381 cm (.150 in.) and .0076 cm (.003 in.), respectively. Each honeycomb land was tested with the baseline four knife straight-through seal at three clearance values: .013 cm (.005 in.), .025 cm (.010 in.), and .051 cm (.020 in.). A photograph showing the 2D honeycomb lands is presented in Figure 17.

The honeycomb land flow parameters, presented in Figures 43, 44, and 45 for the three clearances tested, were obtained up to the maximum facility supply pressure. The purpose of testing to high seal pressure ratios was to verify the unusual trend of the flow parameter near the choking point. Figure 43, which illustrates the .013 cm (.005 in.) clearance tests, shows the flow parameter decreasing from its maximum as pressure ratio is increased beyond the critical value. The .025 cm (.010 in.) clearance tests, shown in Figure 44, indicate a similar effect at the largest cell size, however, the flow parameter decrease is much less than for the lower clearance. This phenomenon was not evident at the highest clearance tested, .051 cm (.020 in.).

A possible explanation for the flow parameter characteristic of the honeycomb land as pressure ratio is increased at the .013 cm (.005 in.) and .025 cm (.010 in.) clearances tested could be predicated on an increased level of turbulence within the knife seal cavity resulting from the flow disturbance generated by the honeycomb cells. This flow field variation could cause the flow parameter to pass through a maxima.

The aerodynamic flow area between the knife edge and honeycomb cell could undergo changes with local pressure and Mach number, also. As the seal pressure ratio increases, the flow may have less tendency to expand into the honeycomb cell, particularly for the smaller cell sizes. This action would have the effect of reducing the aerodynamic clearance. Figures 43, 44, and 45 show that the flow parameter falls off less in absolute magnitude as the honeycomb land cell size is reduced.

A comparison of the smooth and honeycomb lands is presented in Table 13. A honeycomb land can reduce leakage up to 20% at .051 cm (.020 in.) clearance. However, at .013 cm (.005 in.) clearance the two larger cell size honeycomb lands leaked almost twice as much as a smooth land. Therefore, it can be concluded that a honeycomb land may be employed to reduce seal leakage but with consideration given to the operating clearance and the honeycomb cell size selection.

Cell Depth Effect on the Honeycomb Lands. The honeycomb land cell depth effect on seal leakage was also investigated on the 2D air seal test rig. Two depths, .254 cm (.100 in.) and .127 cm (.050 in.) were evaluated in addition to the cell depth of .381 (.150 in.). The honeycomb cell depth was decreased by laying a strip of wax of the desired thickness onto

the honeycomb land, forcing it down into the land cells, and then applying heat to melt the wax. The liquid wax wicked into the corners of the cells and solidified at the predetermined depth. Testing was conducted using the baseline four knife straight-through seal. The results are summarized in Figures 46, 47, and 48 for the .013 cm (.005 in.), .025 cm (.010 in.), and .051 cm (.020 in.) radial clearances, respectively.

Figure 46 shows that a cell depth of .254 cm (.100 in.) is optimum for the .079 cm (.031 in.) cell honeycomb at .013 cm (.005 in.) clearance. The two larger cell honeycomb lands indicated higher flow than a smooth land, thus they would not be used at .013 cm (.005 in.) clearance to reduce leakage.

Figure 47 shows an optimum cell depth of .254 cm (.100 in.) for the .079 cm (.031 in.) and the .159 cm (.062 in.) honeycomb cell sizes at .025 cm (.010 in.) clearance. The large cell honeycomb again indicated higher flow than a smooth land. The .079 cm (.031 in.) cell size honeycomb produces the minimum leakage of those tested at .025 cm (.010 in.) clearance.

Figure 48 shows that the optimum honeycomb land cell depth at .051 cm (.020 in.) clearance is .254 cm (.100 in.) for the three honeycomb land cell sizes tested. However, the minimum leakage honeycomb is the .318 cm (.125 in.) cell size at .051 cm (.020 in.) clearance.

The effectiveness of honeycomb material in reducing straight-through seal leakage appears to be a function of the cell depth and the ratio of cell size to clearance. The data obtained from these tests indicate that the optimum cell depth is .254 cm (.100 in.) when the cell size to clearance ratio is less than about 6.2.

Seal Rotation Effect on the Honeycomb Land. A honeycomb land design was also evaluated on the 3D air seal test rig. A cell size of .159 cm (.062 in.) and a cell depth of .254 cm (.100 in.) were selected for testing at radial clearances of .025 cm (.010 in.) and .051 cm (.020 in.). The honeycomb cell size and depth selections were based on the 2D rig test results and the range of clearances to be evaluated in the 3D rig tests.

The static and dynamic test results with the baseline four knife straight-through seal are presented in Figures B-15 and B-16, Appendix B. These data at a seal pressure ratio of 2.0 are summarized in Table 14. The smooth land test data are also included for comparison purposes. At .025 cm (.010 in.) clearance, the initial effect of rotation on the honeycomb land is to reduce leakage relative to the static level. As rotational speed increases, the leakage increases slightly above the static level. The .051 cm (.020 in.) clearance results, however, show the honeycomb land leakage decreasing slightly at each speed condition tested.

The 3D rig static test results for the honeycomb lands at a 2.0 pressure ratio show 5% less leakage than the smooth land at .025 cm (.010 in.) clearance. However, seal knife rotational effects cause the honeycomb land leakage to increase with knife tip speed until a leakage 7% higher than the smooth land occurs at 239 m/s (785 ft/sec). The honeycomb land at .051 cm (.020 in.) clearance shows about 25% less leakage than the solid-smooth land, both statically and dynamically. These results are summarized in Table 15, which also includes a comparison of the 3D rig abradable land performance.

A comparison of the 2D rig and 3D rig honeycomb land test results shows excellent agreement at .051 cm (020 in.) clearance. At .025 cm (.010 in.) clearance, the honeycomb land shows a variation in performance level between the 2D and 3D rigs. This variation might mean that the location of the seal knife edge relative to the honeycomb cell sidewall is an influential parameter at small clearances. Additional testing may be warranted with the .025 cm (.010 in.) radial clearance honeycomb land to investigate the performance difference between the 2D rig and 3D rig test results.

FIGURE 43. 2D RIG FOUR KNIFE STRAIGHT SEALS WITH SMOOTH AND HONEYCOMB LANDS

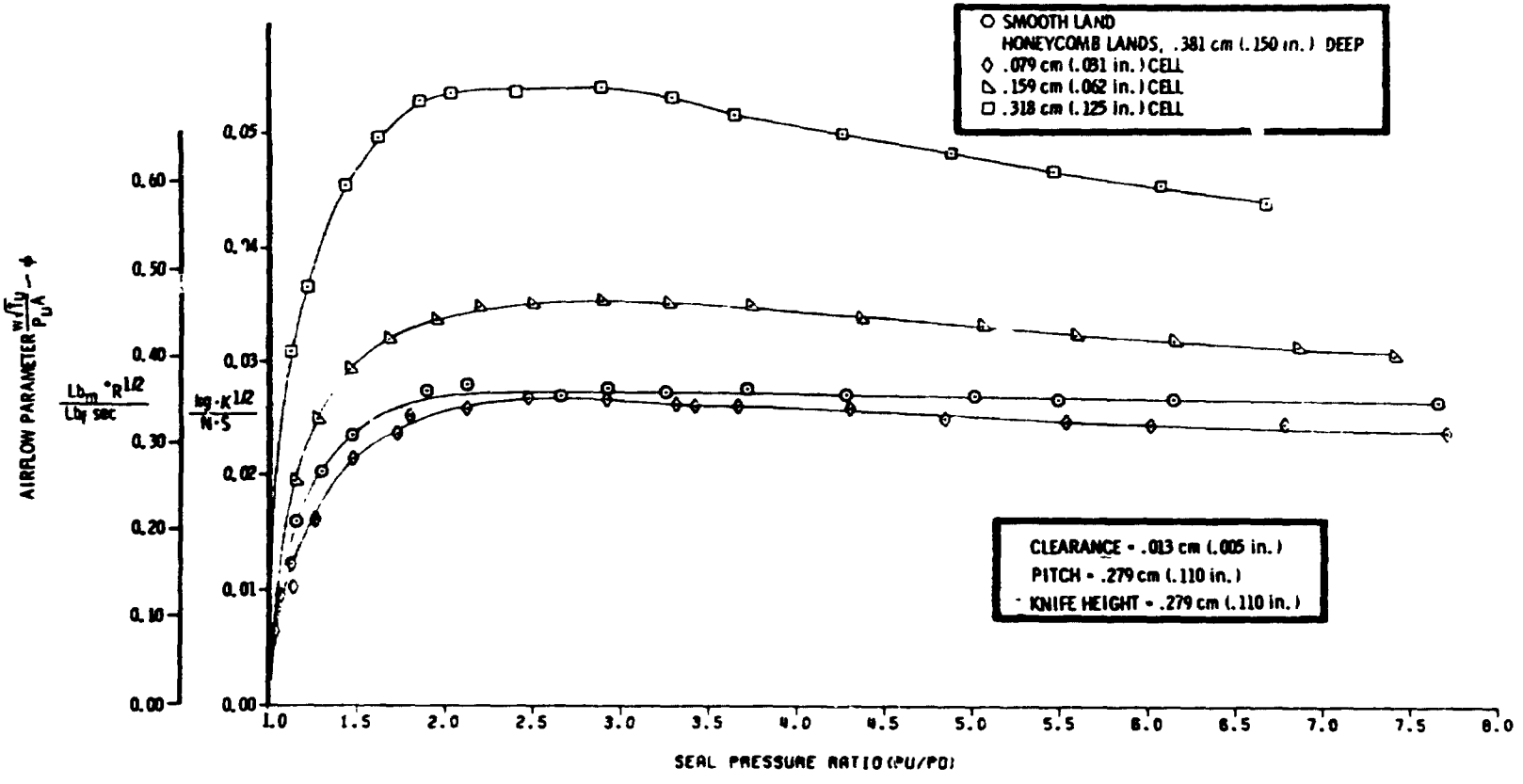

FIGURE 44. 2D RIG FOUR KNIFE STRAIGHT SEALS WITH SMOOTH AND HONEYCOMB LANDS

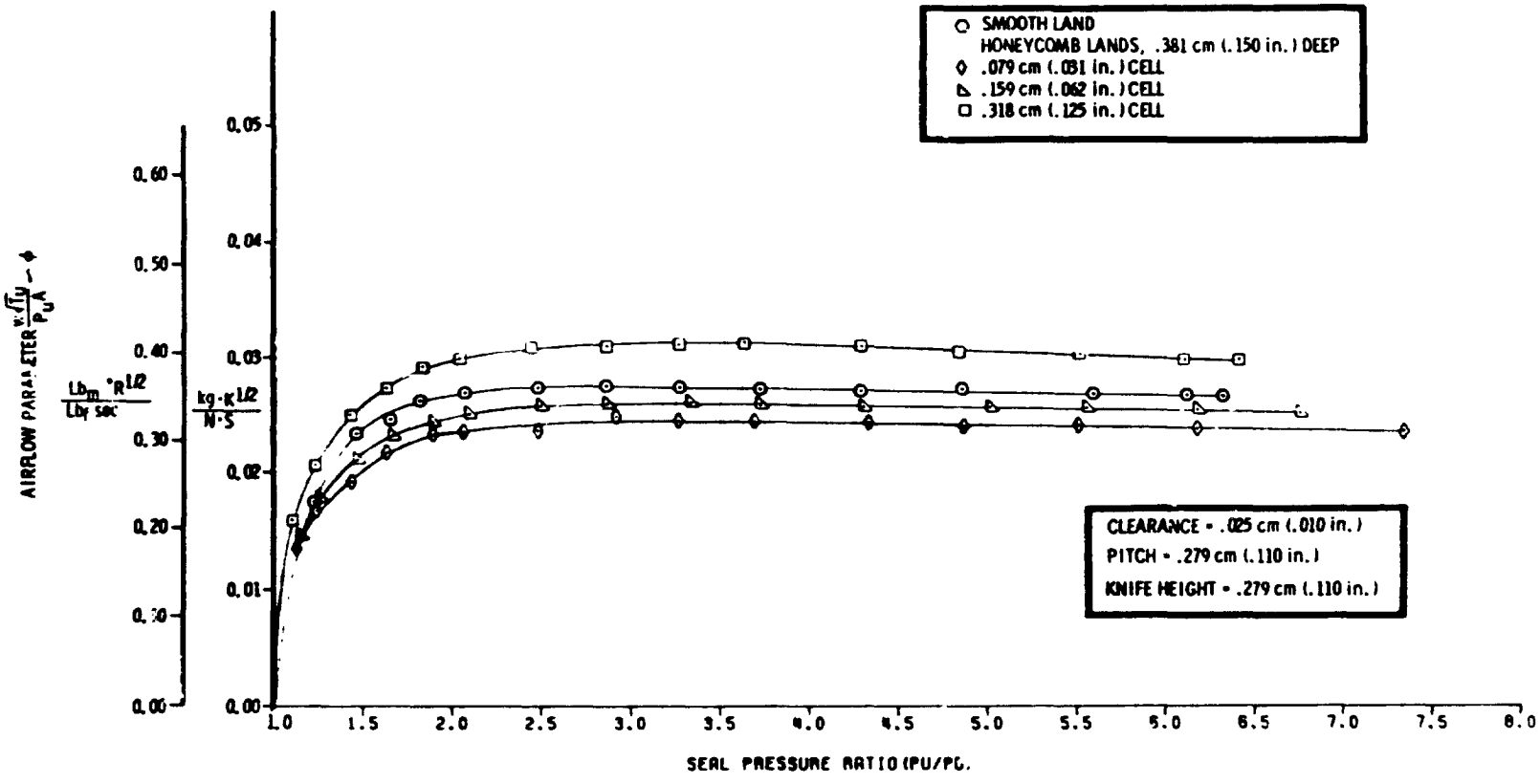

FIGURE [illegible] 2D RIG FOUR KNIFE STRAIGHT SEALS WITH SMOOTH AND HONEYCOMB LANDS

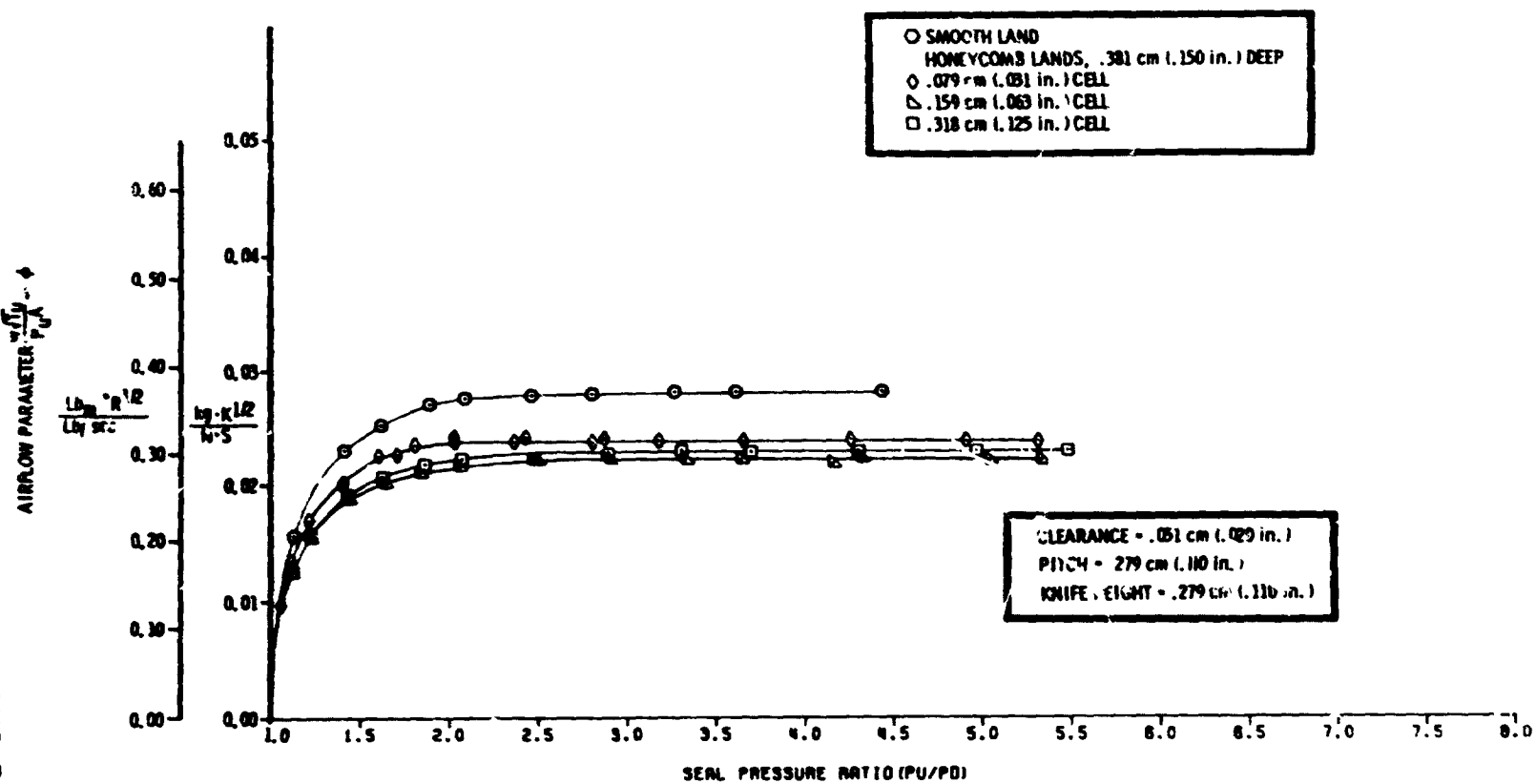

FIGURE 46. EFFECT OF HONEYCOMB CELL DEPTH ON FOUR KNIFE STRAIGHT SEAL LEAKAGE

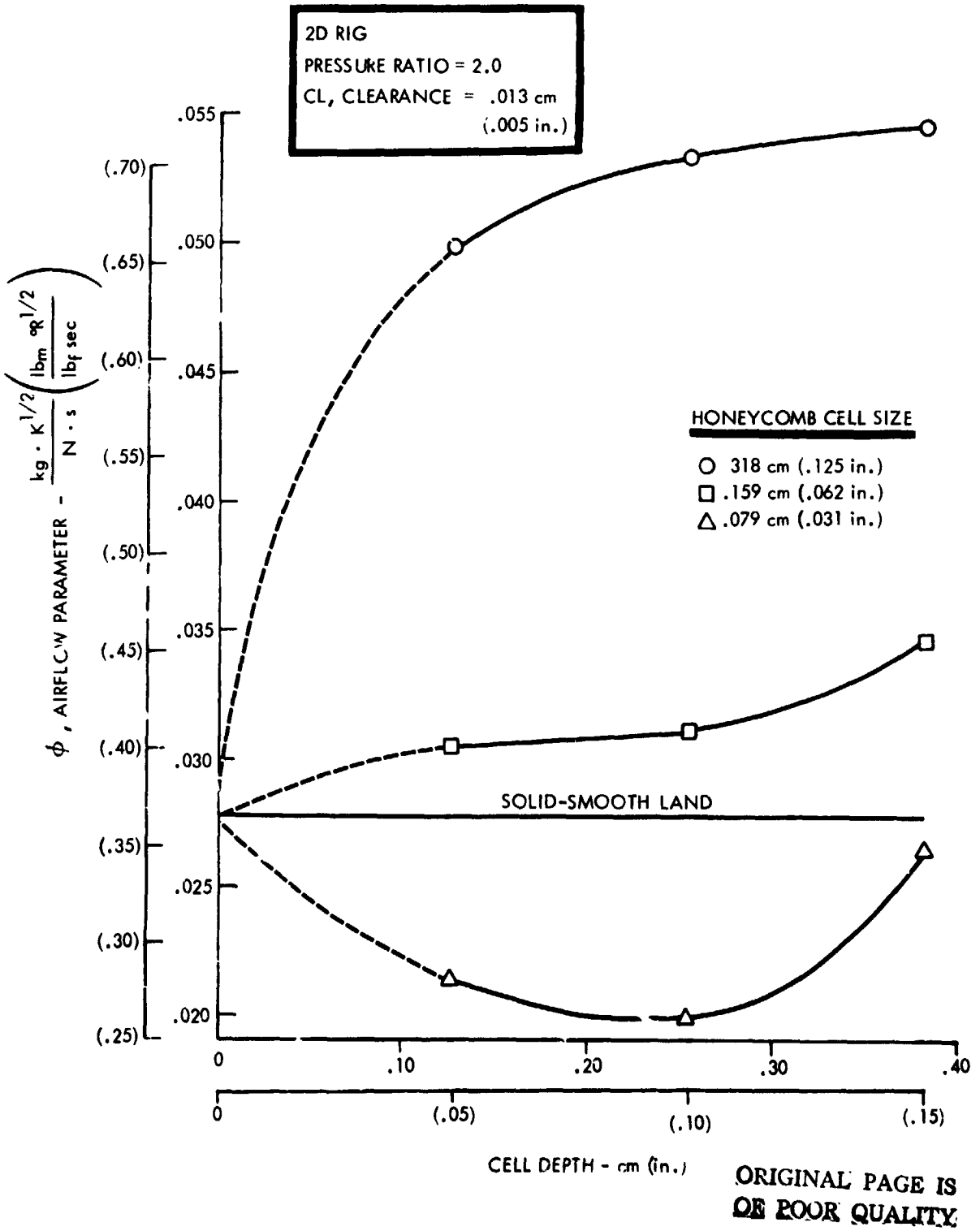

FIGURE 47. EFFECT OF HONEYCOMB CELL DEPTH ON FOUR KNIFE STRAIGHT SEAL LEAKAGE

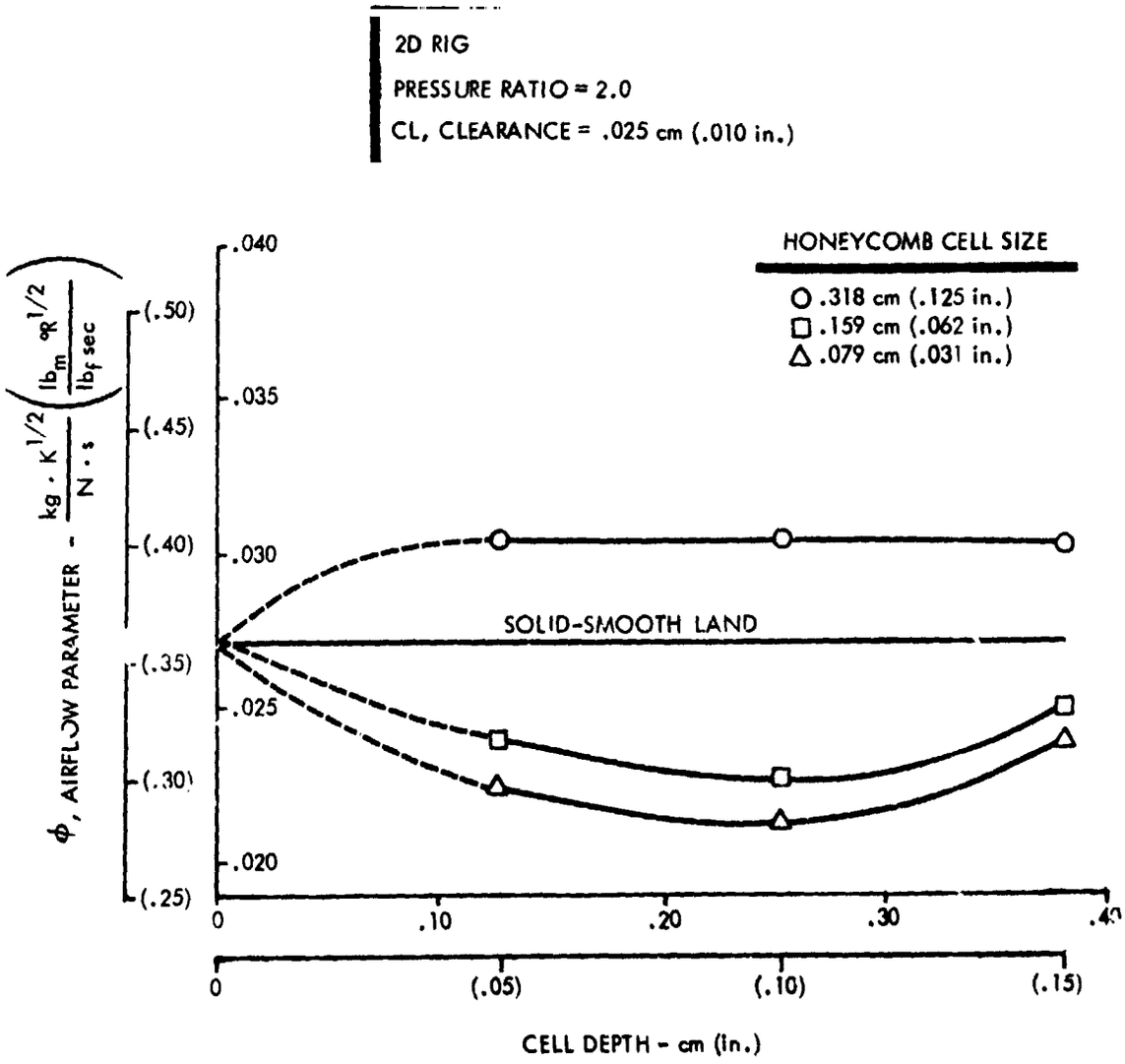

FIGURE 48. EFFECT OF HONEYCOMB CELL DEPTH ON FOUR KNIFE STRAIGHT SEAL LEAKAGE

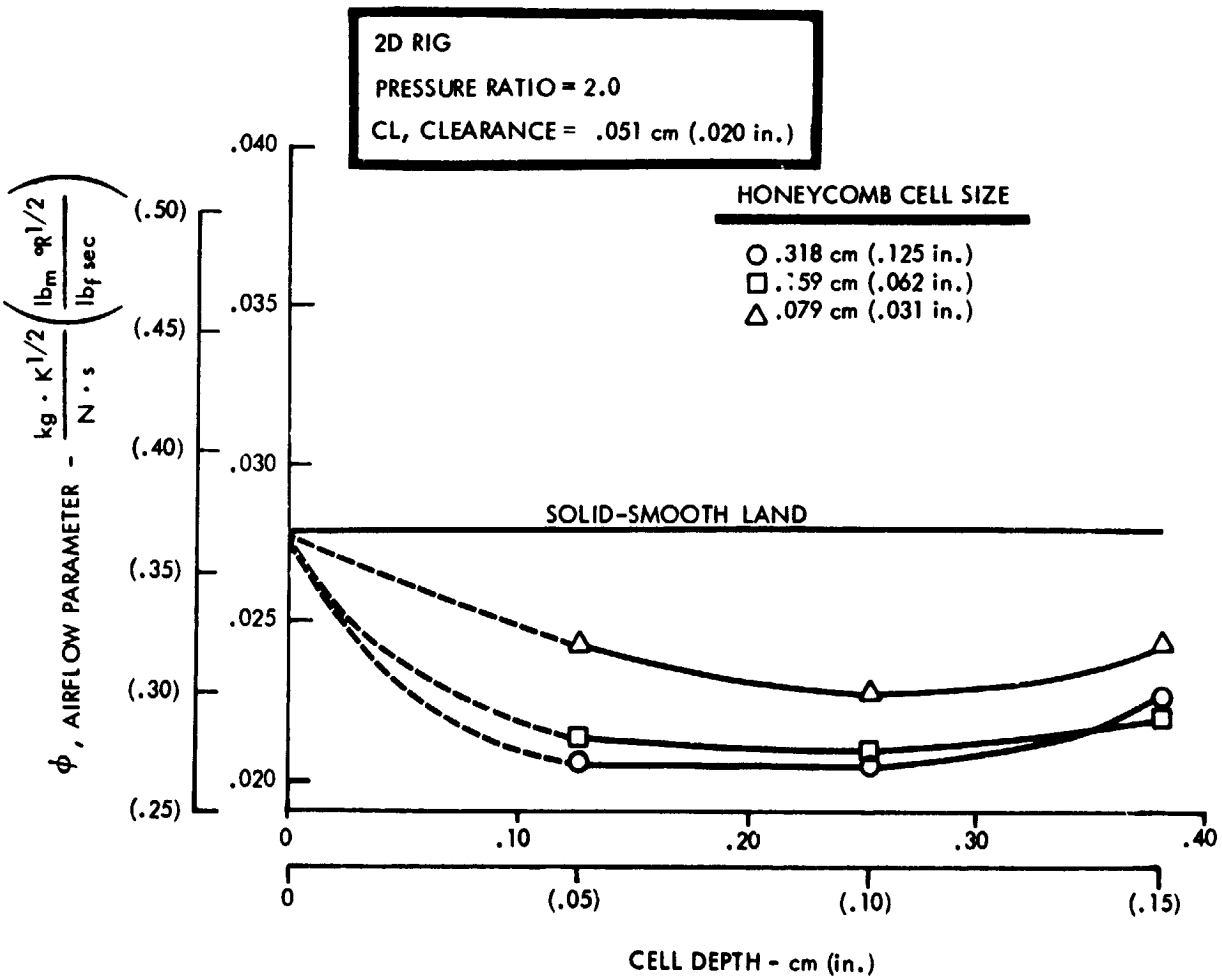

TABLE 13. COMPARISON OF SMOOTH AND HONEYCOMB LAND PERFORMANCE AT PRESSURE RATIOS OF 2.0 AND 3.0

2-D Rig, Seal Configuration:

Four Vertical Knives

Pitch = .279 cm (.110 in.)

Knife Height = .279 cm (.110 in.)

Knife Edge Thickness = .025 ∿.038 cm (.010 ∿ .015 in.)

Land Cell Depth = .381 cm (.150 in.)

NOTE: + Indicates leakage greater than smooth land at comparable clearance
- Indicates leakage less than smooth land at comparable clearance.

Land Type	CL, Clearance cm	CL, Clearance in.	Pressure Ratio	Φ, Flow Parameter $\frac{kg \cdot K^{\frac{1}{2}}}{N \cdot s}$	Φ, Flow Parameter $\frac{lb_m \cdot °R^{\frac{1}{2}}}{lb_f \cdot sec}$	ΔΦ/Φ From Smooth Land %	Pressure Ratio	Φ, Flow Parameter $\frac{kg \cdot K^{\frac{1}{2}}}{N \cdot s}$	Φ, Flow Parameter $\frac{lb_m \cdot °R^{\frac{1}{2}}}{lb_f \cdot sec}$	ΔΦ/Φ From Smooth Land %
Smooth	.013	.005	2.0	.0277	.365	0.0	3.0	.0279	.368	0.0
	.025	.010	2.0	.0272	.358	0.0	3.0	.0279	.368	0.0
	.051	.020	2.0	.0277	.365	0.0	3.0	.0285	.375	0.0
Honeycomb .079 cm(.031 in) Cell	.013	.005	2.0	.0264	.347	-4.9	3.0	.0271	.356	-3.1
	.025	.010	2.0	.0240	.316	-11.7	3.0	.0249	.328	-10.7
	.051	.020	2.0	.0242	.319	-12.6	3.0	.0244	.321	-14.4
Honeycomb .159 cm(.062 in) Cell	.013	.005	2.0	.0345	.454	+24.4	3.0	.0359	.472	+28.4
	.025	.010	2.0	.0252	.331	- 7.5	3.0	.0263	.346	- 5.9
	.051	.020	2.0	.0219	.288	-21.1	3.0	.0227	.299	-20.3
Honeycomb .318 cm(.125 in) Cell	.013	.005	2.0	.0544	.716	+96.2	3.0	.0548	.721	+96.2
	.025	.010	2.0	.0302	.398	+11.2	3.0	.0317	.417	+13.5
	.051	.020	2.0	.0226	.298	-18.4	3.0	.0234	.308	-17.9

TABLE 14. EFFECT OF ROTATION ON THE PERFORMANCE OF A FOUR KNIFE STRAIGHT SEAL AT A PRESSURE RATIO OF 2.0 WITH A SMOOTH LAND AND HONEYCOMB LAND

Land	Kt, Knife Pitch cm	Kt, Knife Pitch in.	CL, Clearance cm	CL, Clearance in.	Φ, Flow Parameter $\frac{kg \cdot K^{\frac{1}{2}}}{N \cdot s}$	Φ, Flow Parameter $\frac{lb_m \cdot °R^{\frac{1}{2}}}{lb_f \cdot sec}$	ΔΦ/Φ % From Static Performance At Knife Tip Speed, V V=80 m/s (261 ft/sec)	V=159 m/s (523 ft/sec)	V=239 m/s (785 ft/sec)
					Static V=0.0				
Solid-Smooth	.279	.110	.025	.010	.0266	.350	-2.6	-6.0	-8.9
			.051	.020	.0283	.372	+1.3	-1.9	-6.7
.159 cm (.062 in.) Cell Honeycomb	.279	.110	.025	.010	.0253	.333	-1.2	-1.2	+2.2
			.051	.020	.0205	.270	-0.7	-2.2	-2.6

TABLE 15. COMPARISON OF ABRADABLE AND HONEYCOMB SEAL LANDS PERFORMANCE WITH SOLID LAND AT PRESSURE RATIO 2.0

LAND	KP, Knife Pitch cm (in.)	CL, Clearance cm (in.)	$\frac{\Delta\phi}{\phi} \sim$ % FROM SOLID-SMOOTH LAND PERFORMANCE				
			2D RIG	3D RIG			
			Static	Static V= 0.0	V=80 m/s (261 ft/sec)	V=159 m/s (523 ft/sec)	V=239 m/s (785 ft/sec)
SOLID-SMOOTH	.279 (.110)	.025 (.010)					
"ABRADABLE A"			+ 9.8	+ 3.4	+ 4.4	+ 4.0	+ 2.2
HONEYCOMB *			-16.8	- 4.9	- 3.5	0.0	+ 6.9
SOLID-SMOOTH		.051 (.020)					
"ABRADABLE A"			+ 9.9	- 1.1	- 3.2	- 3.8	- 4.9
HONEYCOMB *			-24.7	-27.4	-28.9	-27.7	-24.2

$$\frac{\Delta\phi}{\phi} = \frac{\phi - \phi_{ss}}{\phi_{ss}}$$

where $\phi_{ss} \sim$ Solid-Smooth Land Flow Parameter

$\phi \sim$ "Abradable A" or Honeycomb Flow Parameter

and $V \sim$ Knife Tip Speed

* .159 cm (.062 in.) Cell Honeycomb, .254 cm (.100 in.) Deep

Optimum Pitch Studies. An experimental study was made to determine if rotation of the seal knife affects the optimum pitch dimension for a conventional straight-through labyrinth seal. The optimum knife pitch value has historically been established from static rig tests. The optimum design pitch is defined in this context as the combination of knife pitch and number of seal knives that provides the lowest leakage at a specified clearance and fits within a specific axial envelope. Using a four knife straight-through seal configuration with a .025 cm (.010 in.) radial clearance, the optimum pitch was calculated to be .279 cm (.110 in.) from the static design parameter, pitch/clearance = 11. Four knife straight-through seal rotors with pitch values of .203 cm (.080 in.) and .356 cm (.140 in.) were also selected for dynamic testing to provide performance information on each side of the optimum pitch seal. The lands evaluated included the smooth, abradable, and honeycomb configurations at .025 cm (.010 in.) and .051 cm (.020 in.) radial clearances which were tested in the 2D rig segment of Task I. All tests in this 3D rig segment of Task I were conducted statically and rotationally at 80 m/s (261 ft/sec), 159 m/s (523 ft/sec), and 239 m/s (785 ft/sec) knife tip velocities.

The solid-smooth, the "Abradable A", and the honeycomb land test results for the three knife pitch values are plotted in Figures 49, 50, and 51, respectively, to show the similar performance characteristics at static and dynamic conditions. Differences in seal leakage do result from rotational effects, but the similarity in flow parameter change with knife pitch from static and dynamic tests indicates that rotation does not significantly affect knife optimum pitch for any of the seal lands tested. The solid-smooth and abradable lands generally show a continuous decrease in the leakage characteristic as pitch increases. The honeycomb land displays a distinct minima in flow parameter at the .279 cm (.110 in.) knife pitch.

These results are cross-plotted in Figures 52 and 53 to show the similarity in the effect of knife pitch on the performance of seals with solid-smooth, abradable, or honeycomb lands. Figures 54, 55, and 56 show the influence of rotation on the seal performance with solid-smooth, abradable, and honeycomb lands, respectively. The second-order effect of rotation on knife pitch is reconfirmed, also. The individual flow parameter curves are included in Appendix B.

Review. The complex nature of labyrinth seal performance and the associated difficulty of predicting performance without adequate knowledge based on test data have been verified by the experimental program. The use of abradable and honeycomb seal lands is a relatively recent development. The prediction of leakage performance for these newer seal materials is based on a limited amount of test data and the assumption of characteristics developed for solid-smooth lands. A summary of the static performance and rotational effects on the seal leakage characteristics for the representative abradable and honeycomb land materials is presented

with the solid-smooth land performance in Table 16. A comparison of the abradable and honeycomb lands relative to a solid-smooth land is presented in Table 17 for static and dynamic conditions. The comparable 2D rig test results are also included in this table. Figures 57 and 58 are plots of the relative performance deviation from the solid-smooth land.

FIGURE 49. EFFECT OF KNIFE PITCH ON SOLID-SMOOTH LAND SEAL PERFORMANCE

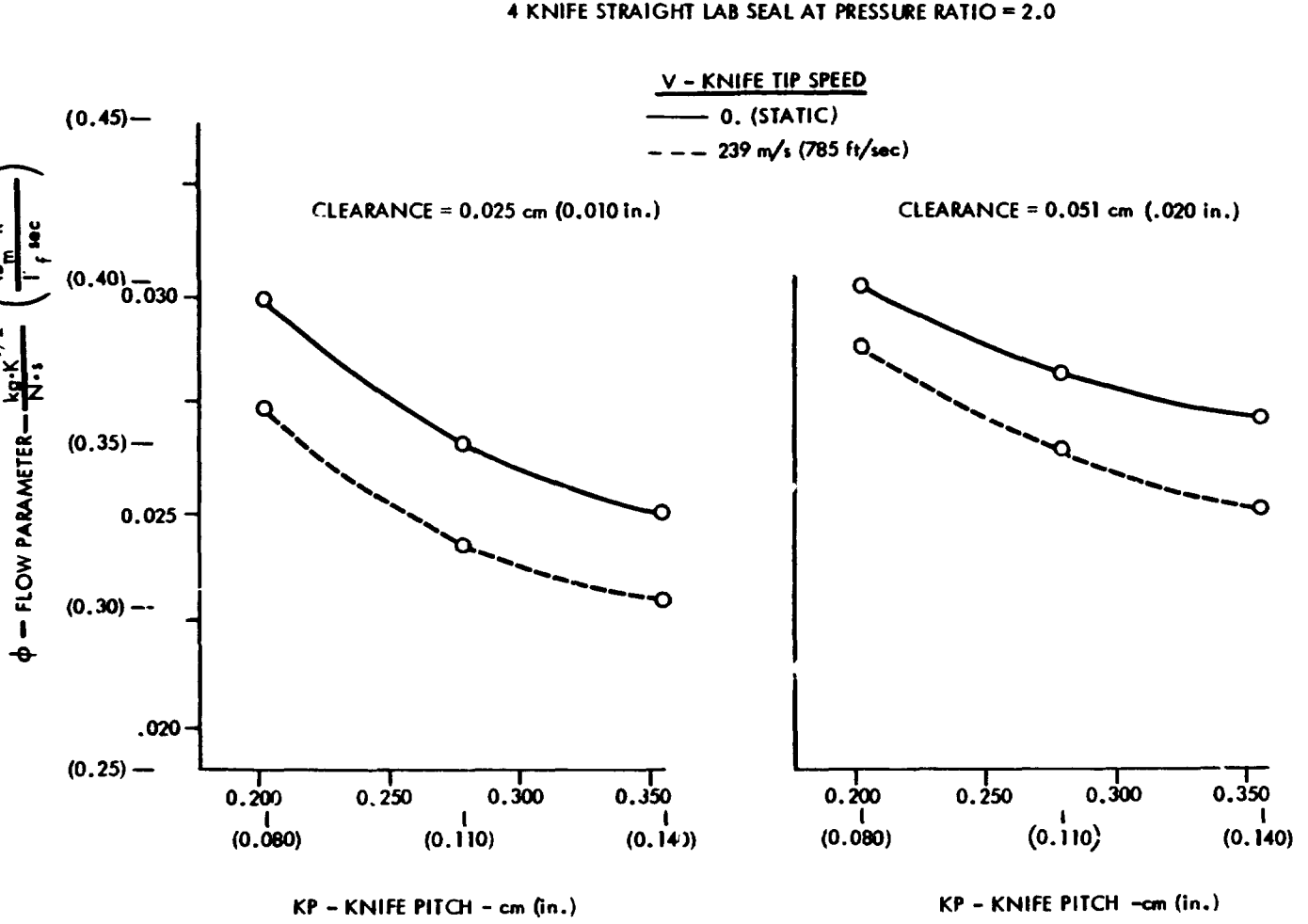

FIGURE 50. EFFECT OF KNIFE PITCH ON "ABRADABLE A" LAND SEAL PERFORMANCE

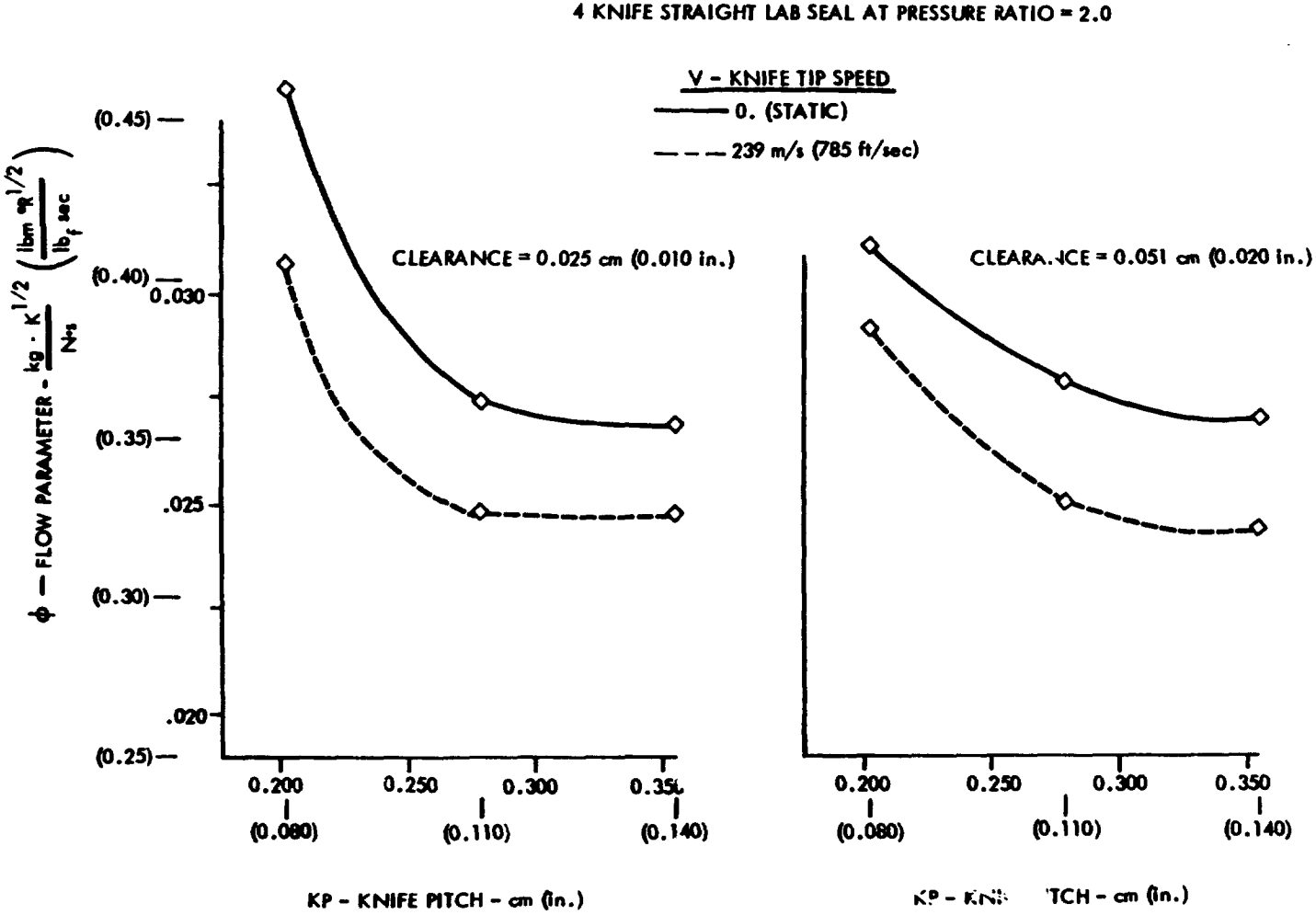

FIGURE 51. EFFECT OF KNIFE PITCH ON HONEYCOMB* LAND SEAL PERFORMANCE

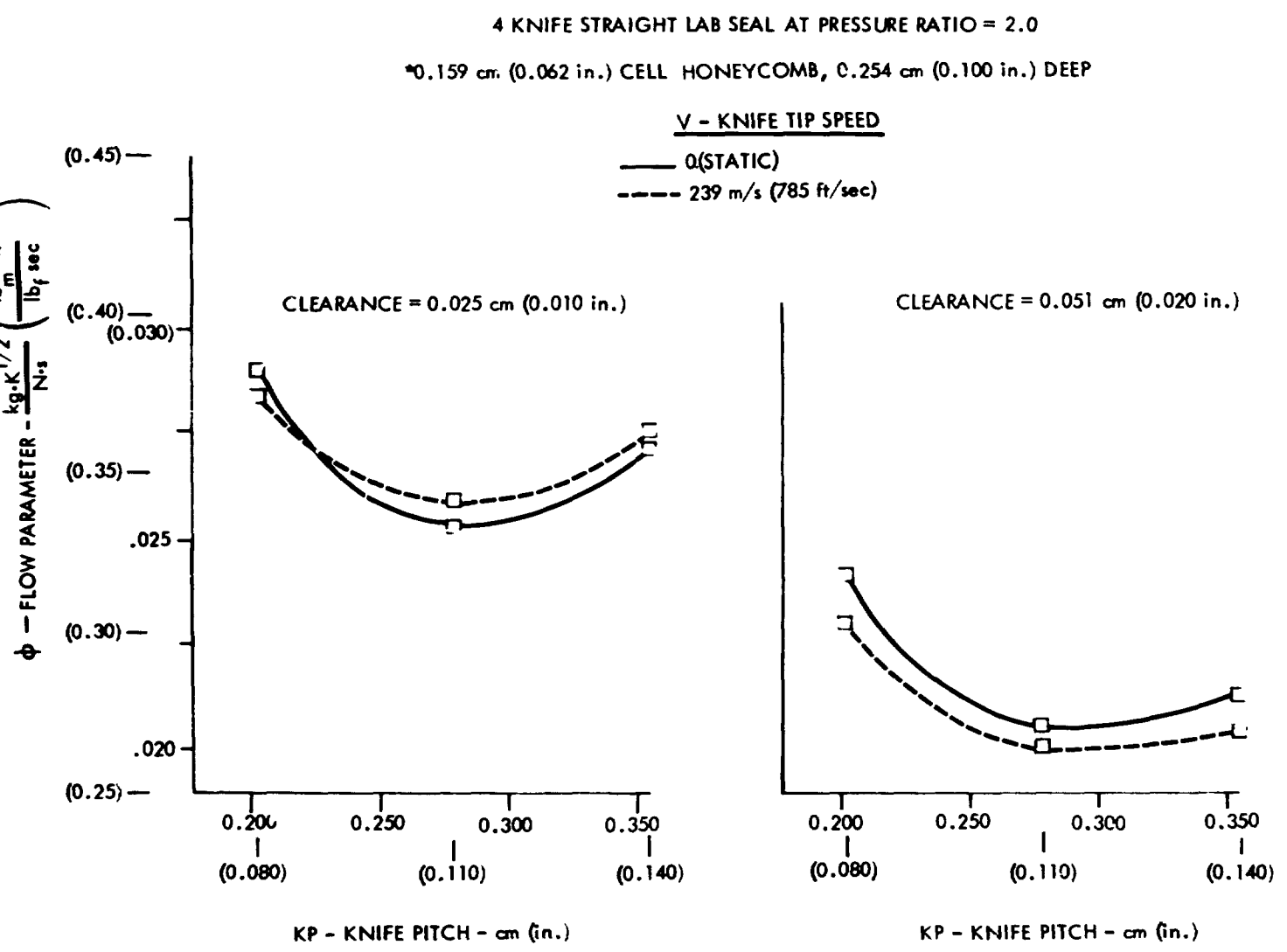

FIGURE 52. EFFECT OF KNIFE PITCH AT 0.025 cm (0.010 in.) CLEARANCE ON SEAL PERFORMANCE

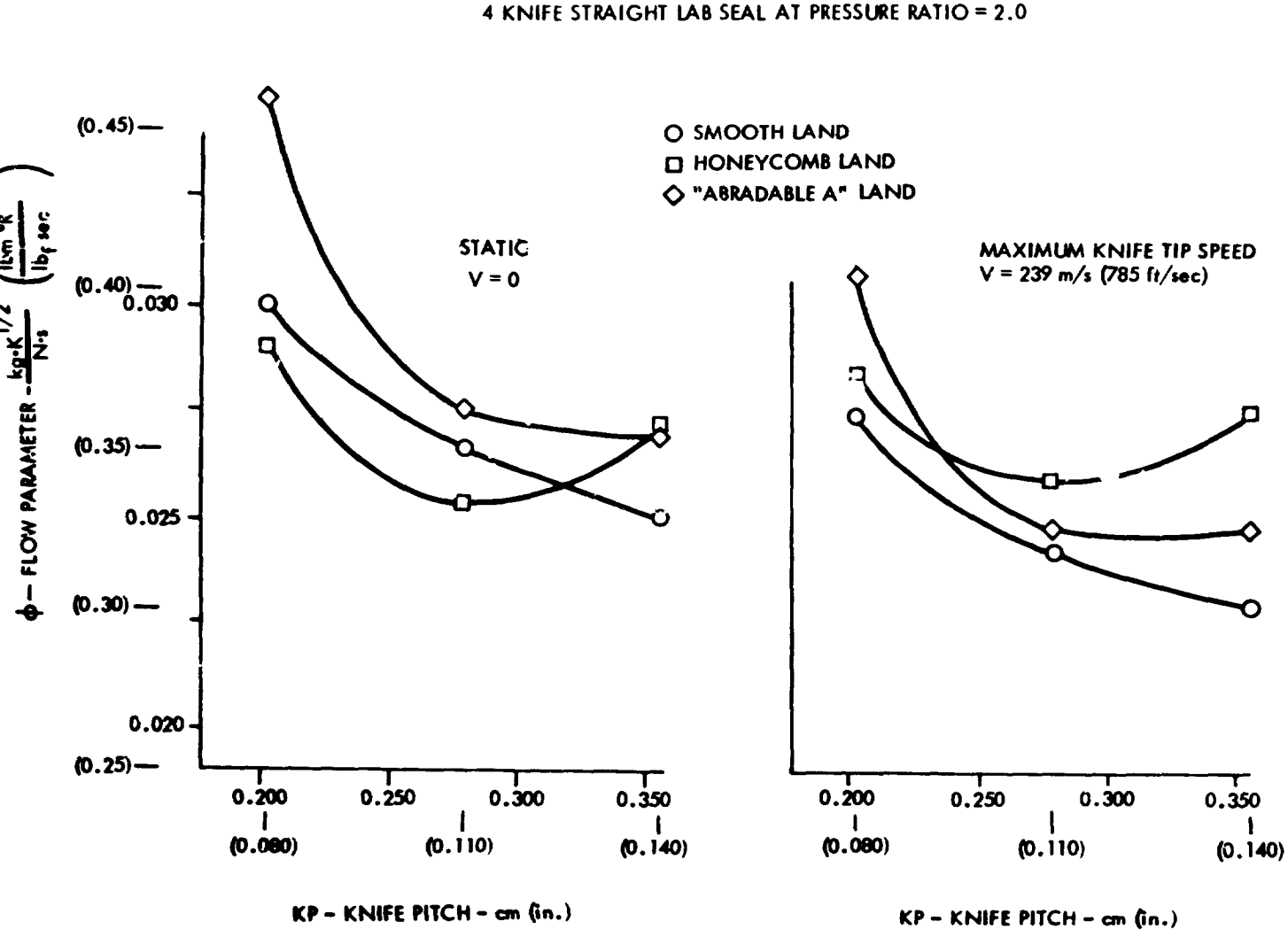

FIGURE 53. EFFECT OF KNIFE PITCH AT 0.051 cm (0.010 in.) CLEARANCE ON SEAL PERFORMANCE

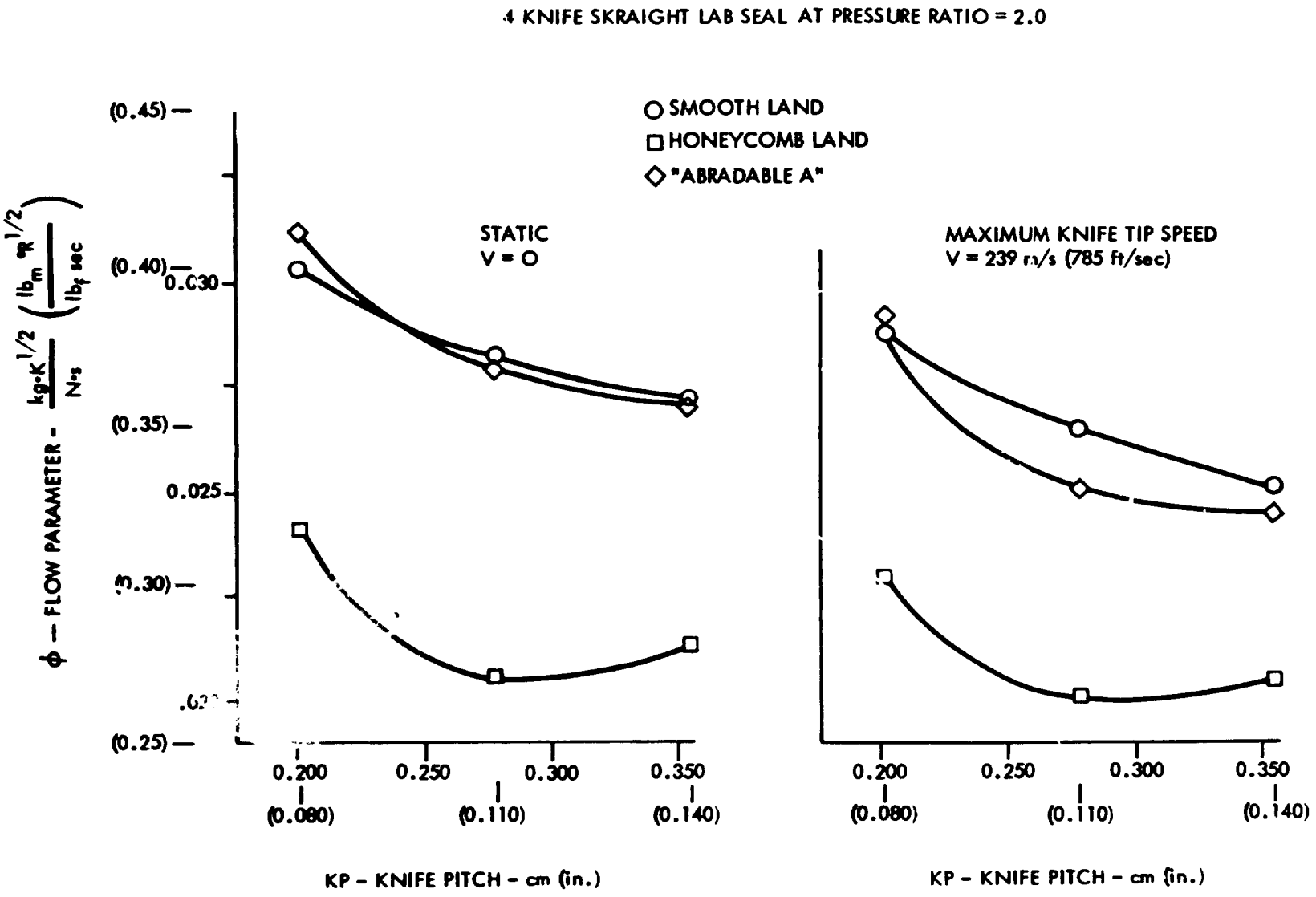

FIGURE 54. EFFECT OF ROTATION ON SOLID-SMOOTH LAND SEAL PERFORMANCE

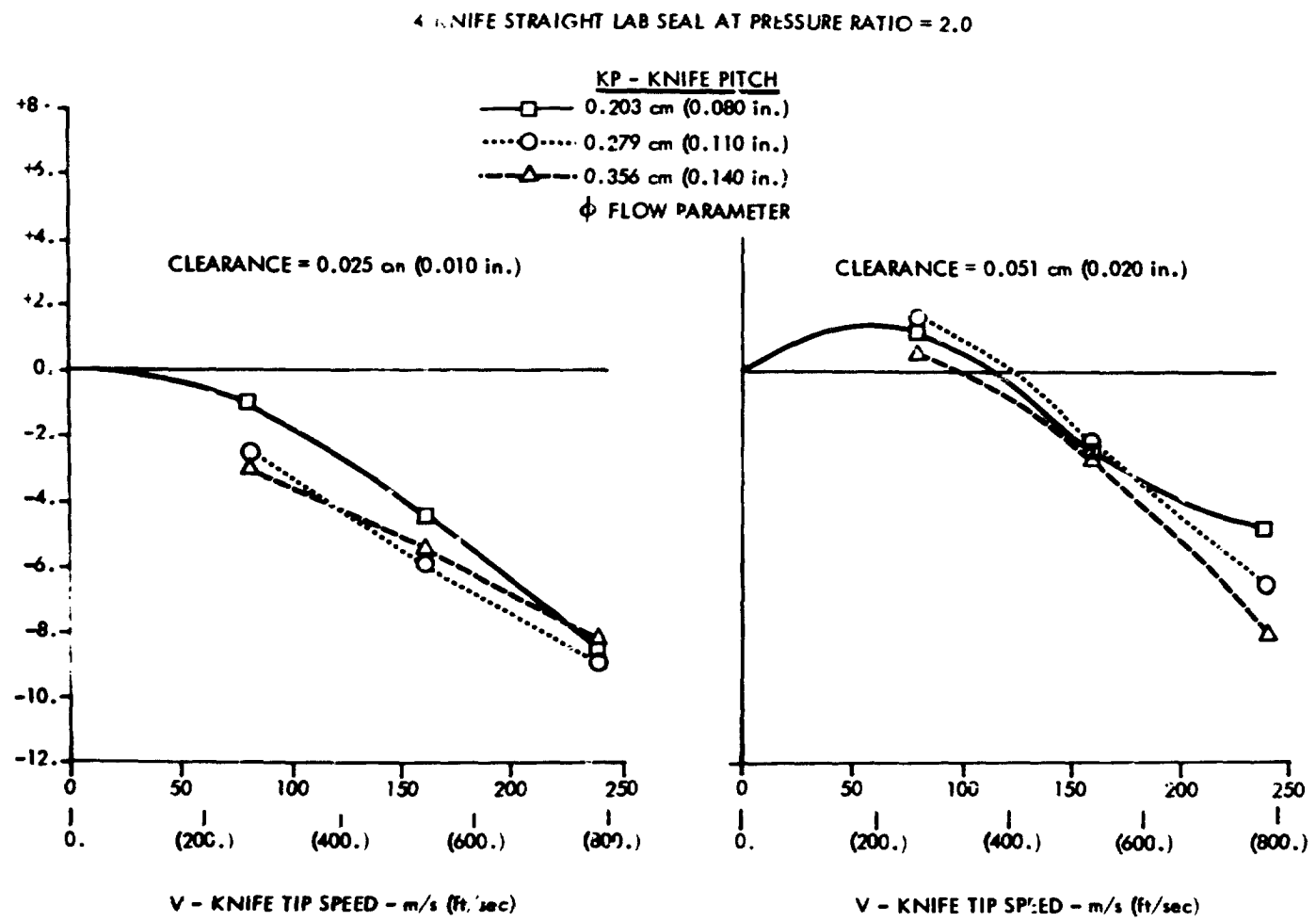

FIGURE 55. EFFECT OF ROTATION ON "ABRADABLE A" LAND SEAL PERFORMANCE

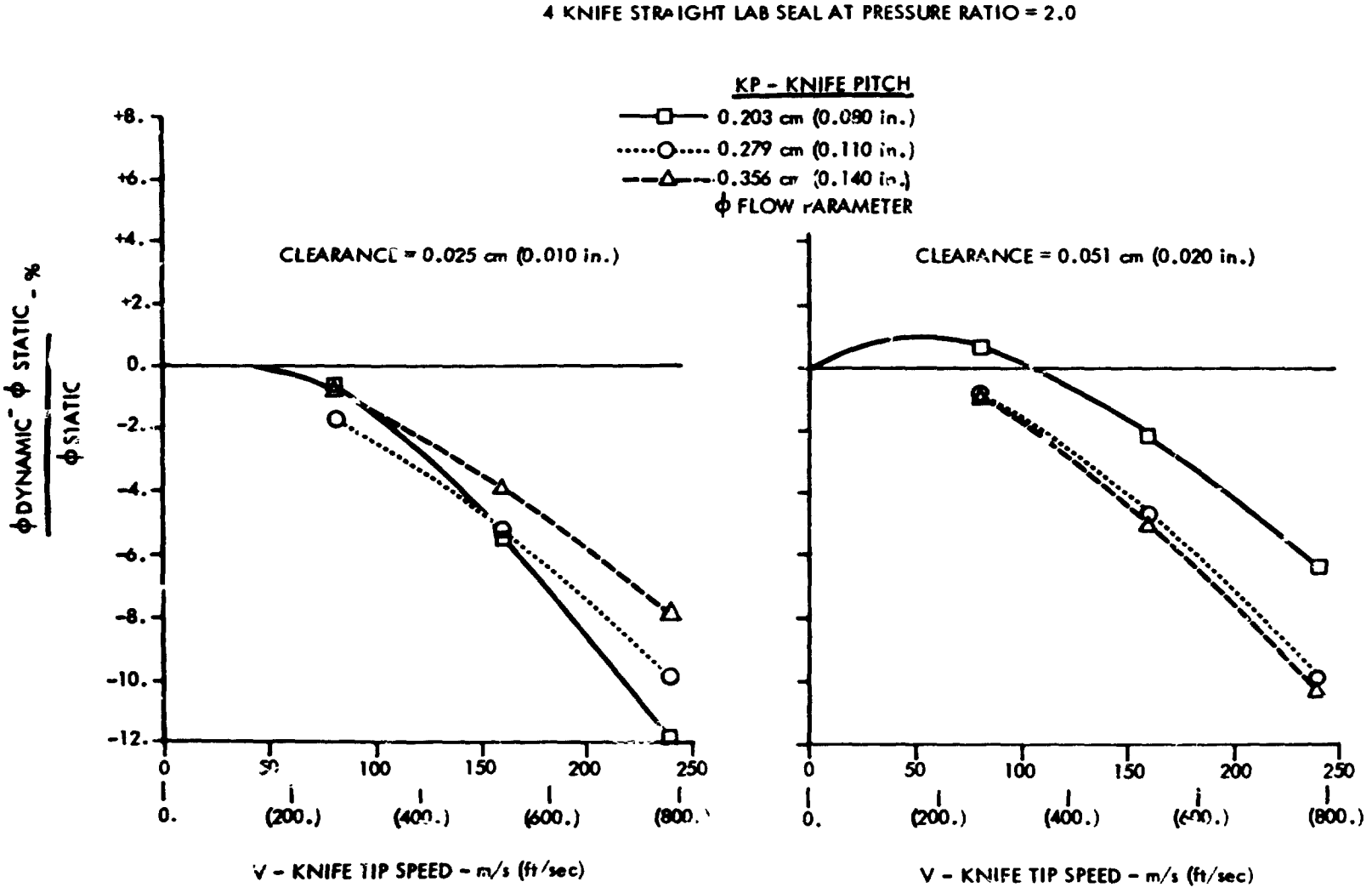

C-2

FIGURE 56. EFFECT OF ROTATION ON HONEYCOMB* LAND SEAL PERFORMANCE

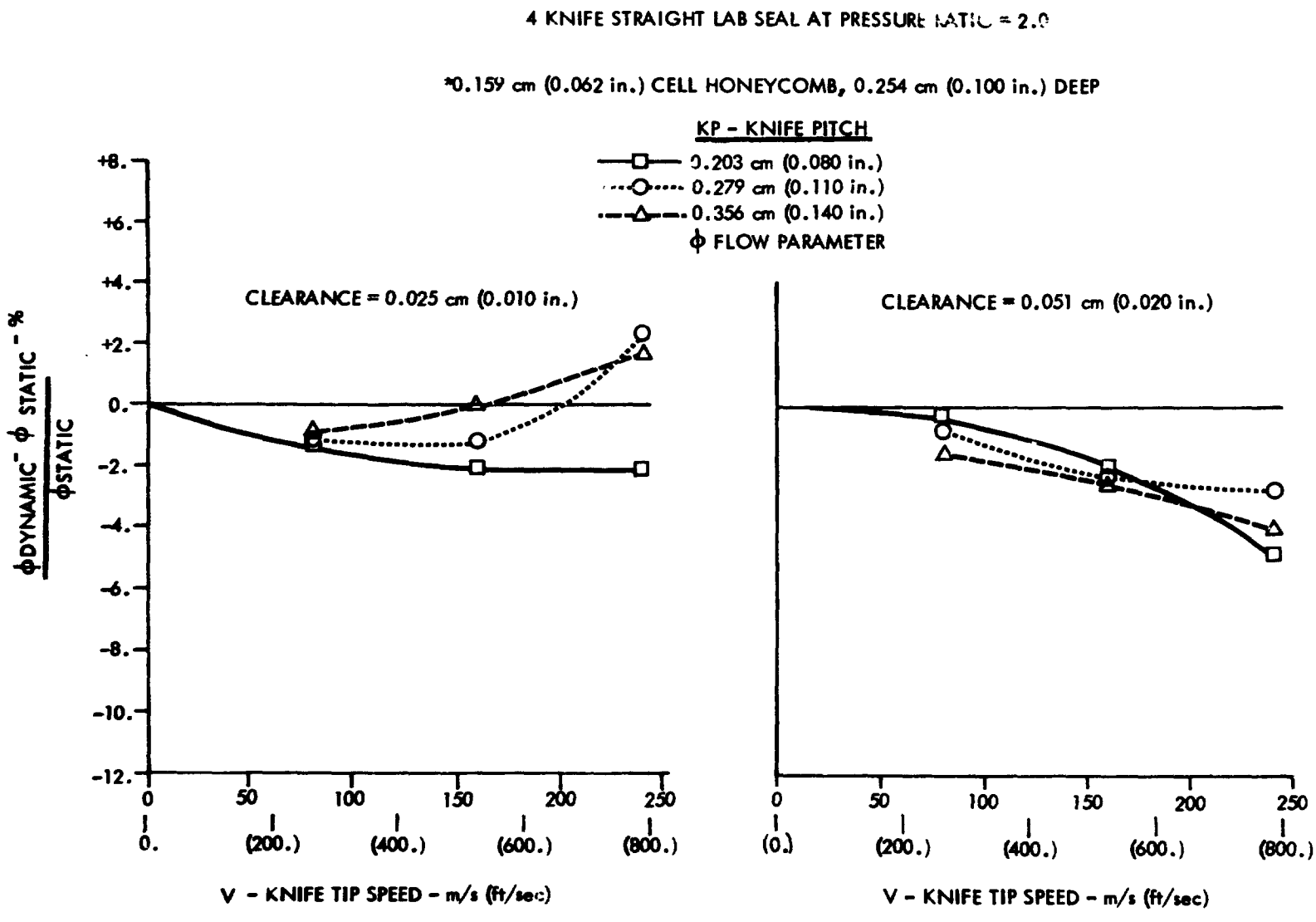

FIGURE 57. EFFECT OF LAND SURFACE AND PITCH ON SEAL PERFORMANCE AT .025 cm (.010 in.) CLEARANCE

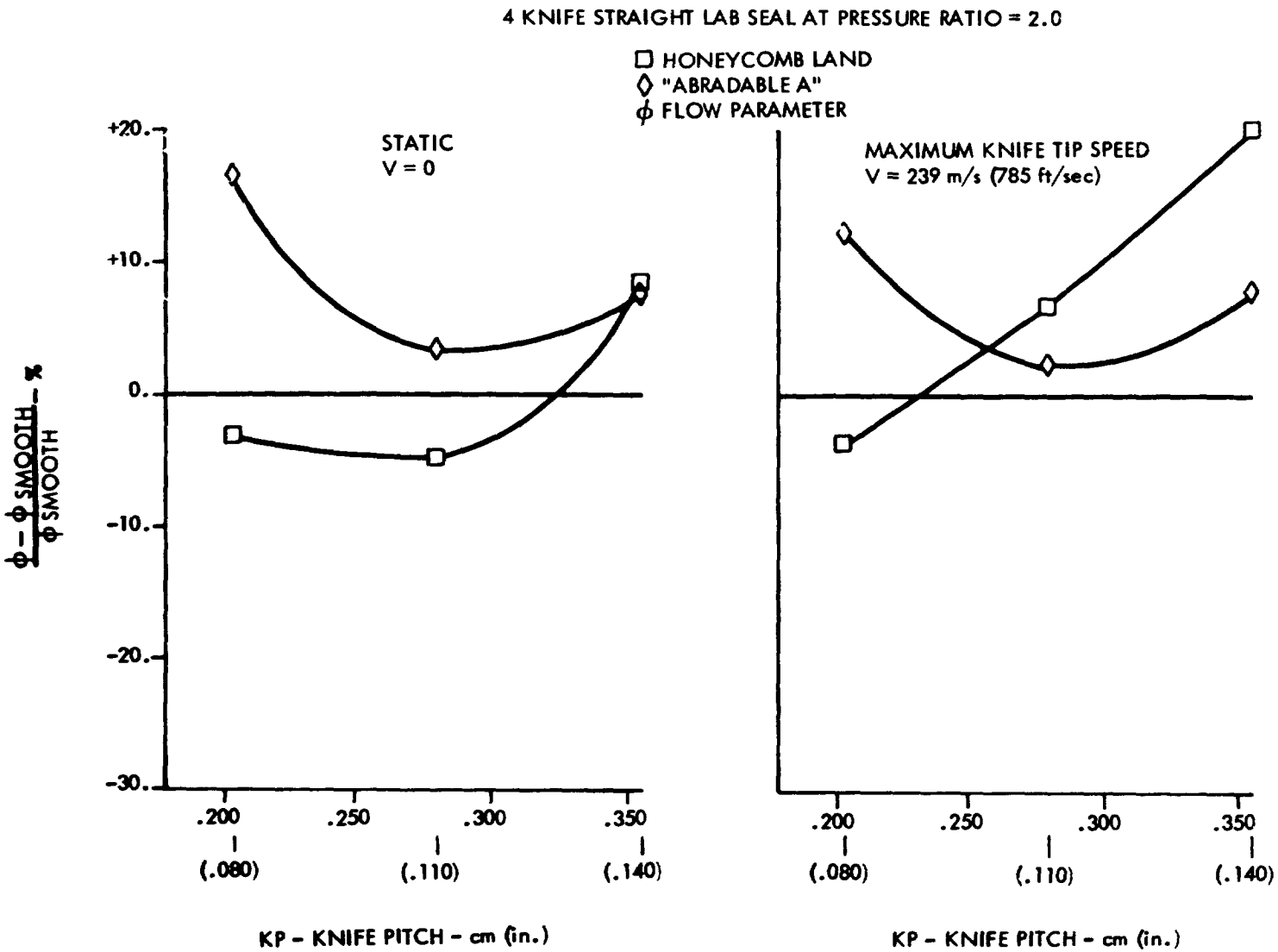

FIGURE 58. EFFECT OF LAND SURFACE AND PITCH ON SEAL PERFORMANCE AT .051 cm (.020 in.) CLEARANCE

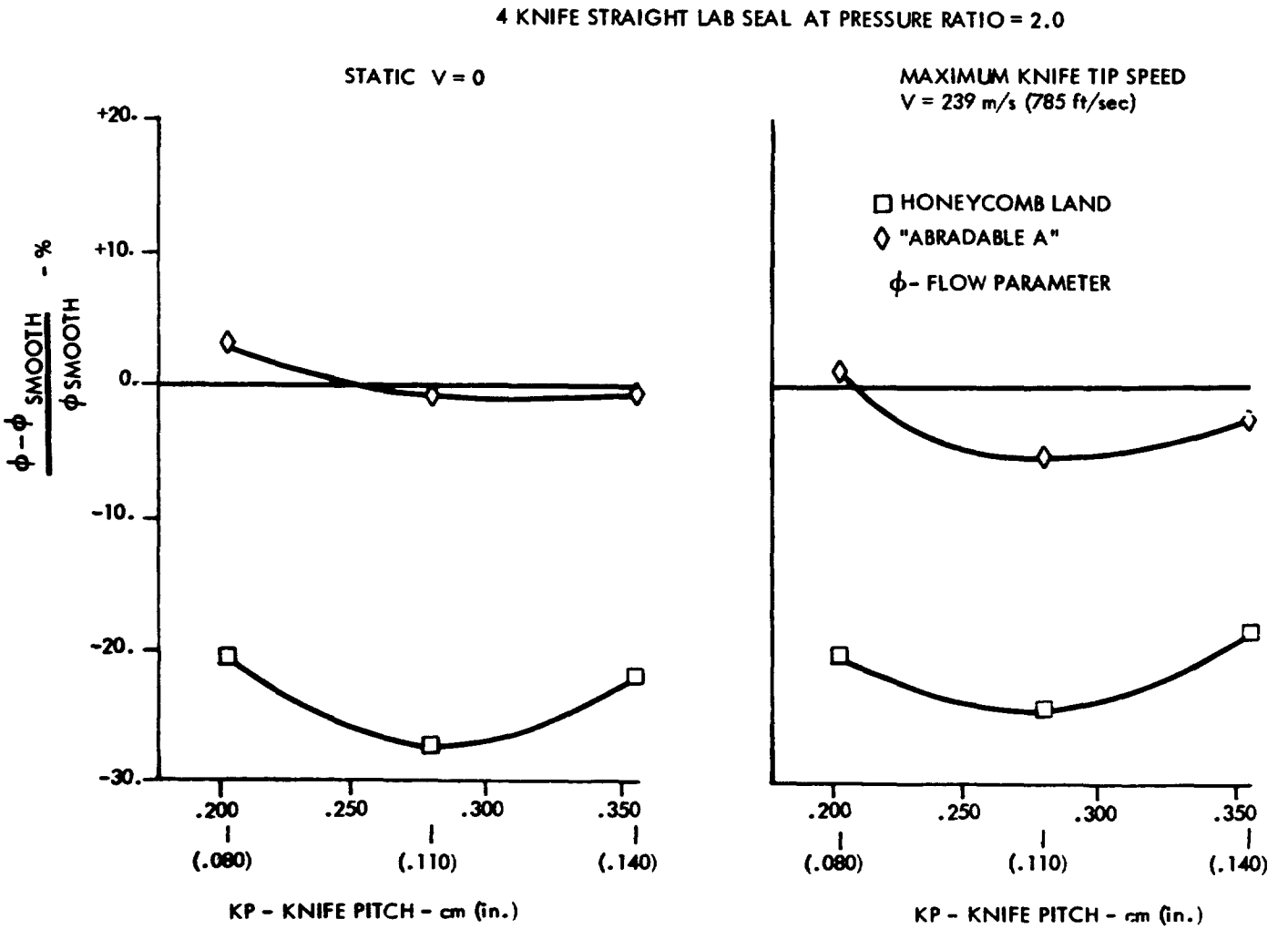

TABLE 16. EFFECT OF ROTATION ON THE PERFORMANCE OF A FOUR KNIFE STRAIGHT SEAL AT A PRESSURE RATIO = 2.0

LAND	KP, Knife Pitch		CL, Clearance		ϕ, Flow Parameter		$\Delta\phi/\phi$ ~ % From Static Performance At Knife Tip Speed, V		
	cm	in.	cm	in.	$\frac{kg \cdot K^{\frac{1}{2}}}{N \cdot s}$	$\frac{lb_m \cdot °R^{\frac{1}{2}}}{lb_f \cdot sec}$			
					Static V=0.0		V=80 m/s (261 ft/sec)	V=159 m/s (523 ft/sec)	V=239 m/s (785 ft/sec)
SOLID-SMOOTH	.203	.080	.025	.010	.0300	.395	-1.0	-4.6	-8.6
			.051	.020	.0303	.399	+1.3	-2.5	-4.8
	.279	.110	.025	.010	.0266	.350	-2.6	-6.0	-8.9
			.051	.020	.0283	.372	+1.3	-1.9	-6.7
	.356	.140	.025	.010	.0250	.329	-3.0	-5.5	-8.2
			.051	.020	.0273	.359	+5.6	-2.8	-8.1
"ABRADABLE A"	.203	.080	.025	.010	.0250	.460	-0.7	-5.4	-12.0
			.051	.020	.0312	.411	+0.7	-2.2	-6.3
	.279	.110	.025	.010	.0275	.362	-1.6	-5.5	-9.9
			.051	.020	.0280	.368	-0.8	-4.6	-10.3
	.356	.140	.025	.010	.0269	.354	-0.9	-4.0	-7.9
			.051	.020	.0271	.357	-0.8	-5.0	-9.8
.159 cm(.062 in) Cell Honeycomb	.203	.080	.025	.010	.0290	.382	-1.3	-2.1	-2.1
			.051	.020	.0241	.317	-0.3	-1.9	-4.7
	.279	.110	.025	.010	.0253	.333	-1.2	-1.2	+2.4
			.051	.020	.0205	.270	-0.7	-2.2	-2.6
	.356	.140	.025	.010	.0271	.357	-0.8	0.0	+1.7
			.051	.020	.0213	.280	-1.4	-2.5	-3.9

TABLE 17. COMPARISON AT A PRESSURE RATIO = 2.0 OF A HONEYCOMB AND AN ABRADABLE LAND WITH SOLID LAND SEAL PERFORMANCE STATICALLY AND DYNAMICALLY

LAND	KP, Knife Pitch cm	KP, Knife Pitch in.	CL, Clearance cm	CL, Clearance in.	$\Delta\phi/\phi$ ~ % FROM SOLID-SMOOTH LAND PERFORMANCE				
					2D RIG	KNIFE TIP SPEED - 3D RIG			
					Static	Static V=0.0	V=80 m/s (261 ft/sec)	V=159 m/s (523 ft/sec)	V=239 m/s (785 ft/sec)
Solid-Smooth	.203	.080	.025	.010					
"Abradable A"						+16.5	+16.9	+15.4	+12.2
Honeycomb						- 3.3	- 3.6	- 0.8	- 3.6
Solid-Smooth			.051	.020					
"Abradable A"						+ 1.0	+ 2.5	+ 3.3	+ 1.3
Honeycomb						-20.6	-21.8	-20.1	-20.5
Solid-Smooth	.279	.110	.025	.010					
"Abradable A"					+ 9.8	+ 3.4	+ 4.4	+ 4.0	+ 2.2
Honeycomb					-16.8	- 4.9	- 3.5	0.0	+ 6.9
Solid-Smooth			.051	.020					
"Abradable A"					+ 9.9	- 1.1	- 3.2	- 3.8	- 4.9
Honeycomb					-24.7	-27.4	-28.9	-27.7	-24.2
Solid-Smooth	.356	.140	.025	.010					
"Abradable A"						+ 7.6	+10.0	+ 9.3	+ 7.9
Honeycomb						+ 8.5	+11.0	+14.8	+20.2
Solid-Smooth			.051	.020					
"Abradable A"						- 0.6	- 1.9	- 2.9	- 2.4
Honeycomb						-22.0	-23.5	-21.8	-18.5

Aerodynamic Test Results for an Advanced Labyrinth Seal

An advanced labyrinth seal design, initially tested under contracts to the Navy (N00140-73-C-0005 and N00140-74-C-0759), was selected as the basis for the geometry optimization study of Task II (see Figure 4). An experimental program was conducted to determine the influence of individual seal design parameters. The matrix of these test results was analyzed to derive an optimum seal geometry with performance superior to the original design. The performance of the optimum advanced seal was mapped and then evaluated against a conventional stepped seal, which is typical of many contemporary designs.

The conventional stepped seal which was used as a performance baseline for the previous Navy program (Reference 1) and for this NASA study has the following configuration:

KNIVES: Vertical	
KN, number of knives	4
KP, pitch	.699 cm (.275 in.)
KH, height	.386 cm (.152 in.)
Flow direction	LTSD or STLD
LAND: Solid-Smooth	
SH, step height	.318 cm (.125 in.)
Step face	smooth (no notch)

A sketch illustrating the general configuration of the advanced labyrinth seal design selected is shown in Figure 59. The design philosophy used to develop the advanced seal configuration was to improve the sealing efficiency by increasing the turbulence within the knife cavity. An extension of the high turbulence concept to seal designs which optimize the knife-to-knife performance was investigated by employing a mixture of seal geometry (nonconstant design parameters) within an individual four knife advanced seal.

Optimization of an Advanced Labyrinth Seal Design. The influences of the geometric variables were sorted expeditiously and economically with the DDA two-dimensional (2D) air seal test rig. The 2D rig test program was structured in a flexible manner to provide only the necessary information to optimize the performance of the advanced seal. When a geometric parameter under evaluation indicated marginal performance improvement, the investigation was discontinued and redirected. Therefore, the performance curves for several of the geometric parameters presented in this report have a limited range of data relative to other parameters investigated. In other cases,

sufficient matrix information was obtained to define performance trends over a wide range of data for several parameters. The effect of a geometric parameter was evaluated empirically from its measured flow parameter characteristic curve ($w\sqrt{T_U}/P_UA$ versus P_U/P_D). The value for the flow parameters, $w\sqrt{T_U}/P_UA$, at an arbitrary 2.0 pressure ratio, when cross-plotted against the subject geometric parameter, provided the influence information required for design selection.

The specific values of the geometric parameters investigated in the 2D rig to optimize the performance of the advanced seal are presented in Table 18.* Each geometric parameter was evaluated at seal clearances of .025 cm (.010 in.) and .051 cm (.020 in.) since the performance of the advanced seal design was known to be dependent on the seal clearance (Reference 1). Throughout the geometric parameter investigations, a four knife seal configuration was used.

Step Height Effect on Advanced Seal Performance. A summary of the test results for the influence of land step height is presented in Figure 60. The investigation of this parameter over a pitch range of .408 cm (.200 in.) to 1.016 cm (.400 in.), concentrated on the 70° knife angle with selected tests at a 90° knife angle. All tests of step height effects were conducted with the land notched as shown in Figure 59. As step height was varied, the height of the notch varied, and the notch lip thickness was held constant at .064 cm (.025 in.). Data were not obtained for the effect of land step height without the notch in the land.

Both the 70° and 90° knife angle configurations indicated only slight variations in leakage rate at the two clearances investigated. Over the step height range evaluated, the smaller step height gave the lowest leakage. This result had not been anticipated since a conventional stepped seal derives lower leakage from the spoiling effect of the step on the flow streamlines. Although the effect on leakage is small, the performance trend for step height is opposite to that expected. The leakage performance trend with step height is probably due to the complex interaction of the flow field with the step height and land notch configuration.

Based on these 90° and 70° knife angle performance trends, a .305 cm (.120 in.) step height was selected for investigation at the 50° knife angle. The performance of the .305 cm (.120 in.) step with the 50° knife angle, also shown on Figure 60, was almost identical to that for the 70° knife angle. Since the influence of step height on the performance of seals with 90° and 70° knife angles was similar, additional testing of the step height parameter was considered unnecessary.

*The geometric parameters are defined in Appendix H.

The optimum step height for the advanced seal land was identified as .305 cm (.120 in.).

Knife Height Effect on Advanced Seal Performance. The seal knife height was varied by inserting wax strips to reduce the knife height dimension. Figure 61 shows an example of this technique. The seal knife height test results are presented in Figure 62 for the 90° knife angle seal and Figure 63 for the 70° and 50° knife angles.

The optimum knife height is near .508 cm (.200 in.) for the 90° knife angle seal and is independent of clearance in the range evaluated, as indicated in Figure 62. Knife pitch has a minor effect on the selection of the optimum performance knife height. The 70° and 50° knife angle performance shown in Figure 63 generally indicates that a large knife height, .711 cm (.280 in.), is beneficial. However, a shallow knife height is desirable from manufacturing and operating durability aspects.

Since the advanced seal performance is not highly sensitive to the height parameter, a knife height of .381 cm (.150 in.) was selected to compromise the mechanical and fabrication requirements with the performance of the optimized advanced seal design.

Knife Pitch Effect on Advanced Seal Performance. The test results for seal knife pitch are shown in Figures 64 through 66. The 90° and 70° knife angle data of Figure 64 indicate that a small pitch is desirable for minimum leakage. However, the 50° knife angle data show a different trend. A pitch of .762 cm (.300 in.) is the value for minimum leakage with a knife angle of 50°. Reducing the pitch below .762 cm (.300 in.) significantly increases the leakage for a 50° knife angle seal, whereas the 90° and 70° knife angle seals generally show little change. The maximum leakage variation for the advanced seal through the range of knife pitch tested was approximately 12% for the 90°, 70°, and 50° knife angles. The advanced seal configurations exhibited similar leakage sensitivity over the clearance range evaluated.

Additional test results for the influence of seal knife pitch are presented in Figures 65 and 66 for the 70° and 90° knife angle configurations, respectively, where a range of seal step height data were available. These results show that a change in the step height, in general, does not change the optimum pitch value.

The selection of knife pitch must also receive careful consideration from a mechanical design standpoint since it is the major geometric dimension which affects the total allowable axial seal movement in a stepped seal. For a typical stepped seal design, an axial travel distance of ±.254 cm (±.100 in.) is required to prevent the seal knives from (1) disengaging from the lands or (2) rubbing the stationary land, both of which will result in excessive leakage. Any physical contact between the knives and the vertical faces of the land steps will cause hardware damage and a possible catastrophic failure.

Based on the test results and mechanical design considerations, a pitch of .762 cm (.300 in.) was selected for the optimized seal design. This pitch yields the minimum leakage for 50° and 90° knife angle seal configurations and is near the optimum for a 70° knife angle. The .762 cm (.300 in.) pitch value also provides sufficient axial knife movement for satisfactory operation in advanced engine environments.

The effect of pitch on the performance of the advanced seal design was greater than expected since most designers do not consider pitch to be a performance parameter. The scope of this program did not include an evaluation of the effects of seal knife pitch on a conventional stepped labyrinth seal (without a notched land step). It is evident from the results of this program that the design of conventional stepped seals might be improved if data for the effects of knife pitch on performance were obtained.

Knife Angle Effects on Advanced Seal Performance. The test results for the effect of seal knife angle are summarized in Figures 67, 68, and 69 in terms of percent leakage reduction compared to the conventional 90° knife angle as the base. Figure 68 shows that, at the optimum knife pitch, a 50° knife angle reduces leakage 7% at .025 cm (.010 in.) clearance and 12% at .051 cm (.020 in.) clearance. The 70° knife angle reduces leakage 5% and 9% for .025 cm (.010 in.) and .051 cm (.020 in.) clearances, respectively.

Figures 70 and 71 are cross-plots of the data in Figures 67, 68, and 69 as a function of pitch for the 70° and 50° knife angles, respectively. These results show that pitch and knife angle interact to exert a significant influence on the seal performance. Generally, a 70° or 50° knife angle was found to reduce leakage. Only one exception at .025 cm (.010 in.) clearance was found in the range of advanced seal parameters investigated. The 50° knife angle at .508 cm (.200 in.) pitch increased leakage 2%. However, these data indicate that the 50° knife angle is best for a knife pitch of .762 cm (.300 in.) or larger. Since a .762 cm (.300 in.) pitch was selected for the optimized advanced seal design, the 50° knife angle was the optimum choice.

Optimum Advanced Seal Performance. A sketch of the optimum advanced seal design for the LTSD flow direction that was derived from evaluating the geometric parameters is presented in Figure 72. The optimized parameters are:

Step Height:	.305 cm (.120 in.)
Knife Height:	.381 cm (.150 in.)
Knife Pitch:	.762 cm (.300 in.)
Knife Angle:	50°

The performance of the optimum advanced seal in the LTSD configuration was mapped in the 2D test rig. The influence of the axial clearance and the number of knives were determined. The performance contributions from the step notch was investigated, also.

Design parameters related to some requirements of the seal application were studied in the 3D test rig. The effects of flow direction and land materials on the performance of the optimum advanced seal were investigated. The interaction of rotation with seal leakage was measured at 80 m/s (261 ft/sec), 159 m/s (523 ft/sec), and 239 m/s (785 ft/sec) knife tip speeds.

Performance Mapping in the 2D Test Rig. The aerodynamic test results from the 2D rig for the LTSD optimized advanced seal design are presented in Figures 73 and 74 at .025 cm (.010 in.) and .051 cm (.020 in.) clearances, respectively. The performance of a 2D conventional stepped seal with the same knife pitch, step height, DTC, and LTSD flow direction has been included for comparison purposes. The optimized advanced seal achieved a significant reduction in seal leakage. At a 2.0 seal pressure ratio, leakage reductions of 11% at .025 cm (.010 in.) clearance and 21% at .051 cm (.020 in.) clearance were obtained relative to the 2D conventional stepped seal.

Land Notch Effect on Optimum Advanced Seal Performance. An evaluation of the seal land notch was conducted in the 2D rig for the optimized advanced seal design. The seal land notch was modified from the optimum geometry, Figure 75 (a), to a "half-notch" configuration, shown in Figure 75 (b), to represent a typical machining process which would be employed for economical manufacturing. The optimized seal was also evaluated with a conventional or "no-notch" land, shown in Figure 75 (c). The aerodynamic test results for the "full-notch", "half-notch", and "no-notch" lands in the optimized seal are presented in Figures 76 and 77. At a 2.0 pressure ratio, the performance with the full-notch showed leakage reduced 7% relative to the no-notch land. Similarly, the half-notch reduced leakage about 3%. Based on these results, which are summarized in Table 19, the full-notch land was determined to be an important design feature of the advanced seal configuration.

- Number of Knives Effect on Optimum Advanced Seal Performance. The optimized advanced seal was also evaluated in the 2D rig for three and two seal knives to complement the four knife information. The flow parameter characteristics for the four, three, and two knife optimized advanced seals at .025 cm (.010 in.) and .051 cm (.020 in.) clearances are presented in Figures 78 and 79, respectively. These results show that the overall discharge coefficient for the optimum advanced seal design is lower at the .051 cm (.020 in.) clearance than at the .025 cm (.010 in.) clearance. Table 20 summarizes the overall discharge coefficients at a 2.0 seal pressure ratio for the four, three, and two knife configurations. The discharge coefficients at .025 cm (.010 in.)

clearance are about 20% greater than they are at .051 cm (.020 in.) clearance.

Axial Clearance Effect on Optimum Advanced Seal Performance. The sensitivity of the optimized advanced seal design relative to the axial position of the seal knife on the land was also determined in the 2D rig. The distance-to-contact (DTC) is defined as the minimum axial distance of any part of the seal rotor (knife) from contact with any part of the land.

The nominal DTC for the optimized advanced seal was set at .254 cm (.100 in.) to accommodate a typical design requirement on axial rotor travel. The DTC results for the four, three, and two knife configurations at .051 cm (.020 in.) clearance are summarized in Figure 80. The DTC has a nominal influence on the performance of the optimum advanced seal.

The scope of this program did not include obtaining similar DTC data for a conventional stepped seal. Since the DTC is probably an important consideration in the design and performance of a conventional stepped seal, this information should be generated in the near future to aid the designer and the performance analyst.

Performance Mapping in the 3D Test Rig. The optimized advanced seal design was fabricated in the LTSD configuration, shown in Figure 72, and in the STLD configuration, shown in Figure 81, for testing in the 3D air seal test rig. An "Abradable A" land, a honeycomb land of .159 cm (.062 in.) cell size, and a solid-smooth land were tested in combination with the STLD rotor. The LTSD rotor was tested with the solid-smooth land. The abradable and honeycomb materials were installed in each land as .254 cm (.100 in.) thick inserts. The optimum advanced seal hardware tested in the 3D rig is shown in Figures 82 through 86.

The flow parameters measured in the 3D rig at static and dynamic test conditions for the advanced seal with a solid-smooth land are presented in Figures 87 and 88 for the LTSD and STLD flow directions, respectively. The flow parameters for the abradable and honeycomb advanced seals in the STLD flow direction are presented in Figures 89 and 90, respectively. All testing of the advanced seals in the 3D rig was accomplished at .051 cm (.020 in.) radial clearance. These results are summarized in Table 21.

The 3D rig test results show that the leakage through the LTSD advanced seal with a solid-smooth land was very similar to, but slightly higher than, that in the 2D rig. The 2D rig test results demonstrated a 21% reduction in leakage with the optimized advanced seal design compared with the 2D conventional stepped seal at 2.0 pressure ratio. The 3D rig tests show a 17% reduction in static leakage relative to the same 2D baseline seal.

Rotational Effect on Optimum Advanced Seal Performance. The rotational effect of the seal knife on leakage in the LTSD flow direction is small, as shown in Figure 87. The optimized advanced seal experienced only a 2% leakage reduction from static performance at a 2.0 pressure ratio for the maximum knife tip speed of 239 m/s (785 ft/sec). Negligible change from static performance was measured at 80 m/s (261 ft/sec) and 159 m/s (523 ft/sec) knife tip speeds. The effect of rotation on the optimized advanced seal is similar to the effect of rotation on a conventional LTSD stepped seal (Reference 1).

The rotational effect on the STLD advanced seal leakage is greater than that on the LTSD design, as shown in Figure 88. The maximum rotational speed tested reduces the advanced seal leakage 6% compared to 3% for a conventional STLD stepped seal (Reference 1). The advanced seal leakage flow in the STLD direction shows a reduction, compared to a conventional stepped seal at a 2.0 pressure ratio, of 24% statically and 27% at 239 m/s (785 ft/sec) knife tip speed.

The STLD configuration of the advanced seal design has 9% less leakage statically and 13% less leakage dynamically than the LTSD configuration. A comparison, at a 2.0 pressure ratio, of the advanced seal performance for leakage in the LTSD and STLD flow directions is presented in Figure 91 for the 3D rig static and dynamic test conditions.

The seal rotational effects for the porous material abradable land and honeycomb land are included in Table 21. These data show that rotation reduces leakage 7% for the abradable land at 239 m/s (785 ft/sec). However, the honeycomb land experienced a 6% leakage increase at the same conditions. An increase in honeycomb land leakage flow with seal rotation was also found for a straight-through seal. Figure 92 is a plot summarizing the effects of rotation on the optimized advanced seal using a LTSD solid-smooth land and on the advanced seal using a STLD solid-smooth land, an abradable land, and a honeycomb land.

The performance for the abradable land and the honeycomb land is compared to a solid-smooth land in Table 22 for the STLD configuration of the advanced seal at a 2.0 pressure ratio. A plot of these results in Figure 93 shows the performance penalty to be about 15% for the abradable land and above 50% for the honeycomb land. The abradable land performance is insensitive to seal rotation, but the honeycomb land performance deteriorates with increasing rotor speed. The leakage increase with the "Abradable A" material land was expected and falls within the range of the experimental results discussed earlier for porous abradable material lands. However, the large increase in honeycomb land leakage was unexpected. The tests conducted on conventional straight-through seals in the 2D and 3D seal rigs showed that honeycomb lands reduced leakage, particularly at .051 cm (.020 in.) clearance.

Conventional stepped seal performance with honeycomb lands was not obtained during the course of this program nor was any performance information found in the literature. The unusual response of the advanced seal with a honeycomb land will require more experimental evaluation to provide the necessary information to explain the leakage performance characteristic. In addition, conventional stepped seal performance with honeycomb lands should be generated to provide the engineer with sufficient knowledge to select the best labyrinth seal design for the dynamic environment.

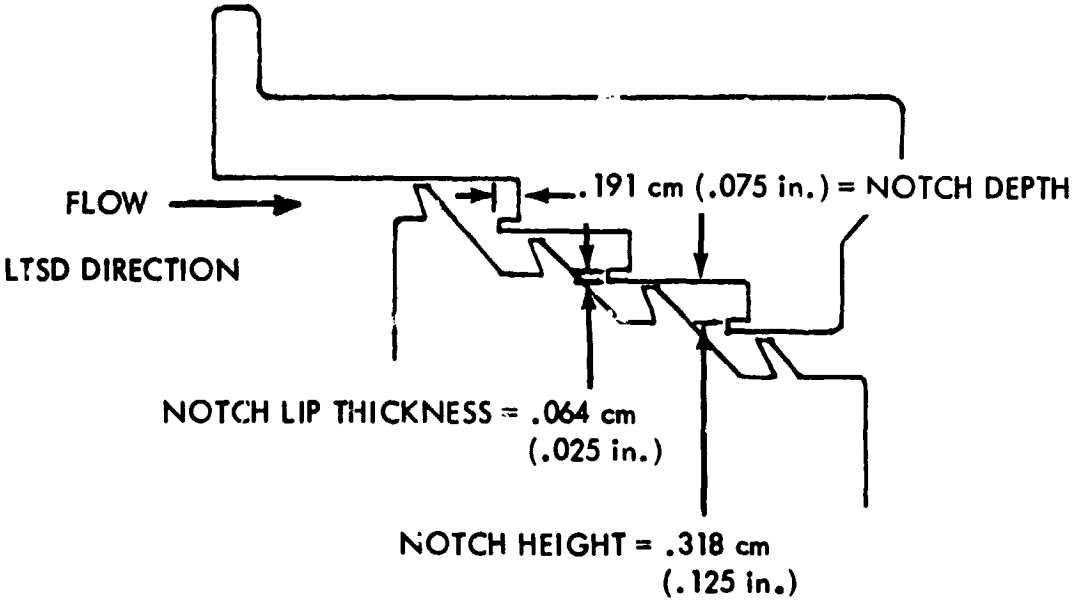

FIGURE 59. ADVANCED SEAL CONFIGURATION FROM REFERENCE 1 FOR PERFORMANCE OPTIMIZATION

FIGURE 60. EFFECT OF STEP HEIGHT ON THE FOUR KNIFE ADVANCED SEAL

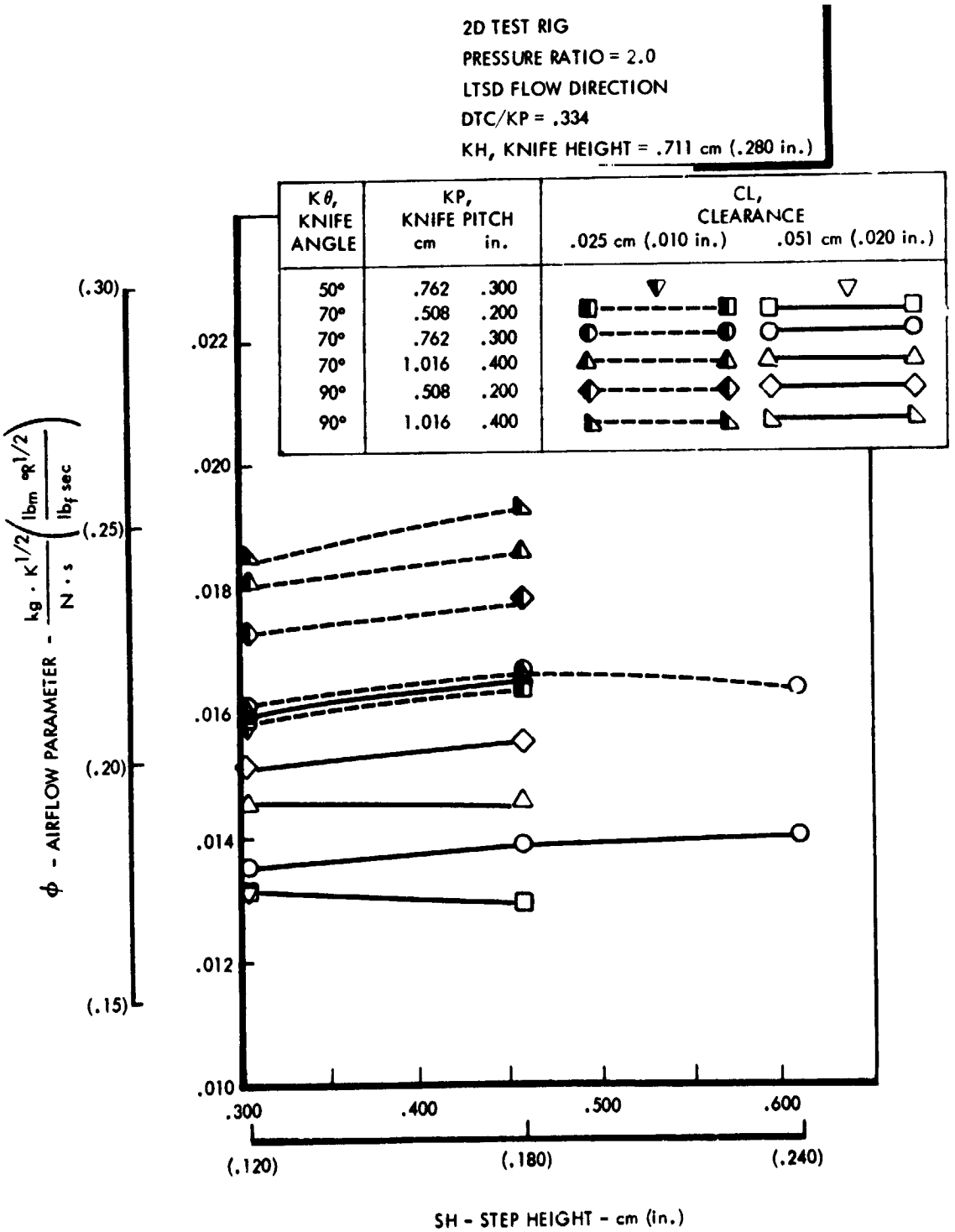

FIGURE 61. WAX-FILL OF 2D TEST RIG SEAL KNIFE HEIGHT

FIGURE 62. EFFECT OF KNIFE HEIGHT ON LEAKAGE THROUGH LTSD ADVANCED SEALS WITH FOUR VERTICAL KNIVES

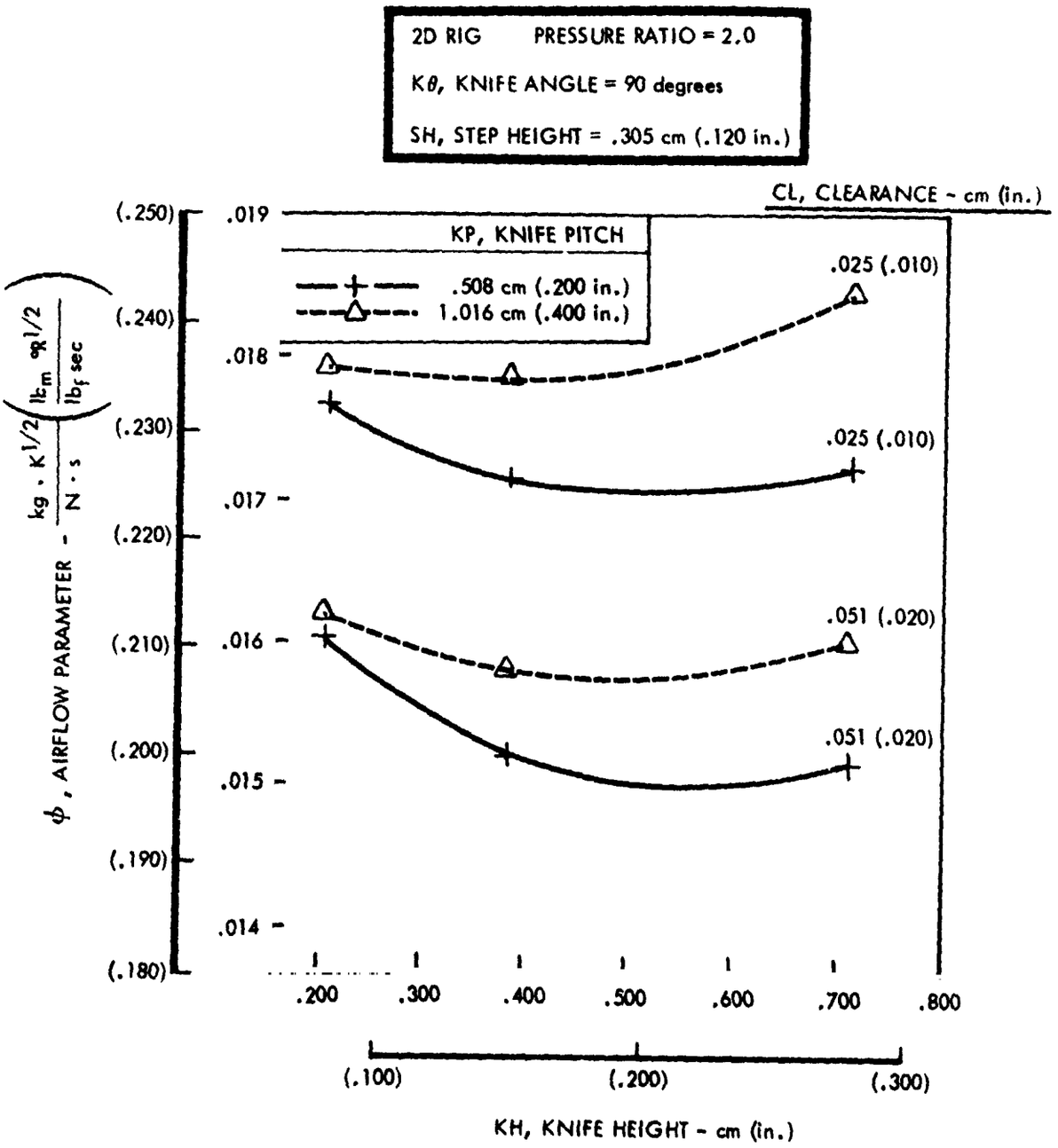

FIGURE 63. EFFECT OF KNIFE HEIGHT ON FOUR SLANTED KNIVES ADVANCED SEAL

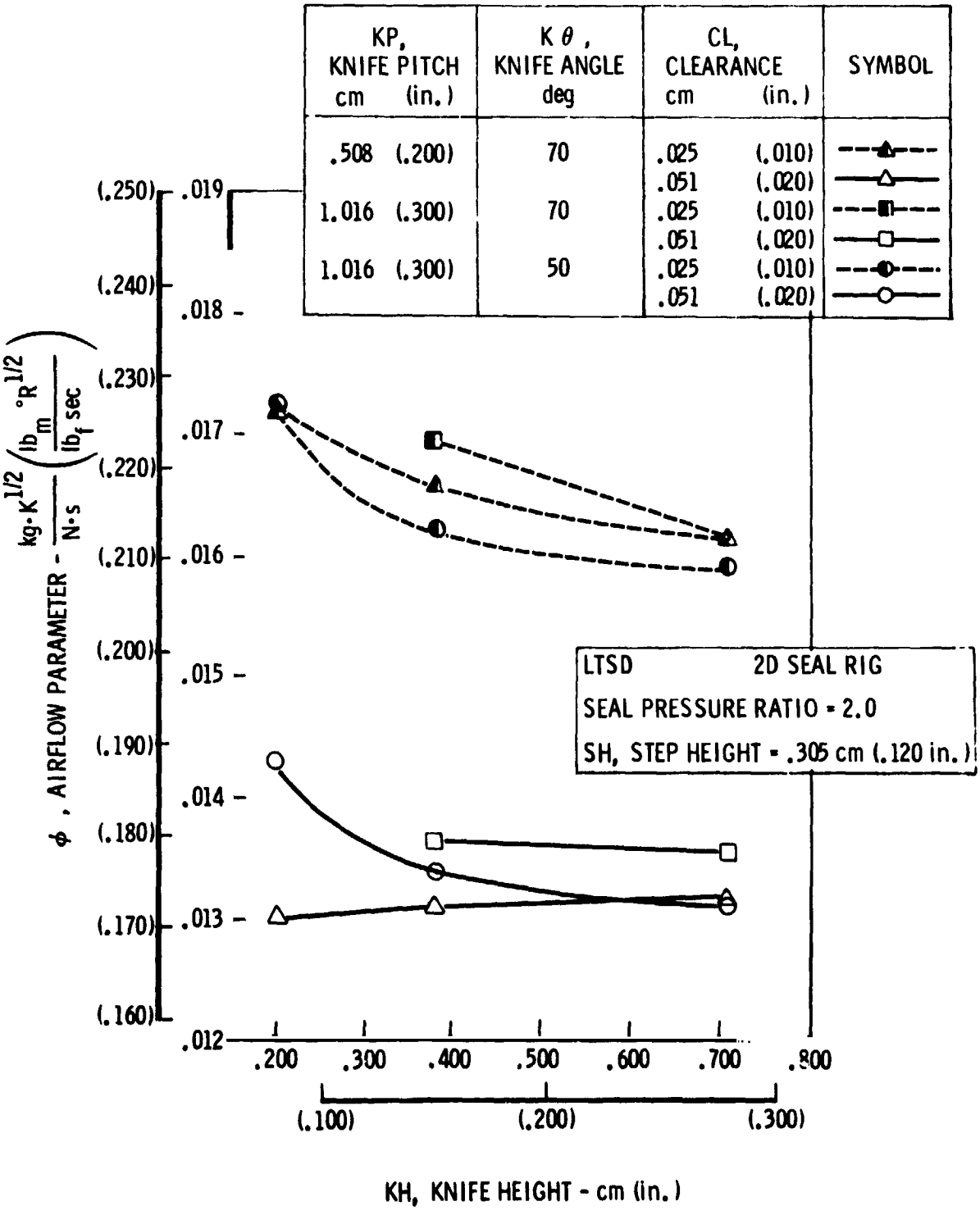

FIGURE 64. EFFECT OF KNIFE PITCH ON FOUR KNIFE ADVANCED SEAL AT THE OPTIMUM STEP HEIGHT

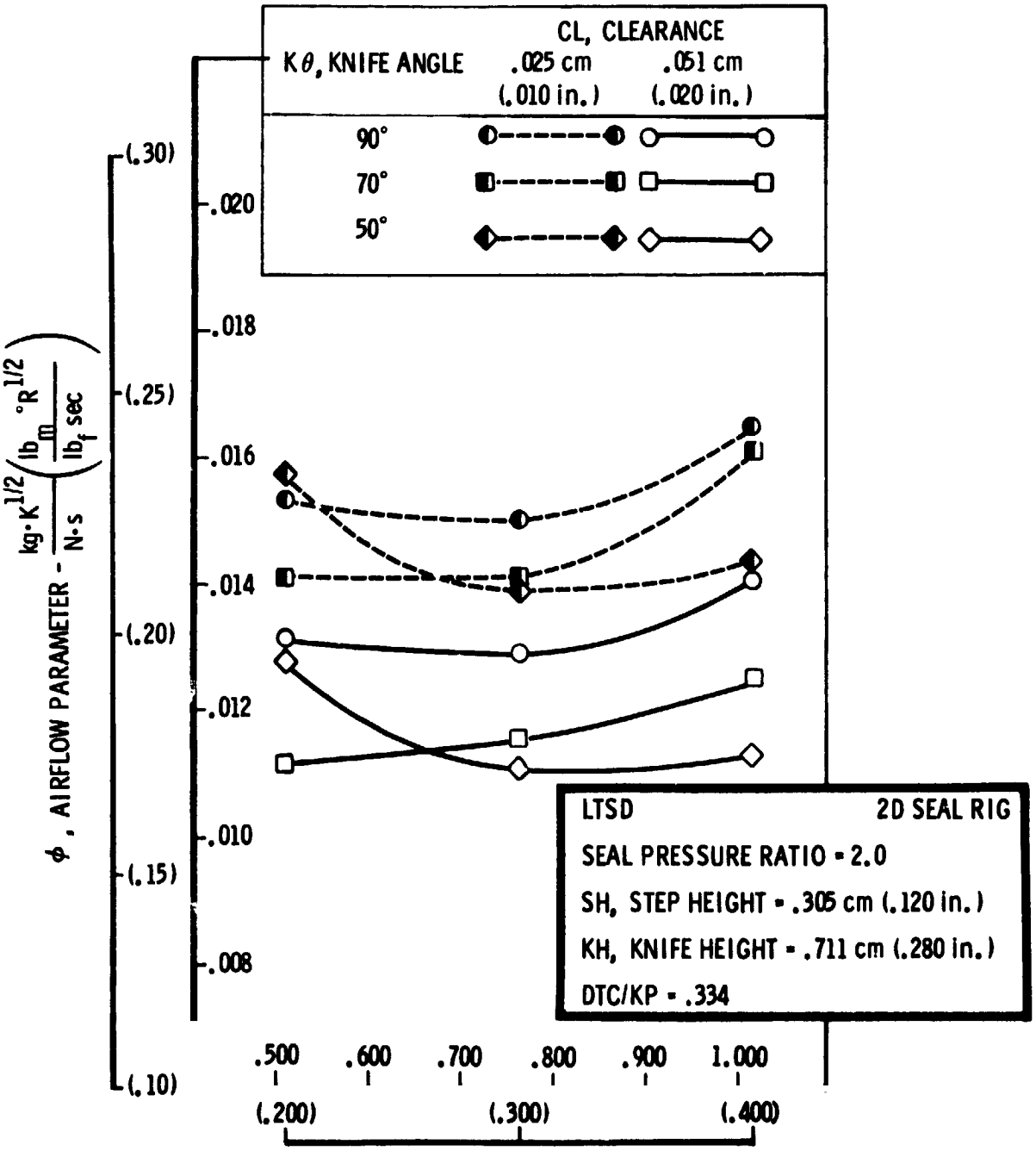

FIGURE 65. EFFECT OF KNIFE PITCH ON FOUR KNIFE ADVANCED SEAL WITH A 70° KNIFE ANGLE

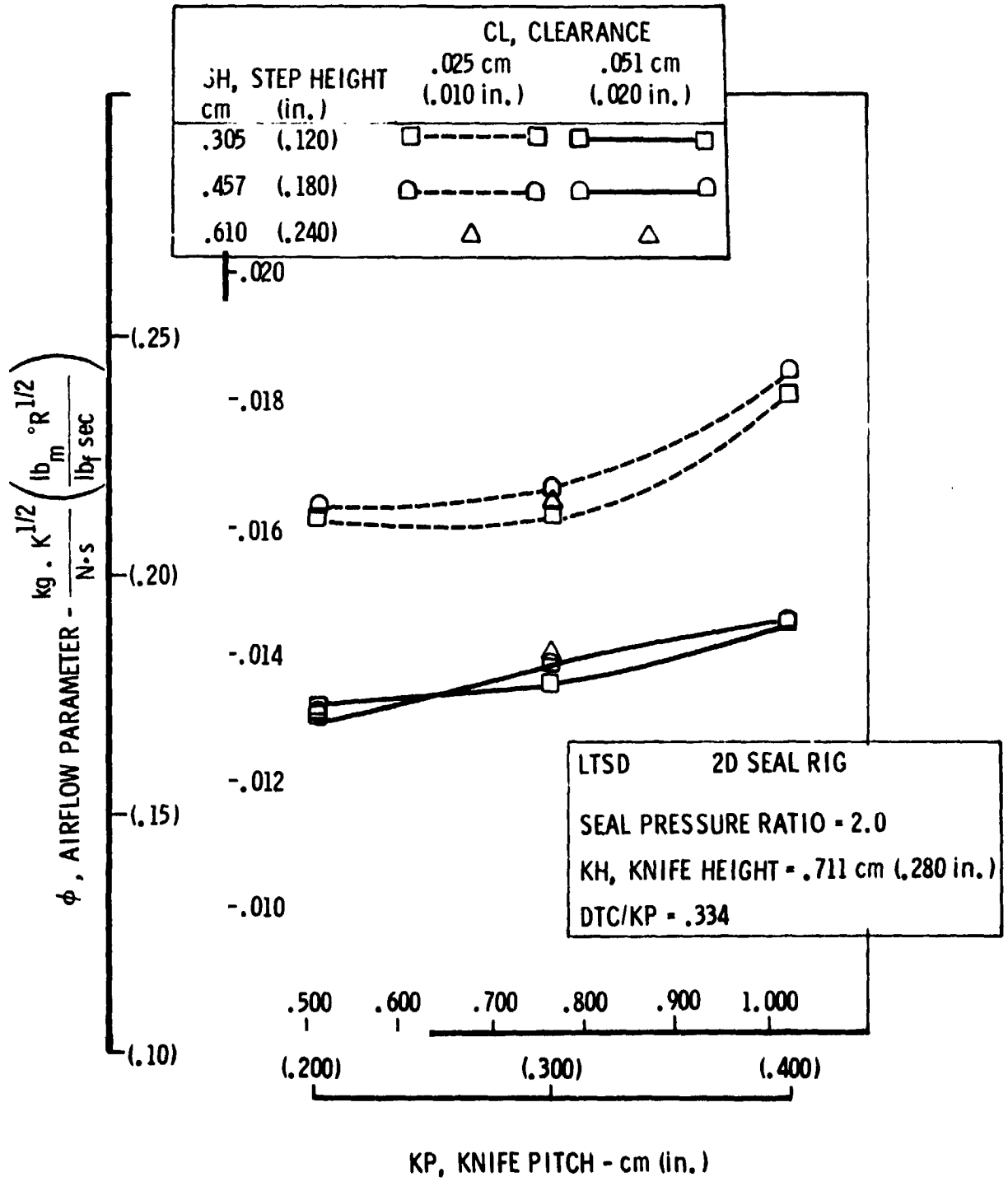

FIGURE 66. EFFECT OF KNIFE PITCH ON FOUR KNIFE STEPPED SEAL WITH A 90° KNIFE ANGLE

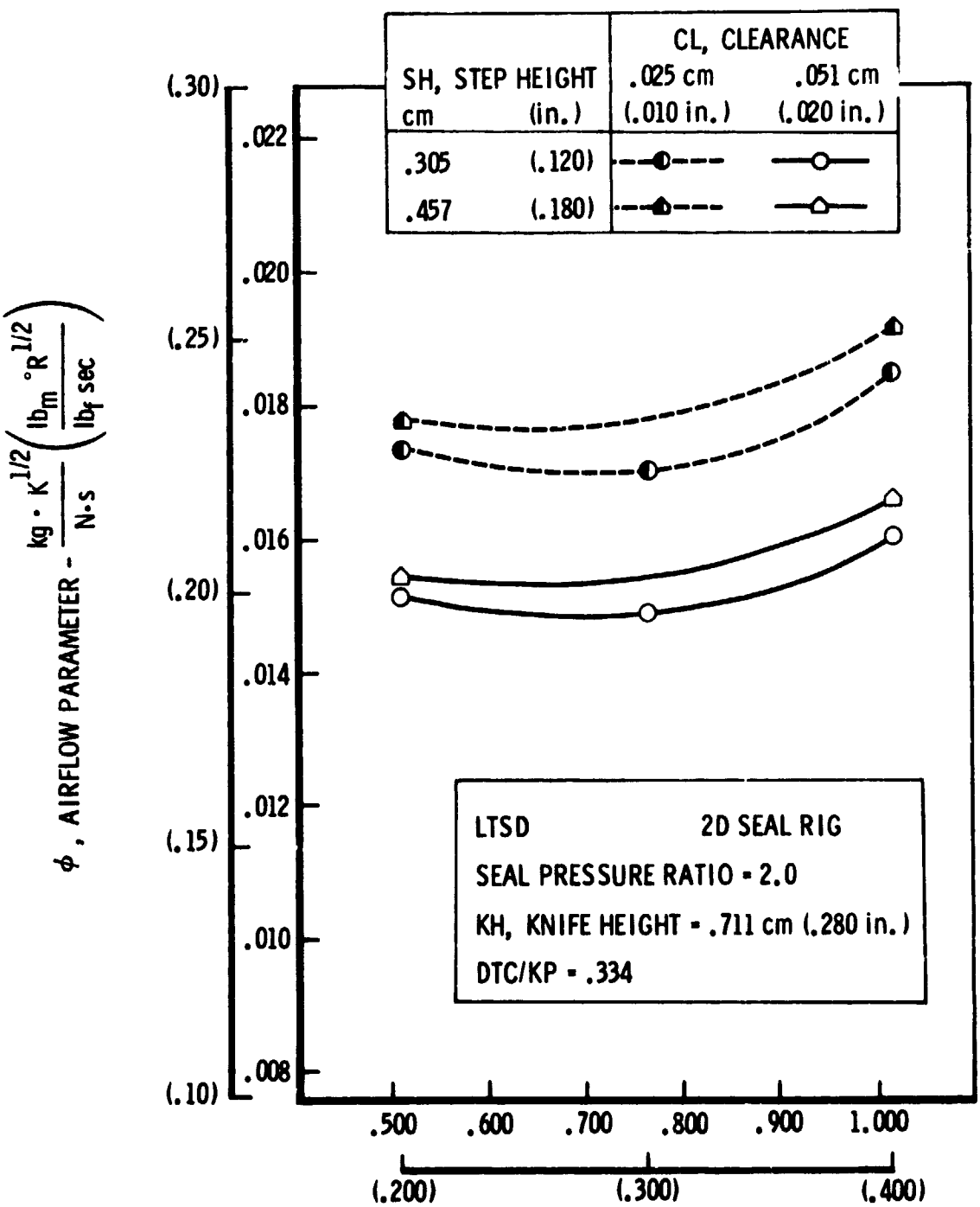

FIGURE 67. EFFECT OF KNIFE ANGLE ON FOUR KNIFE ADVANCED SEAL WITH A KNIFE PITCH = 1.016 cm (.400 in.)

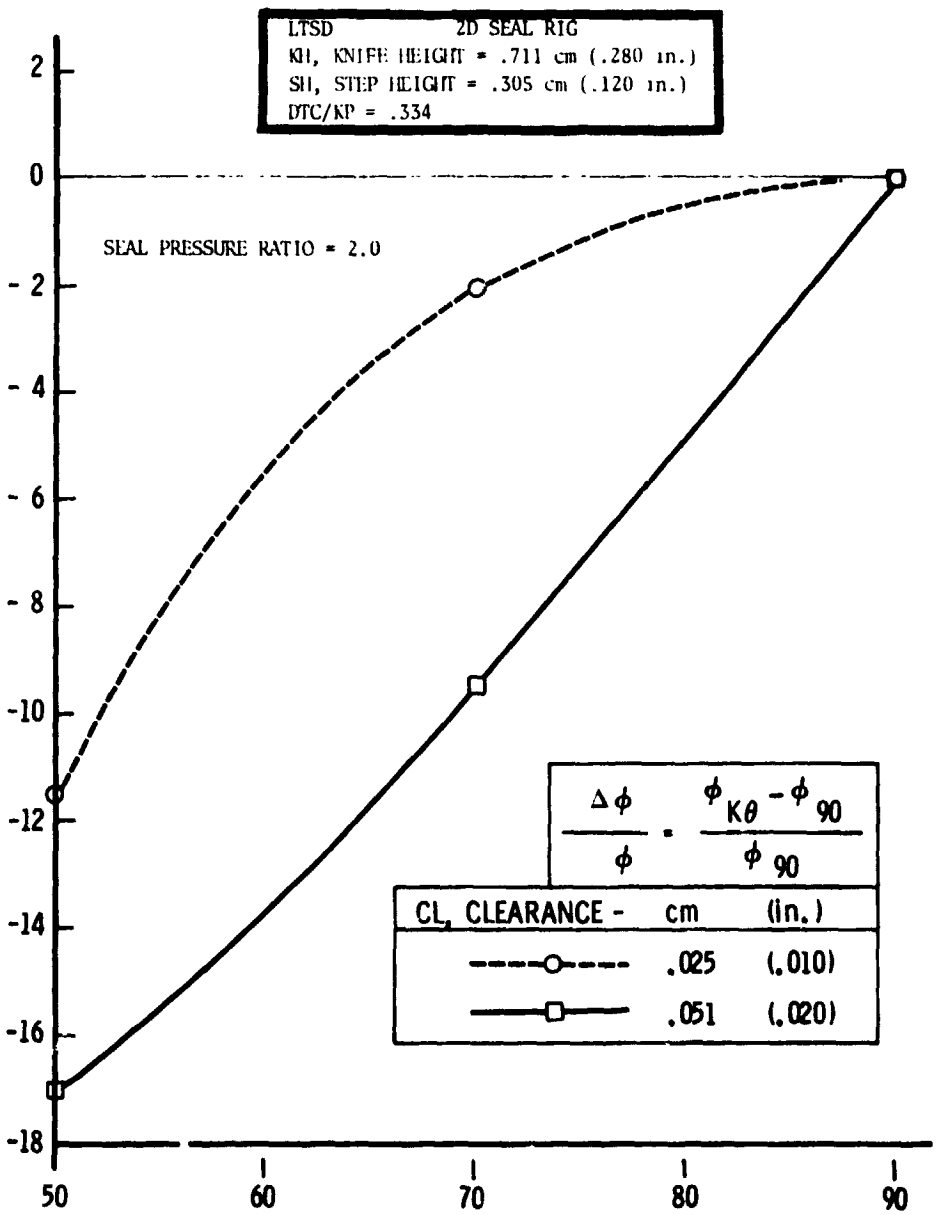

FIGURE 68. EFFECT OF KNIFE ANGLE ON FOUR KNIFE ADVANCED SEAL WITH A KNIFE PITCH = .762 cm (.300 in.)

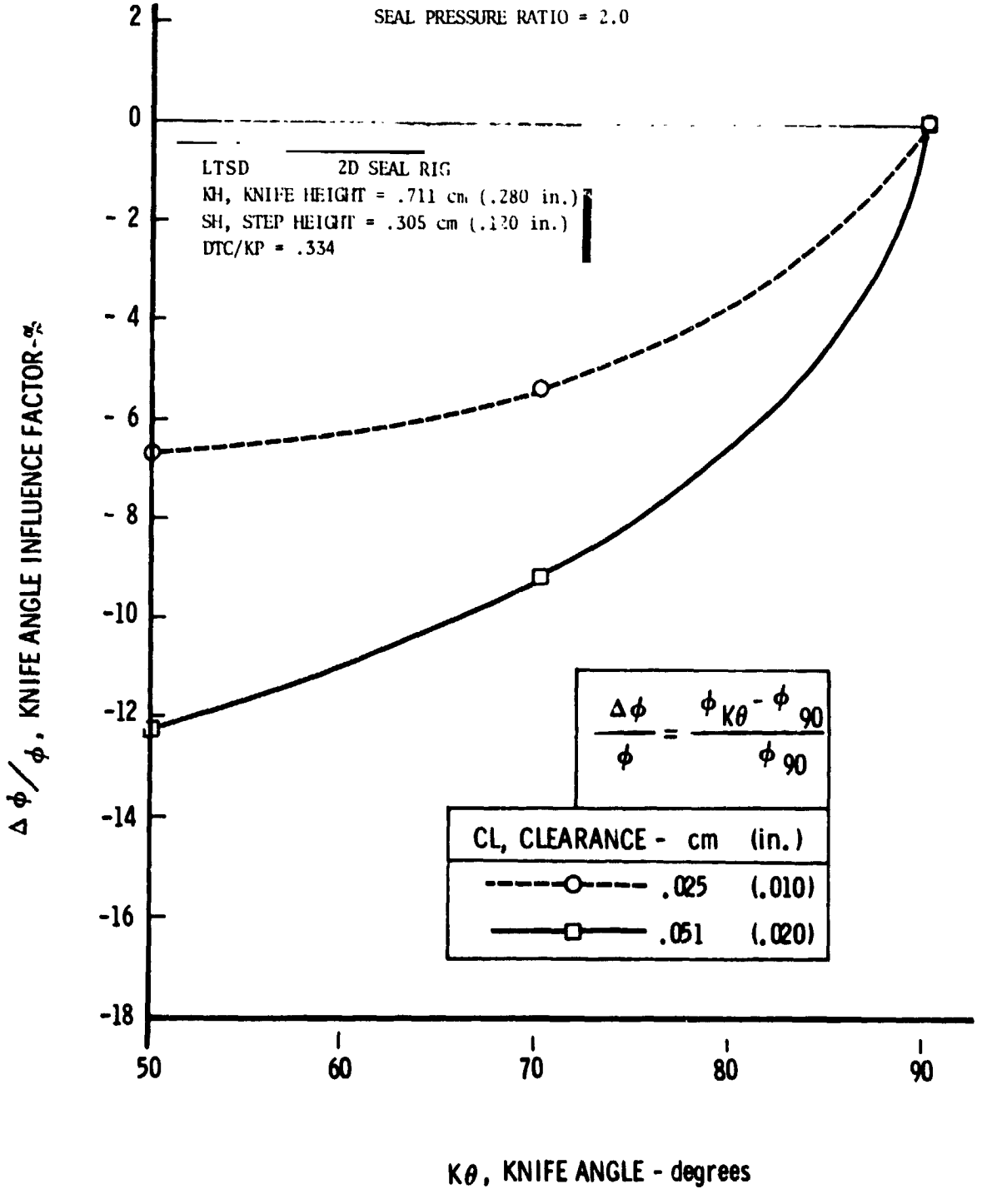

FIGURE 69. EFFECT OF KNIFE ANGLE ON FOUR KNIFE ADVANCED SEAL WITH A KNIFE PITCH = .508 cm (.200 in.)

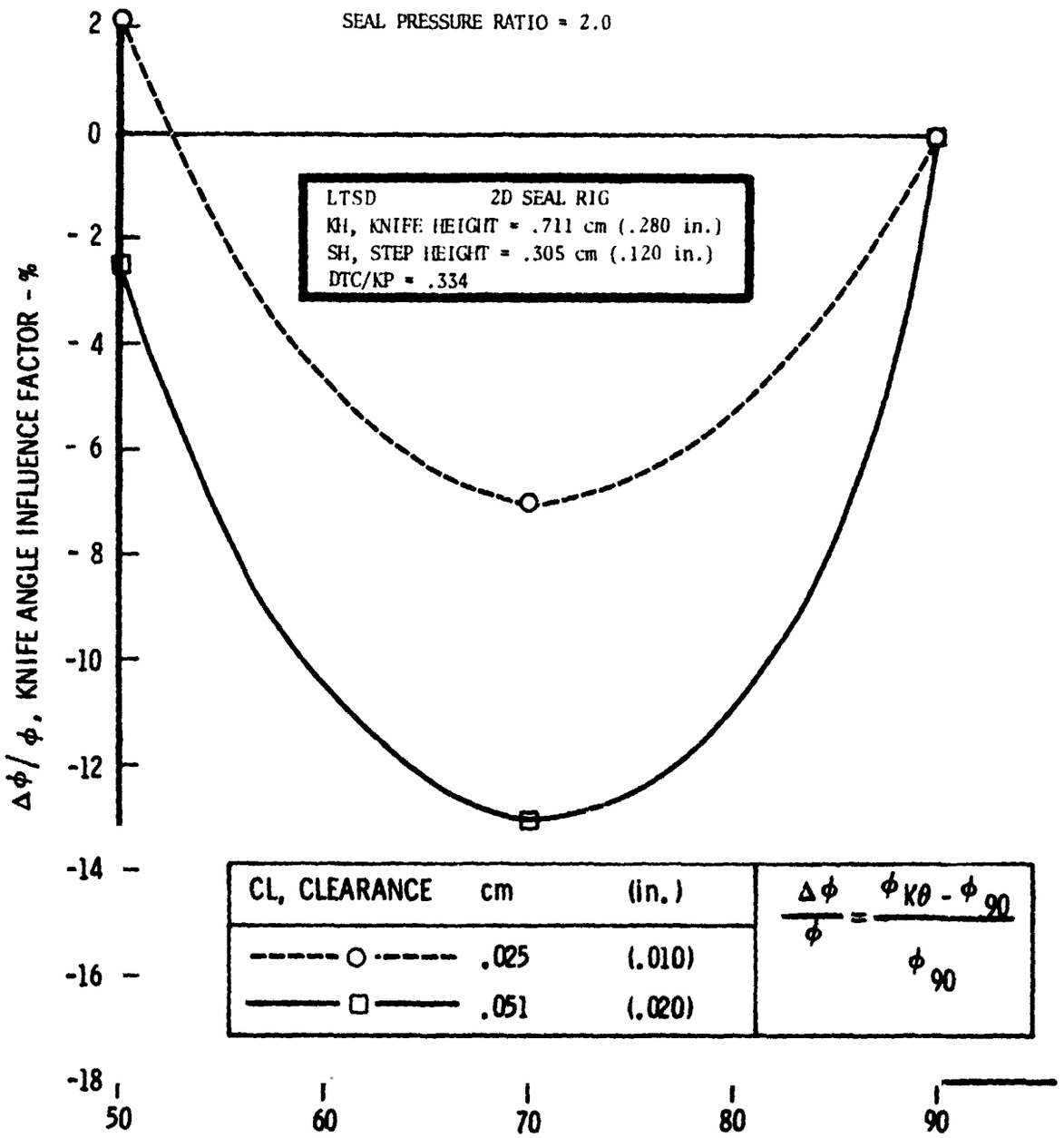

FIGURE 70. EFFECT OF PITCH ON KNIFE ANGLE INFLUENCE FACTOR FOR A FOUR KNIFE ADVANCED SEAL WITH A KNIFE ANGLE = 70°

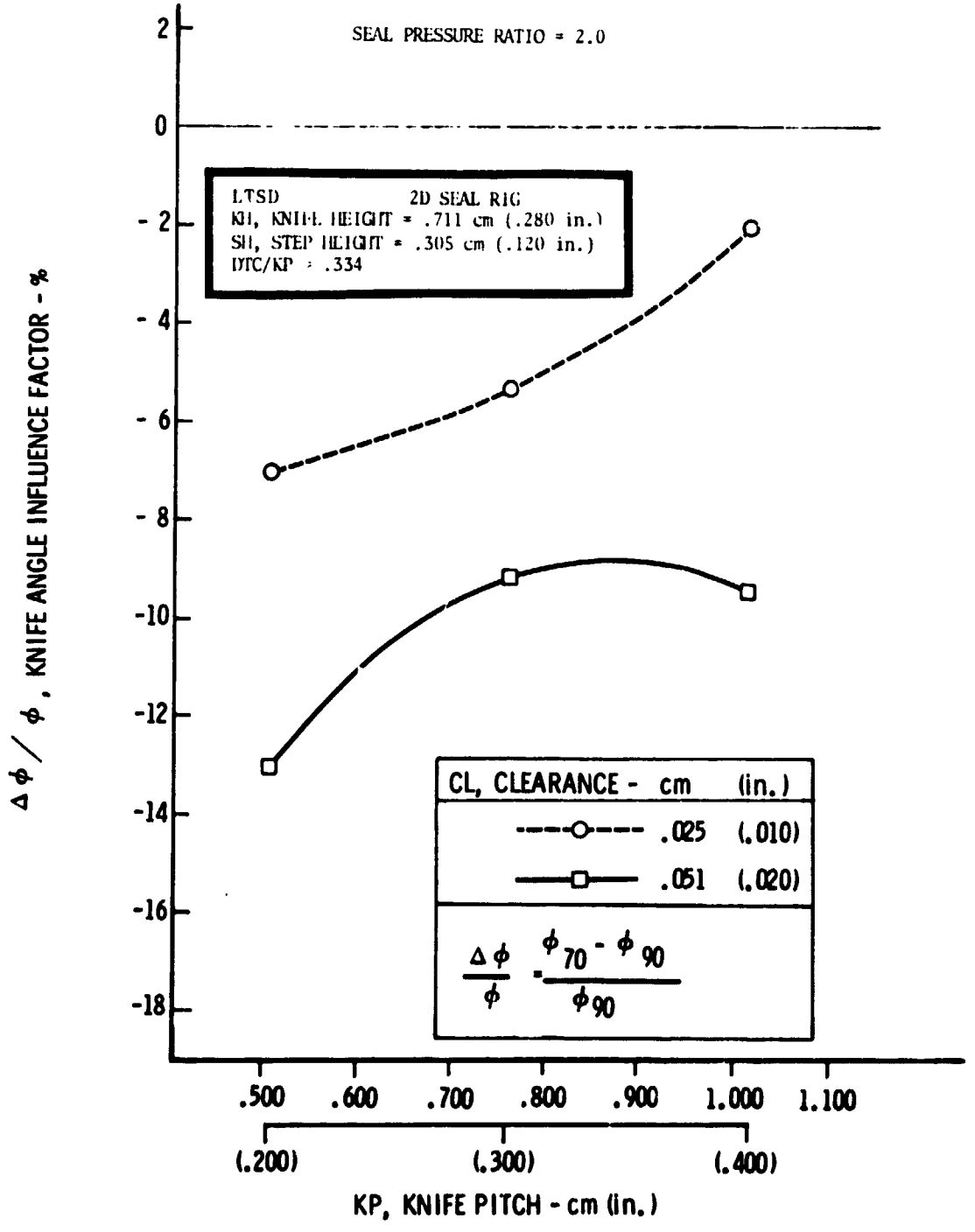

FIGURE 71. EFFECT OF PITCH ON KNIFE ANGLE INFLUENCE FACTOR FOR A FOUR KNIFE ADVANCED SEAL WITH A KNIFE ANGLE = 50°

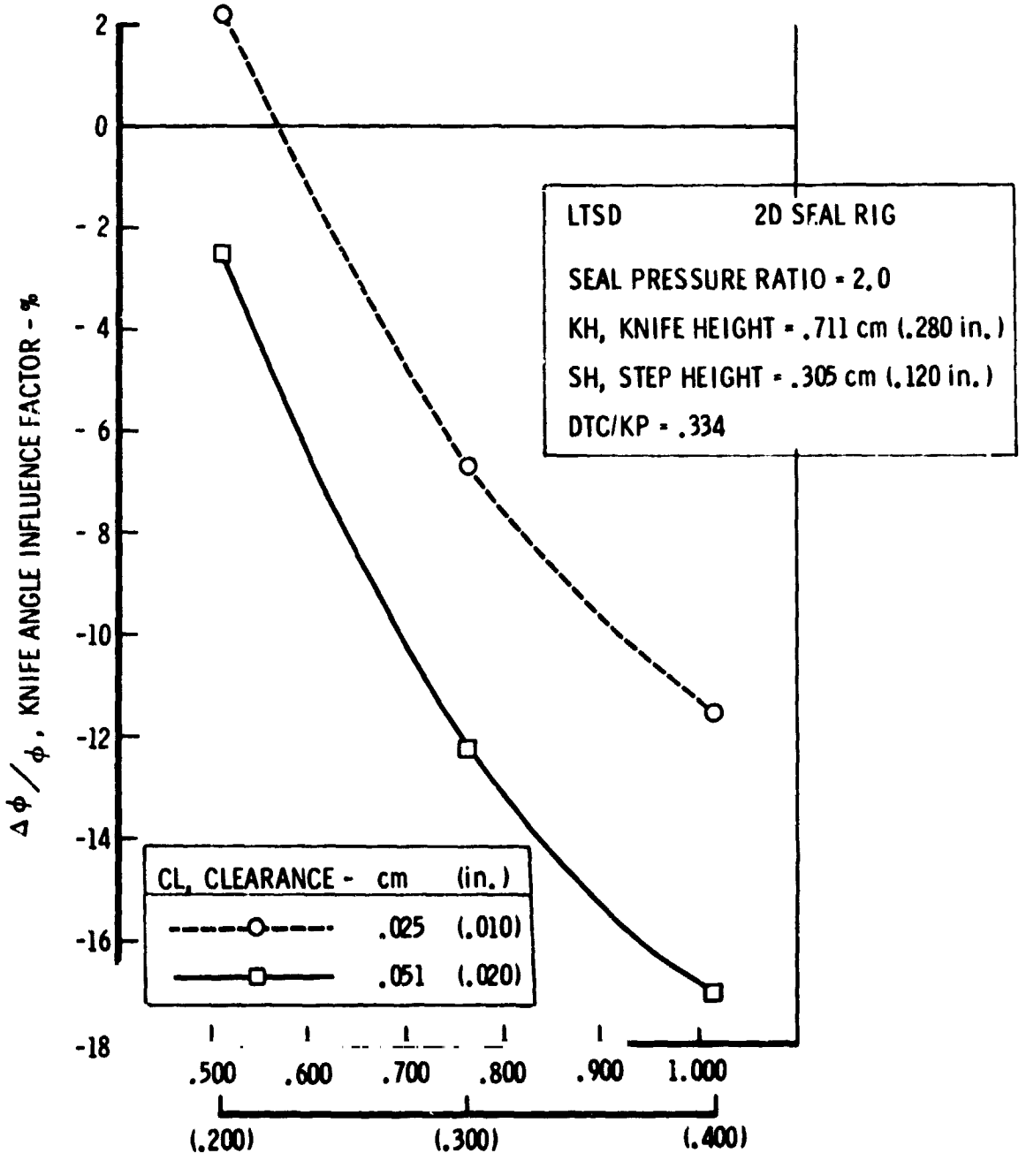

FIGURE 72. LTSD OPTIMIZED ADVANCED SEAL CONFIGURATION

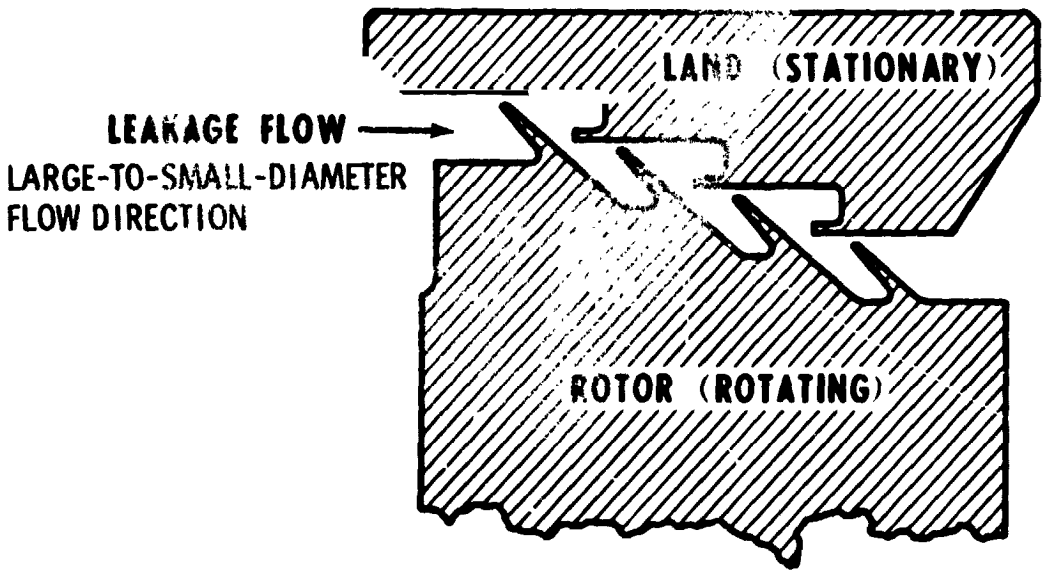

GEOMETRIC DEFINITION

PITCH = .762 cm (0.300 in.)
STEP HEIGHT = .305 cm (0.120 in.)
KNIFE HEIGHT = .381 cm (0.150 in.)
KNIFE ANGLE = 50 DEG

FIGURE 73. COMPARISON OF ADVANCED STEPPED SEAL PERFORMANCE WITH A CONVENTIONAL STEPPED SEAL - CLEARANCE = .025 cm (.010 in.)

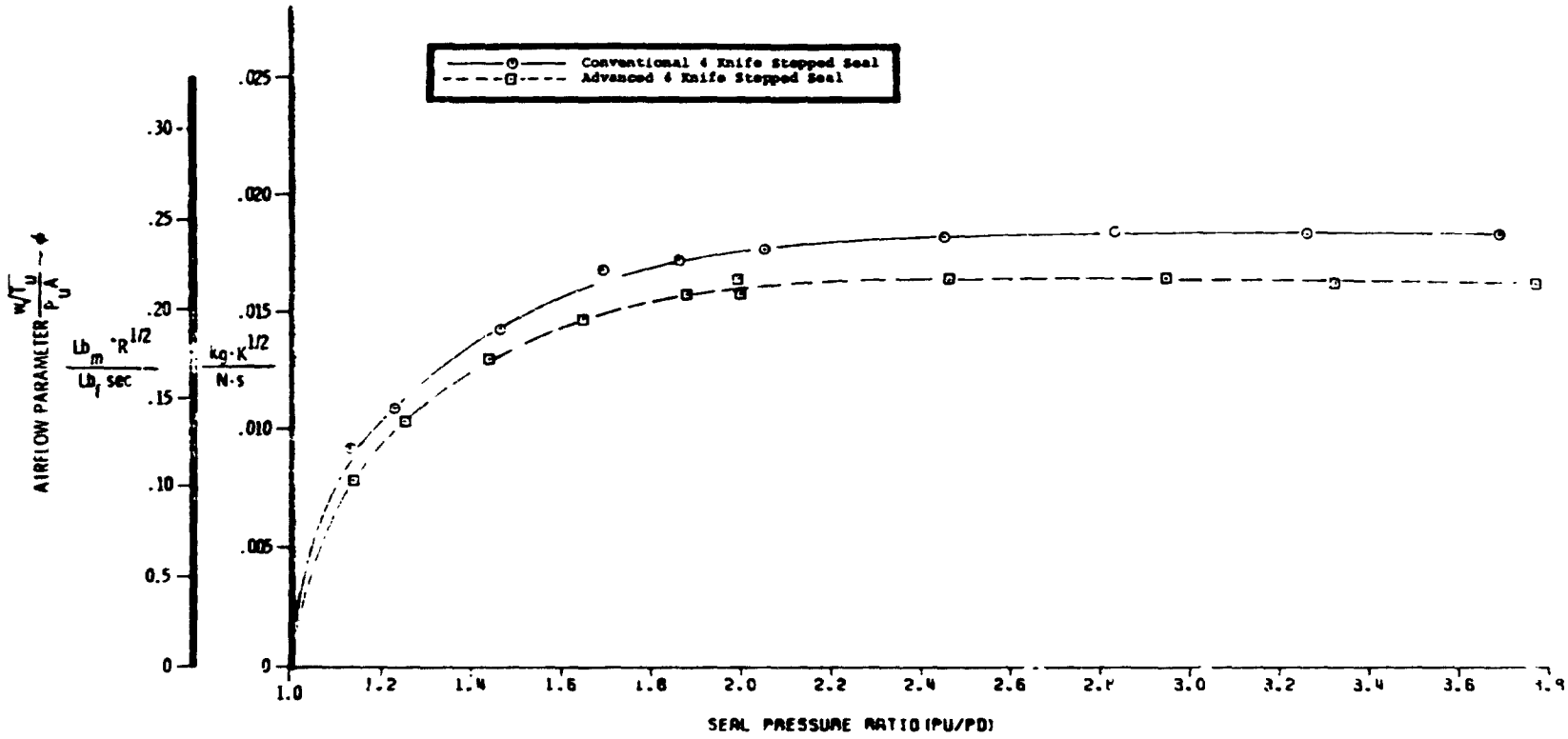

FIGURE 74. COMPARISON OF ADVANCED STEPPED SEAL PERFORMANCE WITH A CONVENTIONAL STEPPED SEAL - CLEARANCE = .051 cm (.020 in.)

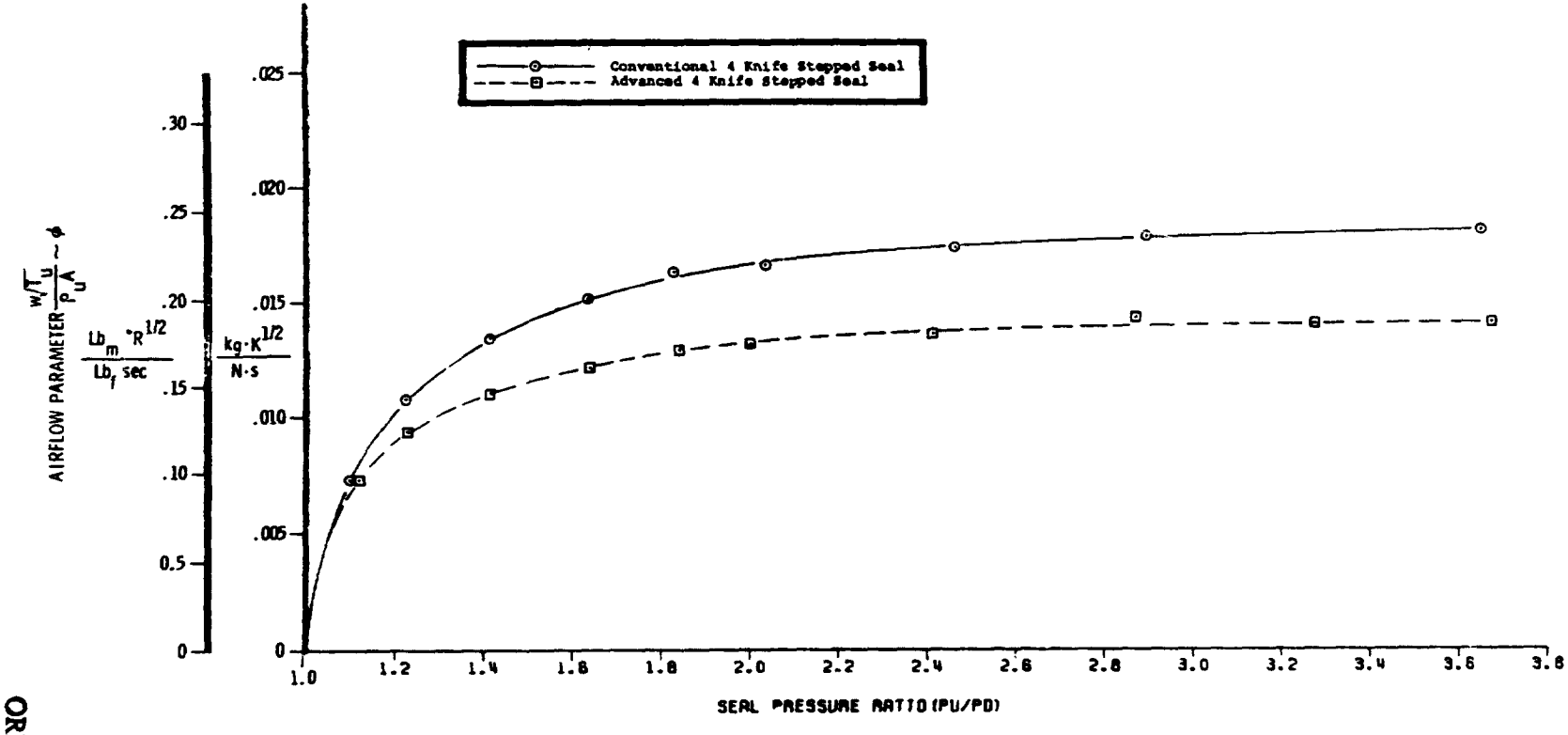

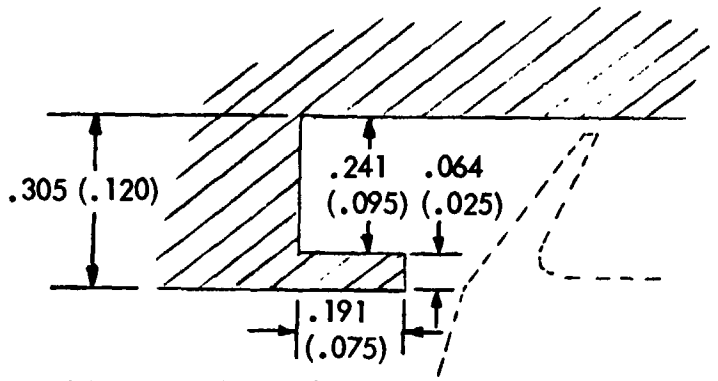

(a) FULL NOTCH ON STEP

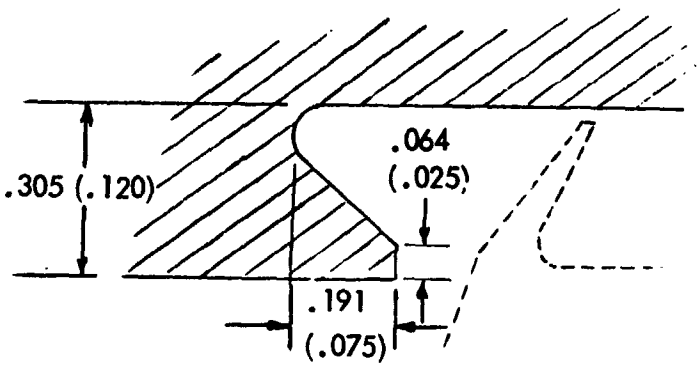

(b) HALF NOTCH ON STEP

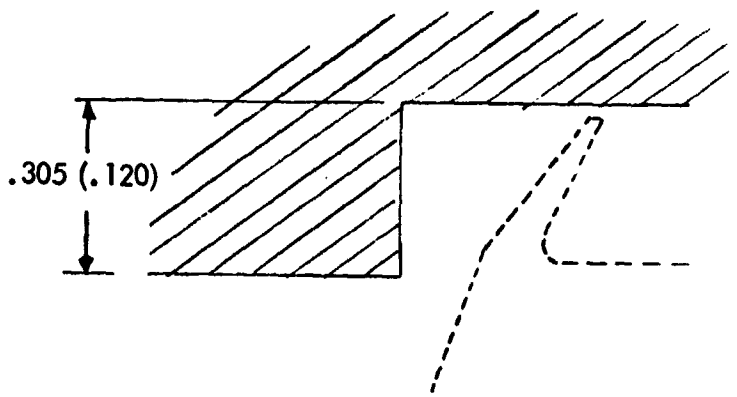

(c) NO NOTCH ON STEP (CONVENTIONAL STEP)

ALL DIMENSIONS ARE IN cm (in.)

FIGURE 75. SKETCH OF FULL-NOTCH, HALF-NOTCH, AND NO-NOTCH LAND CONFIGURATIONS TESTED

FIGURE 76. LAND NOTCH EFFECT ON THE LEAKAGE THROUGH THE LTSD OPTIMUM ADVANCED SEAL

FIGURE 77. LAND NOTCH EFFECT ON THE LEAKAGE THROUGH THE LTSD OPTIMUM ADVANCED SEAL

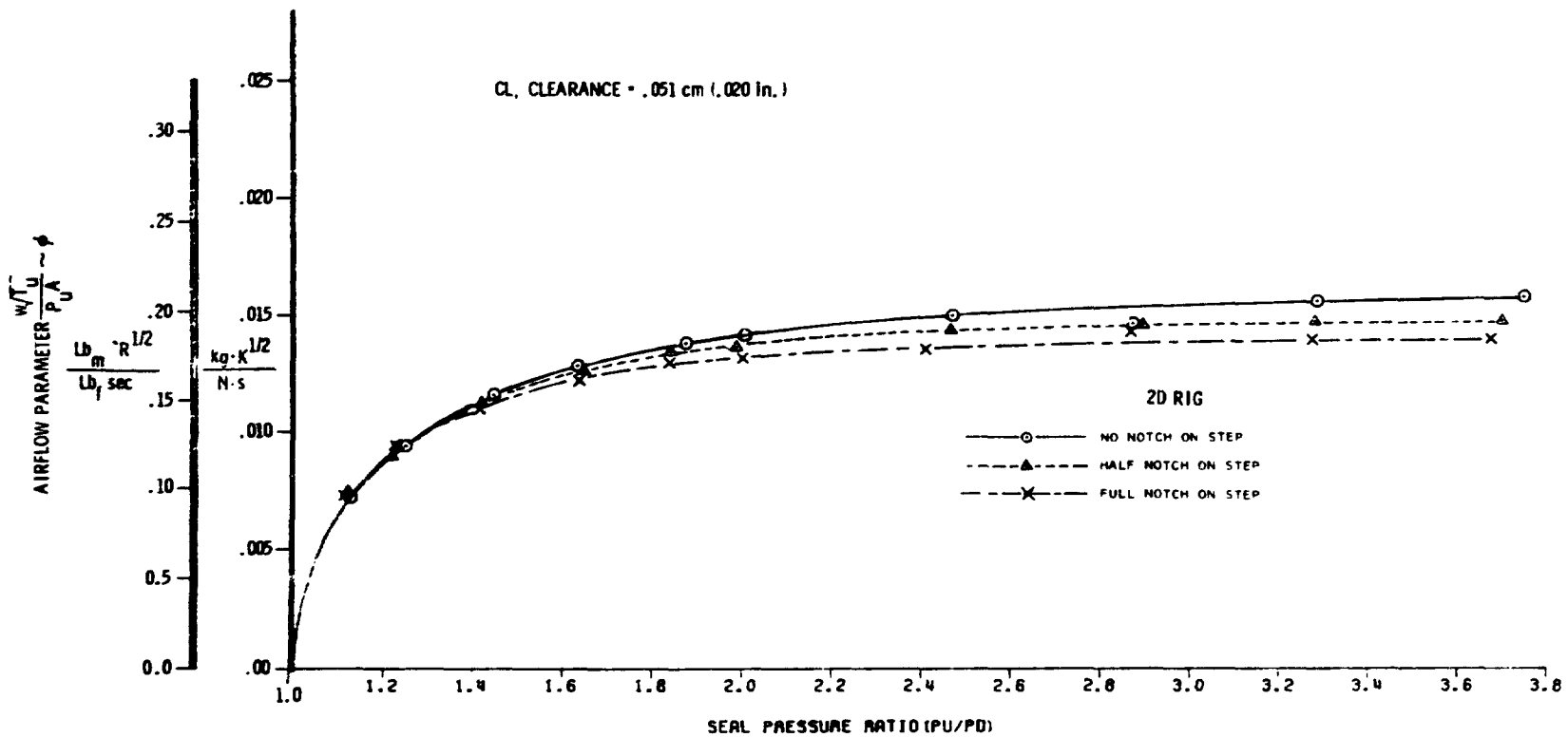

FIGURE 78. EFFECT OF THE NUMBER OF KNIVES ON THE LEAKAGE THROUGH THE LTSD OPTIMUM ADVANCED SEAL

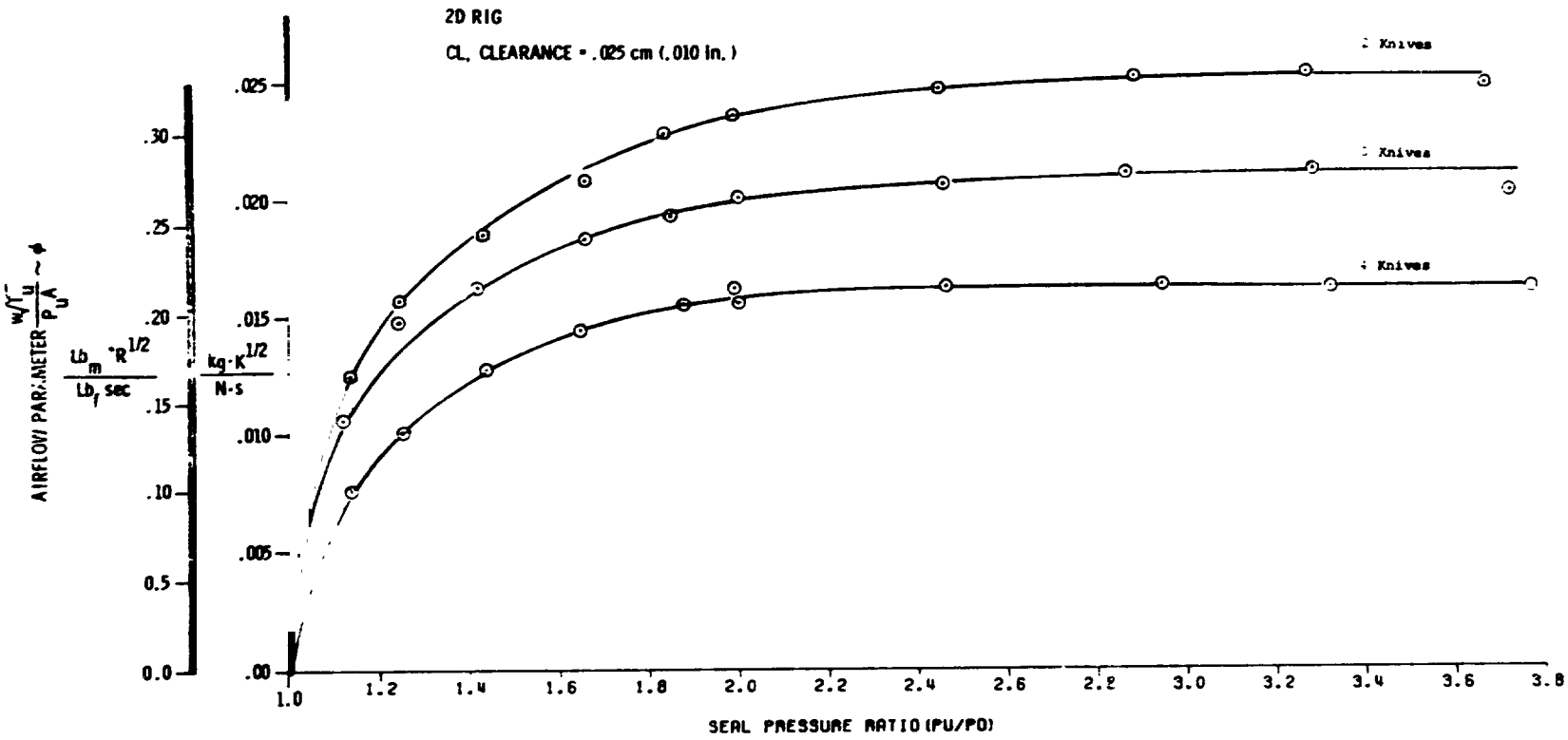

FIGURE 79. EFFECT OF THE NUMBER OF KNIVES ON THE LEAKAGE THROUGH THE LTSD OPTIMUM ADVANCED SEAL

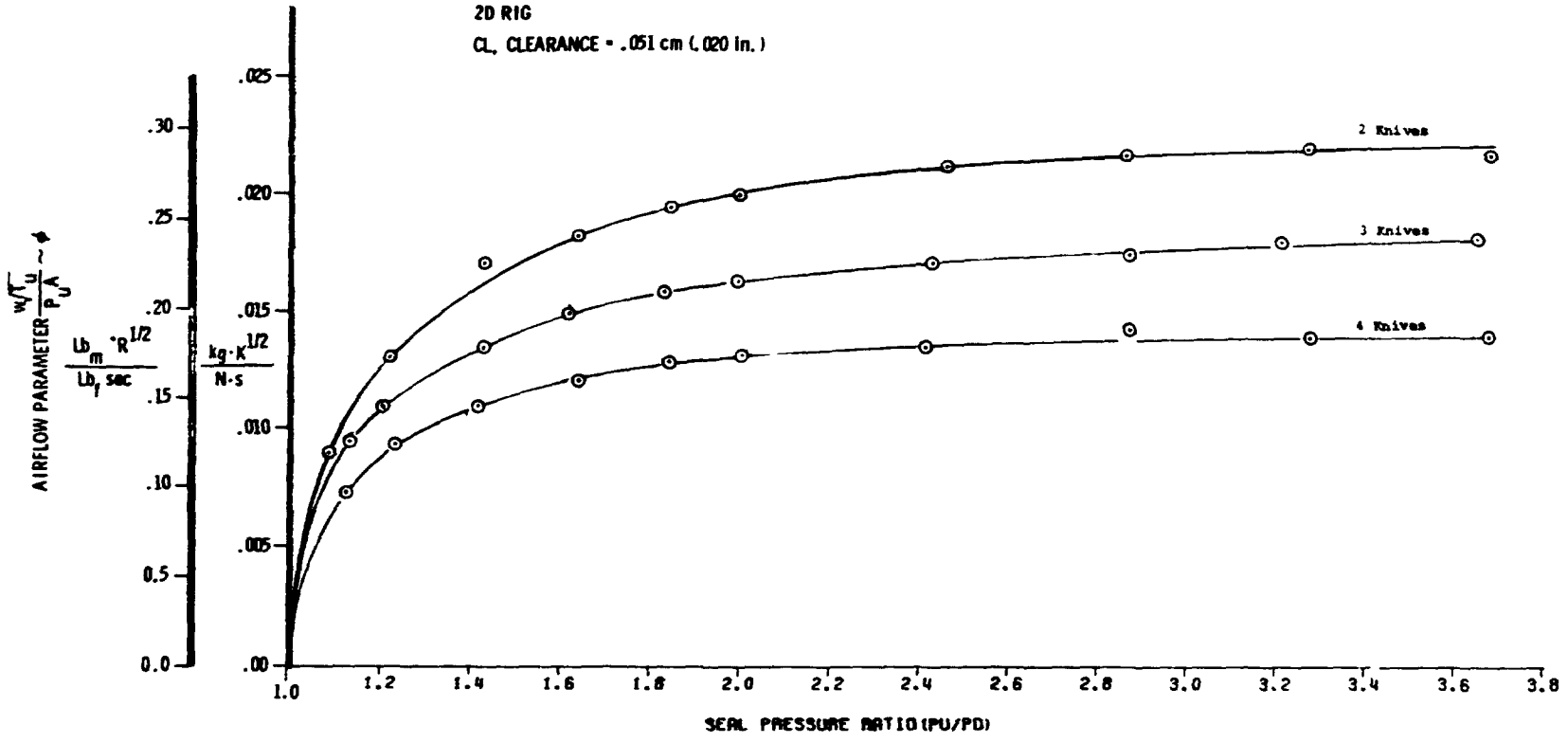

FIGURE 80. EFFECT OF DISTANCE-TO-CONTACT(DTC) AND NUMBER OF KNIVES ON LEAKAGE THROUGH THE OPTIMUM ADVANCED SEAL AT A CLEARANCE = .051cm(.020 in.)

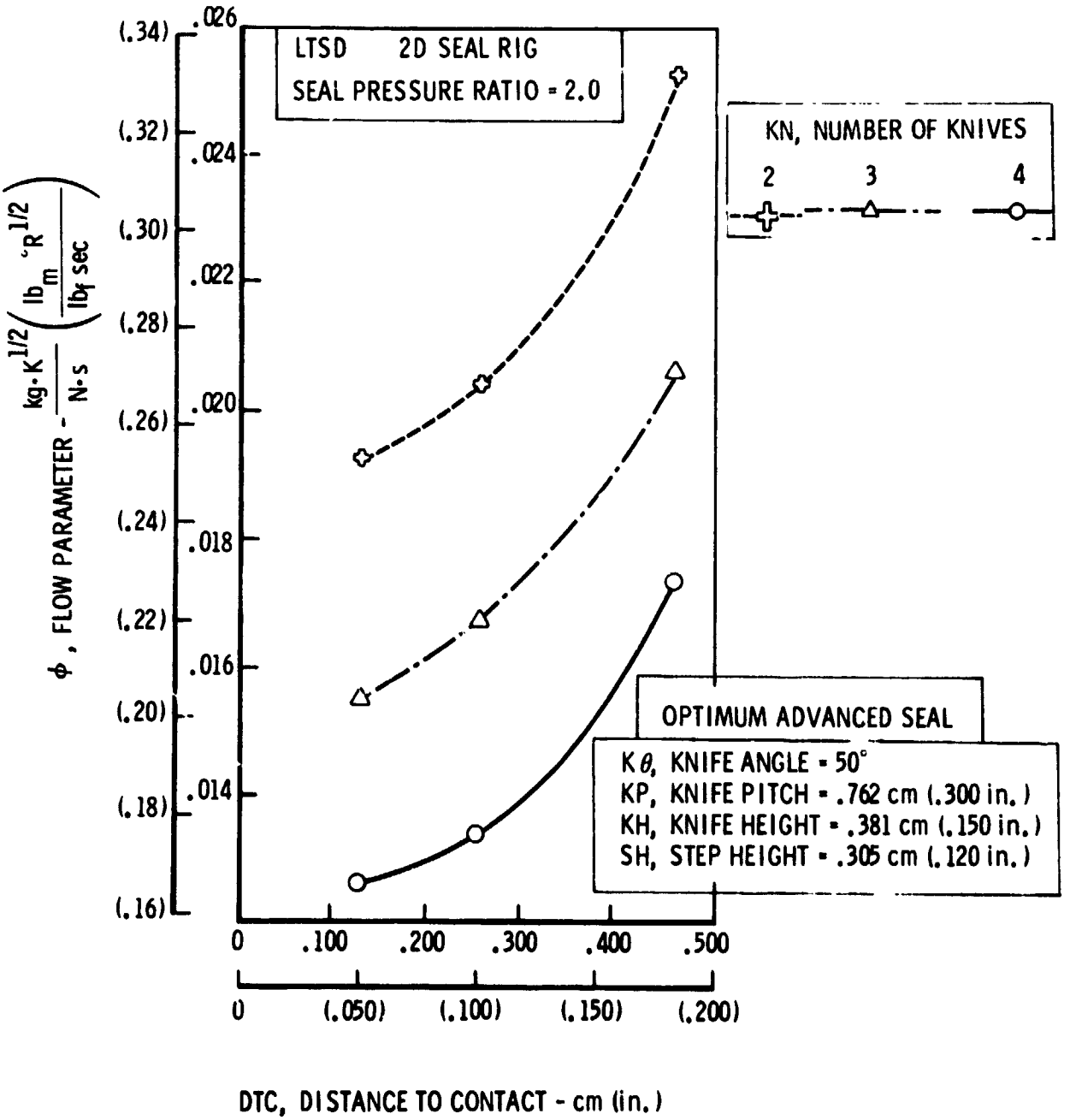

FIGURE 81. STLD OPTIMIZED ADVANCED SEAL CONFIGURATION

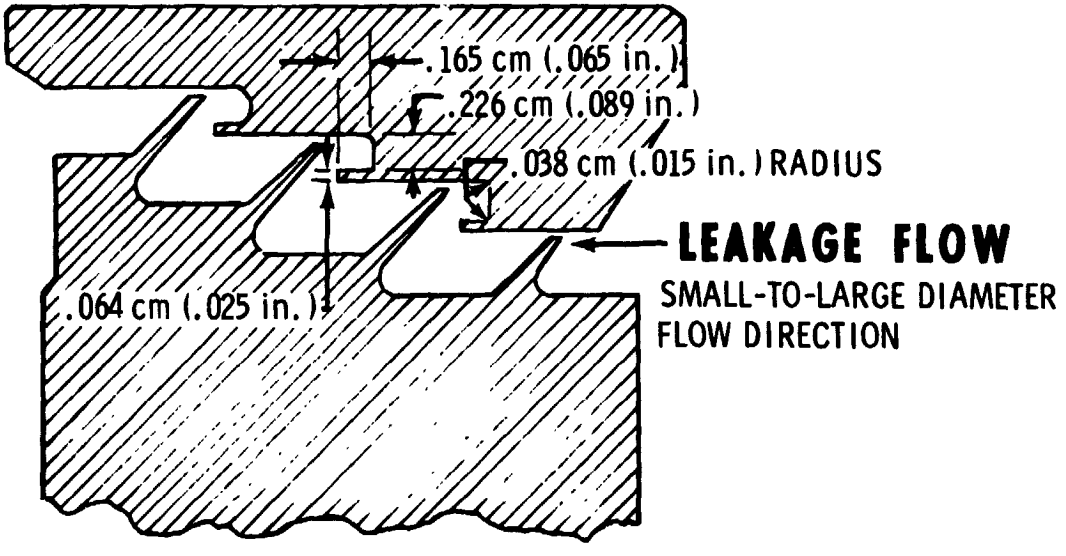

GEOMETRIC DEFINITION

PITCH = .762 cm (0.300 in.)
STEP HEIGHT = .305 cm (0.120 in.)
KNIFE HEIGHT = .381 cm (0.150 in.)
KNIFE ANGLE = 50 DEG

FIGURE 82. SOLID-SMOOTH LAND OF THE OPTIMIZED ADVANCED SEAL FOR THE 3D RIG

FIGURE 83. "ABRADABLE A" LAND OF THE OPTIMIZED ADVANCED SEAL FOR THE 3D RIG

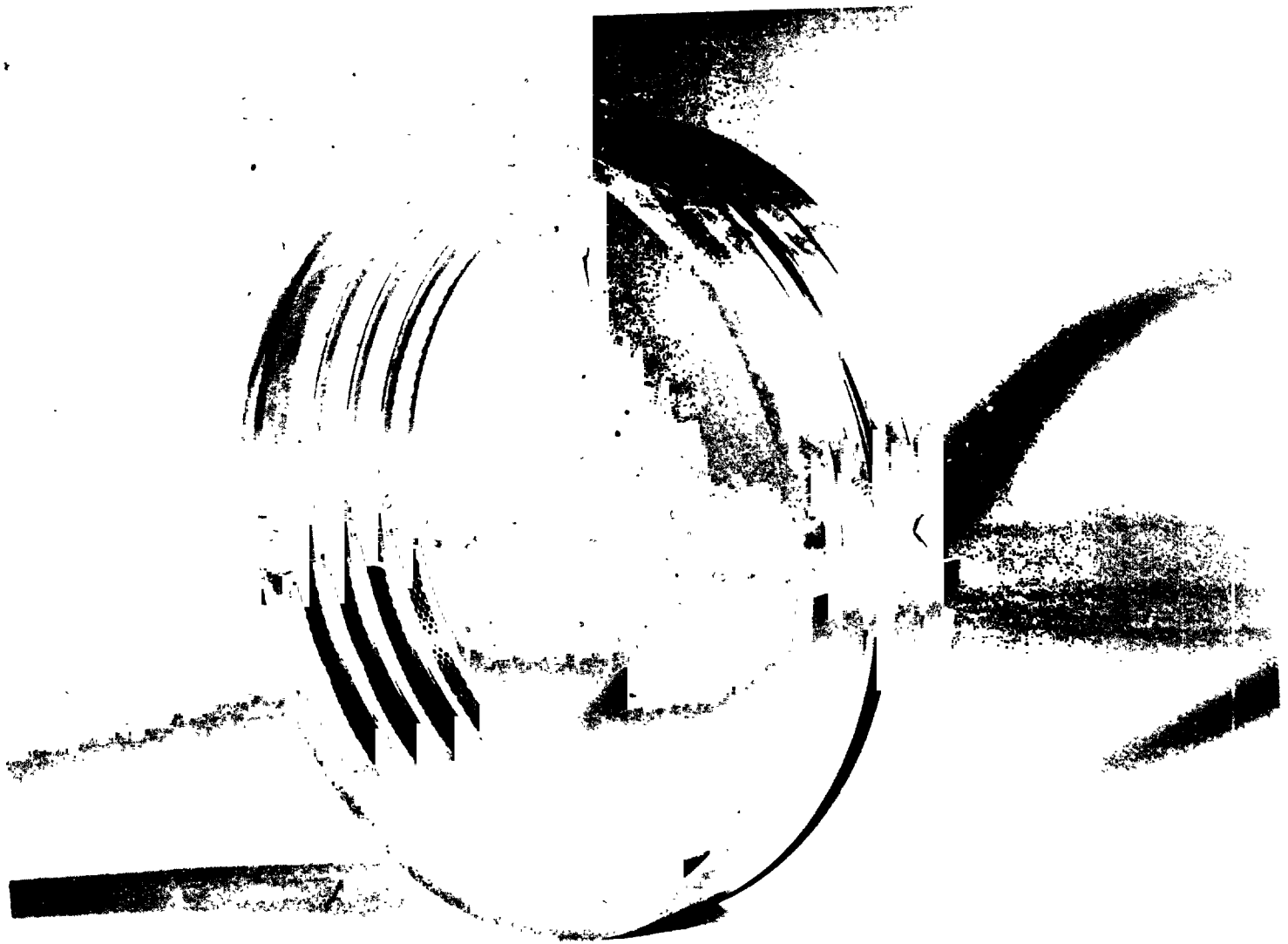

FIGURE 84. HONEYCOMB LAND OF THE OPTIMIZED ADVANCED SEAL FOR THE 3D RIG

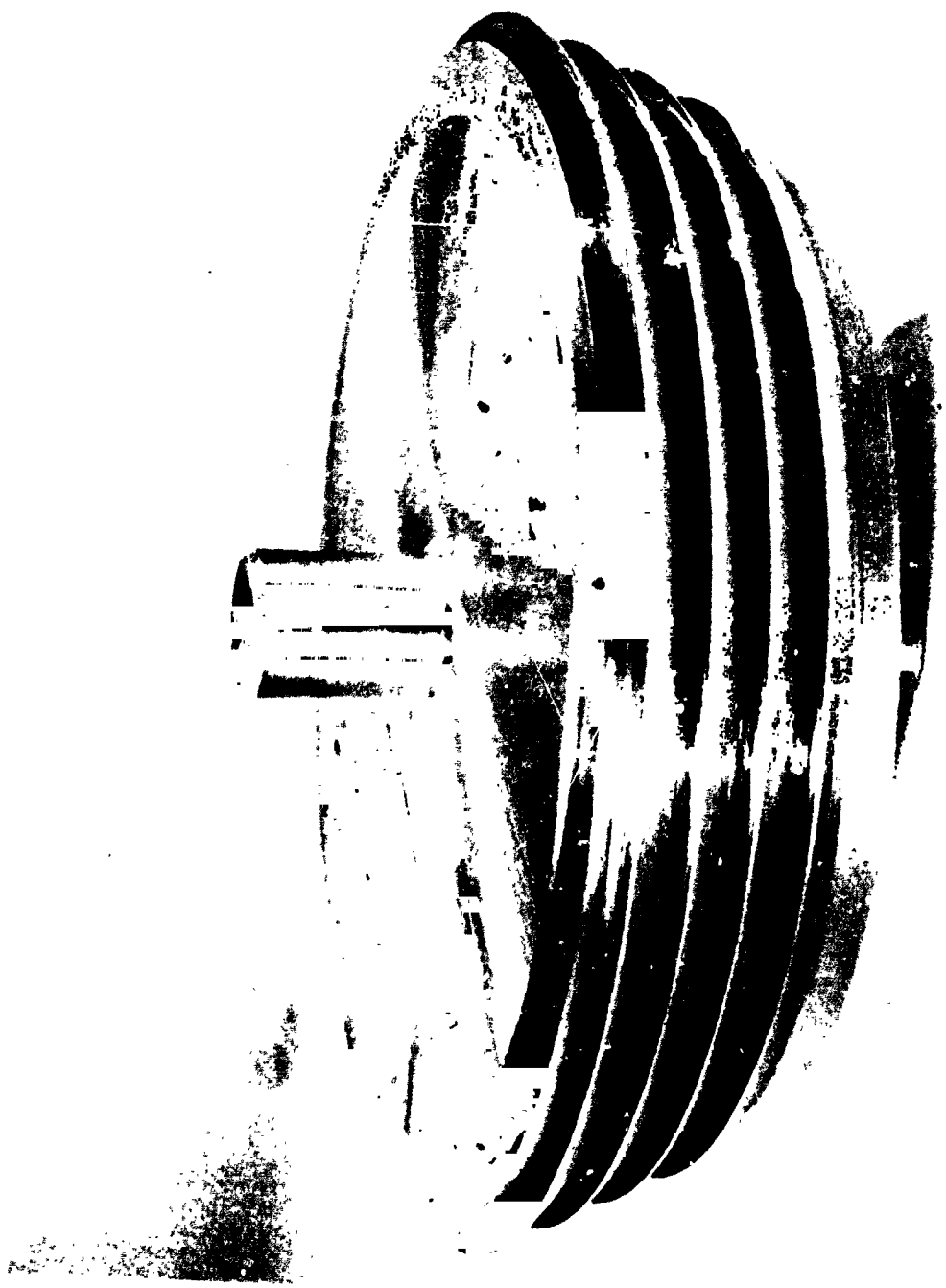

FIGURE 85. LTSD ROTOR OF THE OPTIMIZED ADVANCED SEAL FOR THE 3D RIG

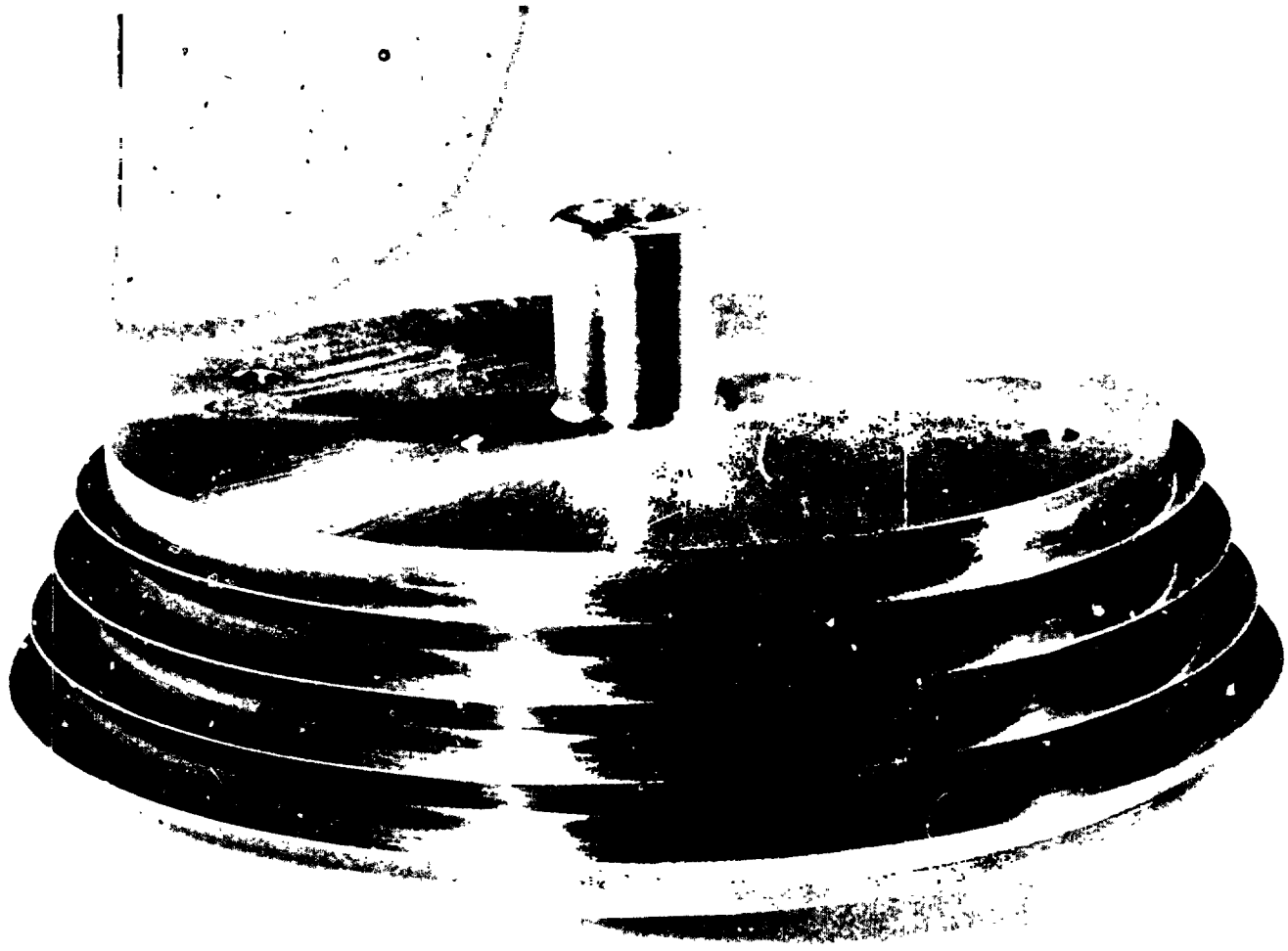

FIGURE 86. STLD ROTOR OF THE OPTIMIZED ADVANCED SEAL FOR THE 3D RIG

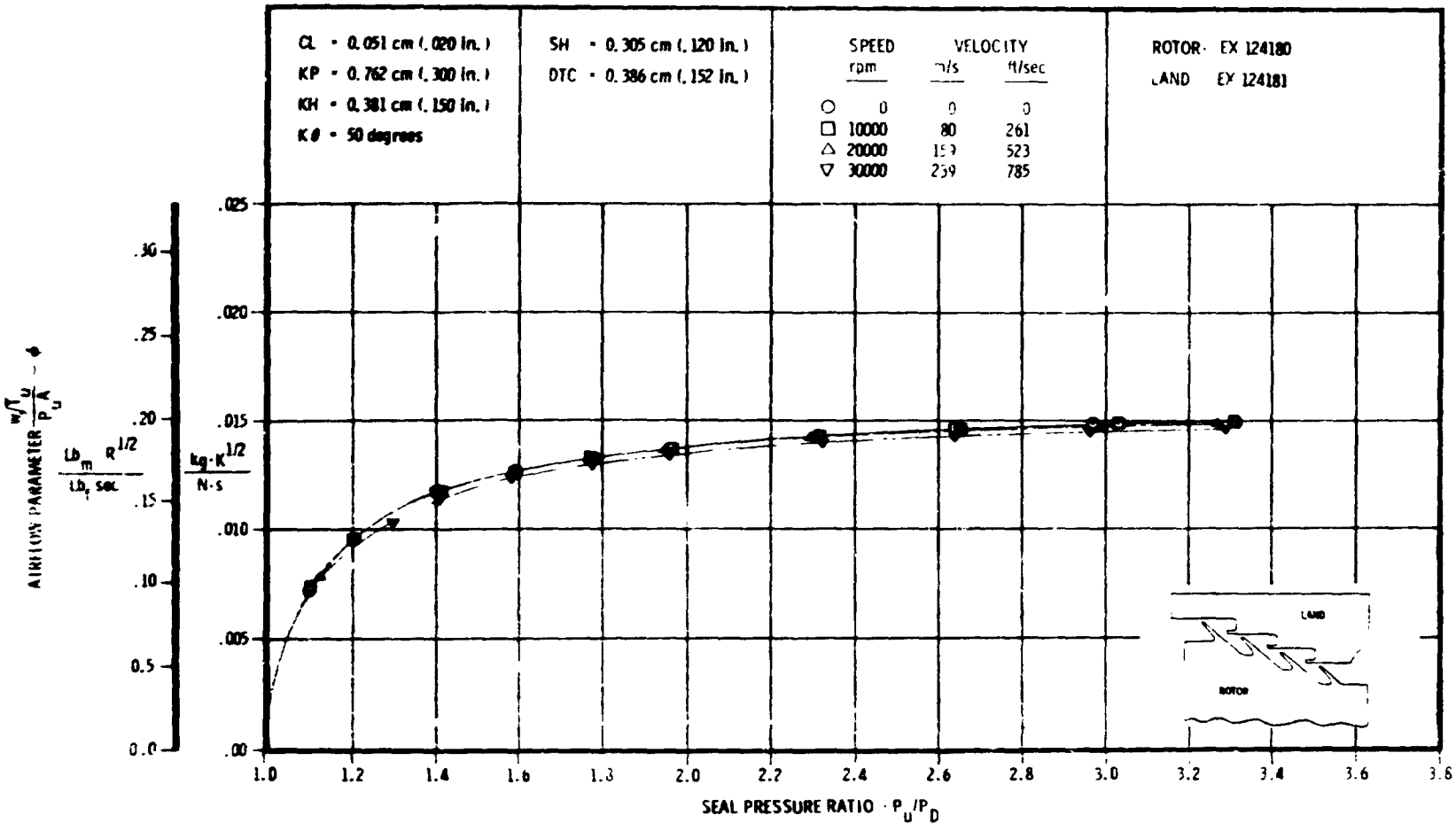

FIGURE 87. FOUR KNIFE LTSD OPTIMUM ADVANCED SEAL WITH SOLID-SMOOTH LAND

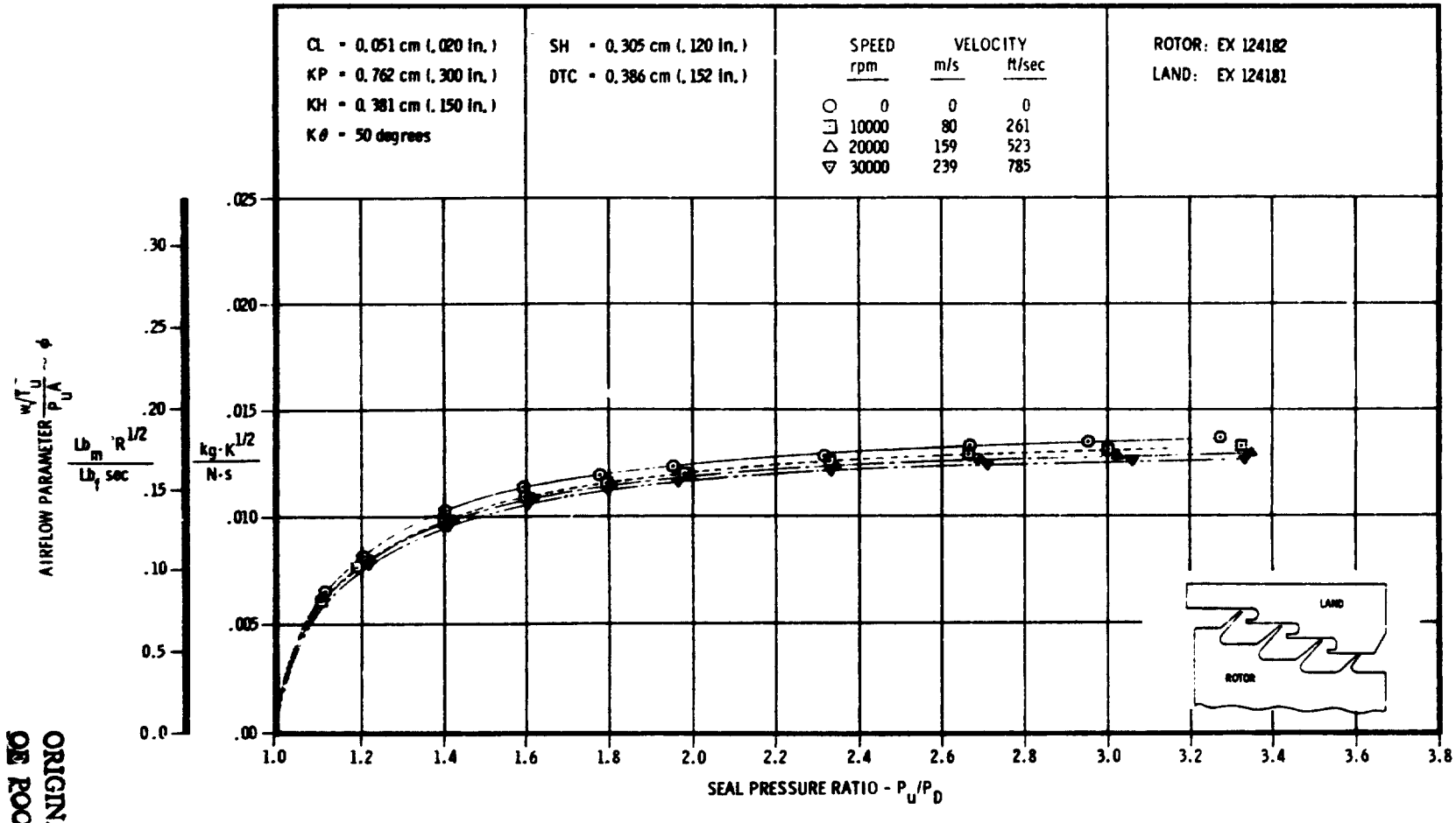

FIGURE 88. FOUR KNIFE STLD OPTIMUM ADVANCED SEA
WITH SOLID-SMOOTH LAND

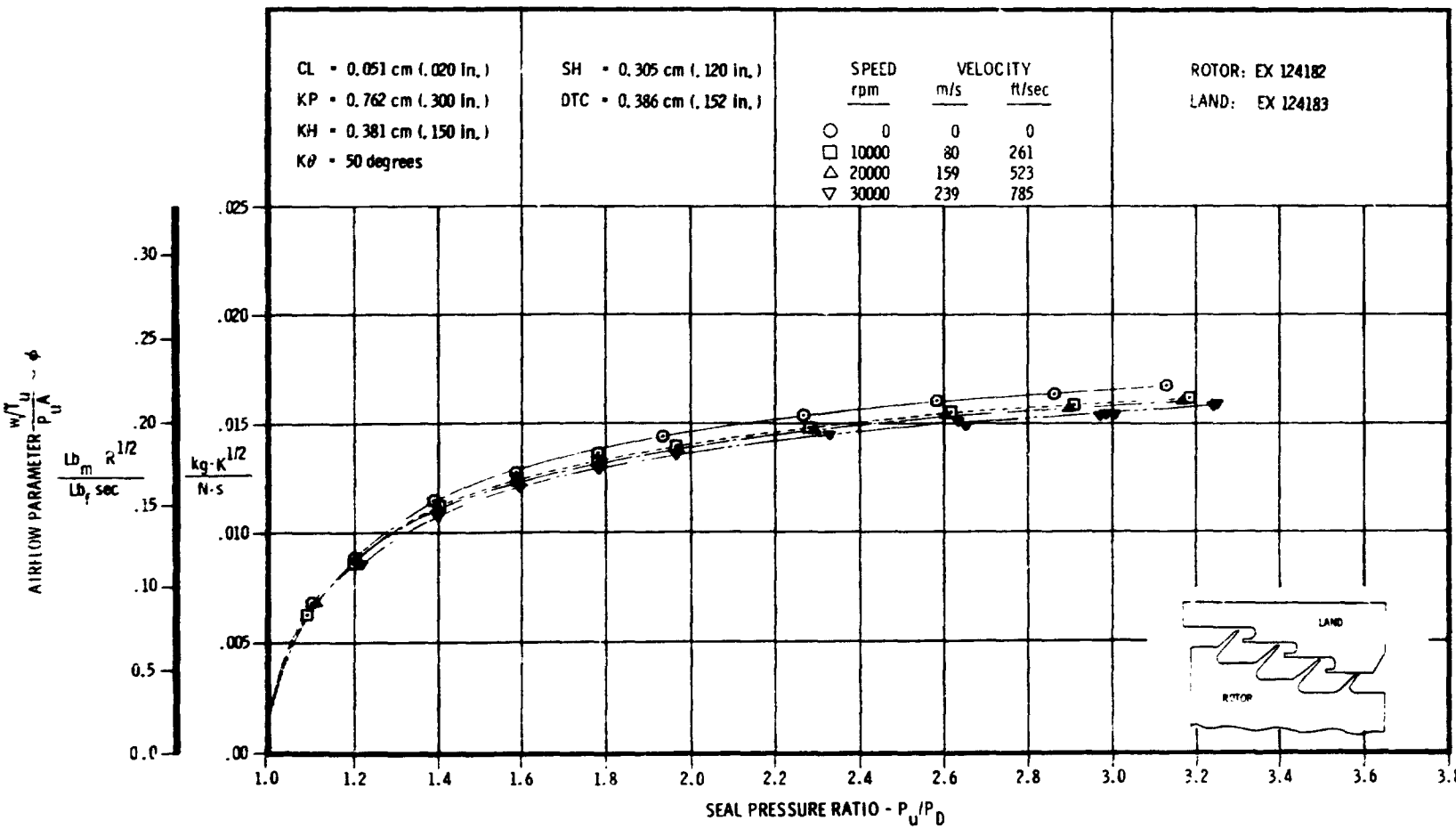

FIGURE 89. FOUR KNIFE STLD OPTIMUM ADVANCED SEAL WITH "ABRADABLE A" LAND

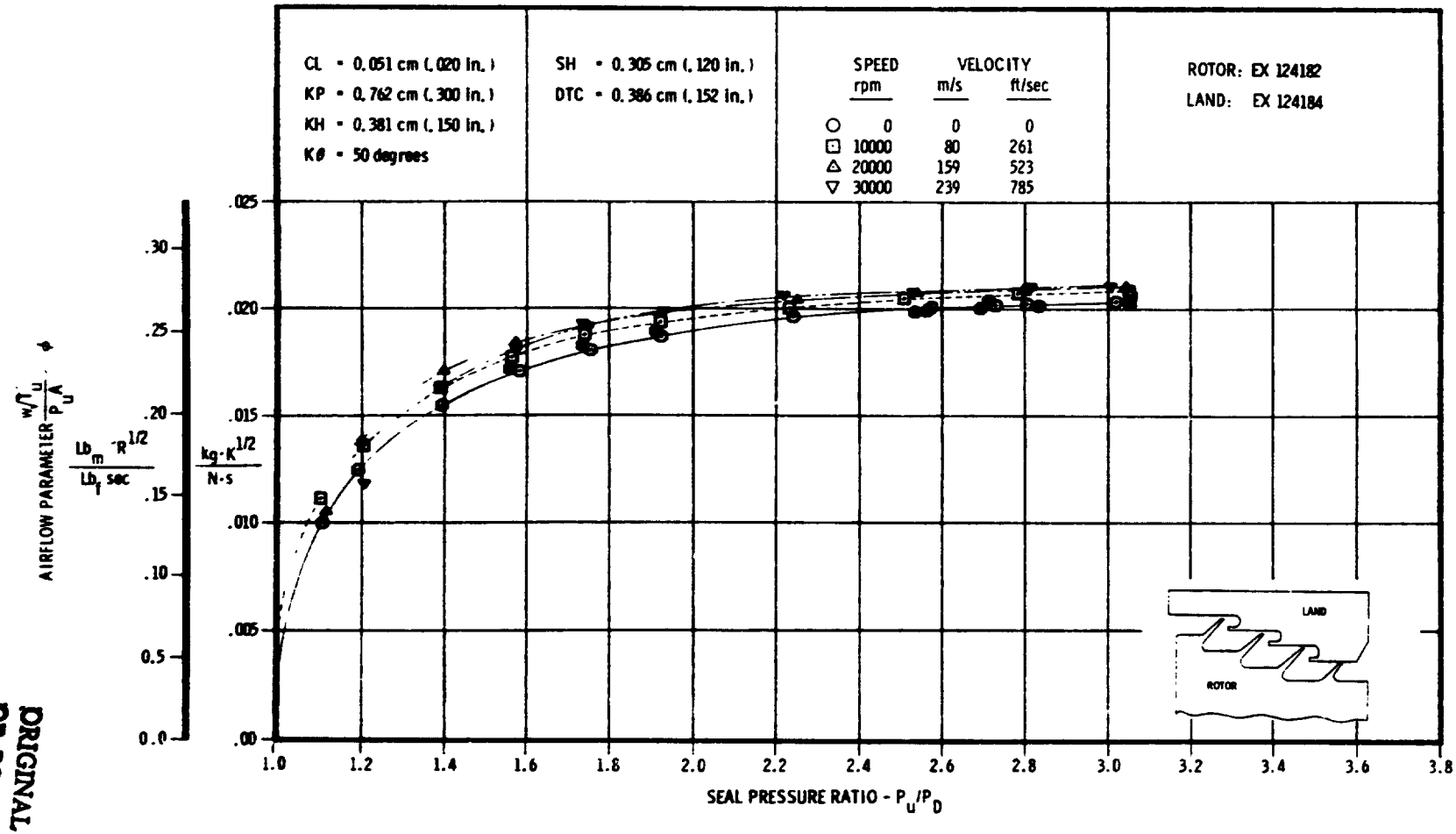

FIGURE 90. FOUR KNIFE STLD OPTIMUM ADVANCED SEAL WITH .159 cm (.062 in.) CELL HONEYCOMB LAND

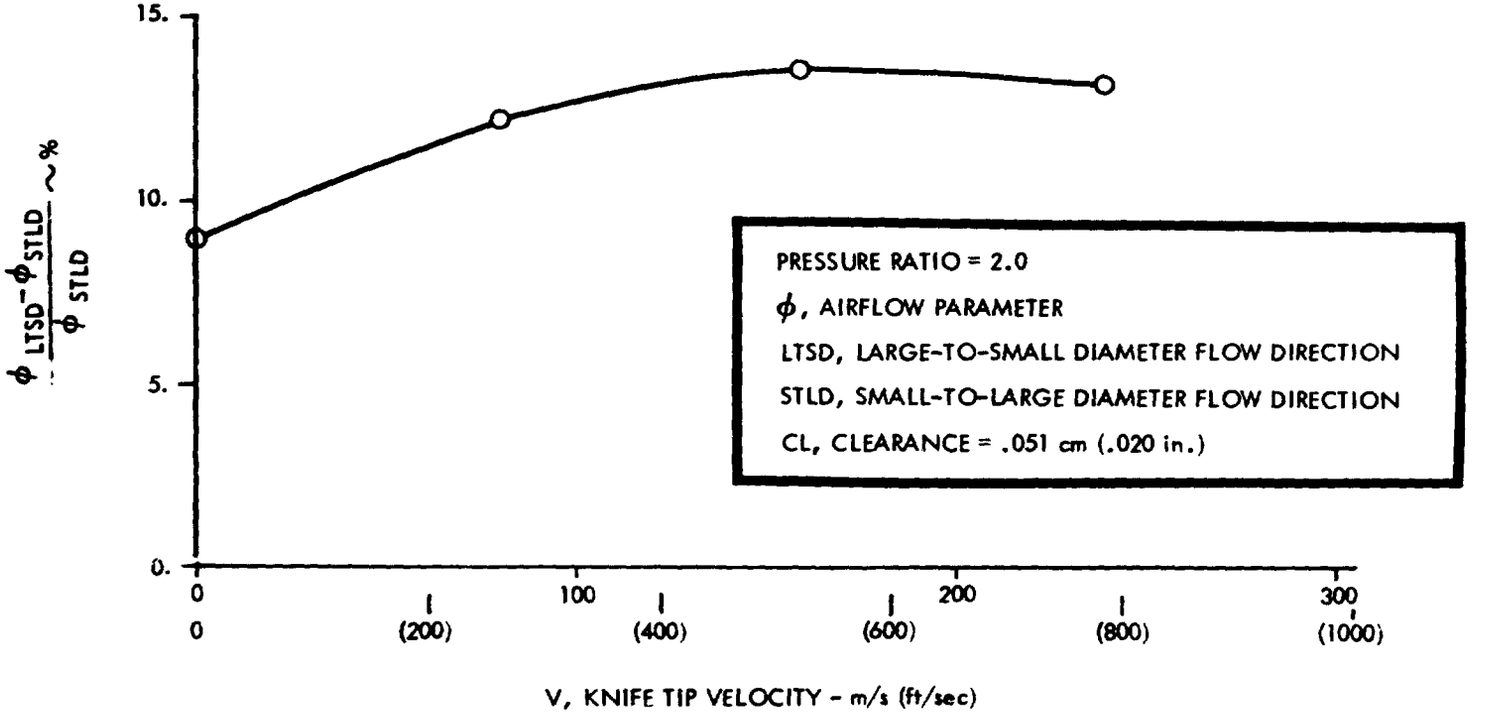

FIGURE 91. EFFECT OF FLOW DIRECTION ON OPTIMIZED ADVANCED SEAL PERFORMANCE

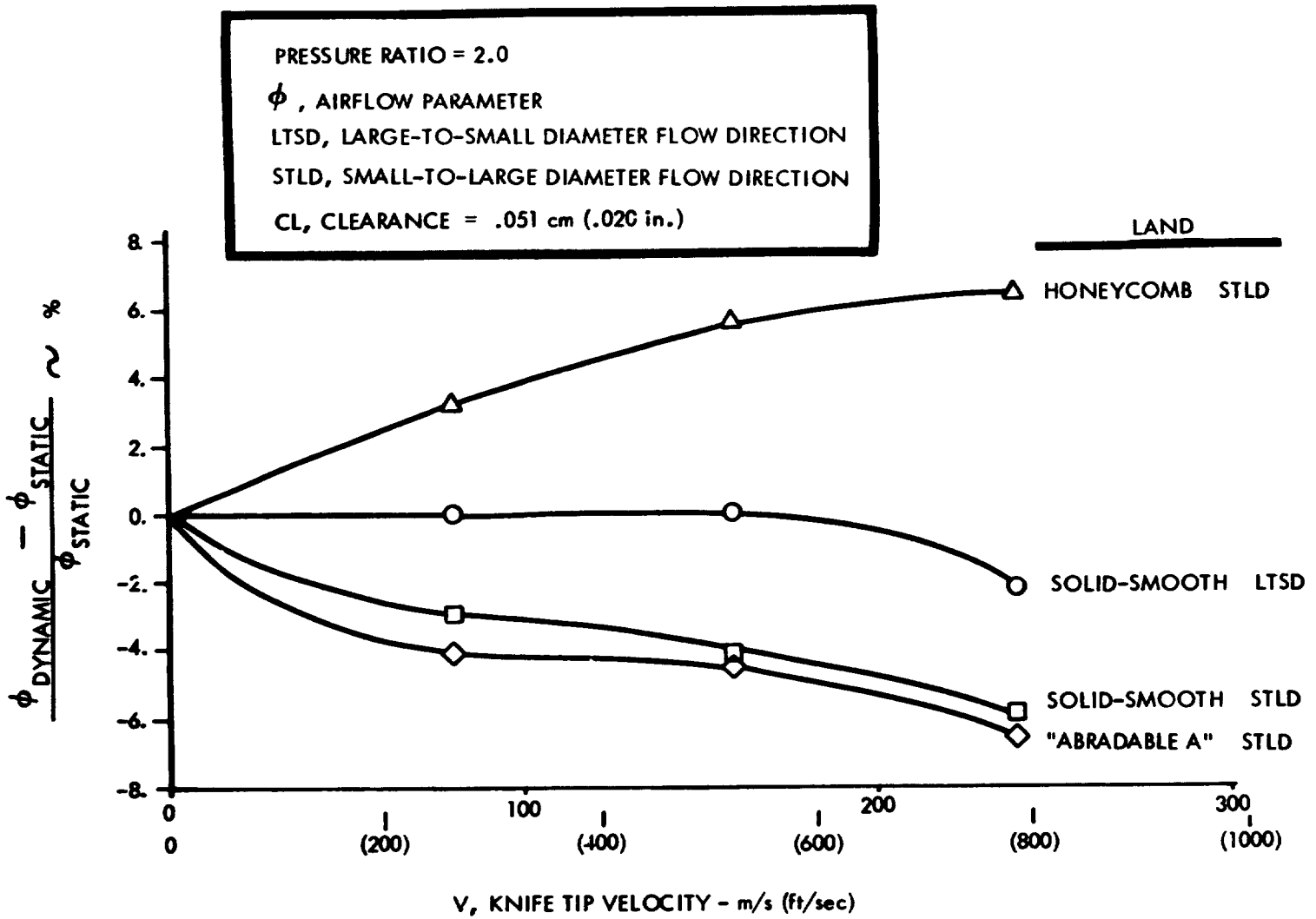

FIGURE 92. EFFECT OF ROTATION ON OPTIMIZED ADVANCED SEAL PERFORMANCE

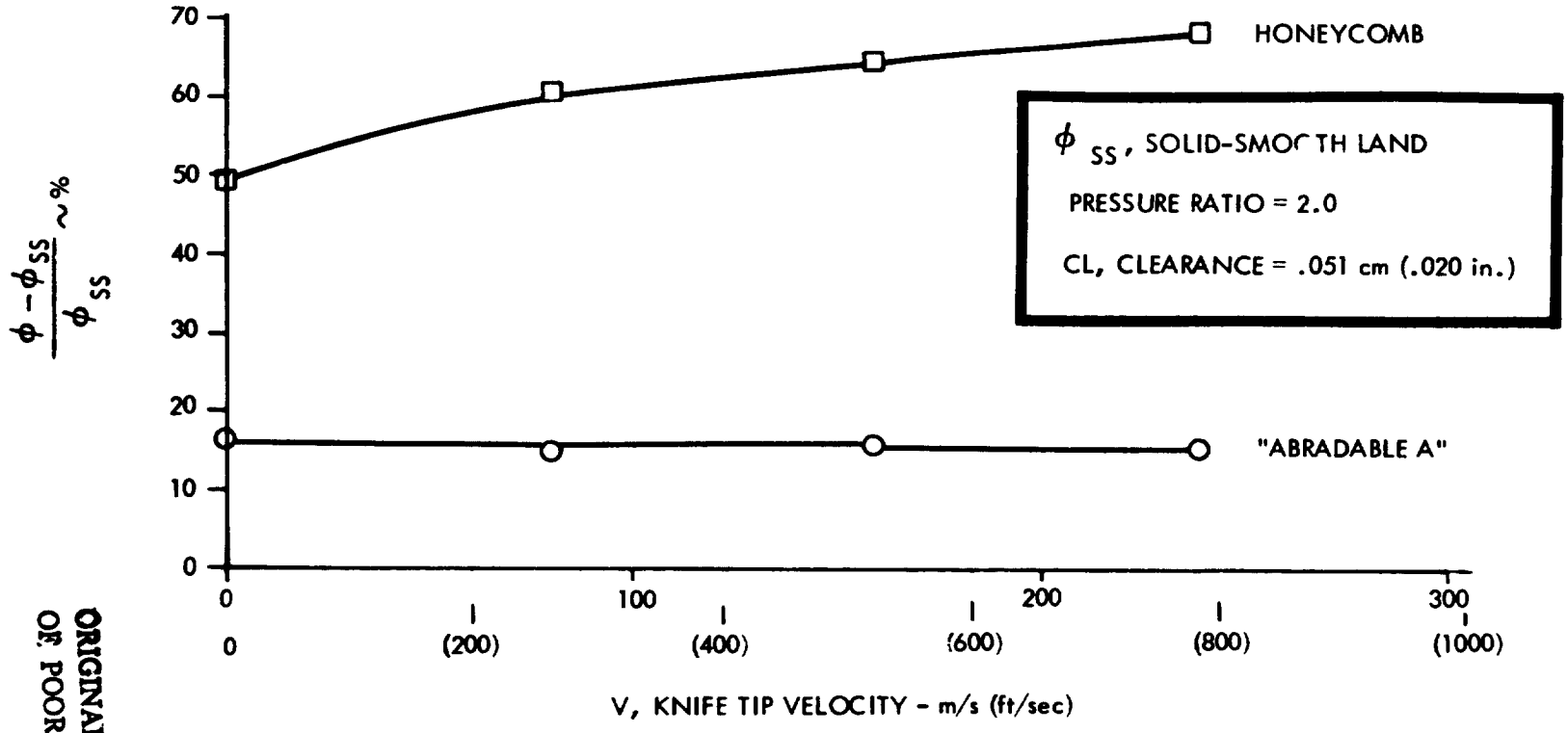

FIGURE 93. EFFECT OF ABRADABLE AND HONEYCOMB LANDS ON OPTIMIZED ADVANCED SEAL PERFORMANCE

TABLE 18. SPECIFIC VALUES OF GEOMETRIC PARAMETERS INVESTIGATED IN THE 2D SEAL RIG TO OPTIMIZE ADVANCED SEAL PERFORMANCE

Land Step Height:	.305 cm (.120 in.)
	.457 cm (.180 in.)
	.610 cm (.240 in.)
Seal Knife Height:	.203 cm (.080 in.)
	.381 cm (.150 in.)
	.711 cm (.280 in.)
Seal Knife Pitch:	.503 cm (.200 in.)
	.762 cm (.300 in.)
	1.016 cm (.400 in.)
Seal Knife Angle:	90°
	70°
	50°

TABLE 19. EFFECT OF LAND NOTCH ON ADVANCED SEAL PERFORMANCE AT A PRESSURE RATIO OF 2.0

Land Configuration	CL, Clearance cm	CL, Clearance in.	ϕ, Flow Parameter $\frac{Kg \cdot K^{1/2}}{N \cdot s}$	ϕ, Flow Parameter $\frac{lb_m \cdot °R^{1/2}}{lb_f \cdot sec}$	$\Delta\phi/\phi$ From the Baseline No Notch Land %
Full-Notch	.025	.010	.0160	.211	-7.58
Half-Notch	.025	.010	.0165	.217	-2.84
No-Notch	.025	.010	.0173	.227	Baseline
Full-Notch	.051	.020	.0135	.177	-7.34
Half-Notch	.051	.020	.0140	.184	-3.95
No-Notch	.051	.020	.0144	.190	Baseline

TABLE 20. SUMMARY OF ADVANCED DESIGN LABYRINTH SEAL DISCHARGE COEFFICIENTS AT A PRESSURE RATIO OF 2.0

2D Rig Seal Configuration	KN, No. of Knives	CL, Clearance cm	CL, Clearance (in.)	C_d, Discharge Coefficient*
Standard Stepped Seal	4	.025	(.010)	.442
Advanced Design	4	.025	(.010)	.401
Advanced Design	3	.025	(.010)	.498
Advanced Design	2	.025	(.010)	.619
Standard Stepped Seal	4	.051	(.020)	.417
Advanced Design	4	.051	(.020)	.331
Advanced Design	3	.051	(.020)	.414
Advanced Design	2	.051	(.020)	.506

* $C_d = \frac{\phi}{\phi_{isentropic}}$

where ϕ, Flow Parameter

TABLE 21. SUMMARY OF ROTATIONAL EFFECTS ON ADVANCED SEAL PERFORMANCE

Land	Flow Direction	Distance To Contact cm (in.)	ϕ-Airflow Parameter $kg\sqrt{K}/s \cdot N$ ($lb_m\sqrt{R}/sec\ psia\ in.^2$) 2D Rig	3D Rig	$\frac{\phi - \phi_s}{\phi_s}$ % 80. m/s (261. ft/sec)	159. m/s (523. ft/sec)	239. m/s (785. ft/sec)
Smooth	LTSD	.259 (.102)	.0134 (.176)	.0140 (.184)	0.0	0.0	-2.2
Smooth	STLD	.368 (.145)		.0128 (.169)	-3.0	-4.1	-5.9
Abradable	STLD	.386 (.152)		.0149 (.196)	-4.1	-4.6	-6.6
Honeycomb	STLD	.379 (.149)		.0192 (.252)	+3.2	+5.6	+6.4

ϕ_s - Static Airflow Parameter, $\frac{w\sqrt{T_U}}{p_U A}$
ϕ - Airflow Parameter, $\frac{w\sqrt{T_U}}{p_U A}$, for Subject Land
Pressure Ratio = 2.0
Radial Clearance = .051 cm (.020 in.)
LTSD - Large-to-Small Diameter
STLD - Small-to-Large Diameter

TABLE 22. PERFORMANCE COMPARISON OF ABRADABLE AND HONEYCOMB LANDS WITH A SOLID-SMOOTH LAND FOR THE ADVANCED SEAL DESIGN

Land	Flow Direction	Distance To Contact cm (in.)	$\frac{\phi - \phi_{ss}}{\phi_{ss}}$ % 0.0 m/s (0.0 ft/sec)	80. m/s (261. ft/sec)	159. m/s (523. ft/sec)	239. m/s (785. ft/sec)
Smooth	STLD	.368 (.145)	Baseline	Baseline	Baseline	Baseline
Abradable	STLD	.386 (.152)	+16.0	+14.6	+15.4	+15.1
Honeycomb	STLD	.379 (.149)	+49.1	+60.5	+64.2	+68.2

ϕ_{ss} - Solid-Smooth Land Airflow Parameter ($w\sqrt{T_U}/p_U A$)
ϕ - Airflow Parameter ($w\sqrt{T_U}/p_U A$) for Subject Land

Pressure Ratio = 2.0
Radial Clearance = .051 cm (.020 in.)
STLD - Small-to-Large Diameter

Non-constant Geometric Parameters Evaluation for Advanced Seal Design. As a further endeavor to reduce seal leakage, the effect of varying selected major geometric parameters from knife-to-knife in a non-constant fashion through the LTSD advanced seal was experimentally investigated on the 2D rig. Previous analytical analysis by DDA had shown that lower knife discharge coefficients for a series of restrictions could be effected by controlling the individual knife pressure ratio to influence the level of internal cavity turbulence. The major geometric variables controlling leakage were determined to be knife pitch, step height, and knife angle at a design specified clearance and DTC.

Two separate stepped seal envelope lengths were investigated to evaluate the merits of non-constant geometry for a four knife advanced seal. Total seal envelope lengths evaluated were 3.05 cm (1.20 in.), based on an equivalent or average individual knife pitch of .762 cm (.300 in.), and 4.06 cm (1.60 in.), based on an equivalent individual knife pitch of 1.016 cm (.400 in.). Figure 94 shows a typical example of non-constant pitch (increasing pitch dimensions along the seal length) applied to a four knife, 70° angle, advanced seal. Table 23 summarizes the configurations tested and compares the performance at a pressure ratio of 2.0 for each configuration to its constant geometry counterpart and to the optimized advanced seal. For particular non-constant geometries, the constant geometry counterpart is the optimized advanced seal. Also given are the respective geometric dimensions along the seal flowpath, noted by number (#1, #2, etc.), the locations of which are illustrated on Figure 94.

In general, the non-constant geometry configurations demonstrated improved performance at .025 cm (.010 in.) clearance with a maximum reduction in flow of 6% compared to the optimized advanced seal. However, at .051 cm (.020 in.) clearance, a 2% to 14% increase in leakage was found.

The best non-constant geometry utilized a 50° knife angle with the knife pitch decreasing along the flowpath at a rate for an equivalent pitch = 1.016 cm (.400 in.). This configuration indicated an 8% reduction in leakage at a clearance of .025 cm (.010 in.) but had a 2% increase at .051 cm (.020 in.) clearance when compared with its constant geometry counterpart at a pressure ratio of 2.0.

A non-constant configuration with increasing pitch and step height was evaluated with the 50° angle knives. This configuration indicated an 8% increase in leakage at a 2.0 seal pressure ratio compared to its constant geometry counterpart at .025 cm (.010 in.) clearance. Therefore, the investigation was not pursued with this combination of non-constant geometry.

The non-constant geometry advanced seal configured with 70° angle knives set at increasing pitch demonstrated the greatest improvement in leakage compared to its constant geometry counterpart, pitch = 1.016 cm (.400 in.). An 11% reduction in leakage at a clearance of .025 cm (.010 in.) and a 6% reduction at .051 cm (.020 in.) was evident at a 2.0 pressure ratio. Compared to the optimized advanced seal, however, it was marginally higher in leakage at .025 cm (.010 in.) clearance and 5% higher at .051 cm (.020 in.).

Two configurations with vertical knives ($K\theta = 90^{o}$) at non-constant pitch showed leakage reductions at both clearances compared to their constant geometry counterparts. The better configuration, equivalent pitch = 1.016 cm (.400 in.), indicated a 7% reduction in leakage compared to the constant geometry advanced seal.

Knives of 90°, 70°, and 50° angles were assembled with a non-constant pitch (knife spacing) for evaluation at an equivalent pitch = 1.016 cm (.400 in.). At a seal pressure ratio = 2.0, this configuration indicated a 6% reduction in flow at .025 cm (.010 in.) clearance compared to the base constant geometry configuration and 3% reduction compared to the optimized advanced seal. At .051 cm (.020 in.) clearance, however, its leakage was 5% higher than the optimized seal.

The non-constant pitch seals have less allowable axial seal travel than their equivalent constant geometry configurations. Varying the stack between the seal knives and adjacent steps within the same seal length limits the axial travel to the minimum distance-to-contact (DTC). The axial seal clearance (DTC) has been noted in Table 23 for both constant and non-constant geometry configurations for this reason.

In summary, the mixed knife angle and/or the non-constant pitch seal geometries tested indicated improved performance (lower leakage) at .025 cm (.010 in.) clearance compared to their constant geometry counterparts. However, combining increasing step height with increasing pitch resulted in a performance loss. At .051 cm (.020 in.) clearance, leakage decreased for the 70° and 90° knife angle configurations, while leakage increased for the others. Also, none of the non-constant geometry configurations showed improvements at both clearances compared to the optimized advanced geometry seal.

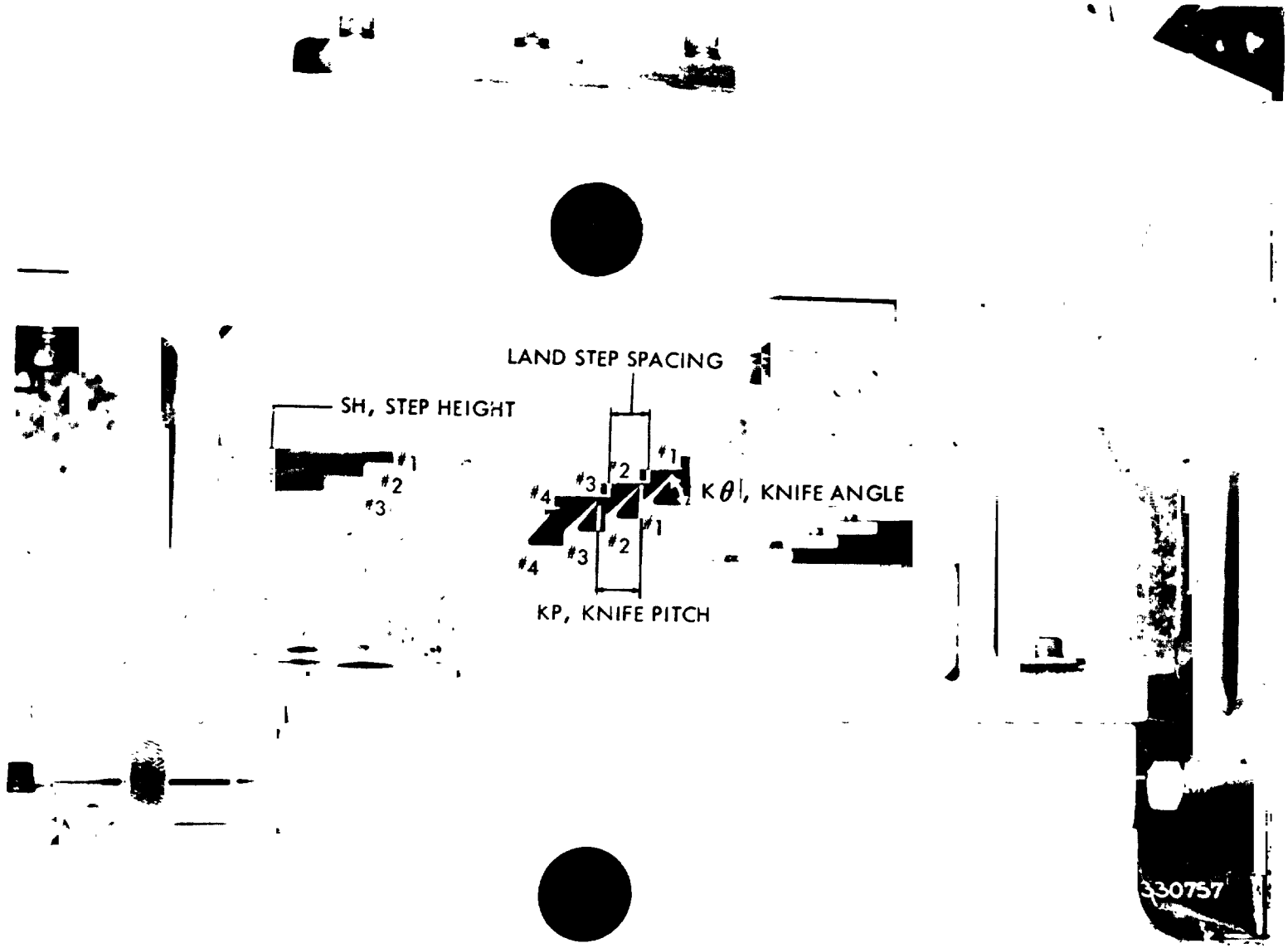

FIGURE 24. NON-CONSTANT PITCH ADVANCED SEAL

TABLE 23. COMPARISON OF NON-CONSTANT GEOMETRY TEST RESULTS AT P_U/P_D = 2.0

NON CONSTANT SEAL CONFIGURATION	CL cm (in.)	DTC cm (in.)	KNIFE ANGLE Kθ ∿ DEGREES θ1	θ2	θ3	θ4	LAND STEP SPACING cm/(in.) θ1	θ2	θ3	θ4	KNIFE PITCH ∿ KP cm(in.) θ1	θ2	θ3	STEP HEIGHT ∿ KH cm/(in.) θ1	θ2	θ3	ϕ @ P_U/P_D = 2.0 kg-Kb/N-s (lbm *Rb/lbf sec)	Δϕ/ϕ ∿ % SIMILAR* CONST GEOM SAME LENGTH	Δϕ/ϕ ∿ % OPTIMIZED SEAL**
NON-CONSTANT PITCH (INCREASING) KP = .762 cm (.300 in.)	.025 (.010) .051 (.020)	.170 (.067) .170 (.067)	50	50	50	50	.508 (.200)	.635 (.250)	.826 (.325)	1.080 (425)	.572 (.225)	.724 (.285)	.940 (.370)	.305 (.120)	.305 (120)	.305 (.120)	.0159 (.208) 0138 (.181)	-0.05 BASE CONF DTC=.254 cm +5.20	-0.05 +5.20
NON-CONSTANT PITCH (INCREASING) KP = 1.016 cm (.400 in.)	.025 (.010) .051 (.020)	.254 (.100) .254 (.100)					.762 (300)	.851 (.335)	1.041 (.410)	1.410 (.555)	.800 (.315)	.889 (.350)	1.041 (.410)				0154 (.202) .0134 (.176)	-6.00 BASE CONF DTC=.340 cm +0.60	-3 40 +2 30
NON-CONSTANT PITCH (INCREASING) KP = 1.016 cm (.400 in.)	.025 (.010) .051 (.020)	.254 (.100) .254 (.100)					1.410 (.555)	1.041 (.410)	.851 (.335)	.762 (.300)	1.041 (.410)	.889 (.350)	.800 (.315)				.0150 (.197) .0135 (.178)	-8.40 BASE CONF DTC=.340 cm +1.70	-5 70 3.50
NON-CONSTANT PITCH & STEP HEIGHT (INCREASING) KP = 1.016 cm(.400 in.) KH = .371 cm(.146 in.)	.025 (.010) NO TEST @ CL = .051 cm(.020 in.)	.254 (.100)					.762 (.300)	.851 (.335)	1.041 (.410)	1.410 (.555)	.800 (.315)	.889 (.350)	1 041 (.410)	.305 (.120)	.457 (180)	.610 (.240)	0176 (.232)	+7.90 BASE CONF DTC=.340 cm KH =.371 cm	+11.00
NON-CONSTANT PITCH (INCREASING) KP = 1.016 cm (.400 in.)	.025 (.010) .051 (.020)	.254 (.100) .254 (.100)	70	70	70	70								.305 (.120)	.305 (.120)	.305 (.120)	.0161 (.212) .0137 (180)	-10.90 BASE CONF DTC=.340 cm -5.80	+1.40 +4.70
NON-CONFORM PITCH (INCREASING) KP = .762 cm (.300 in.)	.025 (.010) .051 (.020)	.170 (.067) .170 (067)	90	90	90	90	.508 (.200)	.635 (.250)	.826 (.325)	1.080 (.425)	.572 (.225)	.724 (.285)	.940 (.370)				.0163 (.215) .0147 (.194)	-4.00 BASE CONF DTC=.254 cm -1.00	+2 90 +12.80
NON-CONSTANT PITCH (INCREASING) KP = 1.016 cm (.400 in.)	.025 (.010) .051 (.020)	.254 (.100) .254 (.100)					762 (.300)	.851 (.335)	1.041 (.410)	1.410 (.555)	.800 (.315)	.889 (.350)	1.041 (.410)				.0172 (.226) .0149 (.196)	-7 00 BASE CONF DTC=.340 cm -7.10	+8 10 +14 00
NON-CONSTANT PITCH & SWEPE ANG. (KP INCREASING) (KB INCREASING) KP = 1.016 cm(.400 in.)	.025 (.010) .051 (.020)	.254 (.100) .254 (.100)	90	70	50	50											0154 (.202) .5137 (.180)	-6.00 BASE CONF DTC=.340 cm Kθ=50° +2.90	-3.30 -4.70

CL - CLEARANCE
DTC - DISTANCE TO CONTACT

*BASE CONF. KP = EQ. KP, KH, KB, KR SAME AS NON-CONSTANT CONF UNLESS NOTED OTHERWISE

**OPTIMIZED SEAL: Kθ = 50° KP = .162 cm(.300 in.) KH = .305 cm(.120 in.) DTC= .254 cm(.100 in.)

Rotational Power Absorption

The relative seal rotational power requirements were measured for all 3D rig seal configurations as a principal part of the 3D dynamic rig investigative effort. The objective of this effort was to determine if the differences in the power requirements of various seal rotors interacting with the land geometry (i.e., smooth, abradable, and honeycomb) could, when applied to engine operating environments, yield seal power requirement variations significant enough to incorporate in engine cycle performance accountability. The experimental technique utilized to determine the rotational power of the 3D seal configuration is explained in detail in Test Rigs and Procedures.*

The rotational power absorption data acquired for all test configurations was initially evaluated graphically in terms of actual measured power versus seal pressure ratio with actual seal rotor speed as a parameter. As an example, Figure 95 illustrates the actual seal rotor power absorption for the four knife straight-through seal at .051 cm (.010 in.) clearance and .356 cm (.140 in.) knife pitch with smooth, "Abradable A", and honeycomb lands. As noted, the actual power levels are in the order of 3.7 kw (5.0 hp) at high seal pressure ratios and rotational speeds. This power level consists of the total turbine-seal rotor drive system losses (windage, friction, etc.). The differences in actual power absorbed by each of the three land surfaces at a given pressure ratio and speed does, however, represent the differences in parasitic power absorption due to the knife-land surface interactions alone. A more useful representation of the power absorption data for engine application purposes is illustrated on Figure E-5, Appendix E, where corrected (or referred) power ($P/\delta\sqrt{\theta}$) is utilized to evaluate the performance for the seal configuration. This provides a direct relation of seal power absorption to environmental conditions within the engine (i.e., seal inlet temperature, inlet pressure, and pressure ratio). A computational method is presented in Appendix E for applying the rotational power absorption data to an engine environment for the evaluation of seal designs. The corrected power absorption data for the straight-through seals with smooth, abradable, and honeycomb lands are plotted in Figures E-1 through E-6. Corresponding data for the advanced seal are presented in Figure E-7.

The vertical dotted lines on Figure 95 and Figures E-1 through E-7 encompass the seal pressure ratio range in which the rotor bearing load was maintained at a constant 670 N (150 lb_f). On either side of this range it was not possible to maintain a constant bearing load due to the rig thrust balance system design and the available line pressure.

*See "3D Rig Power Absorption Analysis", Test Rigs and Procedures section.

The rotational power absorption results for the four knife straight seal configurations are summarized and compared in Table 24 for the .203 cm (.080 in.), .279 cm (.110 in.), and .356 cm (.140 in.) pitch seal rotors using the smooth, abradable, and honeycomb lands. The rotational power absorption differences due to land material are small, typically of the order 5% at .025 cm (.010 in.) radial clearance, 2.0 seal pressure ratio, and 239 m/s (785 ft/sec) knife tip speed.

Table 25 summarizes and compares the effect of pitch on the rotational power absorption for each land configuration tested. This comparison shows that seal pitch has a small effect on rotational power requirements. The total variation due to pitch was 8.5% for the .051 cm (.020 in.) clearance honeycomb lands, with the lowest pitch rotor indicating the lowest power. The combined aerodynamic leakage and power absorption test results for the four knife straight seal indicate that leakage can be reduced with the honeycomb land, but the rotational power absorption is slightly higher.

Table 26 has been provided to show the change in net system performance in terms of specific fuel consumption (SFC). The use of a honeycomb land instead of a smooth land with a conventional four knife straight-through seal at .025 cm (.010 in.) and .051 cm (.020 in.) radial clearances would provide a net system performance improvement which results in a lower SFC.

The rotational power absorption was also measured during the advanced seal configuration tests in both the STLD and the LTSD flow directions at .051 cm (.020 in.) clearance. These results, illustrated in Figure E-7, show that the rotational power absorption for the advanced seal is generally the same in the STLD flow direction and in the LTSD flow direction. Comparison of Figure E-7 with Figure E-5 indicates that the advanced seals and the straight-through seals experience similar levels of rotational power absorption.

Table 27 summarizes the advanced seal rotational power absorption differences for the smooth, abradable, and honeycomb lands. The honeycomb land seal configuration indicated the highest power absorption of the land configurations tested (14% above the smooth land). This is believed to be partially due to the high leakage rates evidenced for this configuration.

Throughout the range of seal design and environments tested, the rotational power absorption maintained a consistent trend and level with speed. From these results it may be concluded that the rotational power absorption of a labyrinth seal is not a significant design consideration.

FIGURE 95. ACTUAL SEAL ROTOR POWER VERSUS SEAL INLET PRESSURE FOR A FOUR KNIFE STRAIGHT SEAL

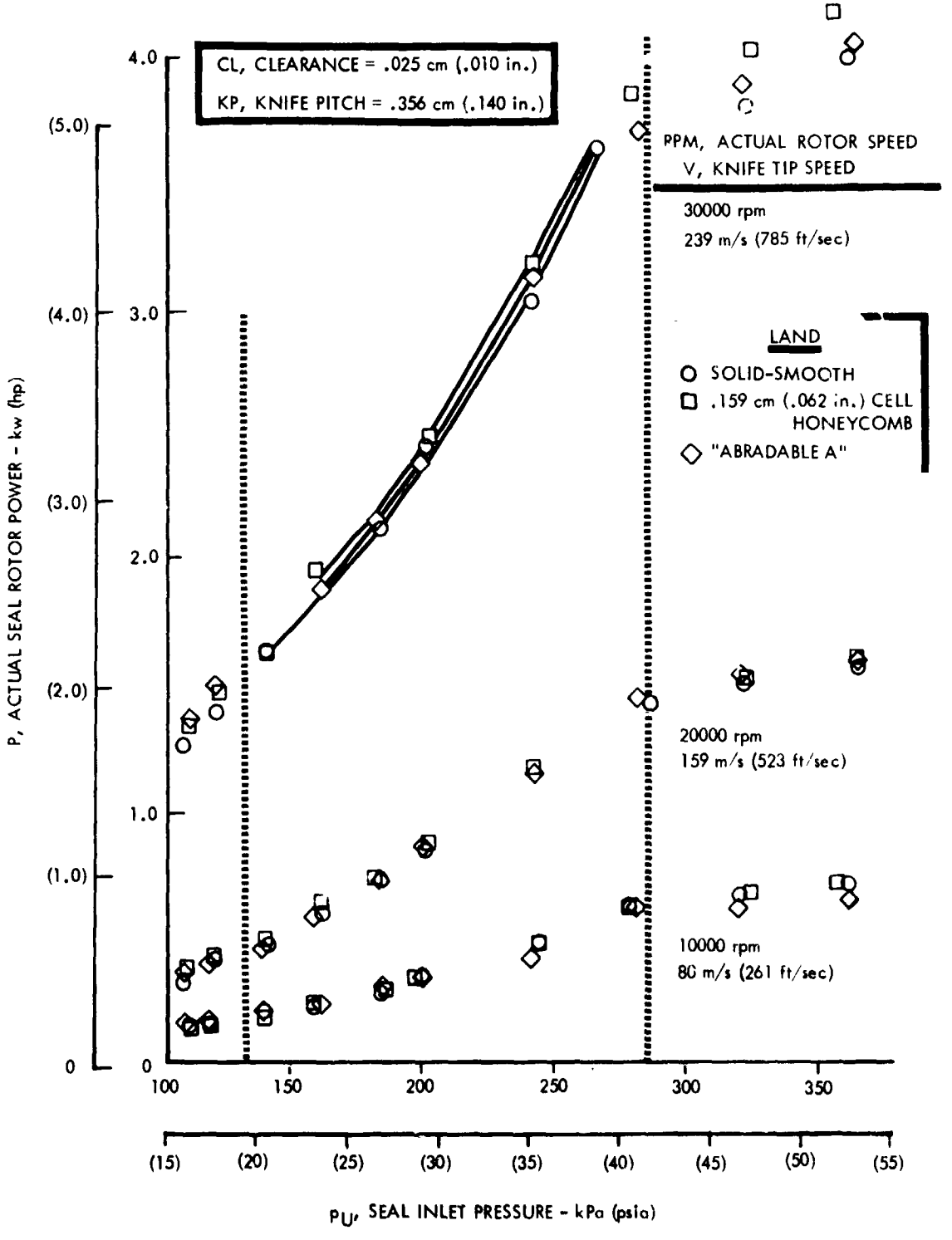

TABLE 24. SUMMARY OF ROTATIONAL POWER ABSORPTION FOR SMOOTH, ABRADABLE, AND HONEYCOMB LANDS WITH FOUR KNIFE STRAIGHT-THROUGH SEAL ROTORS

Land Type	CL, Clear. cm (in.)	KP, Pitch cm (in.)	V, Velocity m/s (ft/sec)	Seal Pressure Ratio	P/δ√θ, Corrected Rotational Power kw (hp)	ΔP/P, Power Change From Smooth Land %
Smooth	.025 (.010)	.203 (.080)	239 (785)	2.	1.150 (1.542)	Baseline
"Abradable A"	.025 (.010)				1.139 (1.528)	0.92
Honeycomb	.025 (.010)				1.195 (1.602)	+3.89
Smooth	.051 (.020)				1.233 (1.654)	Baseline
"Abradable A"	.051 (.020)				1.212 (1.625)	-1.75
Honeycomb	.051 (.020)				1.195 (1.602)	-3.14
Smooth	.025 (.010)	.279 (.110)			1.148 (1.540)	Baseline
"Abradable A"	.025 (.010)				1.180 (1.583)	+2.79
Honeycomb	.025 (.010)				1.213 (1.627)	+5.65
Smooth	.051 (.020)				1.212 (1.625)	Baseline
"Abradable A"	.051 (.020)				1.226 (1.644)	+1.17
Honeycomb	.051 (.020)				1.255 (1.683)	+3.57
Smooth	.025 (.010)	.356 (.140)			1.184 (1.588)	Baseline
"Abradable A"	.025 (.010)				1.207 (1.618)	+1.89
Honeycomb	.025 (.010)				1.239 (1.661)	+4.60
Smooth	.051 (.020)				1.277 (1.712)	Baseline
"Abradable A"	.051 (.020)				1.265 (1.697)	-0.88
Honeycomb	.051 (.020)				1.301 (1.745)	+1.93

TABLE 25. COMPARISON OF ROTATIONAL POWER ABSORPTION AS A FUNCTION OF CLEARANCE, PITCH, AND LAND SURFACE IN A FOUR KNIFE STRAIGHT-THROUGH SEAL

Land Type	CL, Clear. cm (in.)	KP, Pitch cm (in.)	V, Velocity m/s (ft/sec)	Seal Pressure Ratio	P/δ√θ, Corrected Rotational Power kw (hp)	ΔP/P, Power Change From Baseline Pitch %
Smooth	.025 (.010)	.203 (.080)	239 (785)	2.0	1.150 (1.542)	+0.13
	.025 (.010)	.279 (.110)			1.148 (1.540)	Baseline
	.025 (.010)	.356 (.140)			1.184 (1.588)	+3.12
Smooth	.051 (.020)	.203 (.080)			1.233 (1.654)	+1.78
	.051 (.020)	.279 (.110)			1.212 (1.625)	Baseline
	.051 (.020)	.356 (.140)			1.277 (1.712)	+5.35
"Abradable A"	.025 (.010)	.203 (.080)			1.139 (1.528)	-3.47
	.025 (.010)	.279 (.110)			1.180 (1.583)	Baseline
	.025 (.010)	.356 (.140)			1.207 (1.618)	+2.21
"Abradable A"	.051 (.020)	.203 (.080)			1.212 (1.625)	-1.16
	.051 (.020)	.279 (.110)			1.226 (1.644)	Baseline
	.051 (.020)	.356 (.140)			1.265 (1.697)	+3.22
Honeycomb	.025 (.010)	.203 (.080)			1.195 (1.602)	-1.54
	.025 (.010)	.279 (.110)			1.213 (1.627)	Baseline
	.025 (.010)	.356 (.140)			1.239 (1.661)	+2.09
Honeycomb	.051 (.020)	.203 (.080)			1.195 (1.602)	-4.81
	.051 (.020)	.279 (.110)			1.255 (1.683)	Baseline
	.051 (.020)	.356 (.140)			1.301 (1.745)	+3.68

NOTE: The .279 cm (.110 in.) pitch is used for the baseline in each case.

TABLE 26. SUMMARY OF PERFORMANCE IMPROVEMENT FROM USING A HONEYCOMB LAND INSTEAD OF A SMOOTH LAND IN A FOUR KNIFE STRAIGHT SEAL FOR AN ADVANCED HIGH BYPASS RATIO TURBOFAN ENGINE

Land Type	KP, Pitch cm (in.)	CL, Clear. cm (in.)	V, Velocity m/s (ft /sec)	Seal Pressure Ratio	ΔSFC/SFC, Change In Specific Fuel Consumption From a Solid-Smooth Land - %		
					Seal Leakage	Seal Power Absorption	Net Change Per Seal
Honeycomb	.203 (.080)	.051 (.020)	239 (785)	2.0	-.790	-.013	-.803
Honeycomb	.279 (.110)	.051 (.020)	↓	↓	-.850	+.015	-.835
Honeycomb	.356 (.140)	.051 (.020)	↓	↓	-.630	+.008	-.622

Engine Cycle Description:
Altitude = 10688M (35,000 ft.)
Mach Number = .80
Bypass Ratio = 7.0:1
Fan Pressure Ratio = 1.7:1
Overall Pressure Ratio = 38:1
Burner Outlet Temperature = 1700K (3060°R)

TABLE 27. SUMMARY OF ROTATIONAL POWER ABSORPTION FOR A SMOOTH, ABRADABLE, AND HONEYCOMB LAND USING A FOUR KNIFE ADVANCED LABYRINTH SEAL

Land Type	CL, Radial Clearance cm (in.)	V, Velocity m/s (ft /sec)	Seal Pressure Ratio	$P/\delta\sqrt{\theta}$ Corrected Rotational Power kw (hp)	ΔP/P Change From Smooth Land %
Smooth	.051 (.020)	239. (785.)	2.0	1.23 (1.648)	Baseline
"Abradable A"	↓	↓	↓	1.30 (1.74)	+5.6
Honeycomb	↓	↓	↓	1.40 (1.874)	+13.7

CONCLUSIONS

This program experimentally explored labyrinth seal design and performance parameters for which technical information was non-existent or limited in scope. The primary goals of this program were (1) to determine the influence of selected geometric and aerodynamic parameters on the performance of labyrinth seals, and (2) to improve and develop an advanced labyrinth seal design that significantly reduces leakage. The following summary of conclusions derived from the results obtained in this program shows that the program goals were achieved in all categories.

- Honeycomb lands were found to reduce leakage up to 24% for straight-through labyrinth seals.
- Honeycomb cell depth was found to be a significant parameter influencing the leakage of straight-through seals.
- Some abradable lands were found to leak substantially more than a solid-smooth land.
- Grooving a porous abradable seal land signific ntly reduced leakage through the material.
- Moderate surface roughness was found to reduce the leakage of straight-through seals by approximately 23% over a smooth land at .013 cm (.005 in.) clearance and 5% at .051 cm (.020 in.) clearance. Greater roughness increased leakage.
- Rotation reduced leakage up to 10% for smooth and abradable lands in straight-through seals, but it had negligible effect with the honeycomb land.
- Rotation effects do not influence the selection of optimum knife pitch for straight-through seals.
- An advanced seal design using a solid-smooth land was developed that reduced leakage 26.9% compared to a conventional stepped seal.
- Using a honeycomb land with the advanced seal increased leakage 69% compared to the solid-smooth land.
- Rotation effects on the optimized advanced seal for leakage in the large-to-small diameter flow direction were negligible.
- Rotation decreased the advanced seal leakage approximately 6% for flow in the small-to-large diameter direction for the solid-smooth and abradable lands. However, the honeycomb land experienced a 6% leakage increase with rotation compared to the static performance.

- The rotational power absorption for solid-smooth, abradable, and honeycomb lands in a conventional four knife straight-through seal showed small differences. The honeycomb land had the maximum effect indicating a 6% higher power absorption than the smooth land.

- The rotational power absorption for the advanced seal is approximately the same as that for the four knife straight-through seal when both have solid-smooth lands.

- The rotational power absorption for the advanced seal design using a honeycomb land is 13% higher than it is with the solid-smooth land.

The results obtained during the course of this program stimulated additional questions suggesting the need for further work. Based on the results of this program, the following areas of investigation should be included in future labyrinth seal performance evaluation programs:

Conventional Straight-Through Seals

- Effect of grooving solid material lands

- Effect of surface roughness on leakage in a rotational environment

Conventional Stepped Seals

- Effect of step height and knife height

- Effect of pitch

- Effect of axial position on land

- Effect of honeycomb lands

REFERENCES

1. Cox, D. M.; Advanced Labyrinth Seal Development Program; EDR 8539, Detroit Diesel Allison, Division of General Motors Corporation, Indianapolis, Indiana, July 1975. (Contract N00140-74-C-0759, Naval Air Propulsion Test Center, Trenton, New Jersey.)

2. Stocker, H. L.; Exploratory Investigation for Reducing Labyrinth Seal Leakage in High Pressure Ratio Gas Turbines; EDR 7968, Detroit Diesel Allison, Division of General Motors Corporation, Indianapolis, Indiana, September 1973. (Contract N00140-73-C-0005, Naval Air Propulsion Test Center, Trenton, New Jersey.)

BIBLIOGRAPHY

Egli, A.: "Leakage of Steam Through Labyrinth Seals"; Trans. ASME; Vol. 57, No. 3, 1935, pp 115-122.

Jerie, J.; "Flow Through Straight-through Labyrinth Seals"; Proceedings of the Seventh International Congress for Applied Mechanics; Vol. 2, Part 1, 1948, pp 70-82.

Kearton, W. J., and Keh, T. H.; "Leakage of Air Through Labyrinth Glands of the Staggered Type"; Proceedings of the Institute of Mechanical Engineers; Vol. 166, 1952, pp 180-188.

Mahler, F. H.; Advanced Seal Technology; Technical Report AFAPL-TR-72-8, Pratt & Whitney Aircraft Division, United Aircraft Corporation, East Hartford, Connecticut, February 1972. (Contract F33615-71-C-1534, Air Force Aero Propulsion Laboratory, Wright-Patterson AFB, Ohio.)

Meyer, C. A., and Lowrie, III, J. A.; The Leakage Thru Straight and Slant Labyrinths and Honeycomb Seals; ASME 75-WA/PTC-2, August 1974.

Vermes, G.; "A Fluid Mechanics Approach to the Labyrinth Seal Leakage Problem"; Journal of Power Engineering, Trans. ASME; Series A, Vol. 83, No. 2, April 1961, pp 161-169.

Zabriskie, W., and Sternlicht, B.; "Labyrinth Seal Leakage Analysis"; Journal of Basic Engineering, Trans. ASME; Series D, Vol. 81, September 1959, pp 332-340.

APPENDIX A

Four Knife Straight-Through Labyrinth Seal Flow Parameter Curves from the 2D Air Seal Test Rig for Smooth, Abradable, and Honeycomb Lands

The labyrinth seal flow parameter curves contained in Appendix A were derived from testing accomplished in the Detroit Diesel Allison two-dimensional (2D) air seal test rig.

The static test data from the 2D rig include performance for a solid-smooth land, four abradable lands, and three honeycomb cell size lands using a conventional four knife straight-through seal. Nickel-graphite and aluminum-polyester materials were utilized to represent solid abradables, and "Abradable A" and "Abradable B" materials were utilized to represent porous abradables. The cell sizes for the honeycomb lands were .079 cm (.031 in.), .159 cm (.062 in.), and .318 cm (.125 in.). The cell depth was .381 cm (.150 in.). Each land was tested at three clearances: .013 cm (.005 in.), .025 cm (.010 in.), and .051 cm (.020 in.).

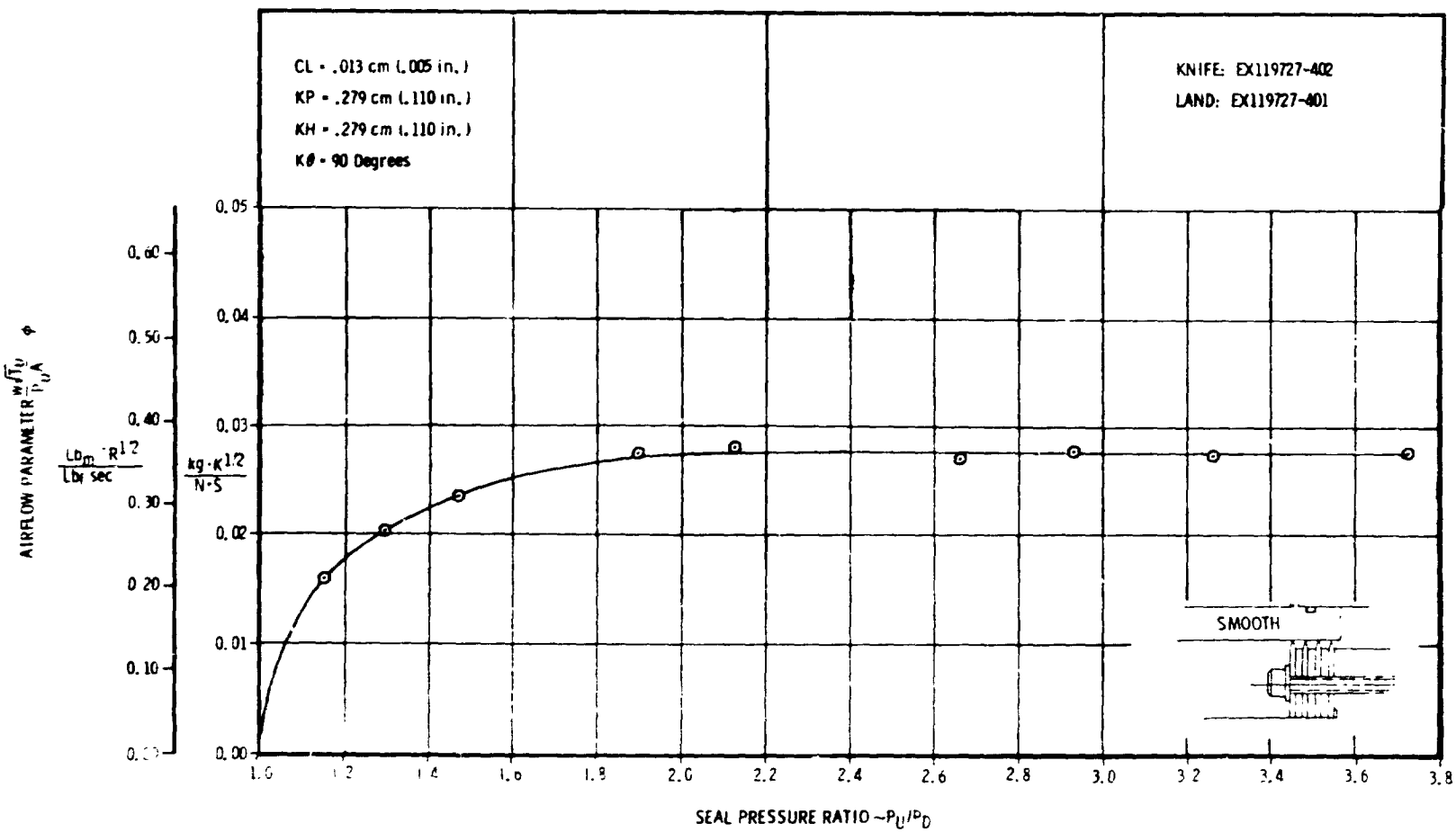

FIGURE A-1. 2D RIG TEST RESULTS OF A 4 KNIFE STRAIGHT-THROUGH SEAL WITH A SOLID-SMOOTH SURFACE LAND

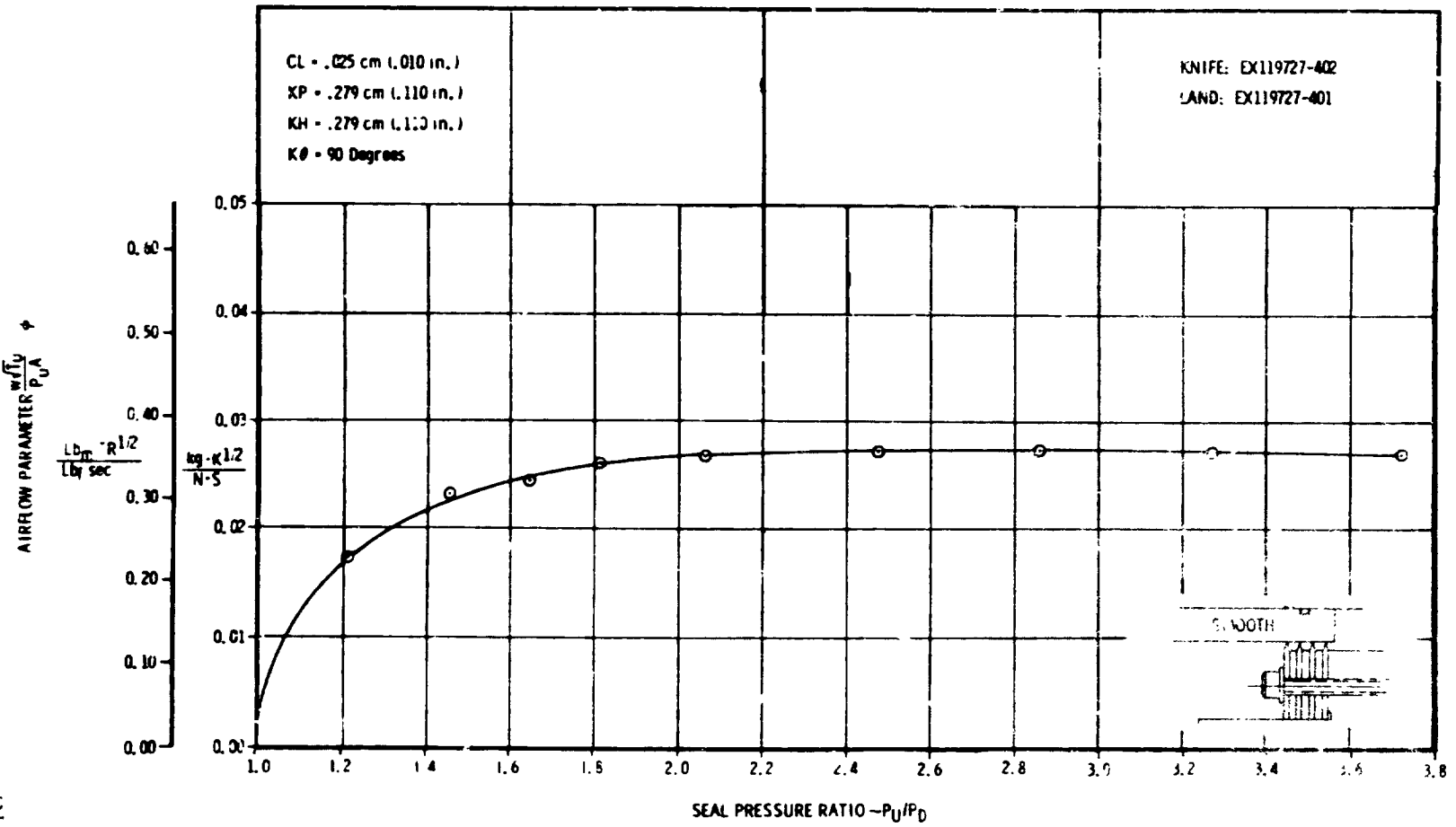

FIGURE A-2. 2D RIG TEST RESULTS OF A 4 KNIFE STRAIGHT-THROUGH SEAL WITH A SOLID-SMOOTH SURFACE LAND

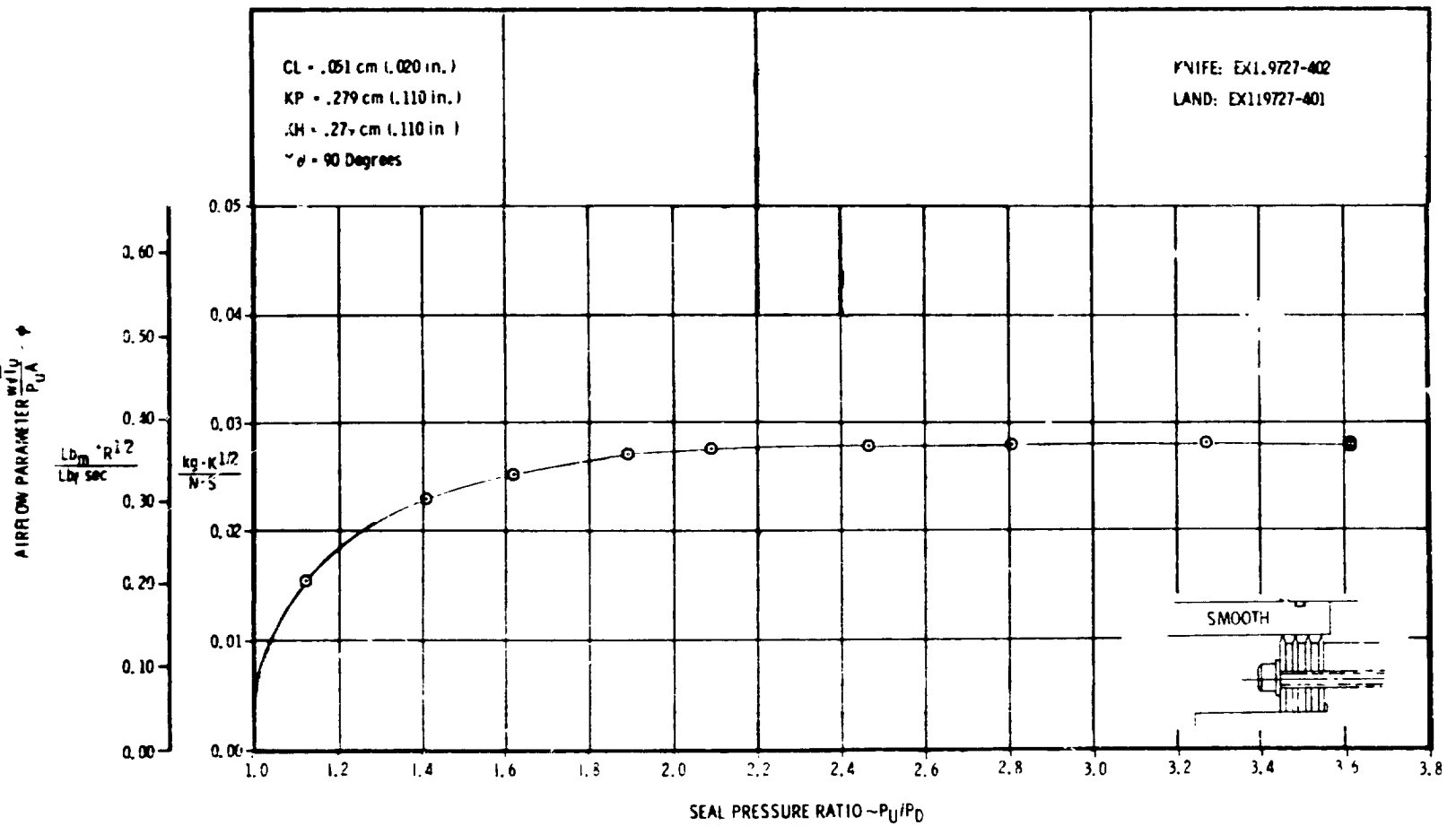

FIGURE A-3. 2D RIG TEST RESULTS OF A 4 KNIFE STRAIGHT-THROUGH SEAL WITH A SOLID-SMOOTH SURFACE LAND

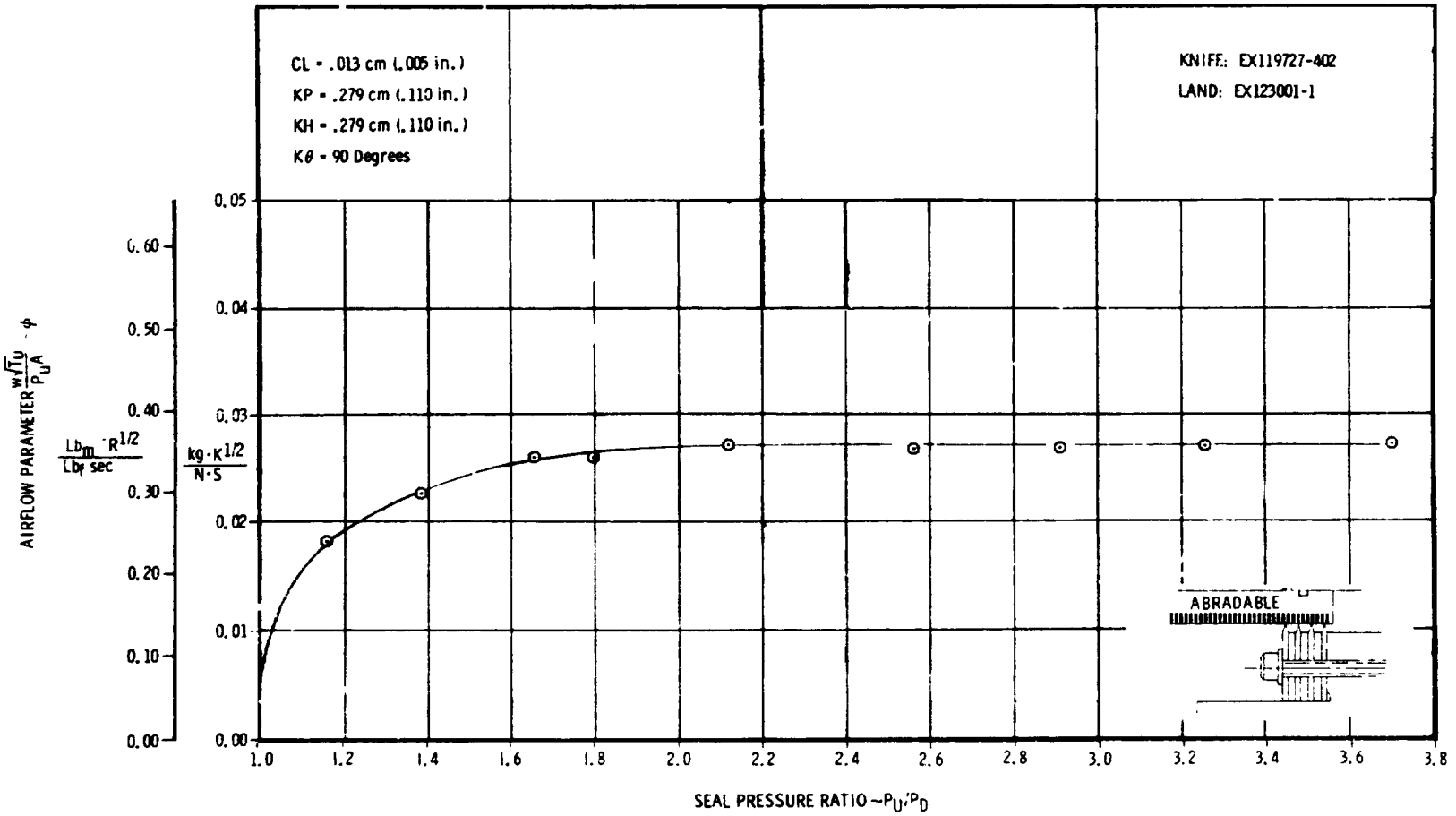

FIGURE A-4. 2D RIG TEST RESULTS OF A 4 KNIFE STRAIGHT-THROUGH SEAL WITH A NICKEL-GRAPHITE SURFACE LAND

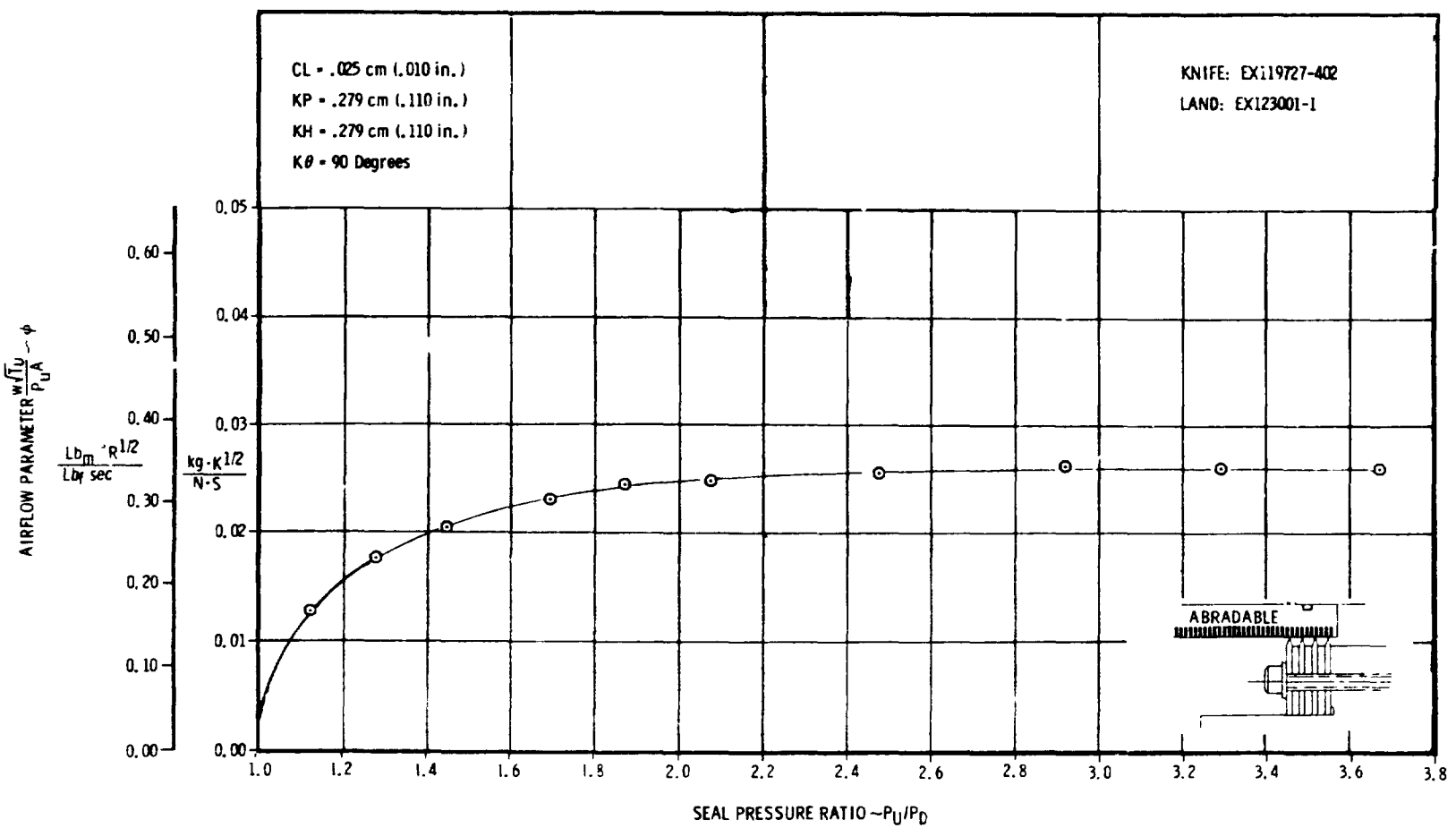

FIGURE A-5. 2D RIG TEST RESULTS OF A 4 KNIFE STRAIGHT-THROUGH SEAL WITH A NICKEL-GRAPHITE SURFACE LAND

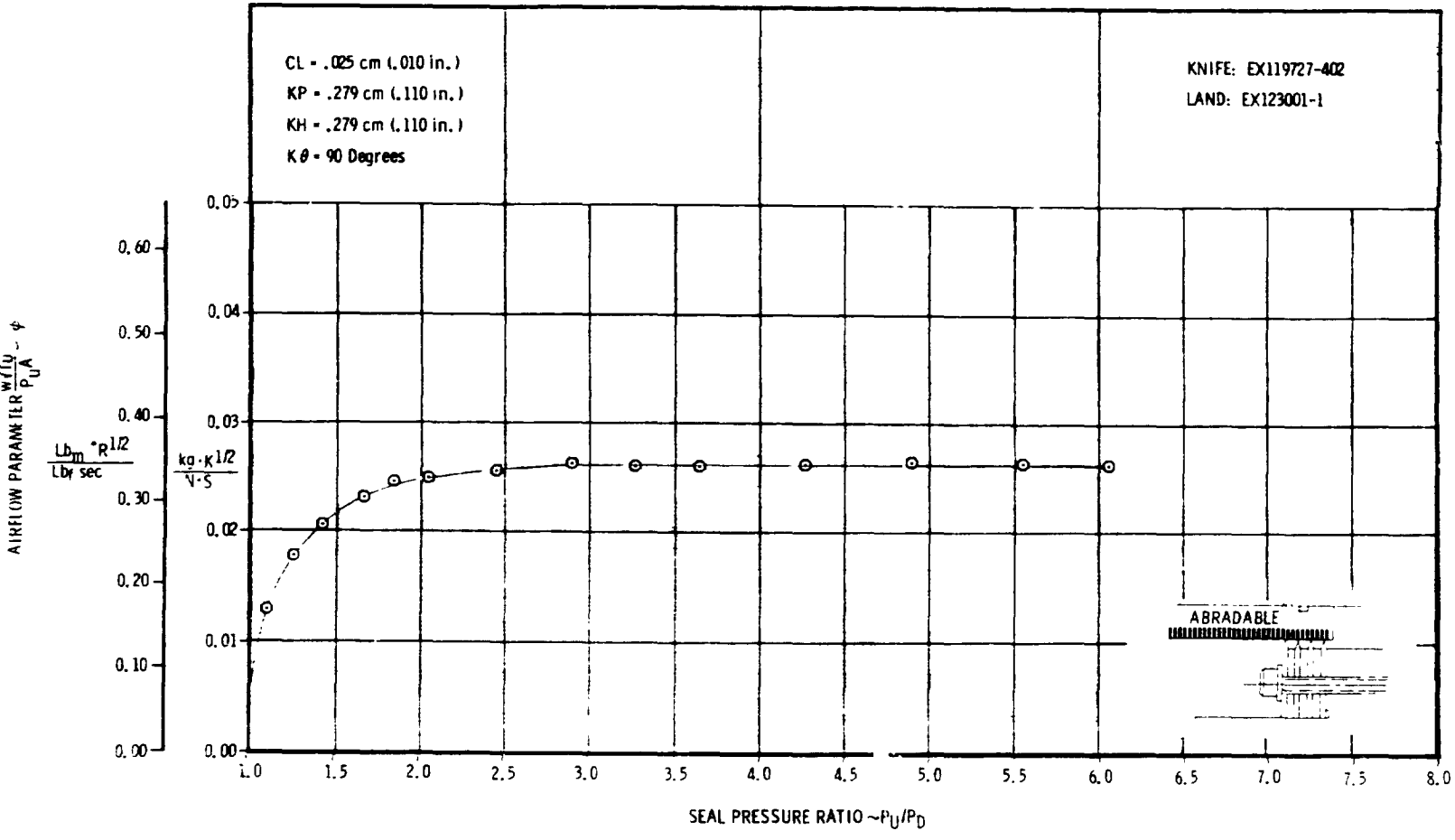

FIGURE A-6 2D RIG TEST RESULTS OF A 4 KNIFE STRAIGHT-THROUGH SEAL WITH A NICKEL-GRAPHITE SURFACE LAND

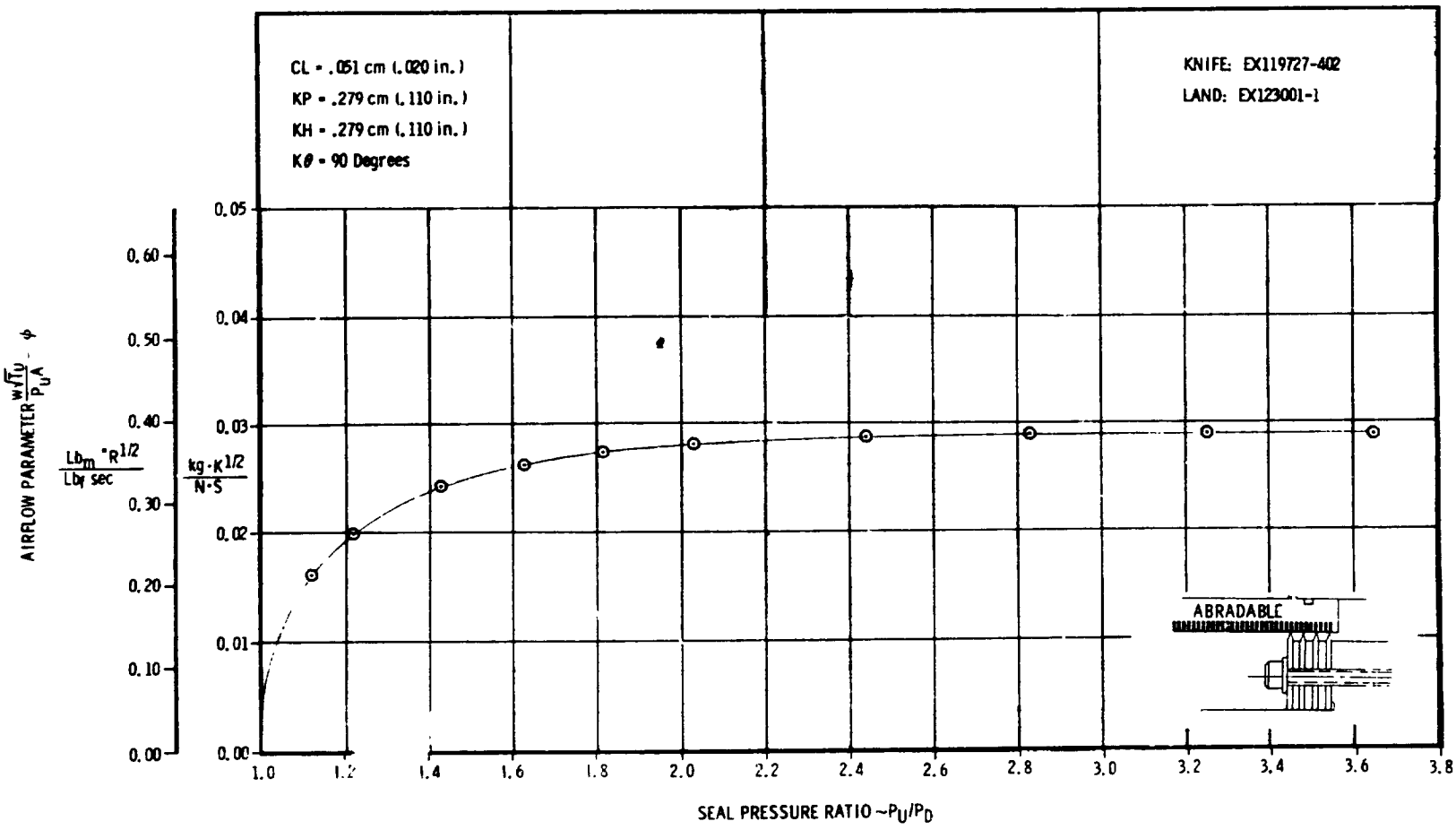

FIGURE A-7. 2D RIG TEST RESULTS OF A 4 KNIFE STRAIGHT-THROUGH SEAL WITH A NICKEL-GRAPHITE SURFACE LAND

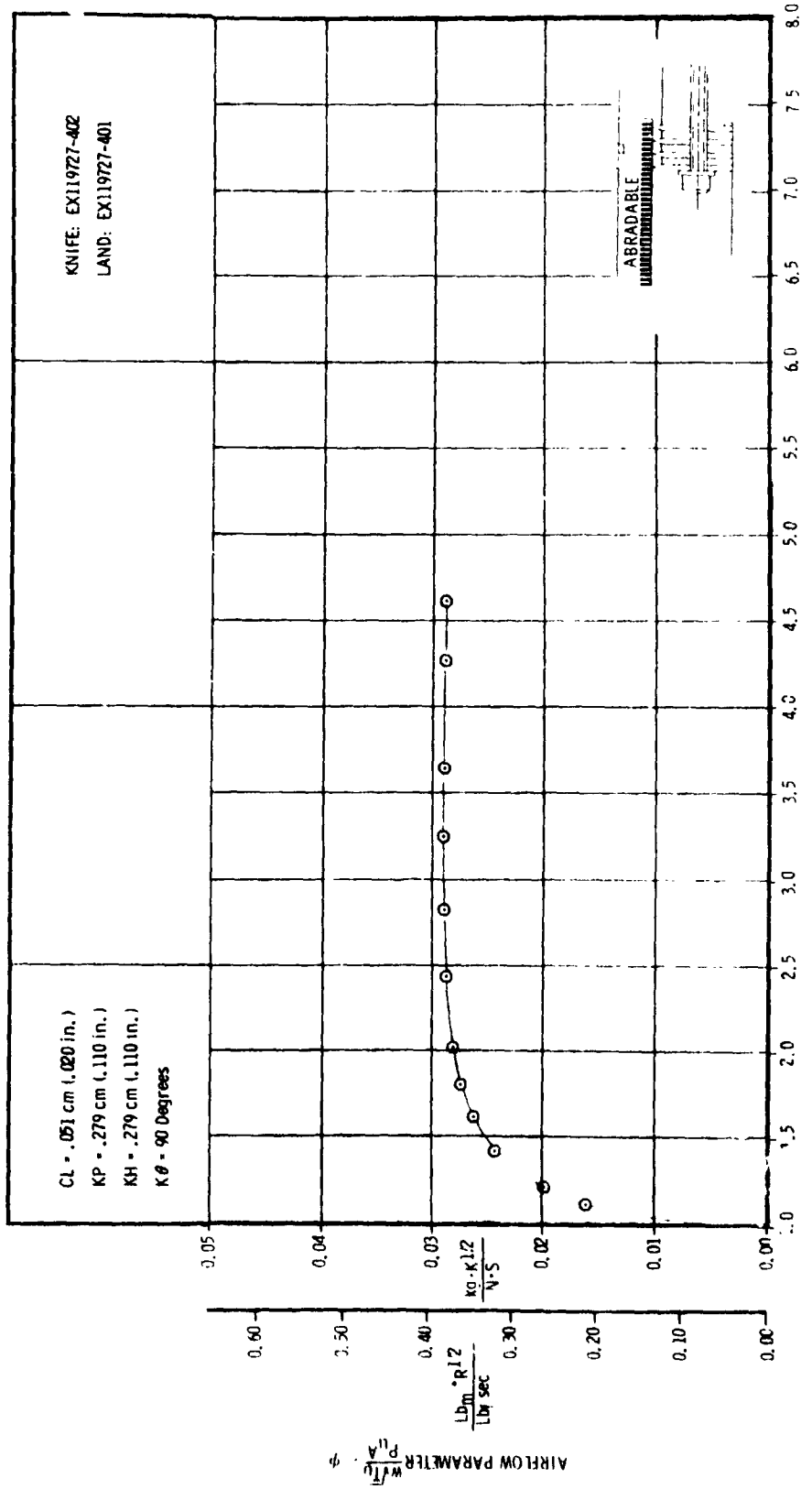

FIGURE A-8 2D RIG TEST RESULTS OF A 4 KNIFE STRAIGHT-THROUGH SEAL WITH A NICKEL-GRAPHITE SURFACE LAND

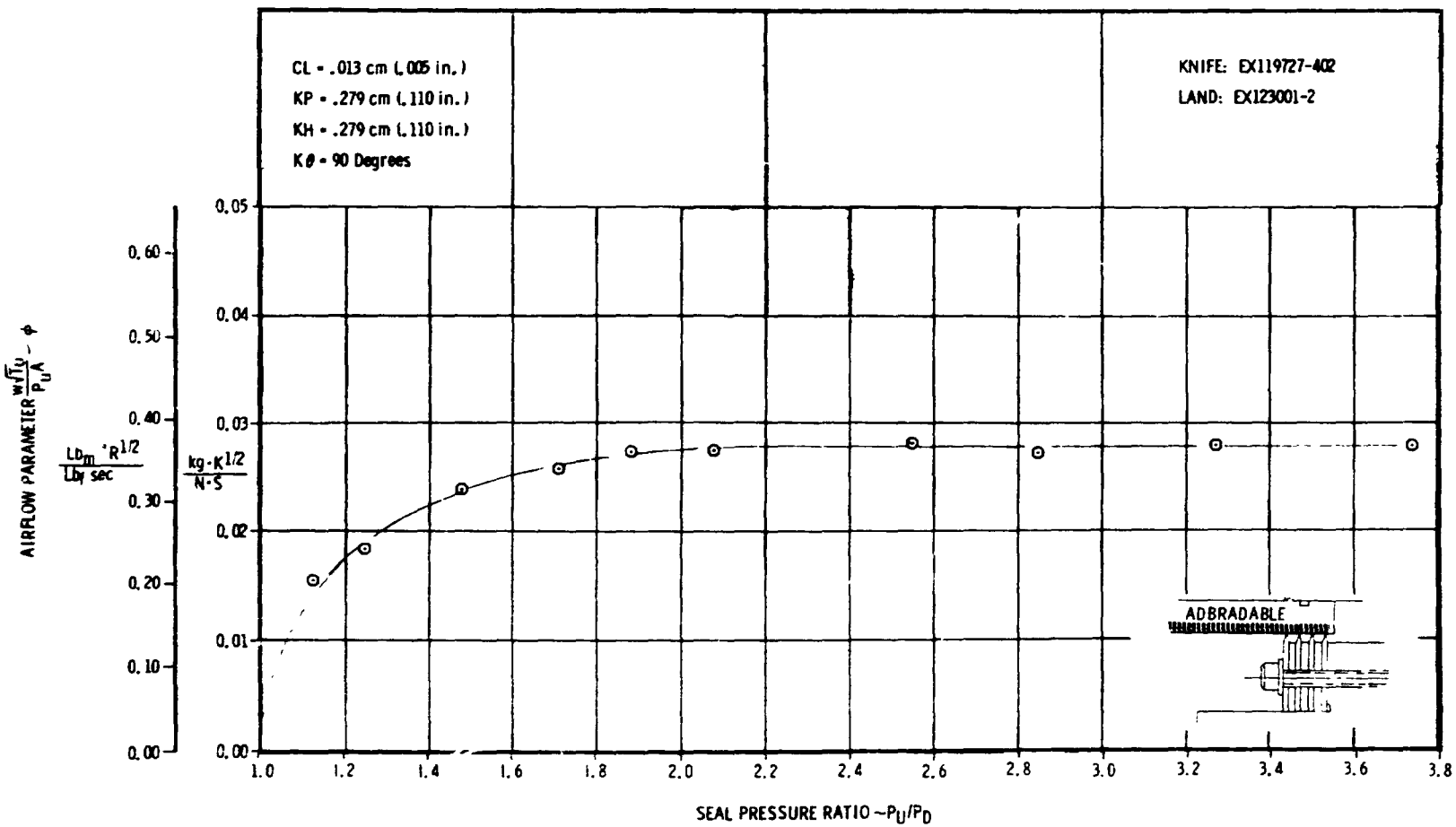

FIGURE A-9. 2D RIG TEST RESULTS OF A 4 KNIFE STRAIGHT-THROUGH SEAL WITH AN ALUMINUM-POLYESTER SURFACE LAND

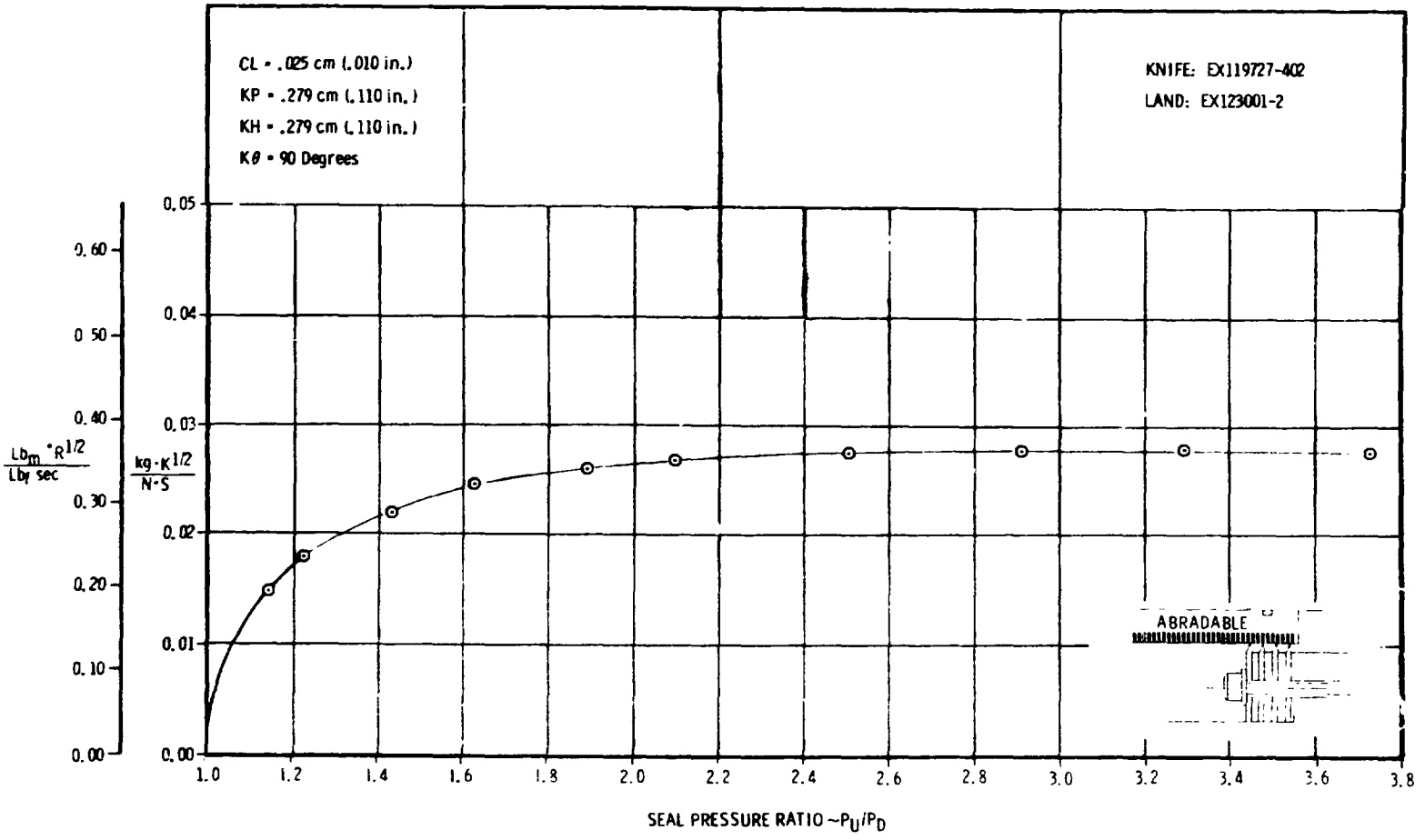

FIGURE A-10. 2D RIG TEST RESULTS OF A 4 KNIFE STRAIGHT-THROUGH SEAL WITH AN ALUMINUM-POLYESTER SURFACE LAND

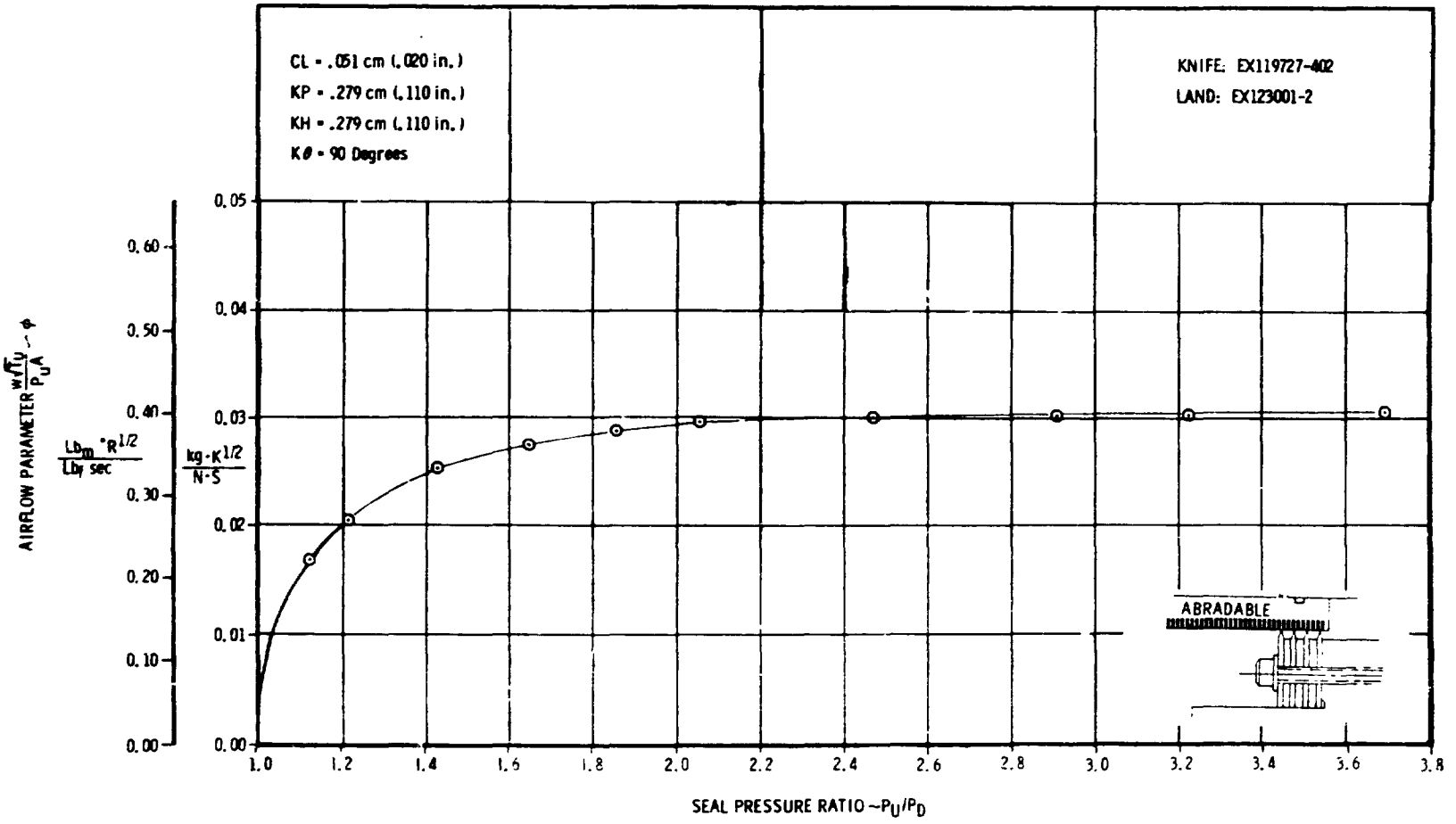

FIGURE A-11. 2D RIG TEST RESULTS OF A 4 KNIFE STRAIGHT-THROUGH SEAL WITH AN ALUMINUM-POLYESTER SURFACE LAND

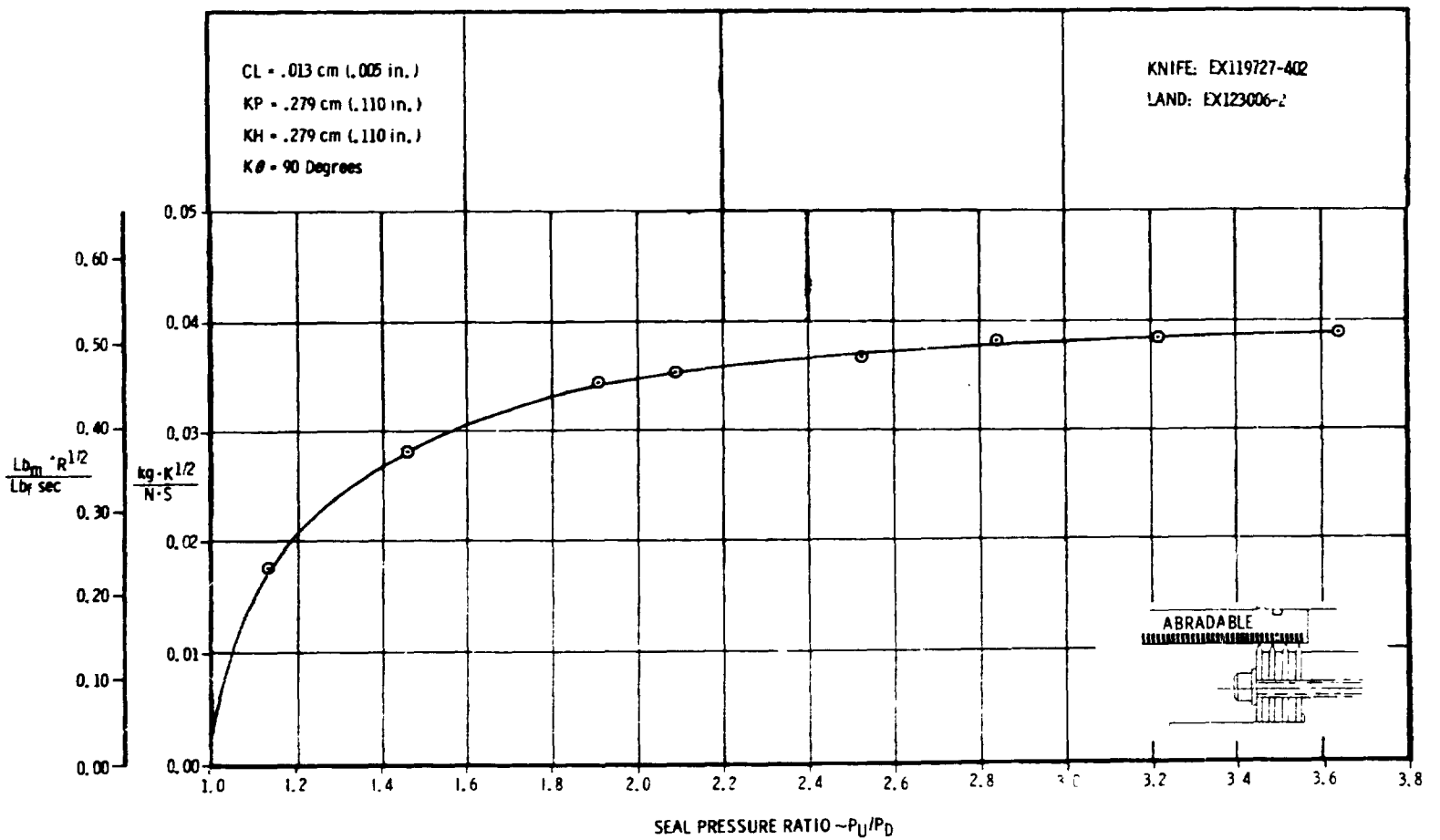

FIGURE A-12. 2D RIG TEST RESULTS OF A 4 KNIFE STRAIGHT-THROUGH SEAL WITH AN "ABRADABLE A" SURFACE LAND

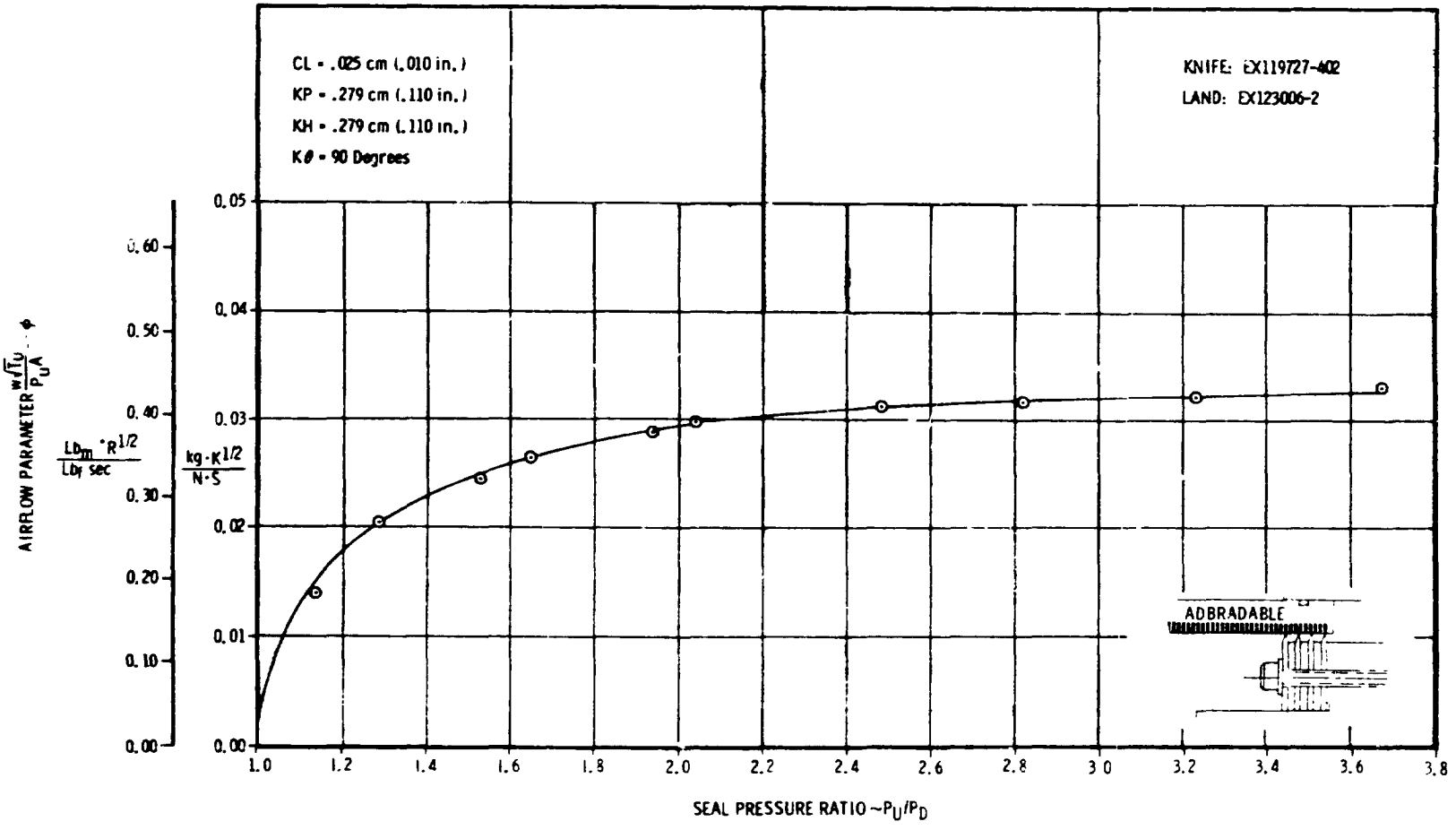

FIGURE A-13. 2D RIG TEST RESULTS OF A 4 KNIFE STRAIGHT-THROUGH SEAL WITH AN "ABRADABLE A" SURFACE LAND

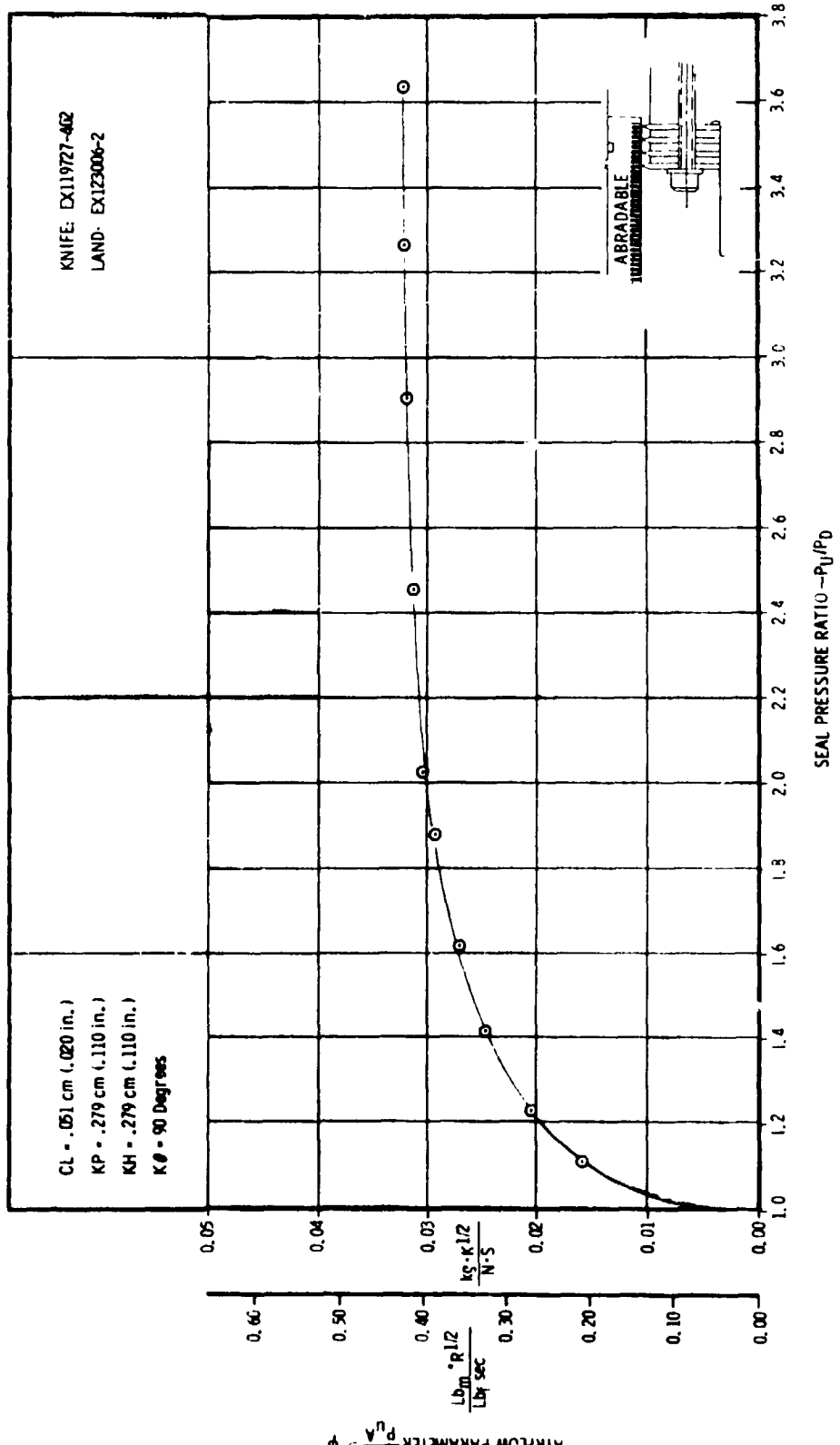

FIGURE A-14. 2D RIG TES: RESULTS OF A 4 KNIFE STRAIGHT-THROUGH SEAL WITH AN "ABRADABLE A" SURFACE LAND

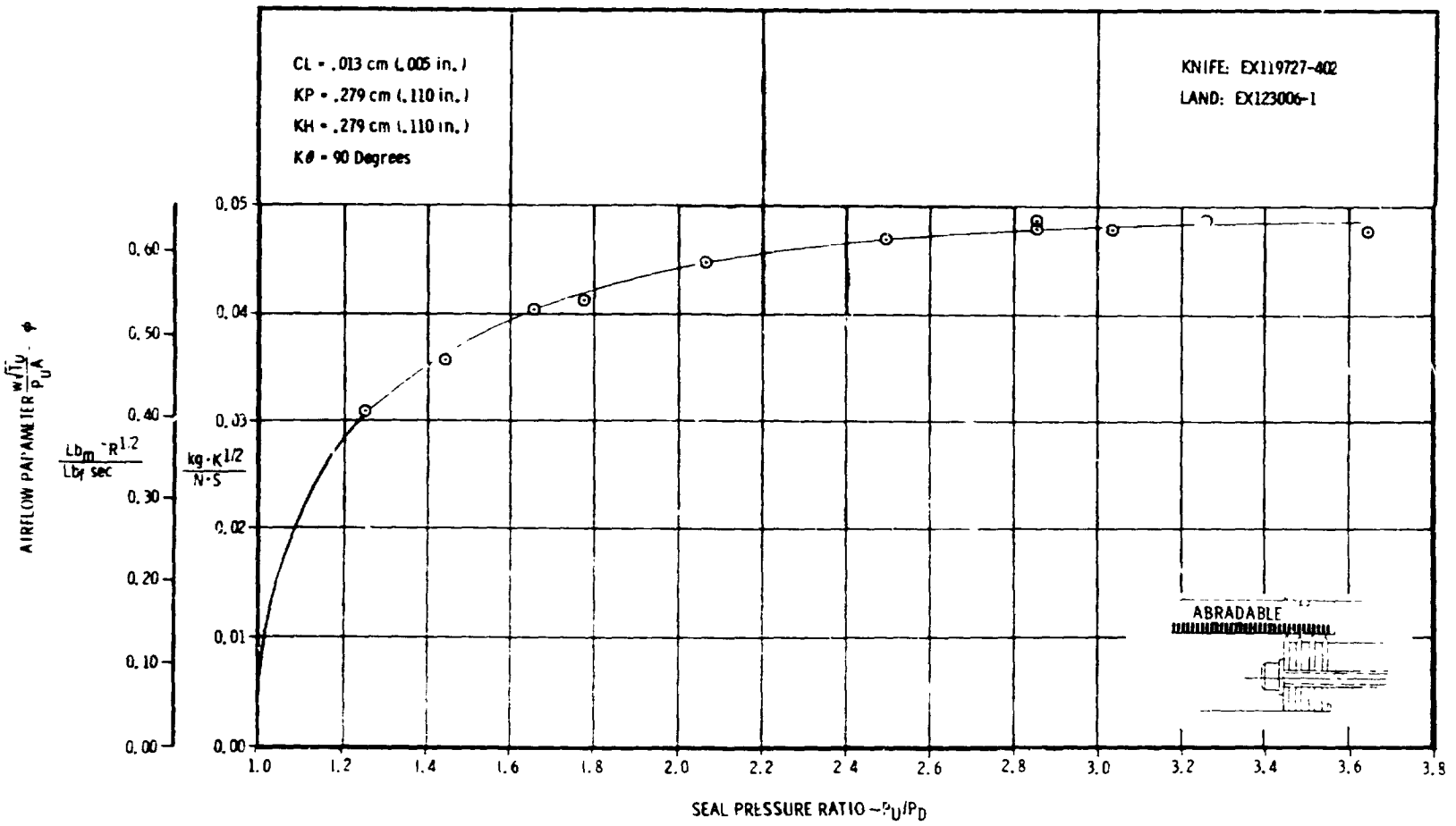

FIGURE A-15. 2D RIG TEST RESULTS OF A 4 KNIFE STRAIGHT-THROUGH SEAL WITH AN "ABRADABLE B" SURFACE LAND

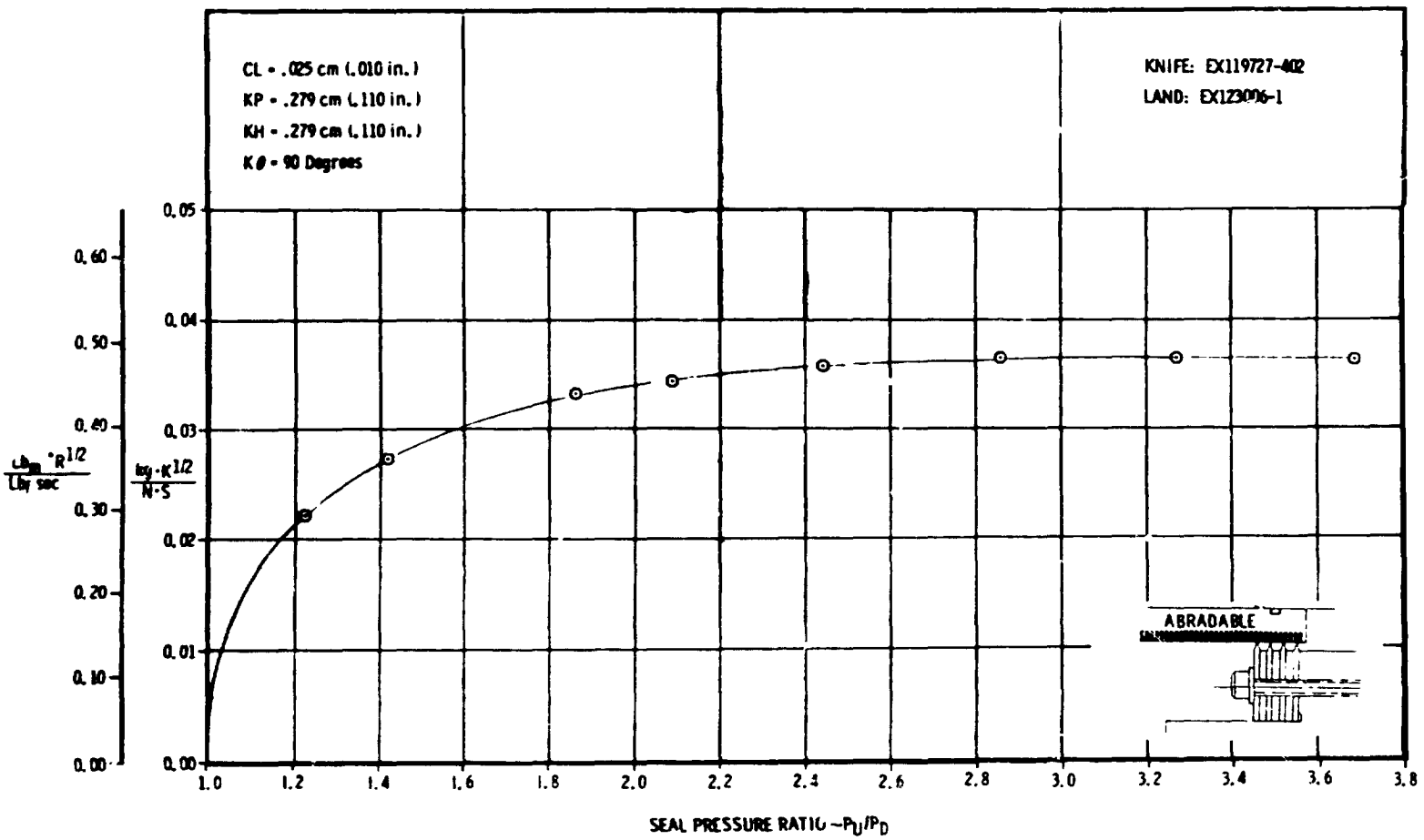

FIGURE A-16. 2D RIG TEST RESULTS OF A 4 KNIFE STRAIGHT-THROUGH SEAL WITH AN "ABRADABLE B" SURFACE LAND

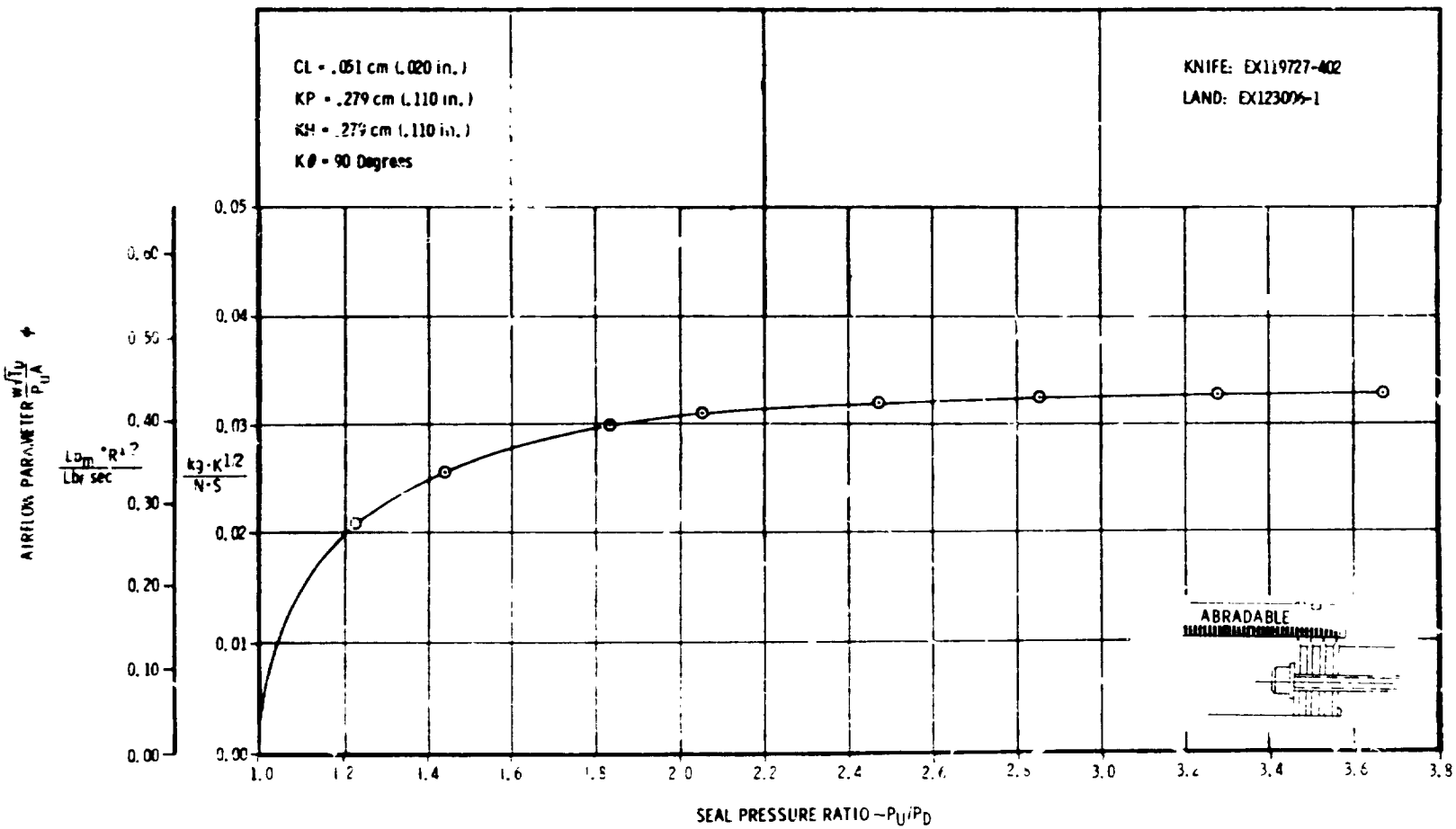

FIGURE A-17. 2D RIG TEST RESULTS OF A 4 KNIFE STRAIGHT-THROUGH SEAL WITH AN "ABRADABLE B" SURFACE LAND

FIGURE A-18. 2D RIG TEST RESULTS OF A 4 KNIFE STRAIGHT-THROUGH SEAL WITH A HONEYCOMB SURFACE LAND

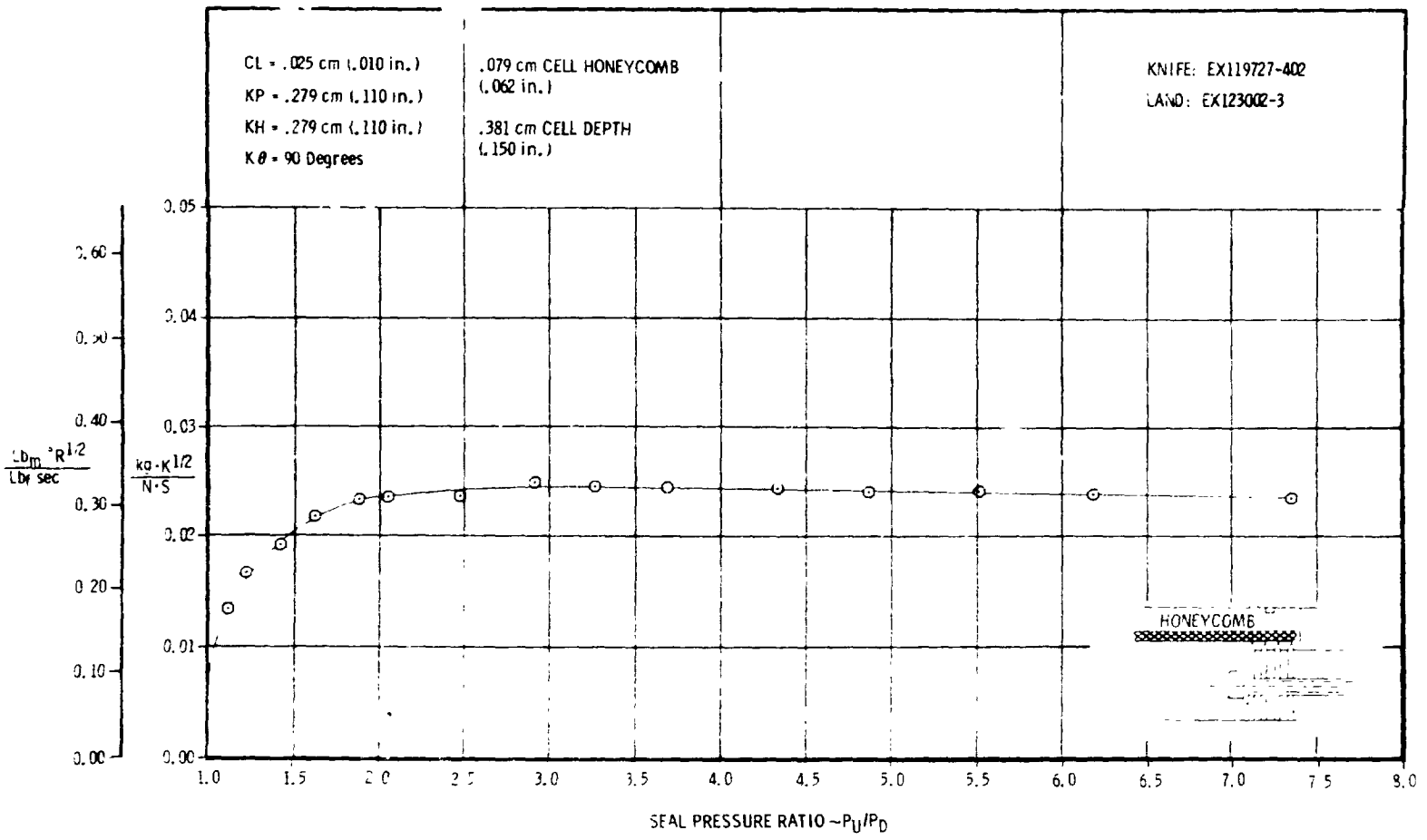

FIGURE A-19. 2D RIG TEST RESULTS OF A 4 KNIFE STRAIGHT-THROUGH SEAL WITH A HONEYCOMB SURFACE LAND

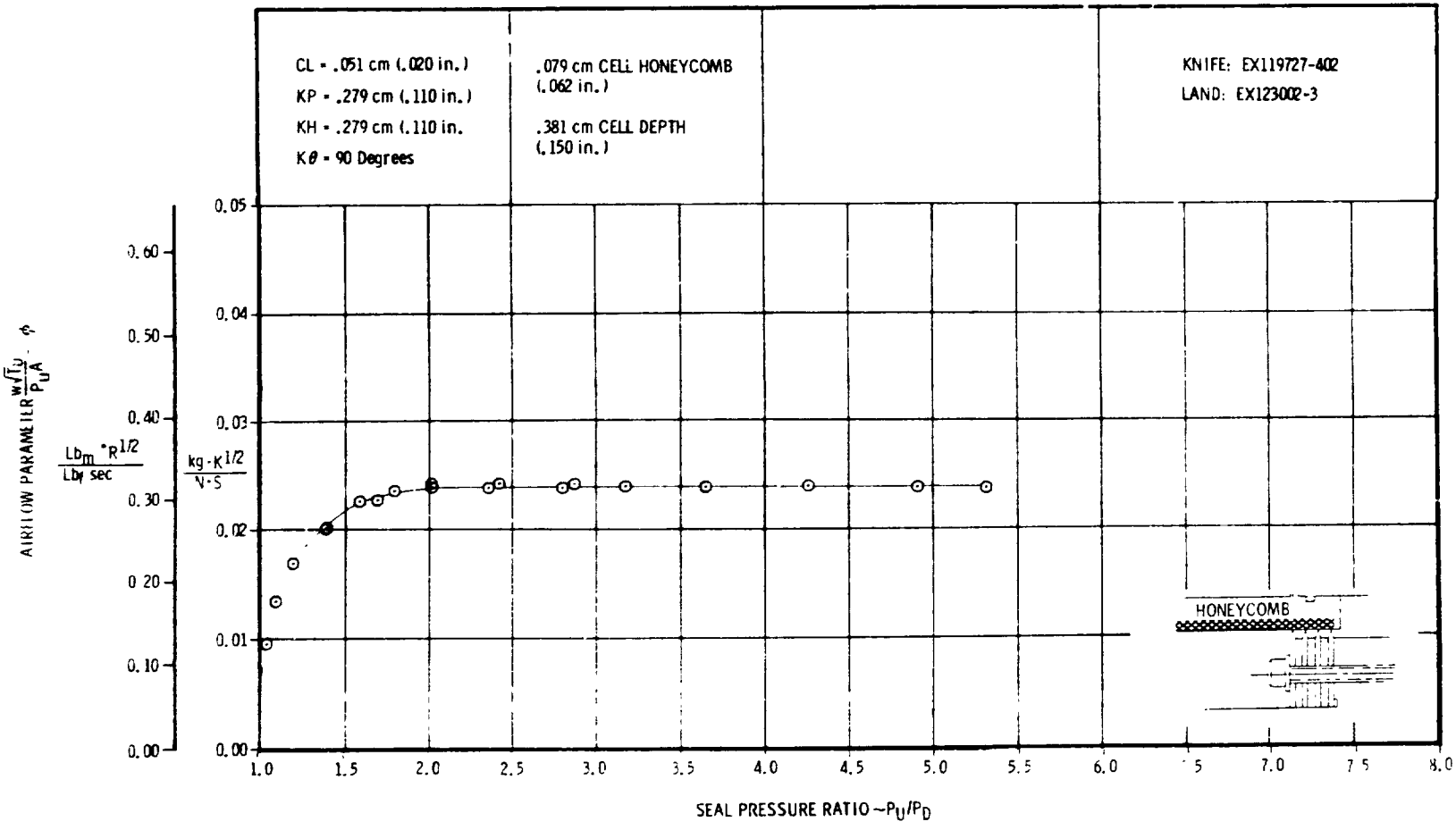

FIGURE A-20. 2D RIG TEST RESULTS OF A 4 KNIFE STRAIGHT-THROUGH SEAL WITH A HONEYCOMB SURFACE LAND

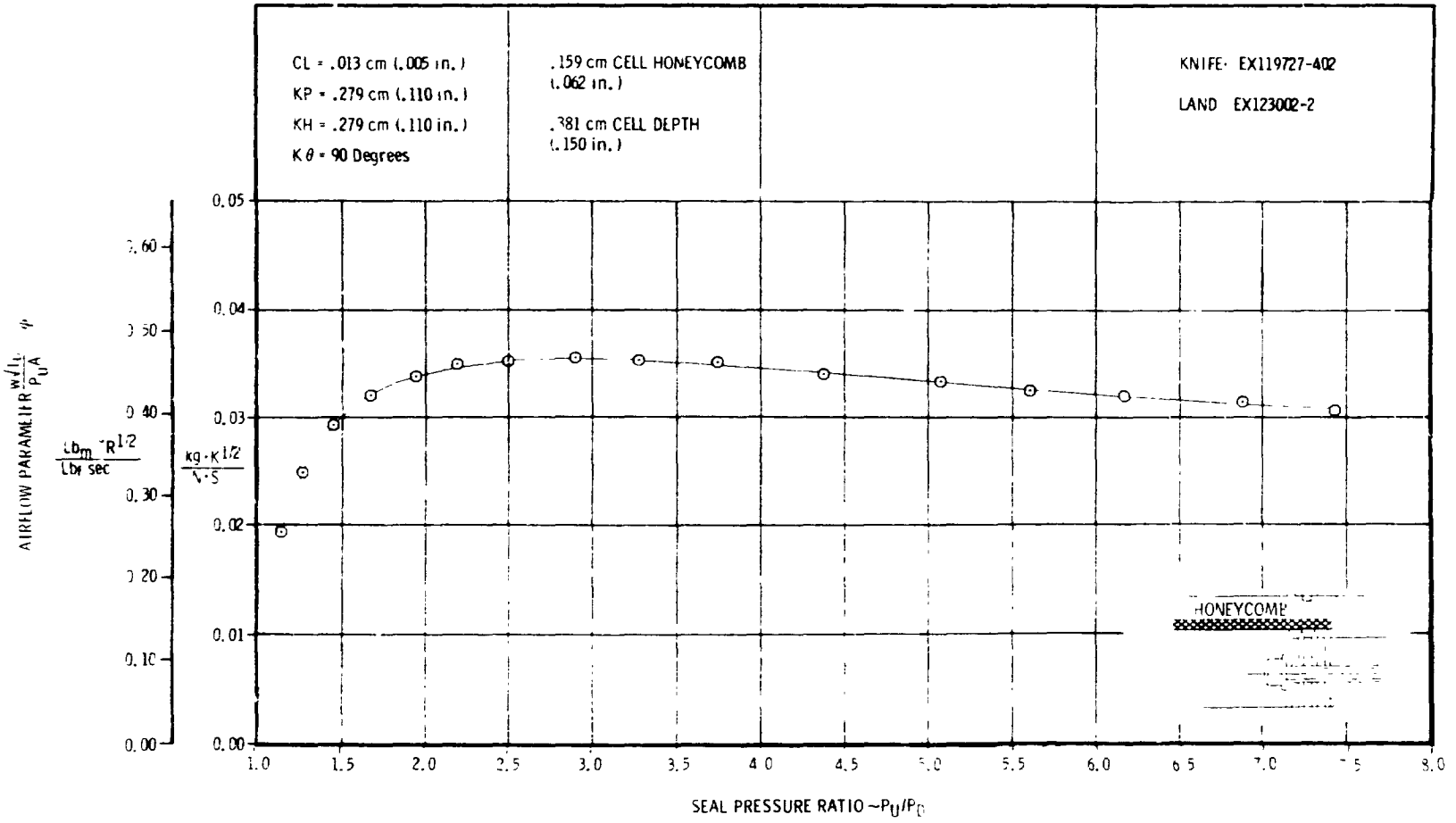

FIGURE A-21. 2D RIG TEST RESULTS OF A 4 KNIFE STRAIGHT-THROUGH SEAL WITH A HONEYCOMB SURFACE LAND

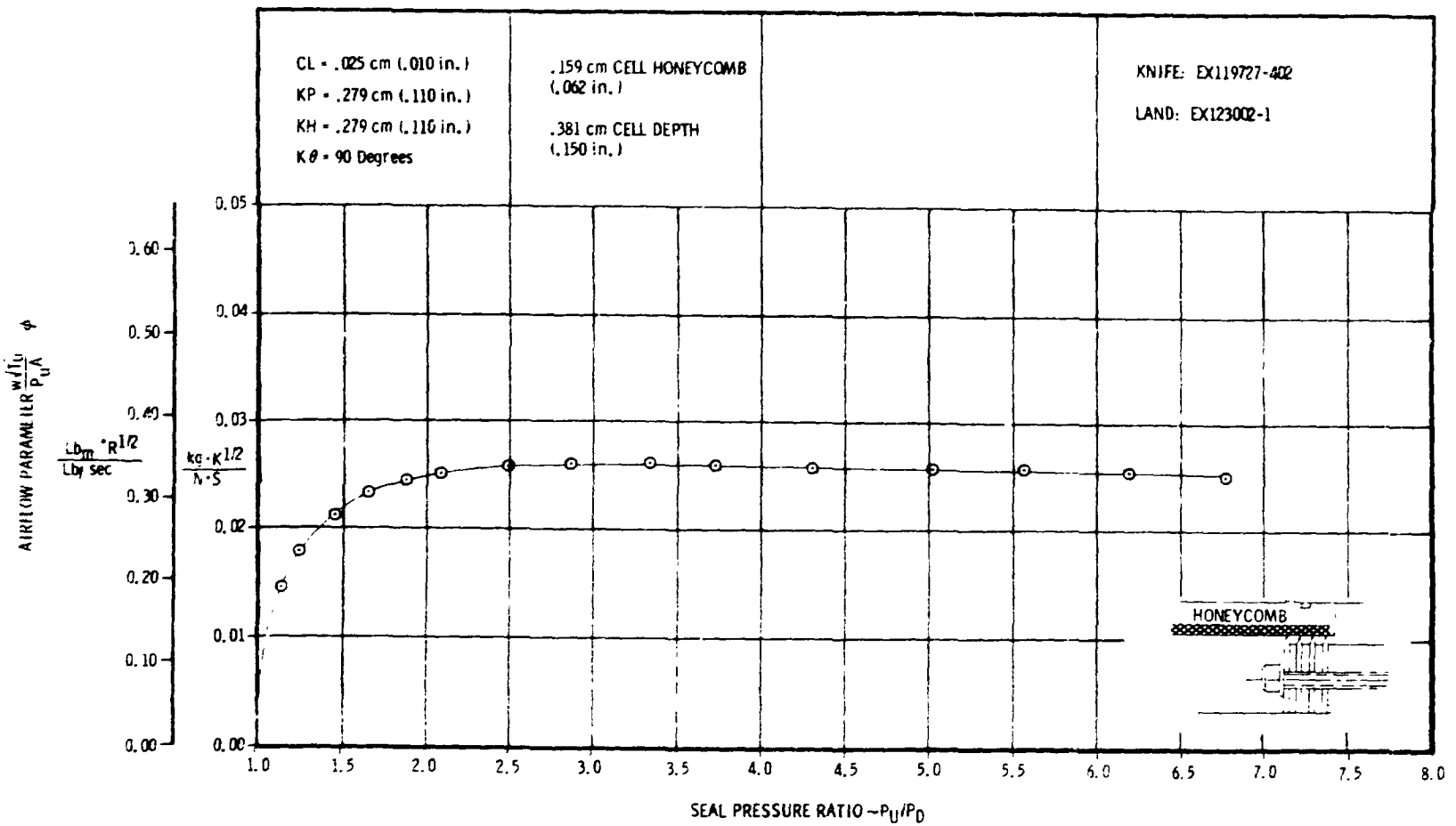

FIGURE A-22. 2D KIG TEST RESULTS OF A 4 KNIFE STRAIGHT-THROUGH SEAL WITH A HONEYCOMB SURFACE LAND

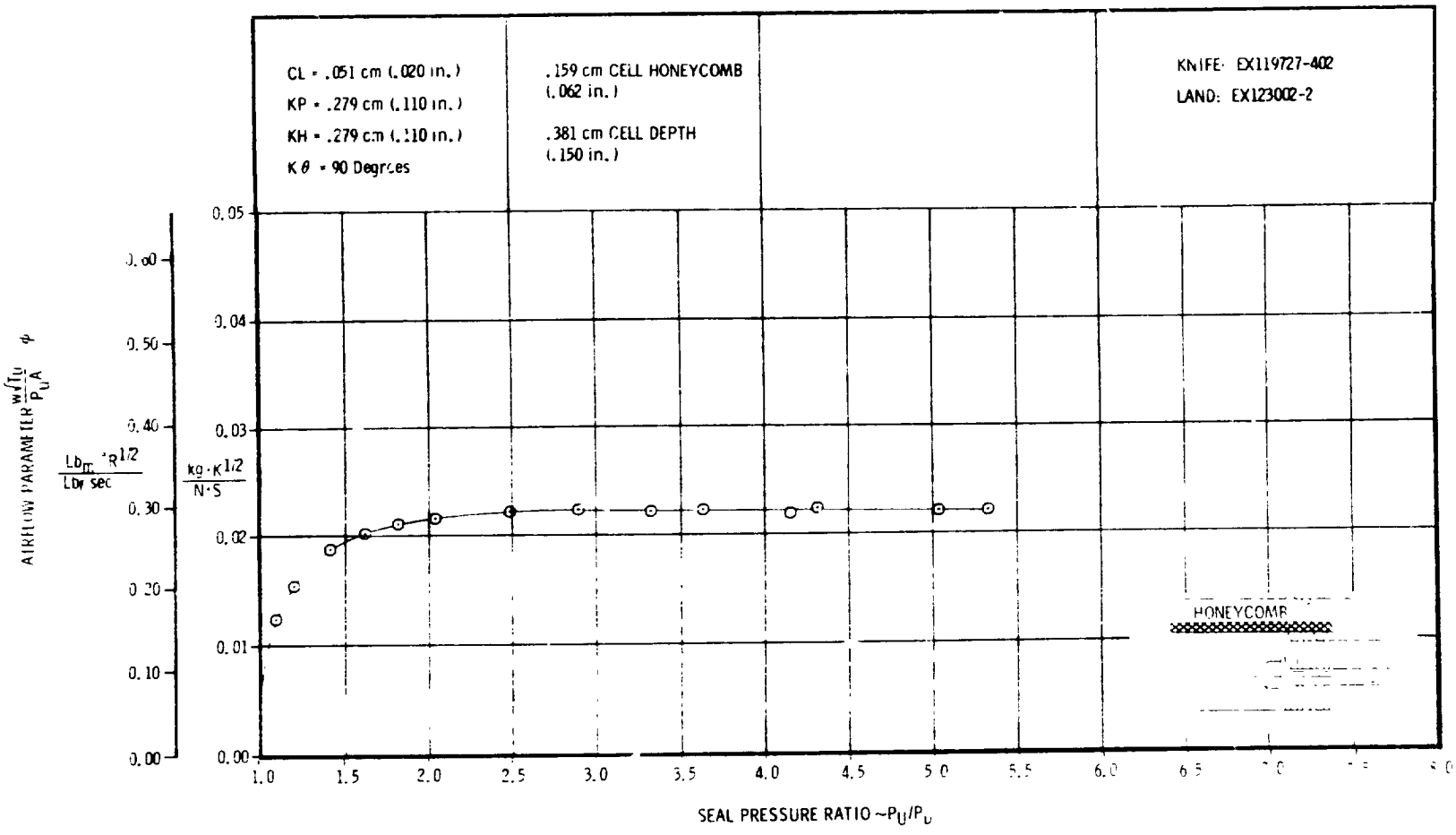

FIGURE A-23. 2D RIG TEST RESULTS OF A 4 KNIFE STRAIGHT-THROUGH SEAL WITH A HONEYCOMB SURFACE LAND

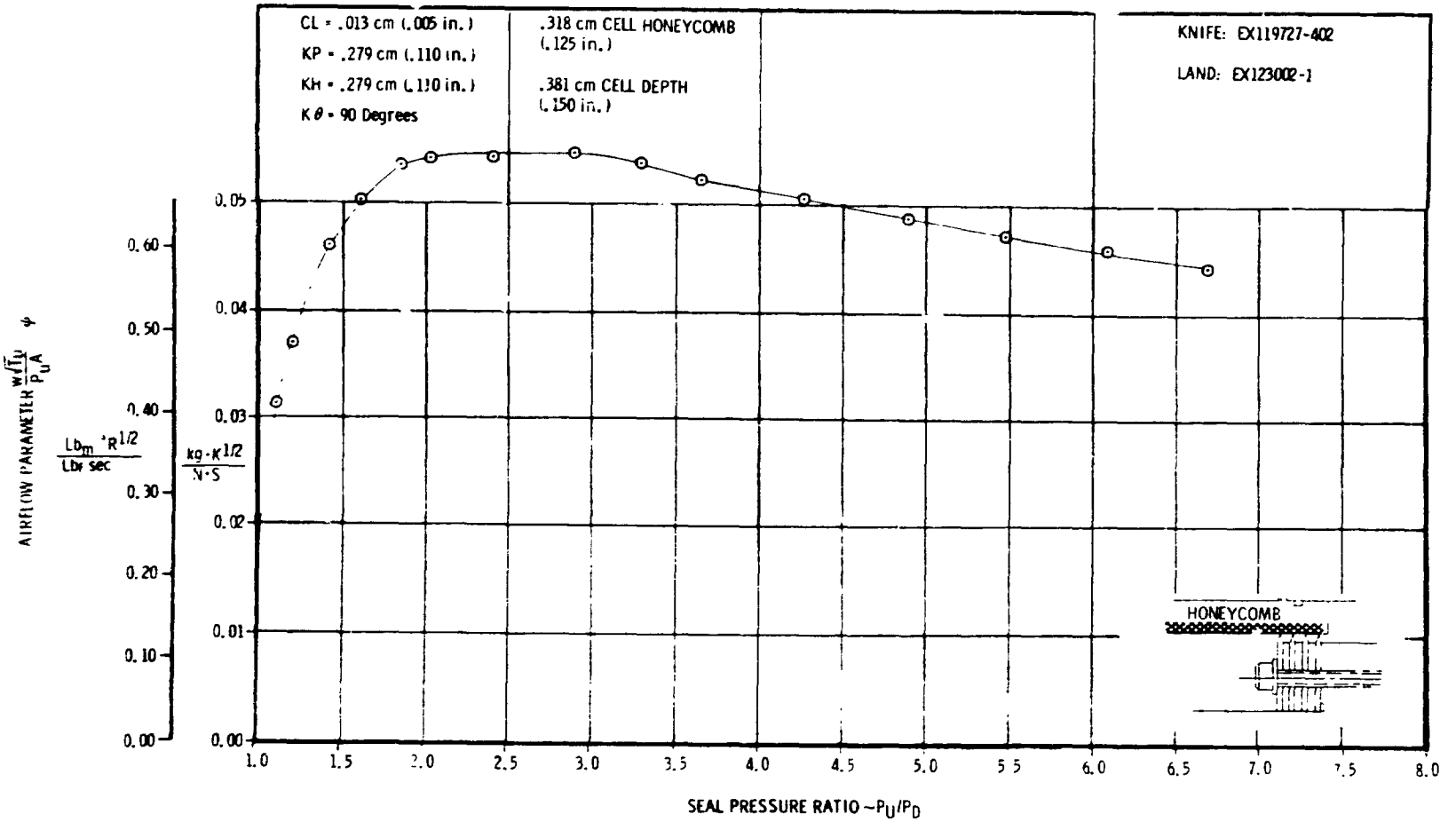

FIGURE A-24.2D RIG TEST RESULTS OF A 4 KNIFE STRAIGHT-THROUGH SEAL WITH A HONEYCOMB SURFACE LAND

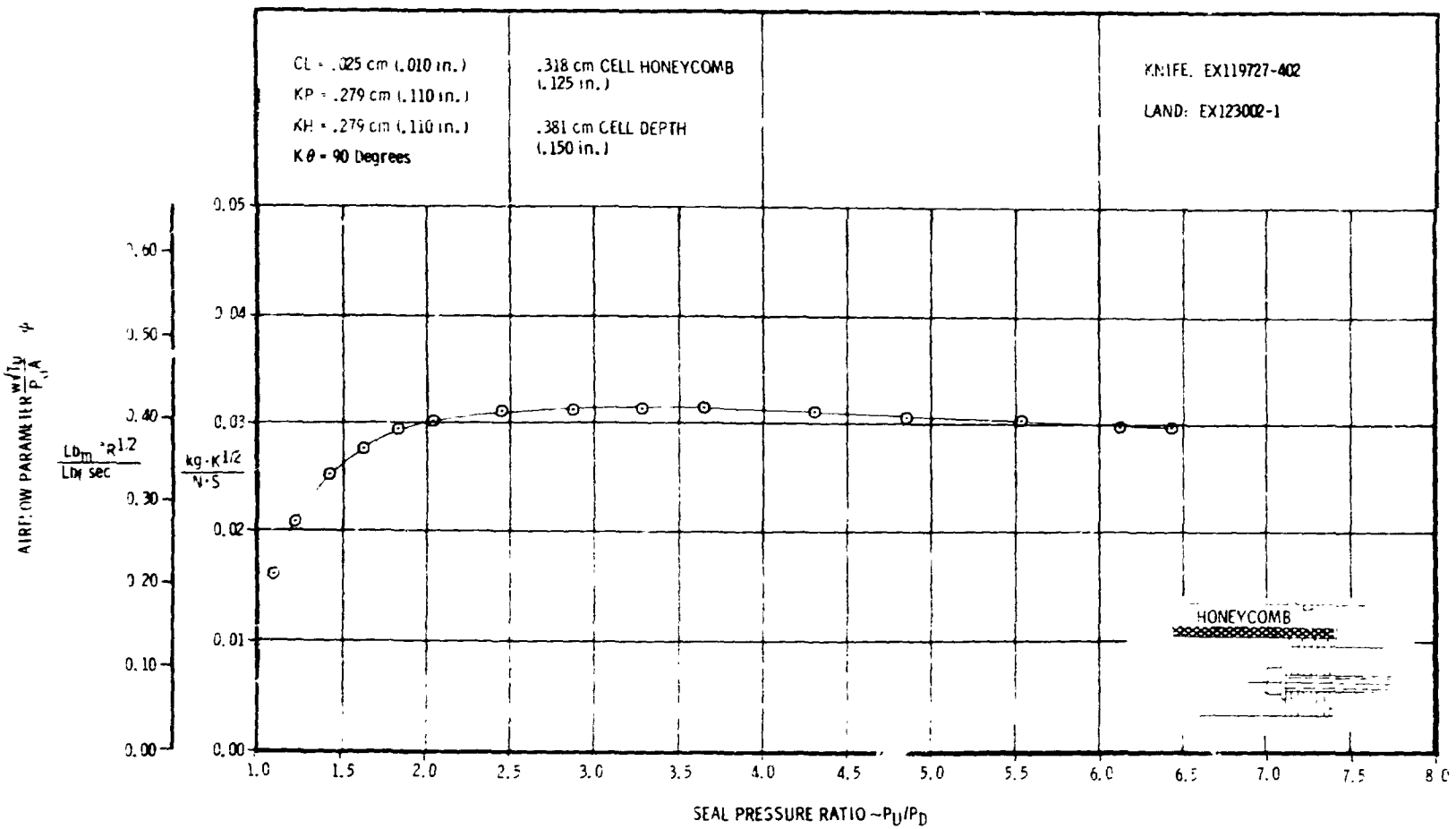

FIGURE A-25. 2D RIG TEST RESULTS OF A 4 KNIFE STRAIGHT-THROUGH SEAL WITH A HONEYCOMB SURFACE LAND

FIGURE A-26. 2D RIG TEST RESULTS OF A 4 KNIFE STRAIGHT-THROUGH SEAL WITH A HONEYCOMB SURFACE LAND

APPENDIX B

Four Knife Straight-Through Labyrinth Seal Flow Parameter Curves from the 3D Air Seal Test Rig for Smooth, Abradable, and Honeycomb Lands

The labyrinth seal flow parameter curves contained in Appendix B were derived from testing accomplished in the Detroit Diesel Allison 15.2 cm (6.00 in.) diameter dynamic air seal test rig (3D rig).

The data include 3D rig static and dynamic test results for solid-smooth, abradable, and honeycomb lands using a conventional four knife straight-through seal design. The "Abradable A" land material represented the porous lands. The honeycomb land cell size was .159 cm (.062 in.), and the cell depth was .254 cm (.100 in.).

Each land was tested with seal knife pitch values of .203 cm (.080 in.), .279 cm (.110 in.), and .356 cm (.140 in.). All configurations were tested at .025 cm (.010 in.) and .051 cm (.020 in.) radial clearances.

In addition to the static test, dynamic tests were run at constant rotational speeds equivalent to knife tip velocities of 80 m/s (261 ft/sec), 159 m/s (523 ft/sec), and 239 m/s (785 ft/sec).

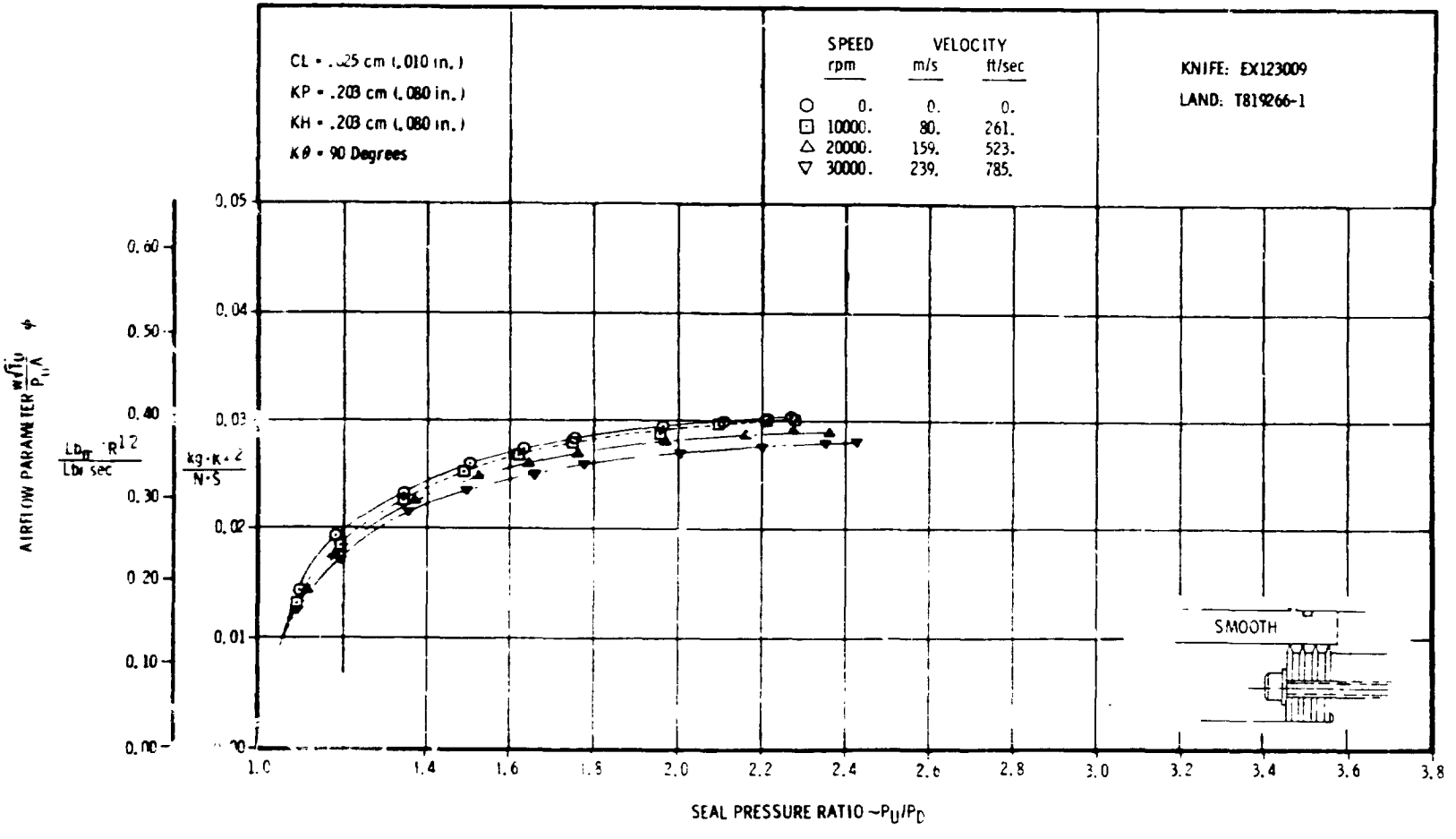

FIGURE B-1. 3D RIG TEST RESULTS OF A 4 KNIFE STRAIGHT-THROUGH SEAL WITH A SOLID-SMOOTH SURFACE LAND

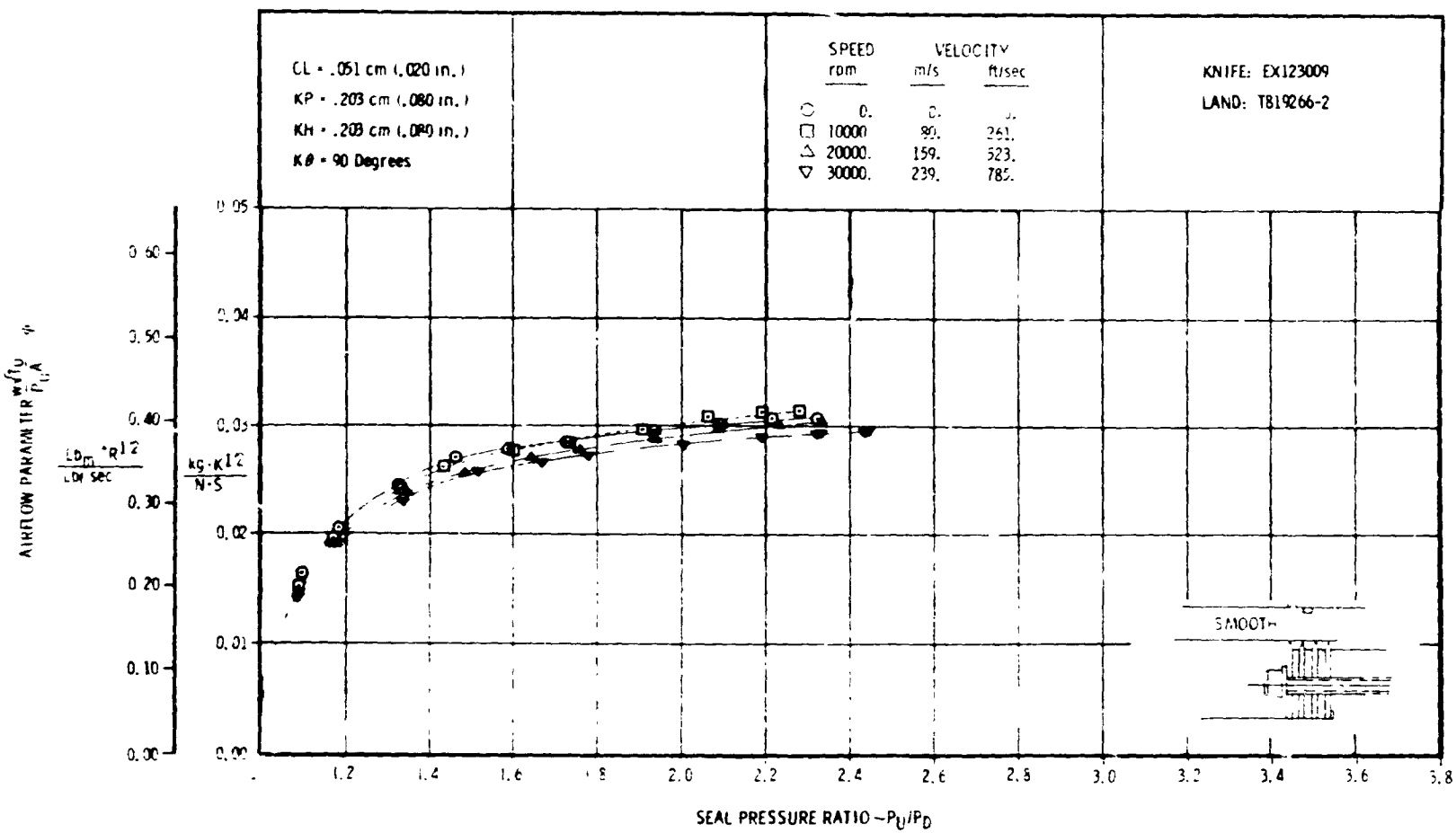

FIGURE B-2. 3D RIG TEST RESULTS OF A 4 KNIFE STRAIGHT-THROUGH SEAL WITH A SOLID-SMOOTH SURFACE LAND

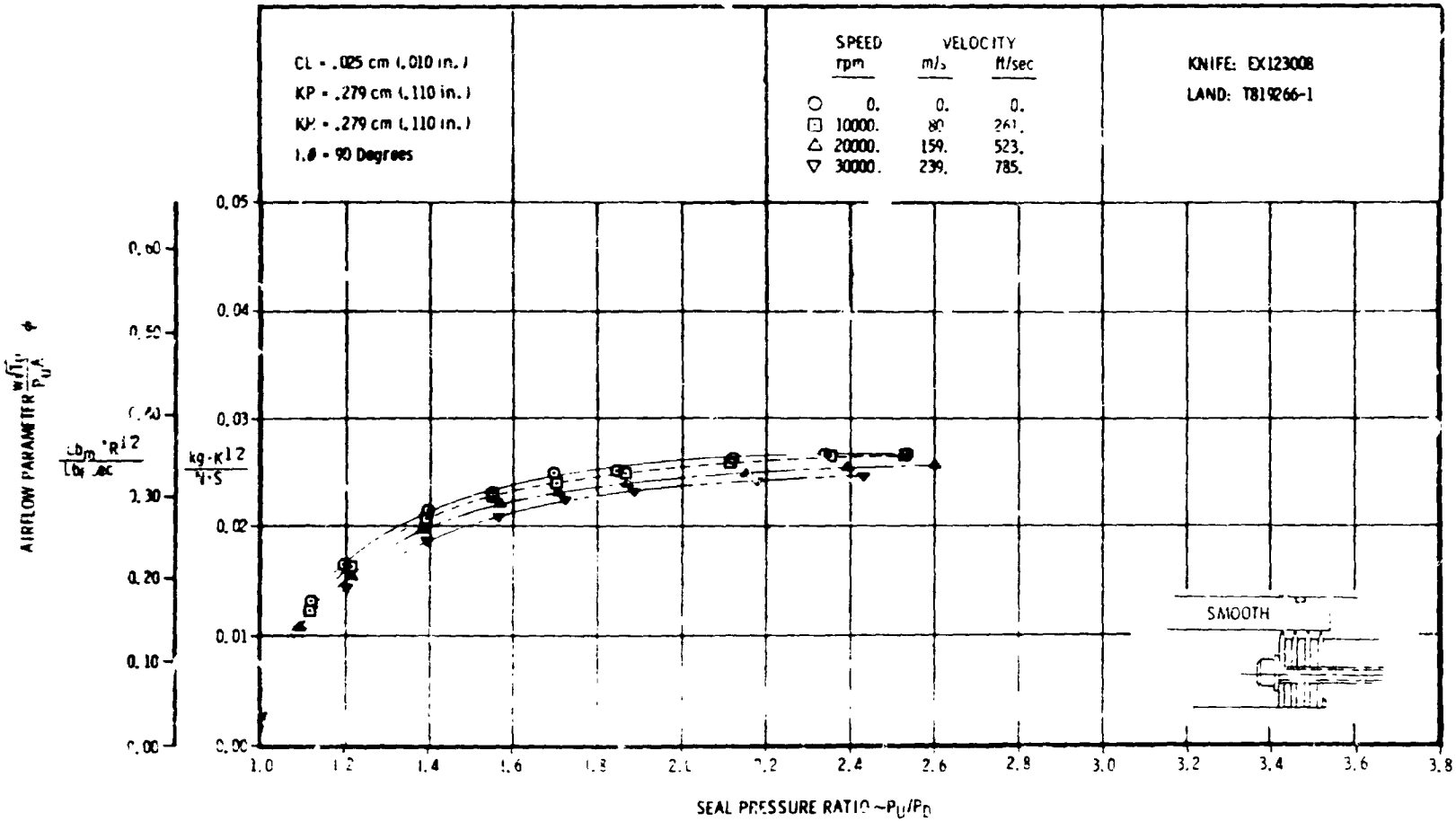

FIGURE B-3. 3D RIG TEST RESULTS OF A 4 K LIFE STRAIGHT-THROUGH SEAL WITH A SOLID-SMOOTH SURFACE LAND

C-3

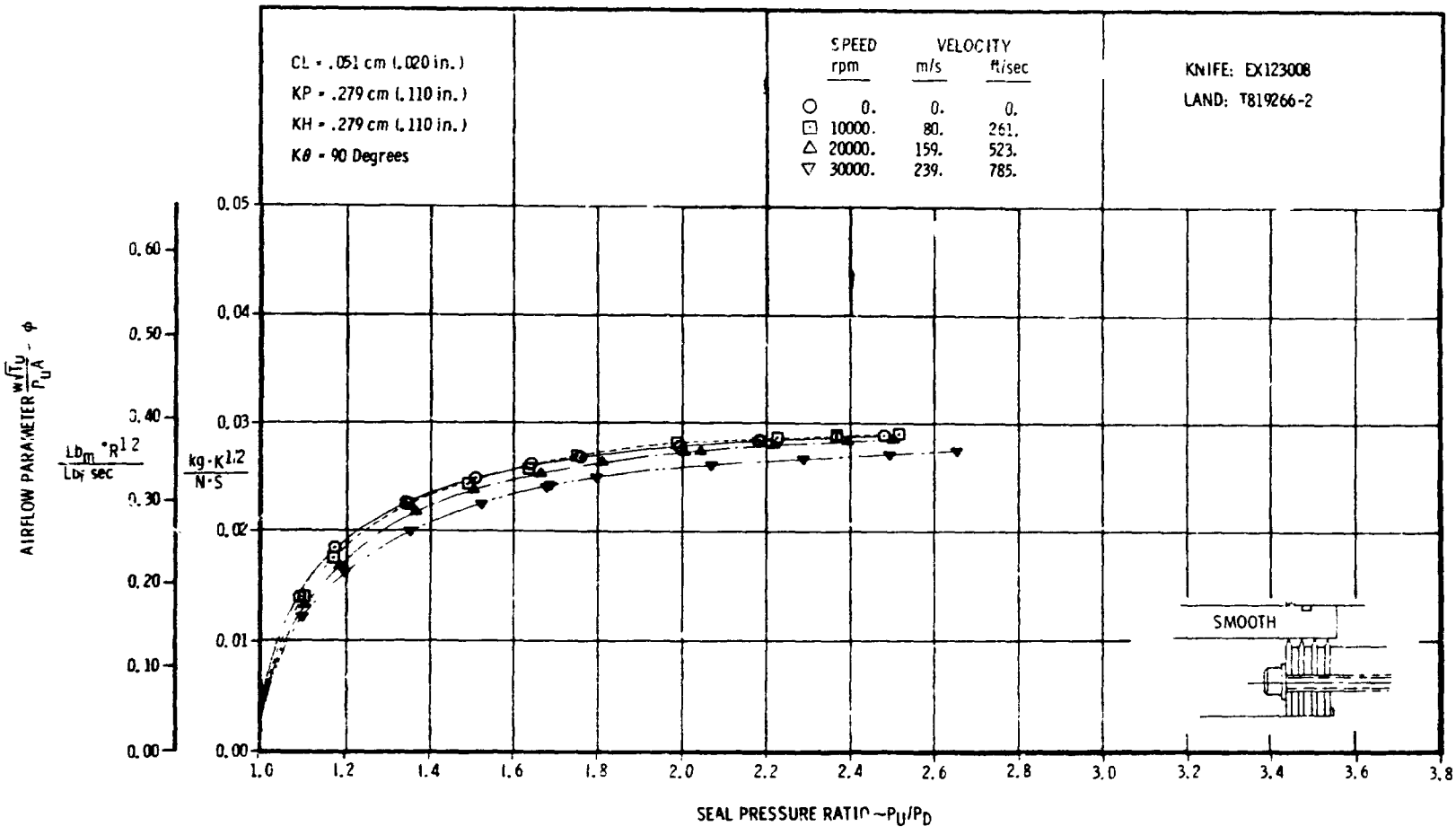

FIGURE B-4. 3D RIG TEST RESULTS OF A 4 KNIFE STRAIGHT-THROUGH SEAL WITH A SOLID-SMOOTH SURFACE LAND

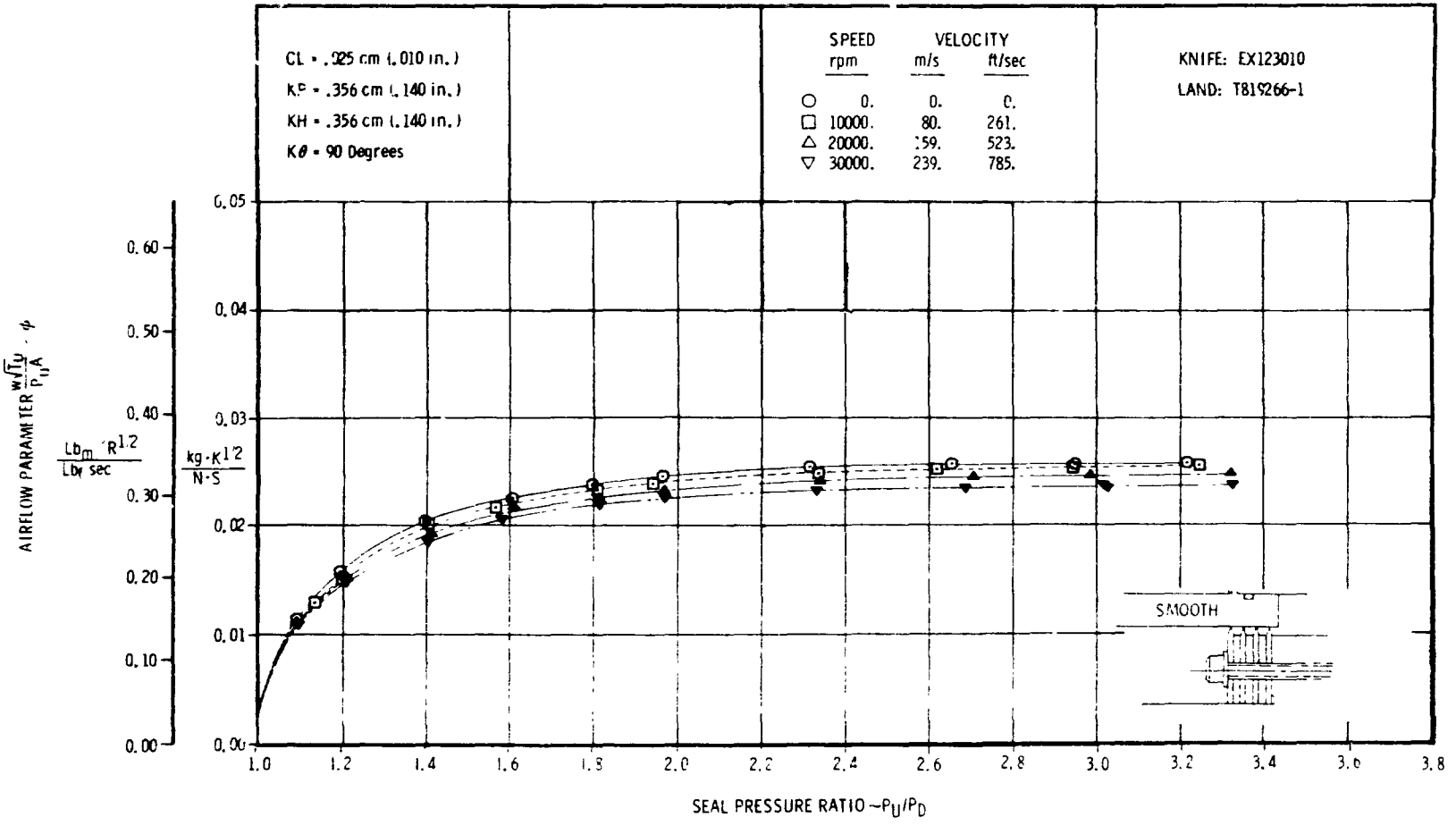

FIGURE B-5. 3D RIG TEST RESULTS OF A 4 KNIFE STRAIGHT-THROUGH SEAL WITH A SOLID-SMOOTH SURFACE LAND

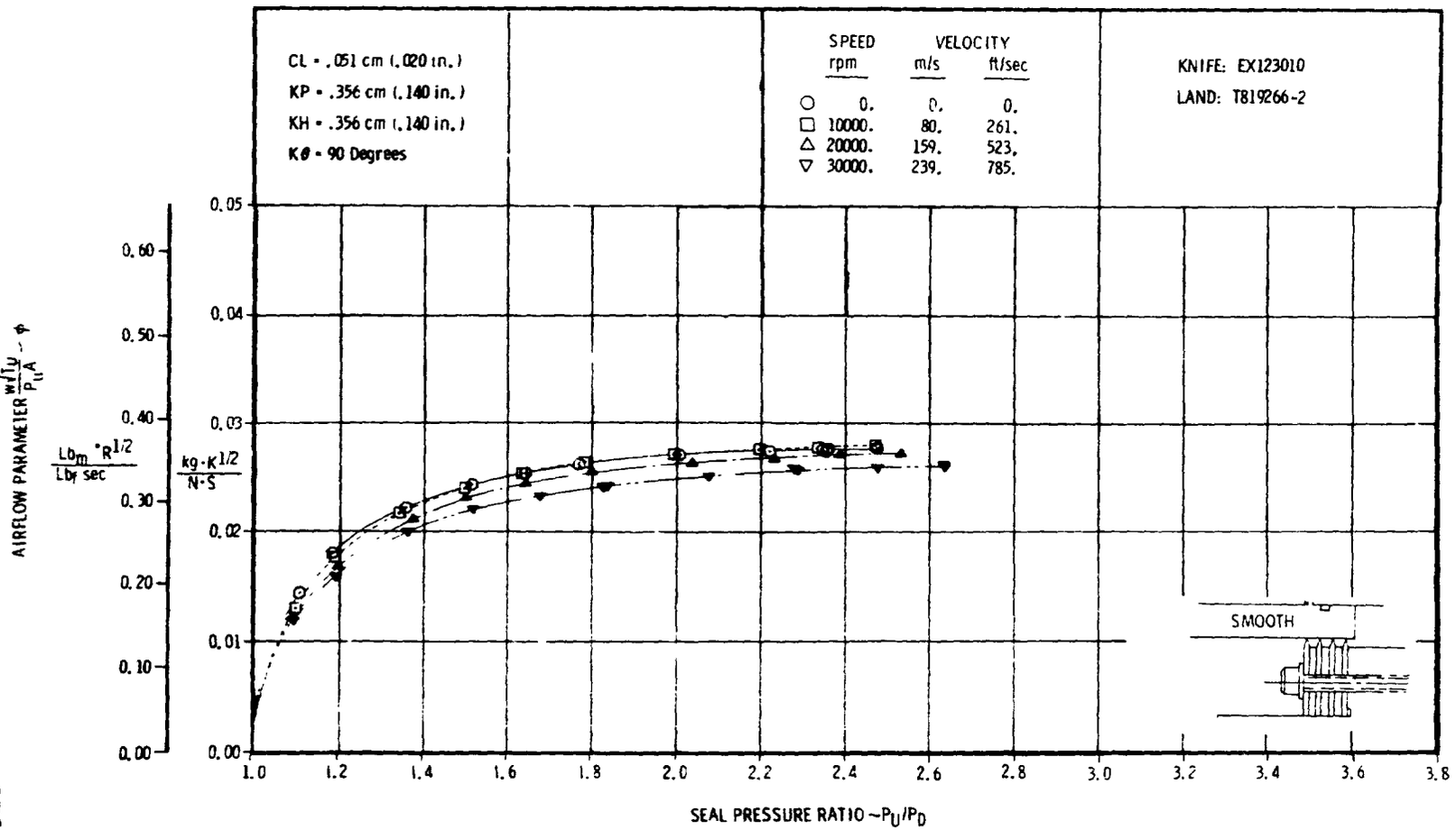

FIGURE B-6. 3D RIG TEST RESULTS OF A 4 KNIFE STRAIGHT-THROUGH SEAL WITH A SOLID-SMOOTH SURFACE LAND

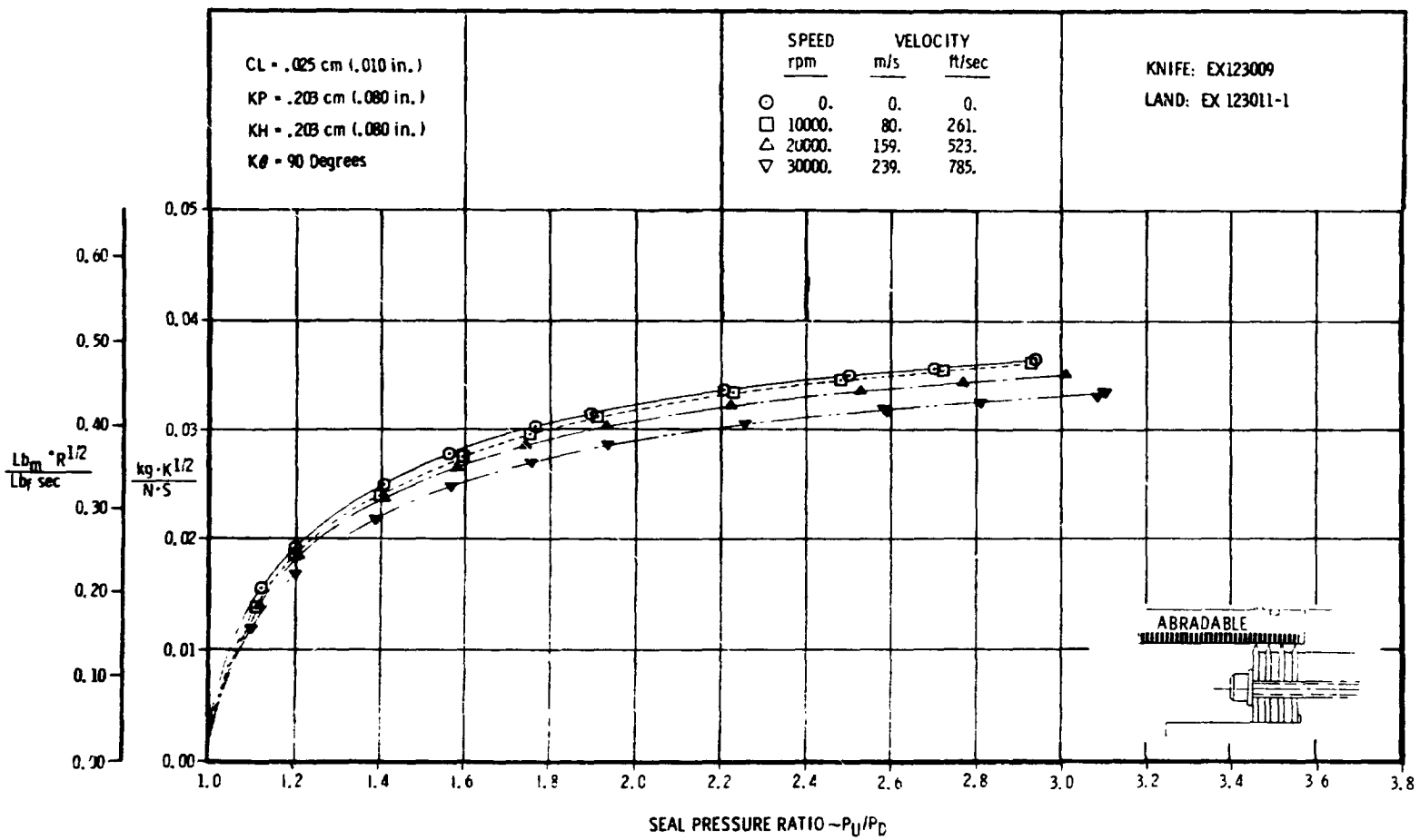

FIGURE B-7. 3D RIG TEST RESULTS OF A 4 KNIFE STRAIGHT-THROUGH SEAL WITH AN "ABRADABLE A" SURFACE LAND

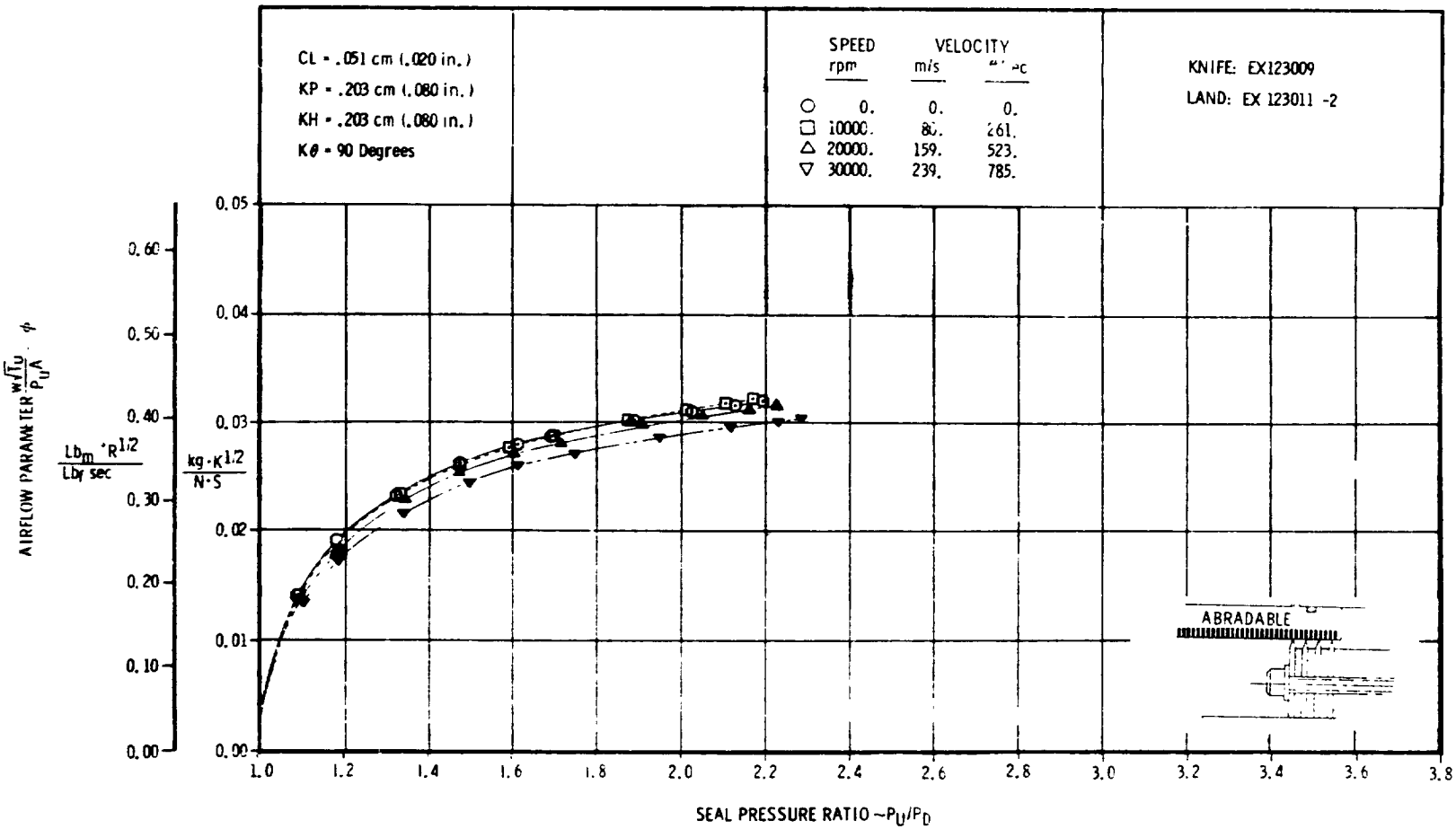

FIGURE B-8. 3D RIG TEST RESULTS OF A 4 KNIFE STRAIGHT-THROUGH SEAL WITH AN "ABRADABLE A" SURFACE LAND

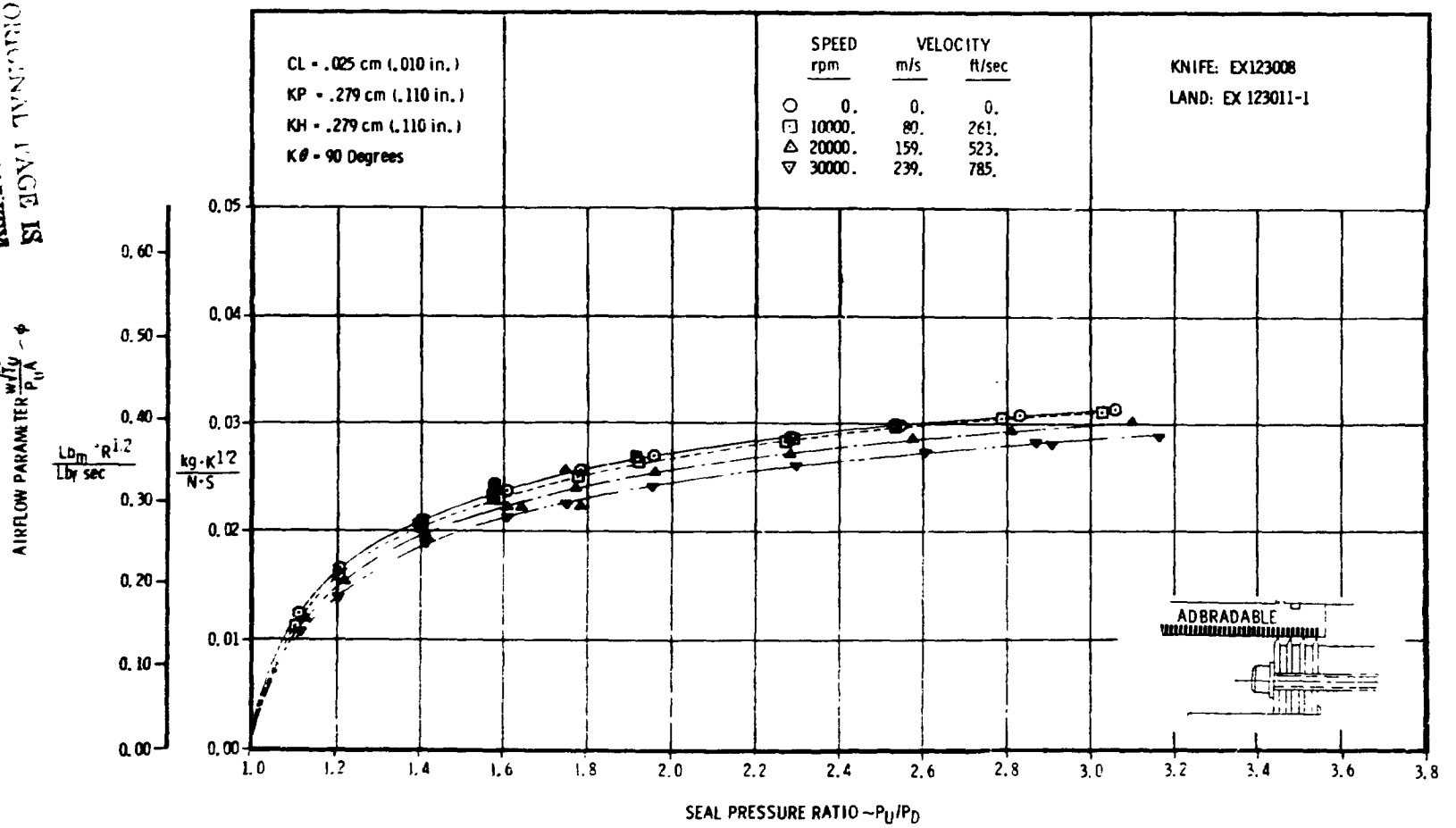

FIGURE B-9. 3D RIG TEST RESULTS OF A 4 KNIFE STRAIGHT-THROUGH SEAL WITH AN "ABRADABLE A" SURFACE LAND

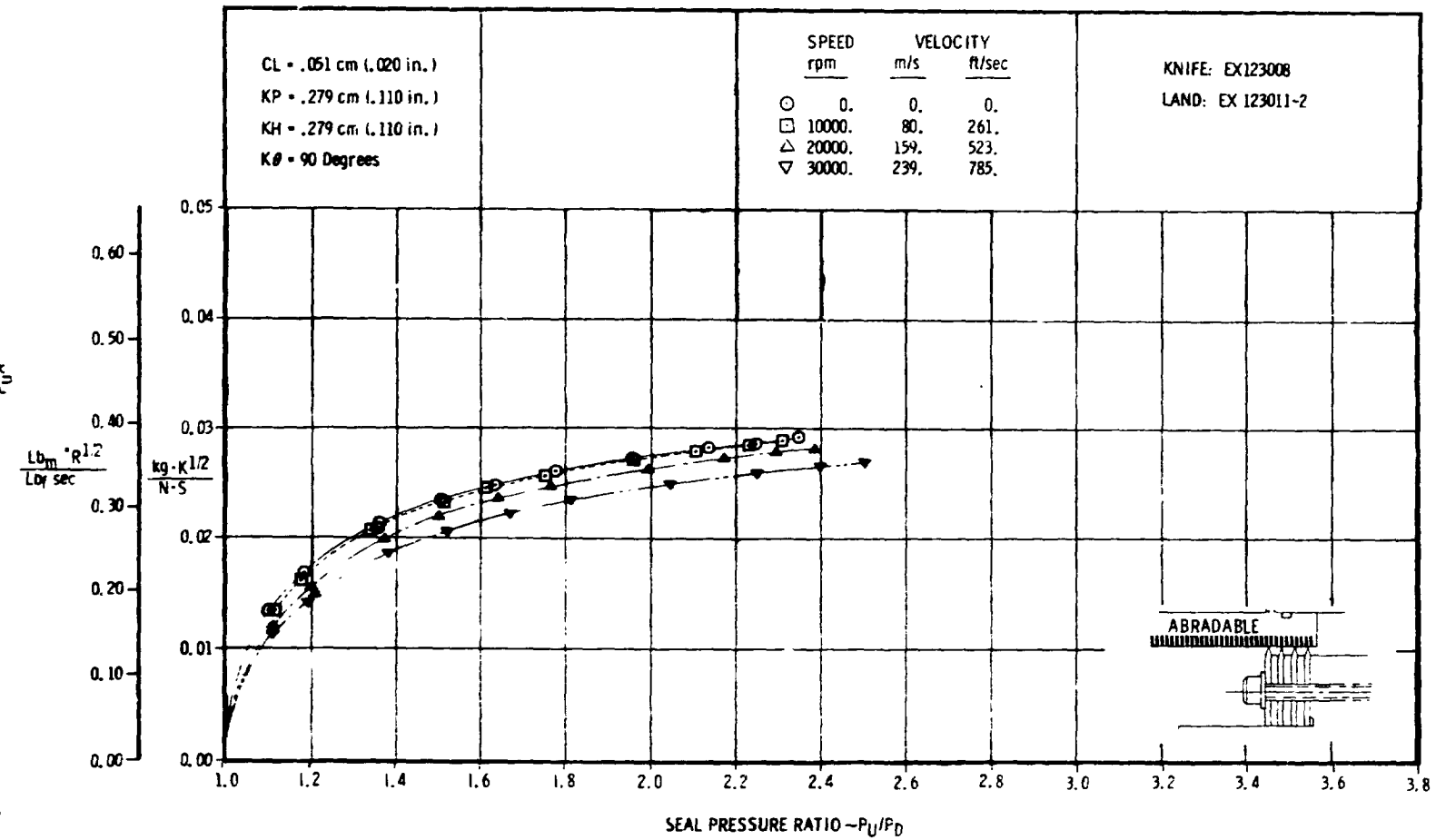

FIGURE B-10. 3D RIG TEST RESULTS OF A 4 KNIFE STRAIGHT-THROUGH SEAL WITH AN "ABRADABLE A" SURFACE LAND

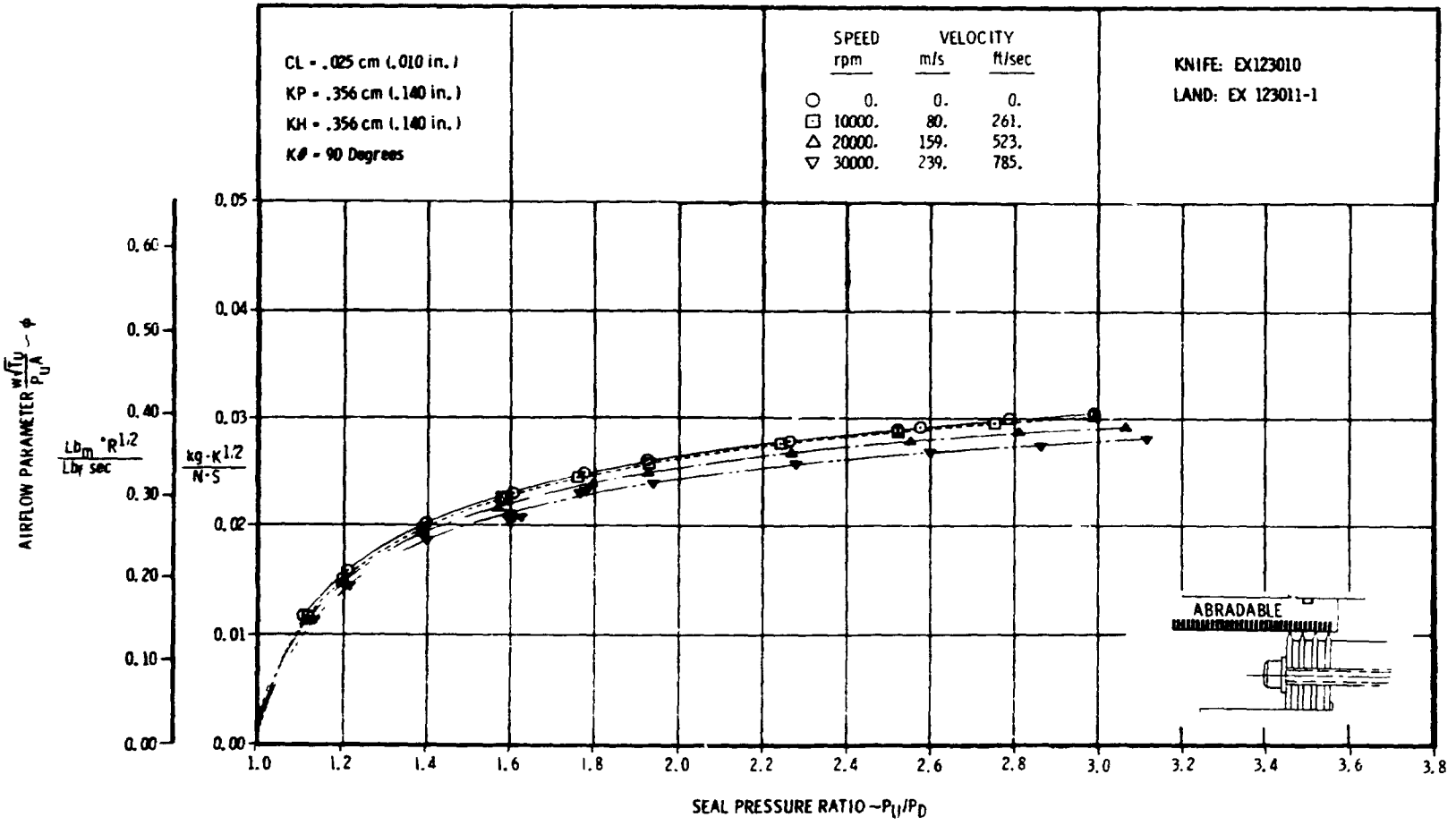

FIGURE B-11. 3D RIG TEST RESULTS OF A 4 KNIFE STRAIGHT-THROUGH SEAL WITH AN "ABRADABLE A" SURFACE LAND

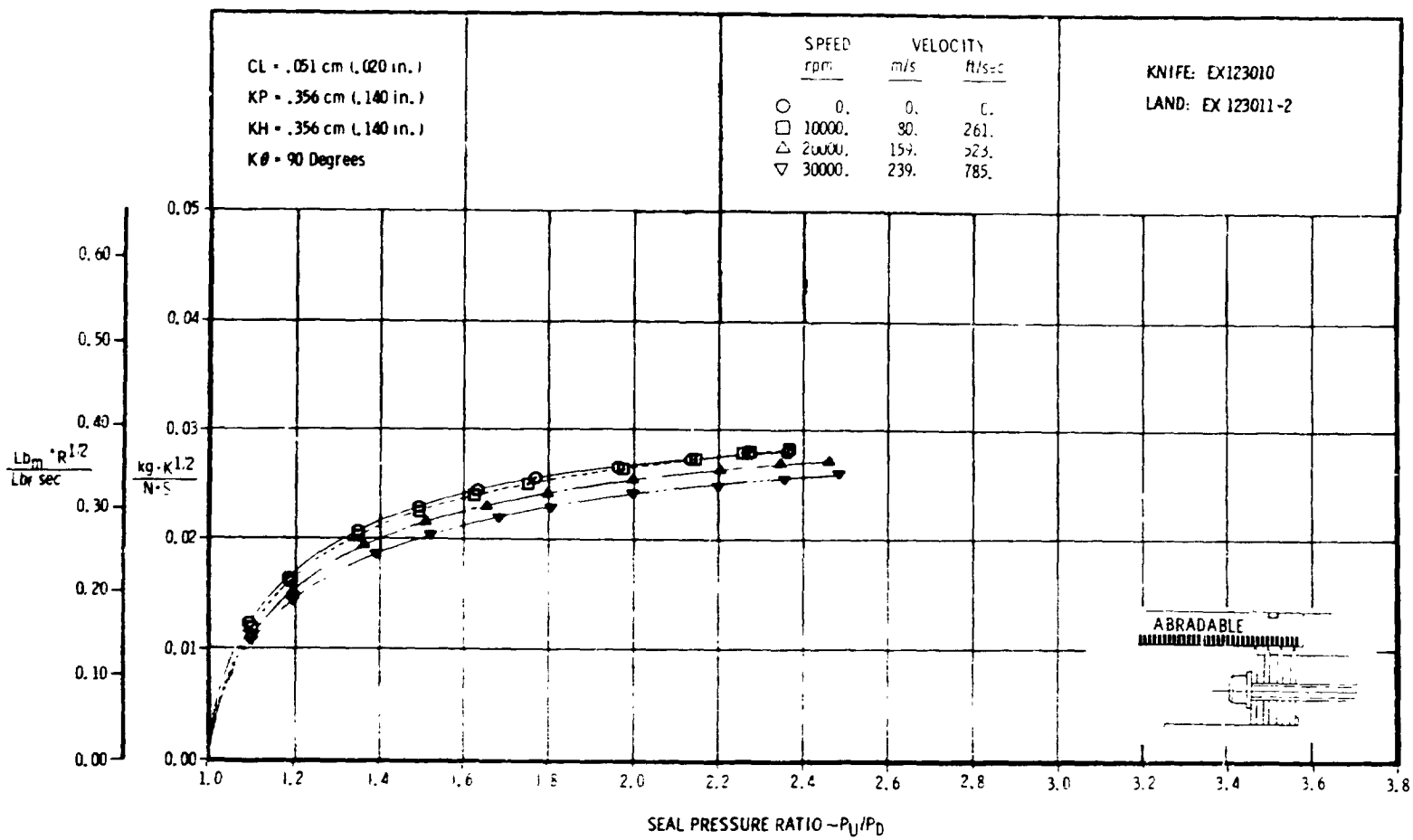

FIGURE B-12. 3D RIG TEST RESULTS OF A 4 KNIFE STRAIGHT-THROUGH SEAL WITH AN "ABRADABLE A" SURFACE LAND

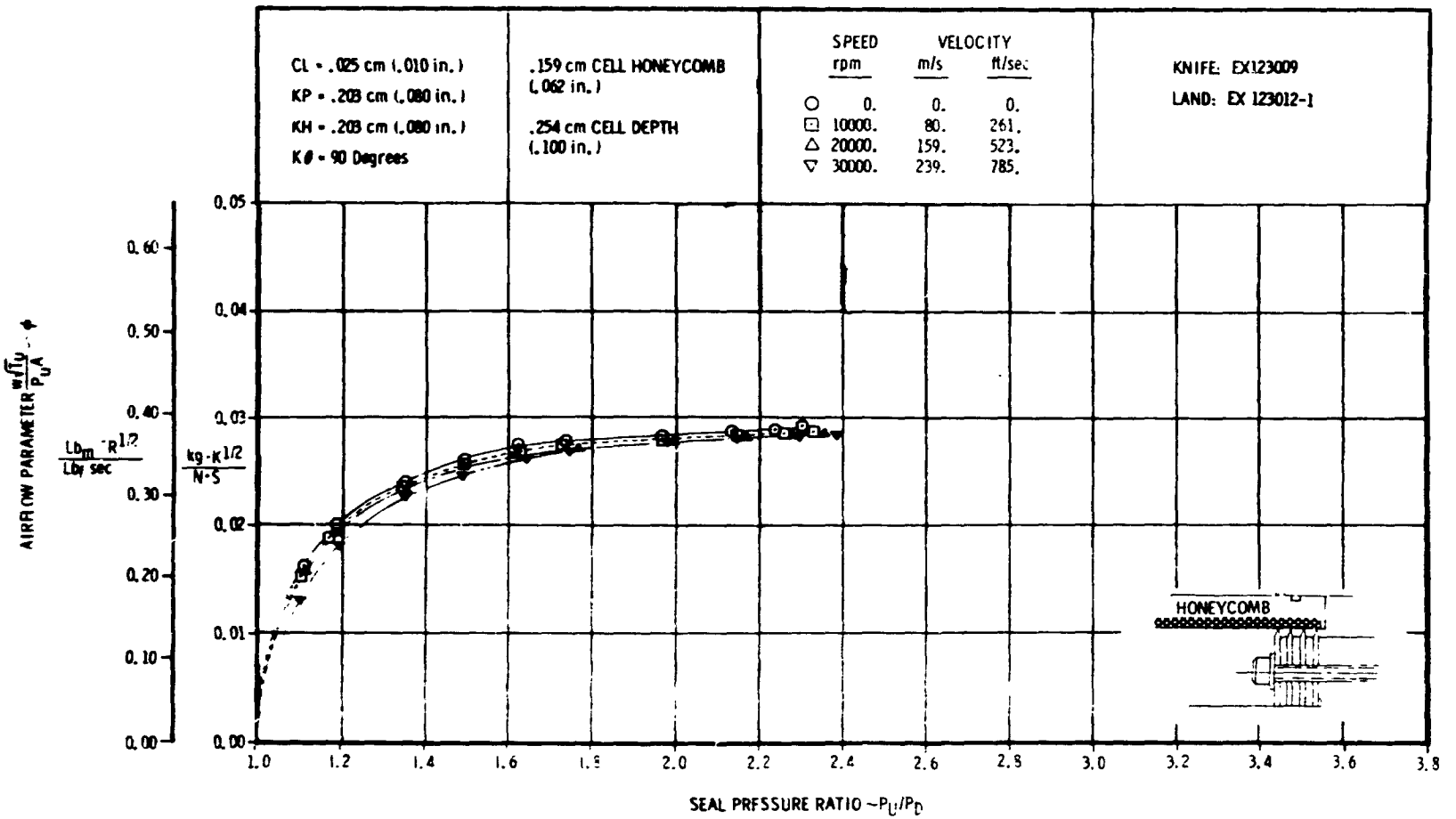

FIGURE 8-13.30 RIG TEST RESULTS OF A 4 KNIFE STRAIGHT-THROUGH SEAL WITH A HONEYCOMB SURFACE LAND

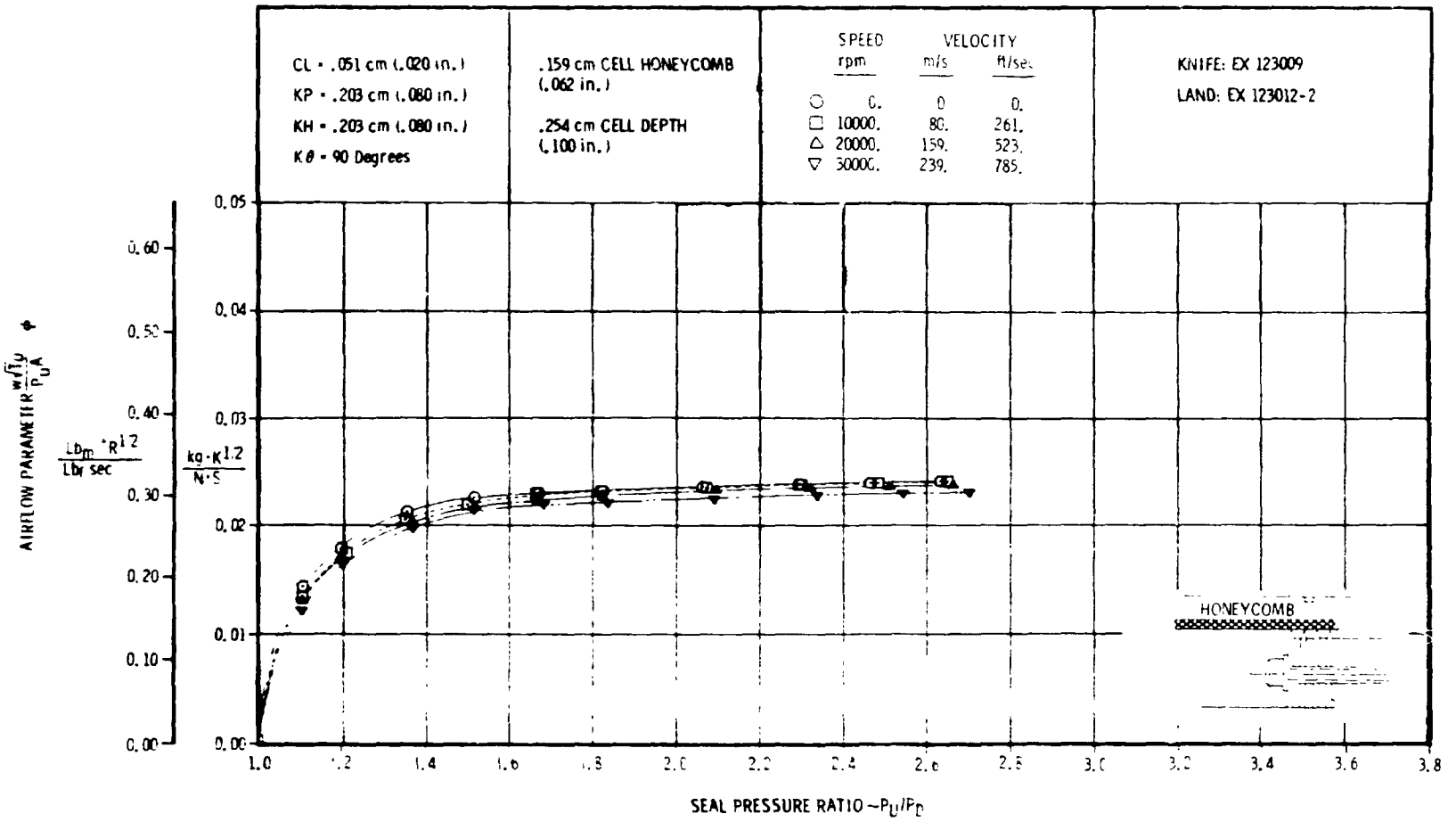

FIGURE B-14. 3D RIG TEST RESULTS OF A 4 KNIFE STRAIGHT-THROUGH SEAL WITH A HONEYCOMB SURFACE LAND

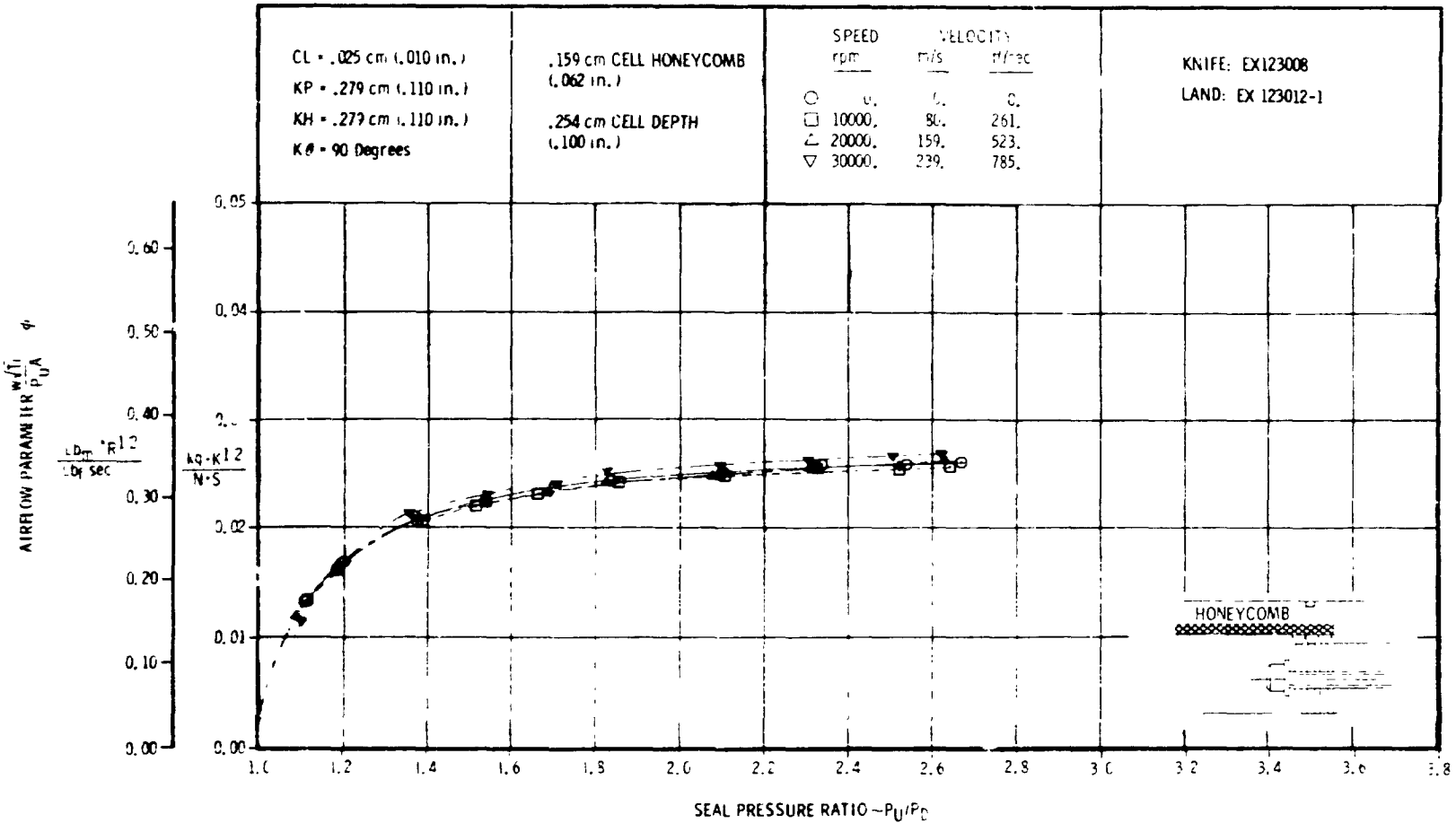

FIGURE B-15. 3D RIG TEST RESULTS OF A 4 KNIFE STRAIGHT-THROUGH SEAL WITH A HONEYCOMB SURFACE LAND

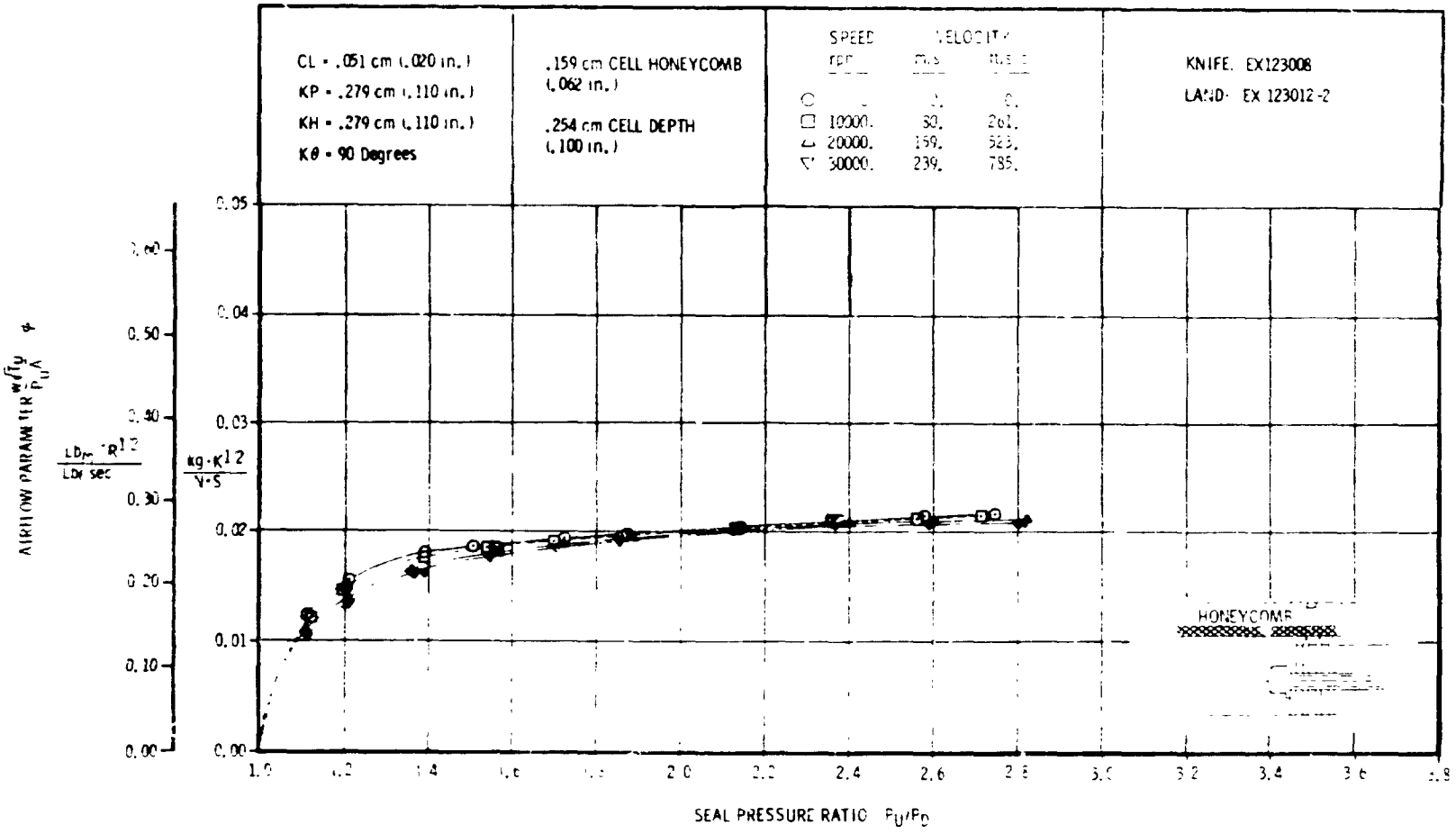

FIGURE B-16.30 RIG TEST RESULTS OF A 4 KNIFE STRAIGHT-THROUGH SEAL WITH A HONEYCOMB SURFACE LAND

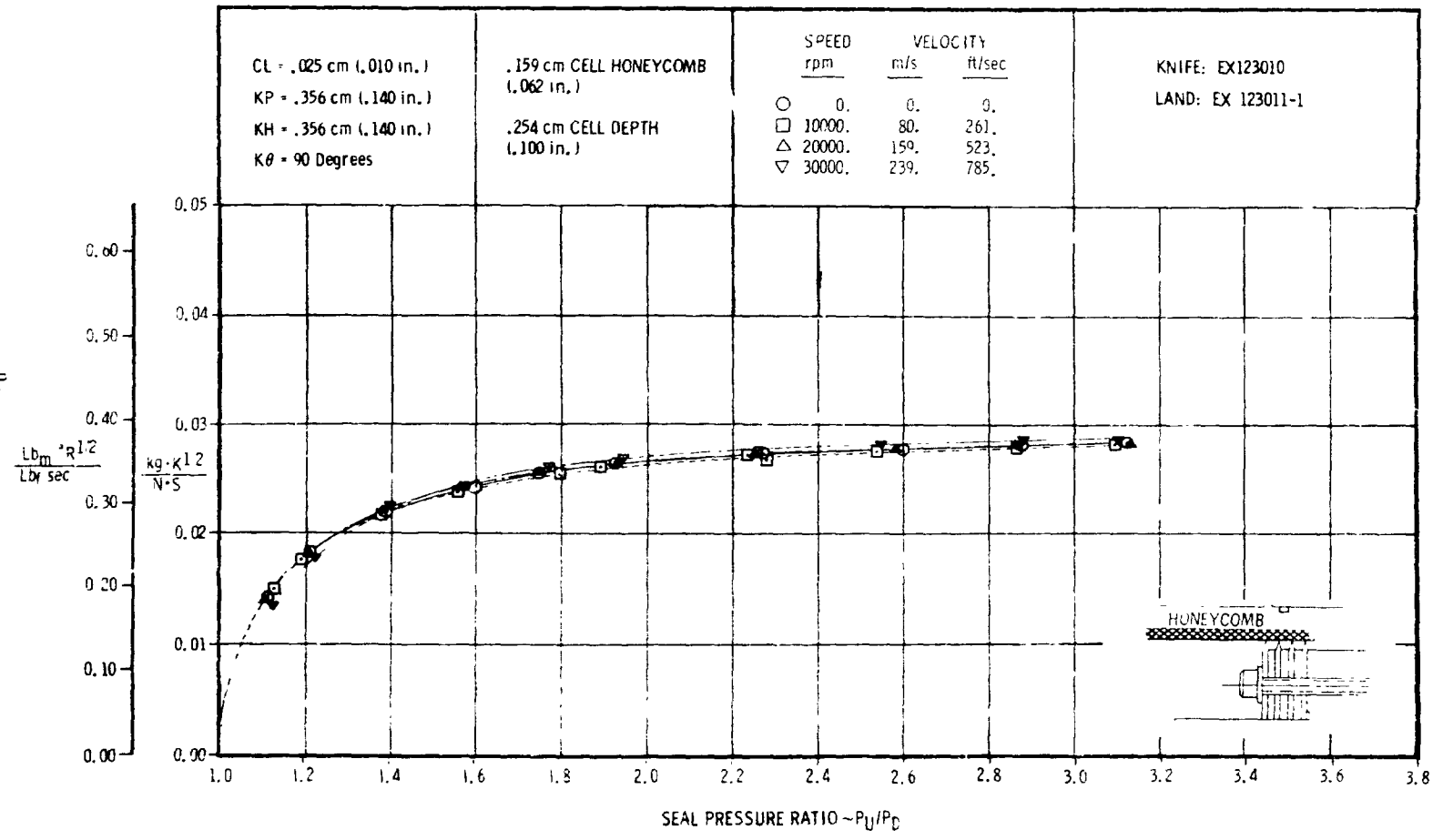

FIGURE B-17. 3D RIG TEST RESULTS OF A 4 KNIFE STRAIGHT THROUGH SEAL WITH A HONEYCOMB SURFACE LAND

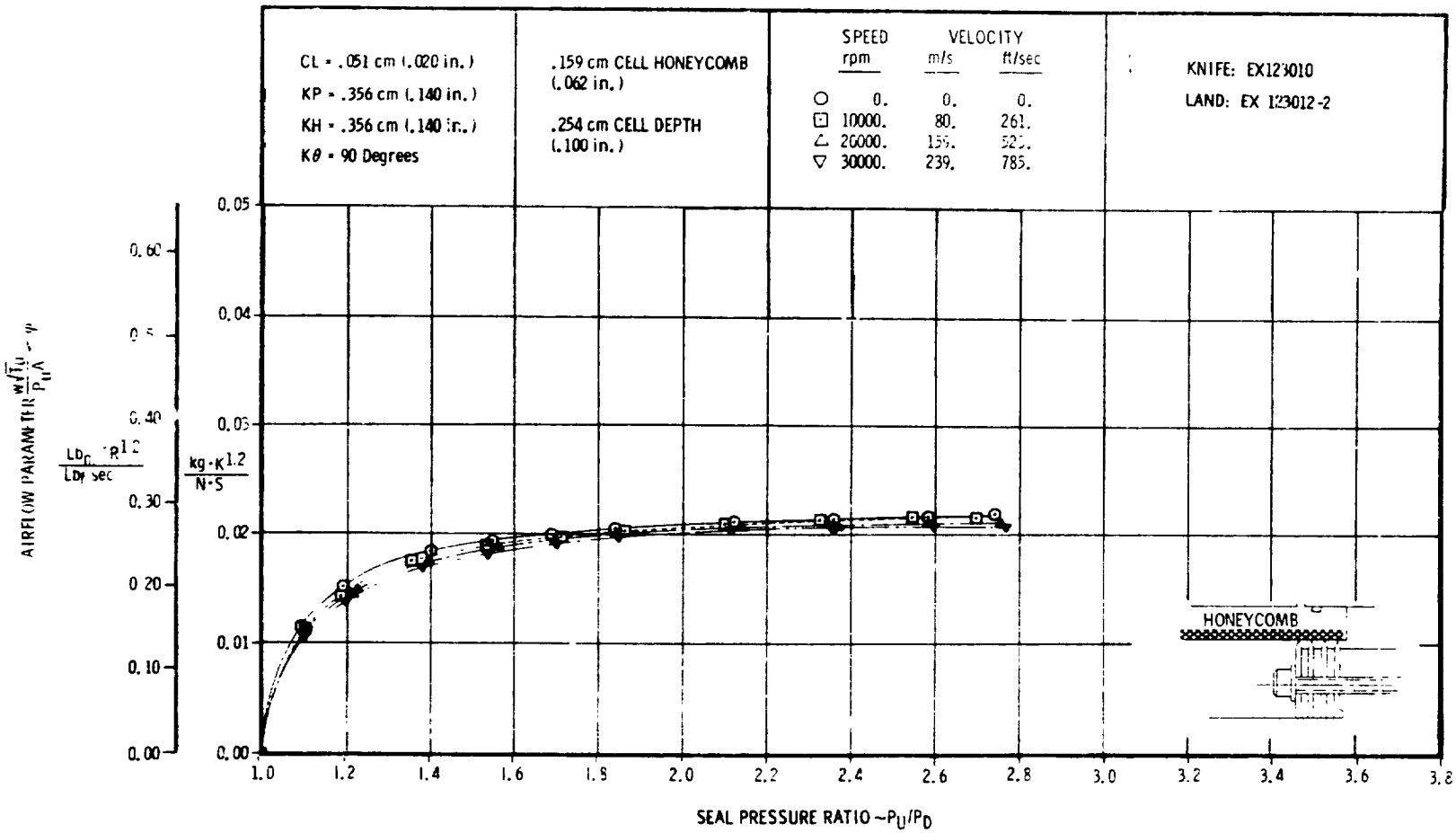

FIGURE B-18. 3D RIG TEST RESULTS OF A 4 KNIFE STRAIGHT-THROUGH SEAL WITH A HONEYCOMB SURFACE LAND

APPENDIX C

2D and 3D Rig Test Results of a Four Knife Straight Seal with Knife Rub Grooves on an "Abradable A" Land

The plots contained in Appendix C illustrate the seal leakage effects due to knife rub grooves in an abradable land. These tests were conducted in the Detroit Diesel Allison 2D and 3D air seal test rigs. The test configuration was a four knife straight-through labyrinth seal with the following geometry:

Knife Pitch	=	.279 cm (.110 in.)
Knife Height	=	.279 cm (.110 in.)
Knife Angle	=	90° (Vertical)
Knife Tip Thickness	=	.025 cm (.010 in.)
Land Material	-	"Abradable A"
Groove Profile Dimensions		

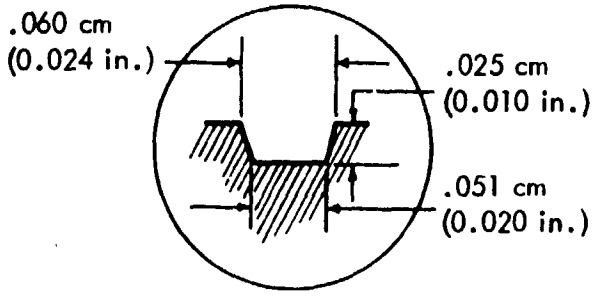

NOTE: All knife clearances are based on the distance from the knife tip to the non-grooved land surface.

The following operating parameters were investigated:

2D Rig: At knife clearances = .013 cm (.005 in.), .025 cm (.010 in.), and .051 cm (.020 in.), the following knife-groove axial positions were tested:

1. Knives directly above the grooves.
2. Knives .013 cm (.005 in.) forward of the grooves.
3. Knives .025 cm (.010 in.) forward of the grooves.
4. Knives .013 cm (.005 in.) aft of the grooves.
5. Knives .025 cm (.010 in.) aft of the grooves.
6. Knives halfway between the grooves.

3D Rig: At a knife radial clearance = .025 cm (.010 in.), the following knife-groove axial positions were tested with 102° and 360° peripheral land grooves:

1. Knives directly above the grooves.
2. Knives .025 cm (.010 in.) forward of the grooves.
3. Knives .025 cm (.010 in.) aft of the grooves.

Knife tip speeds at each condition were:

V = 0 (static).

V = 80 m/s (261 ft/sec).

V = 159 m/s (523 ft/sec).

V = 239 m/s (785 ft/sec).

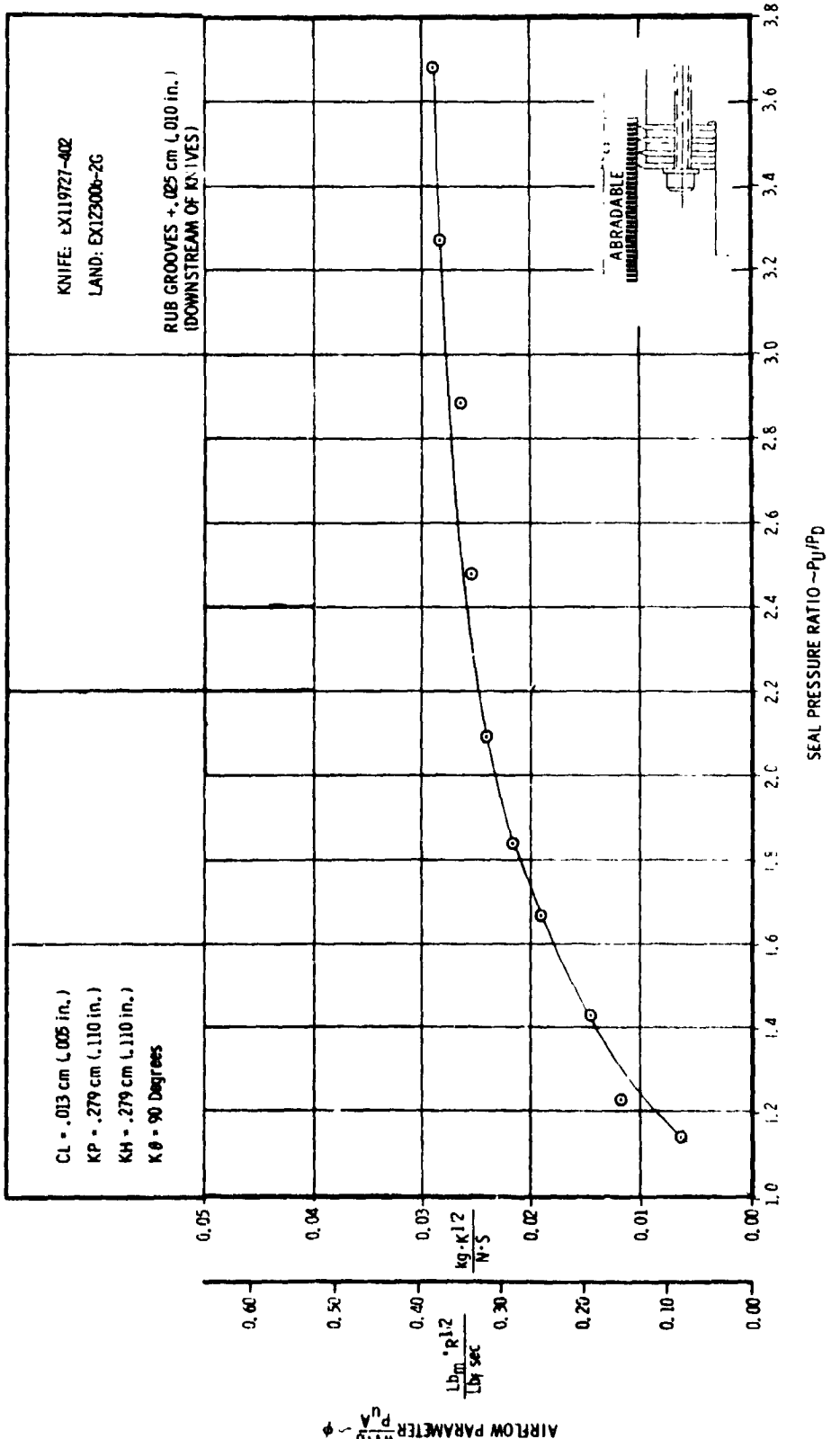

FIGURE C-1. 2D RIG TEST RESULTS OF A 4 KNIFE STRAIGHT-THROUGH SEAL WITH A RUB GROOVED "ABRADABLE A" LAND

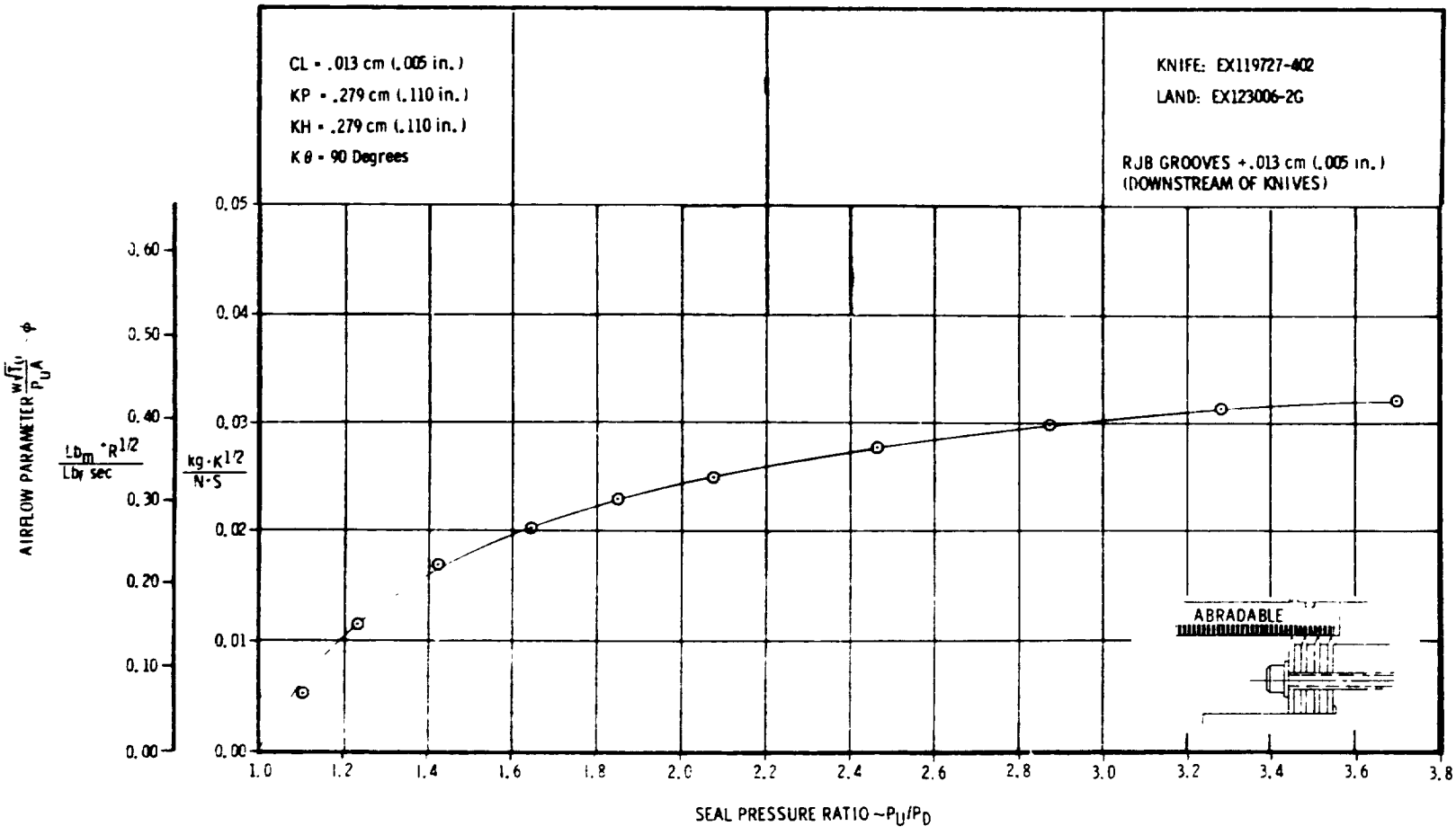

FIGURE C-2. 2D RIG TEST RESULTS OF A 4 KNIFE STRAIGHT-THROUGH SEAL WITH A RUB GROOVED "ABRADABLE A" LAND

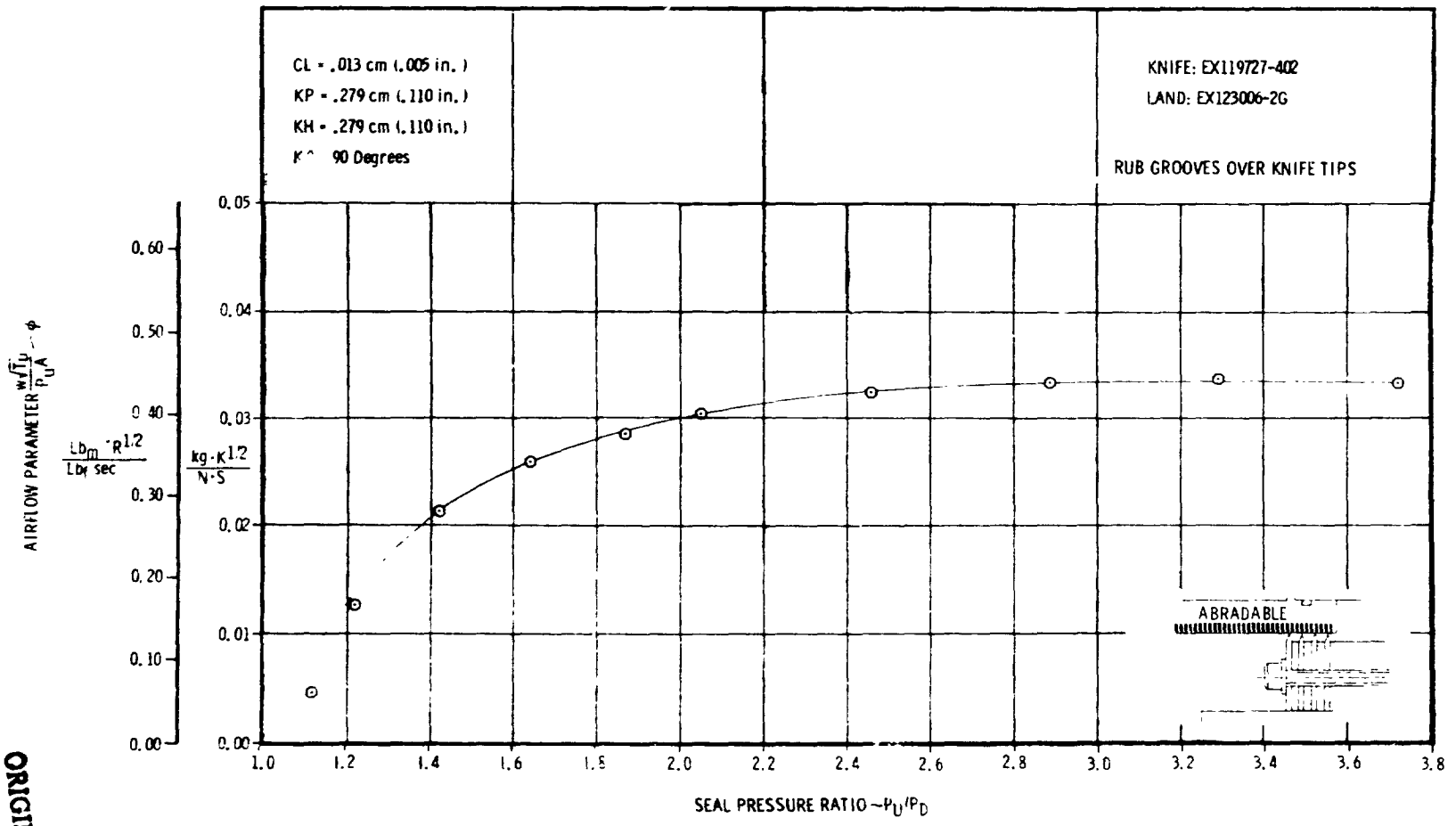

FIGURE C-3. 2D RIG TEST RESULTS OF A 4 KNIFE STRAIGHT-THROUGH SEAL WITH A RUB GROOVED "ABRADABLE A" LAND

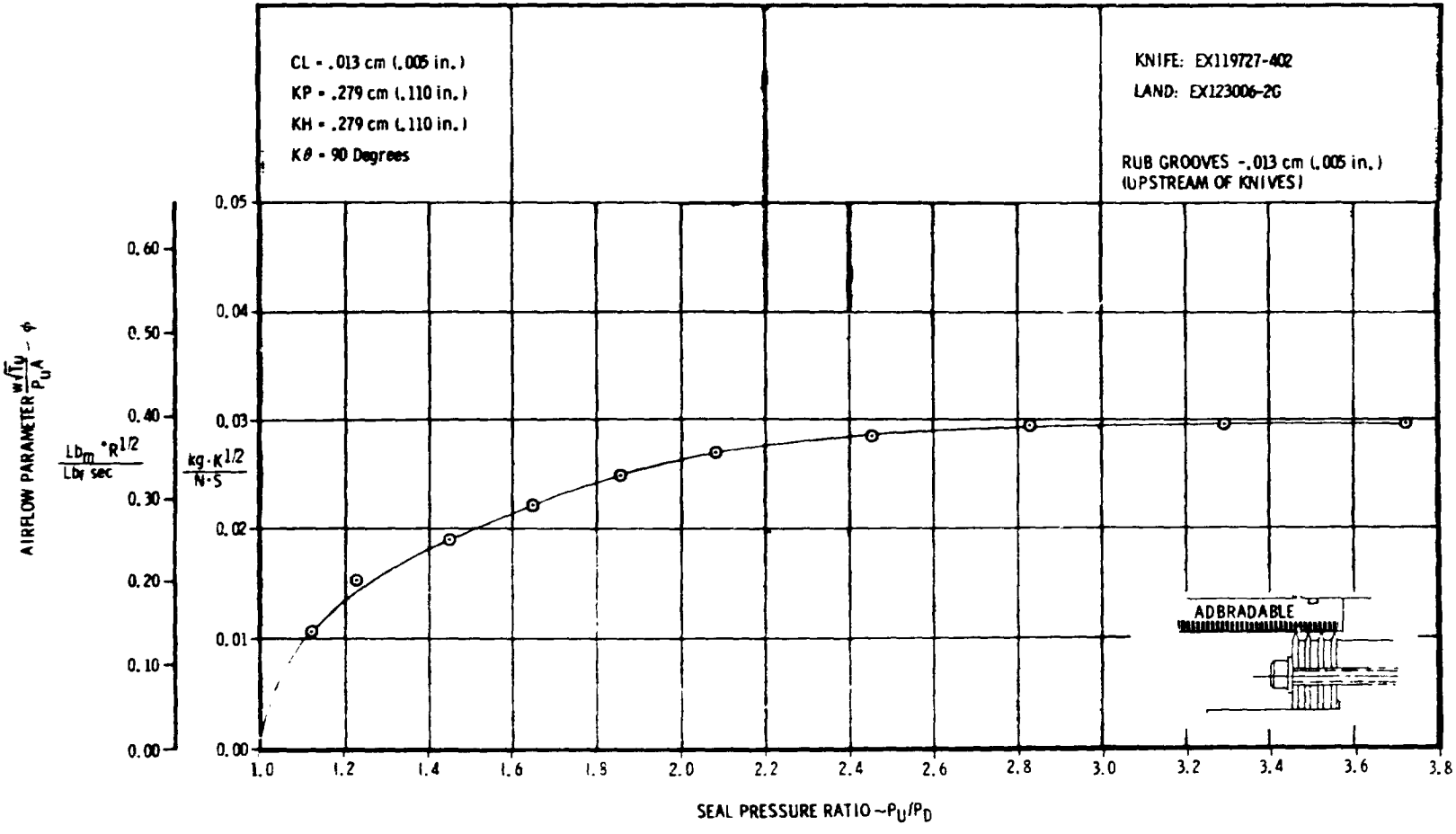

FIGURE C-4. 2D RIG TEST RESULTS OF A 4 KNIFE STRAIGHT-THROUGH SEAL WITH A RUB GROOVED "ABRADABLE A" LAND

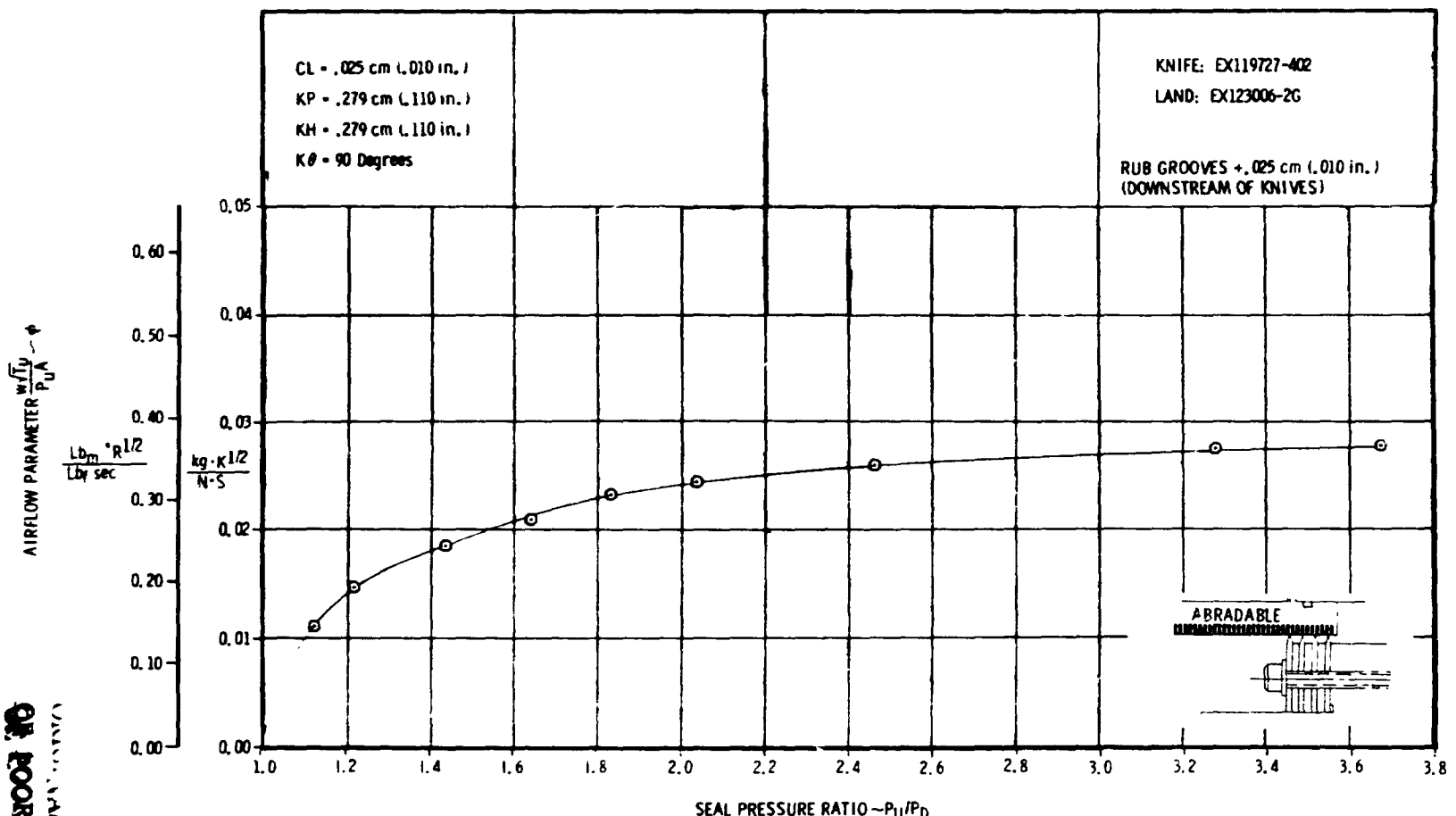

FIGURE C-5. 2D RIG TEST RESULTS OF A 4 KNIFE STRAIGHT-THROUGH SEAL WITH A RUB GROOVED "ABRADABLE A" LAND

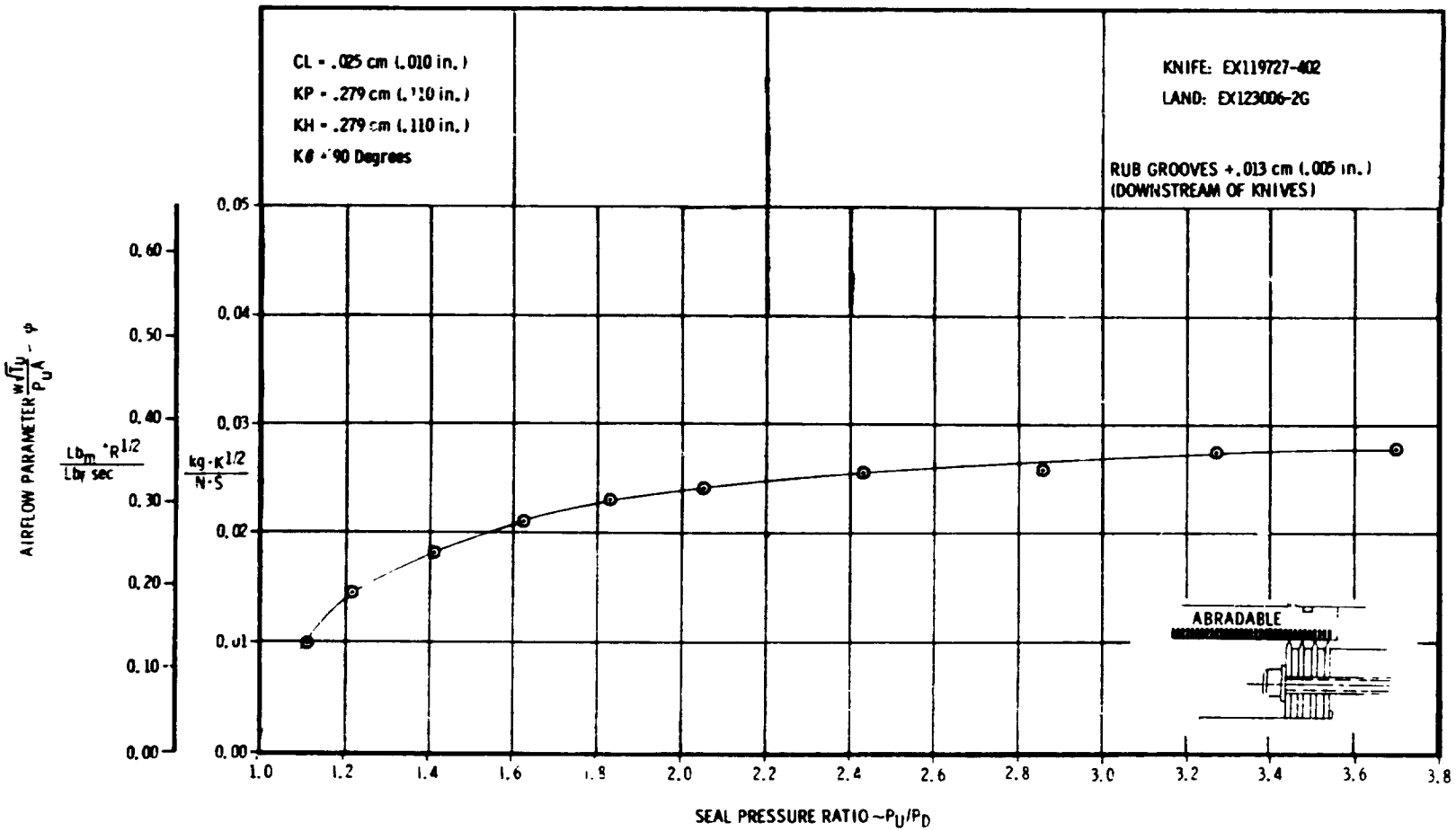

FIGURE C-6. 2L RIG TEST RESULTS OF A 4 KNIFE STRAIGHT-THROUGH SEAL WITH A RUB GROOVED "ABRADABLE A" LAND

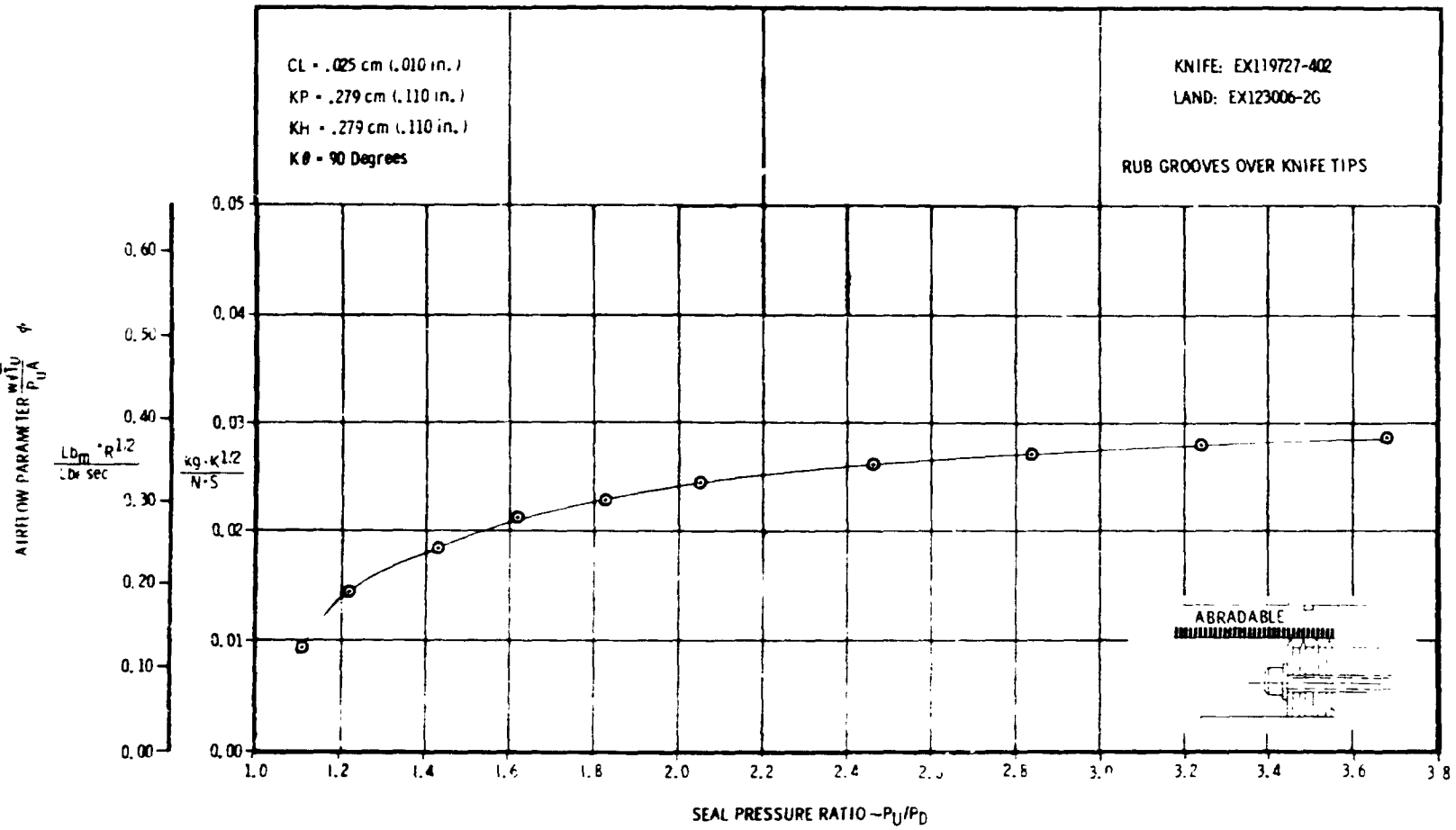

FIGURE C-7. 2D RIG TEST RESULTS OF A 4 KNIFE STRAIGHT-THROUGH SEAL WITH A RUB GROOVED "ABRADABLE A" LAND

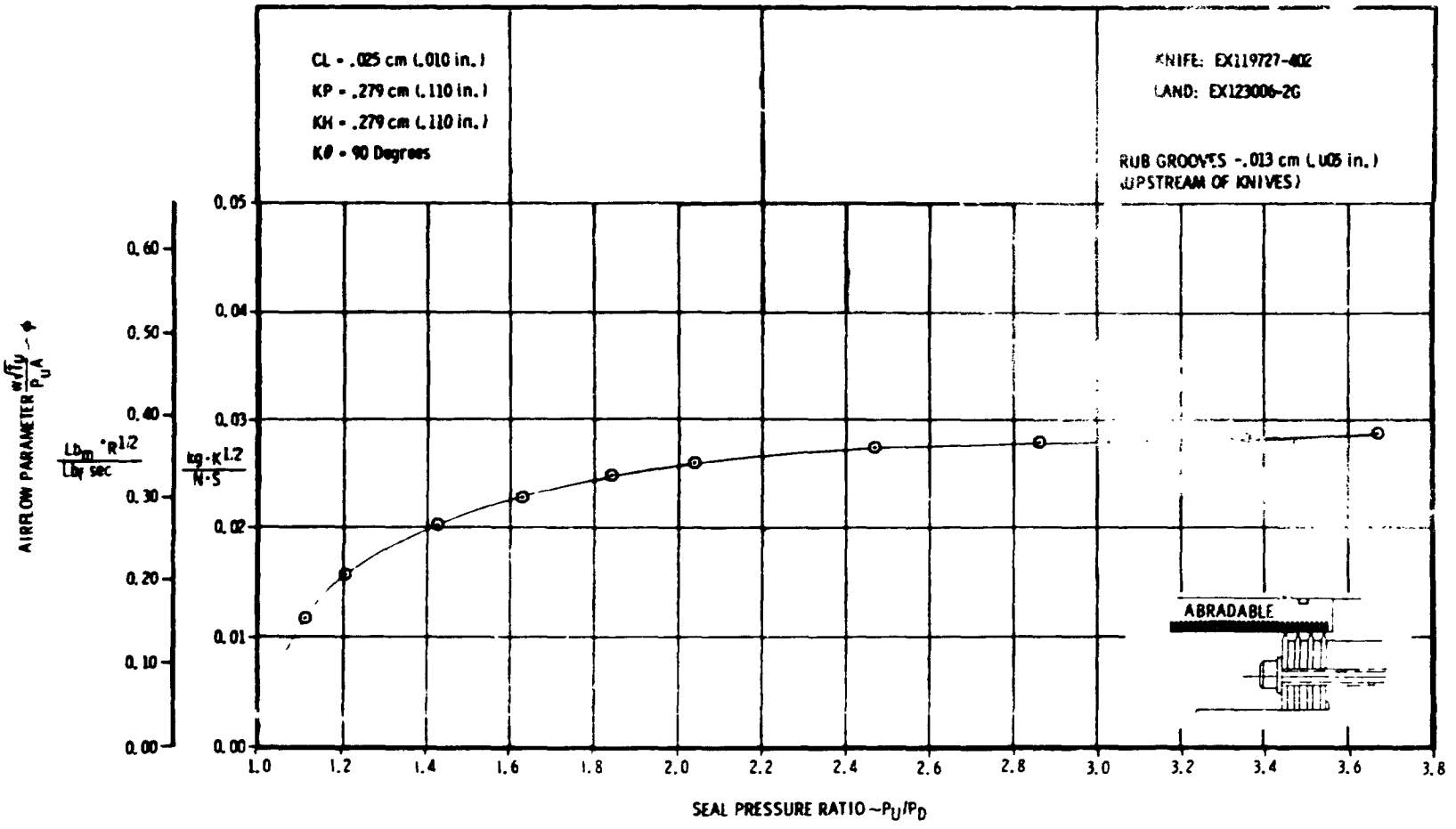

FIGURE C-8. 2D RIG TEST RESULTS OF A 4 KNIFE STRAIGHT-THROUGH SEAL WITH A RUB GROOVED "ABRADABLE A" LAND

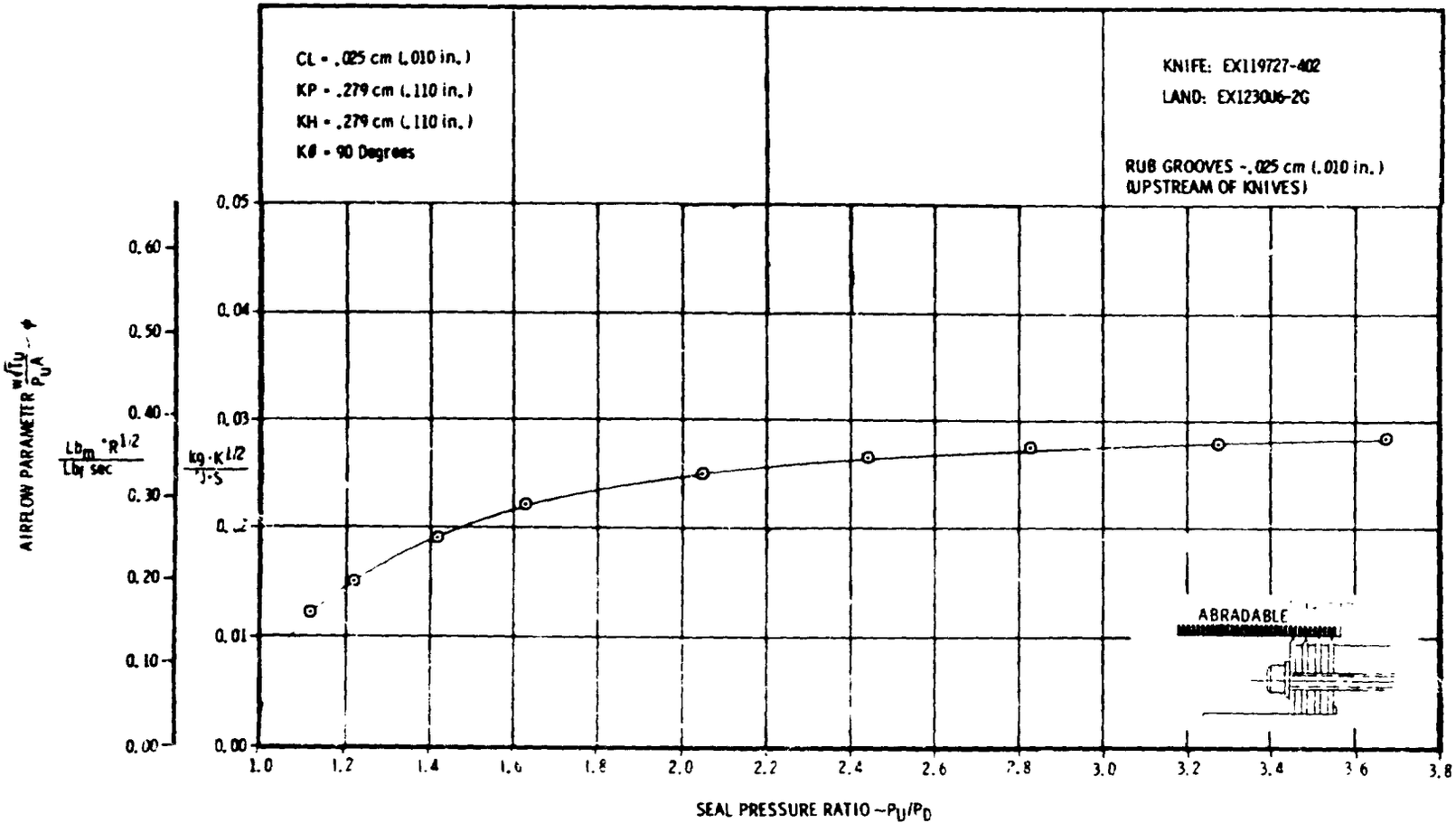

FIGURE C-9. 2D RIG TEST RESULTS OF A 4 KNIFE STRAIGHT-THROUGH SEAL WITH A RUB GROOVED "ABRADABLE A" LAND

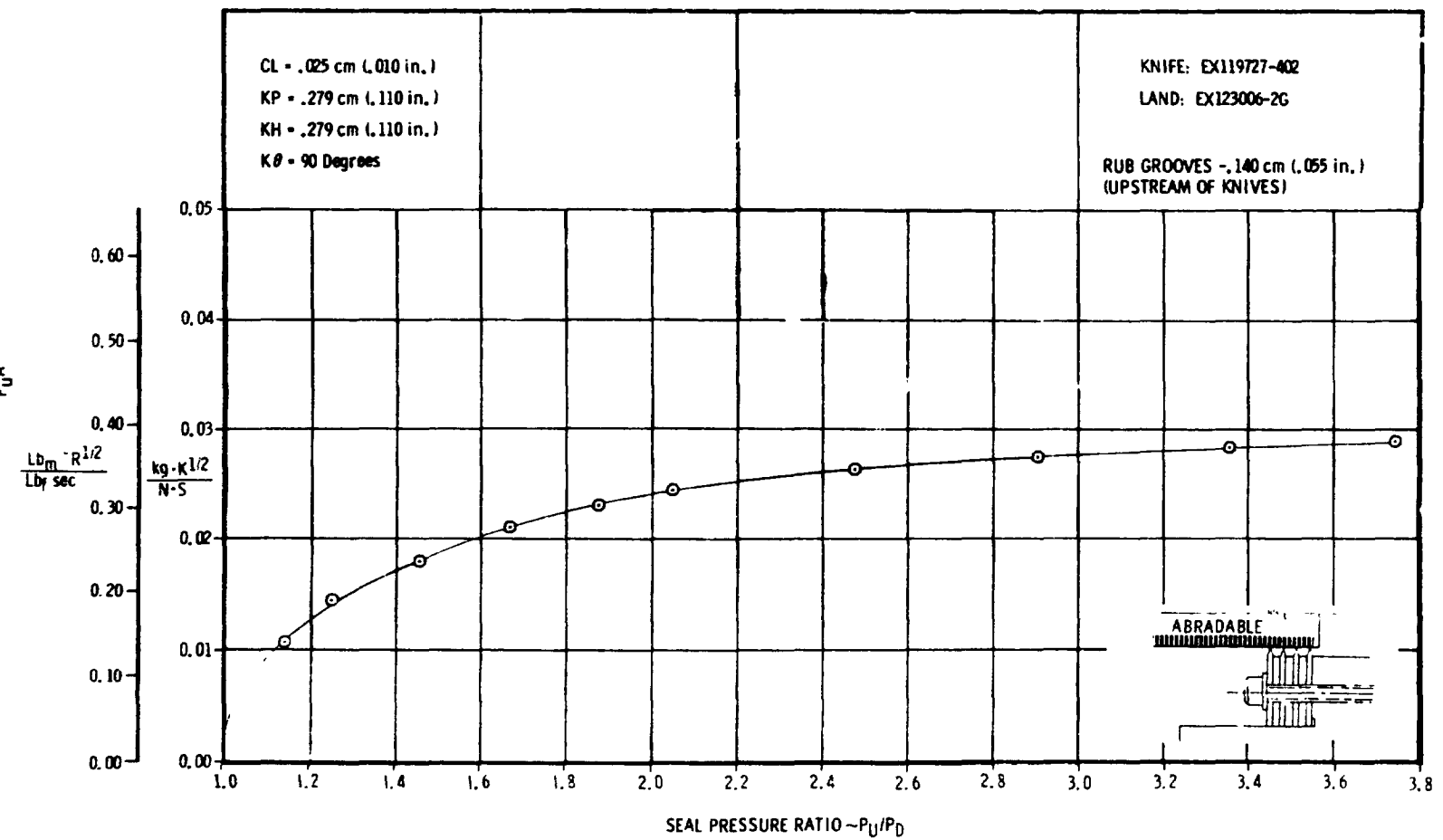

FIGURE C-10. 2D RIG TEST RESULTS OF A 4 KNIFE STRAIGHT-THROUGH SEAL WITH A RUB GROOVED "ABRADABLE A" LAND

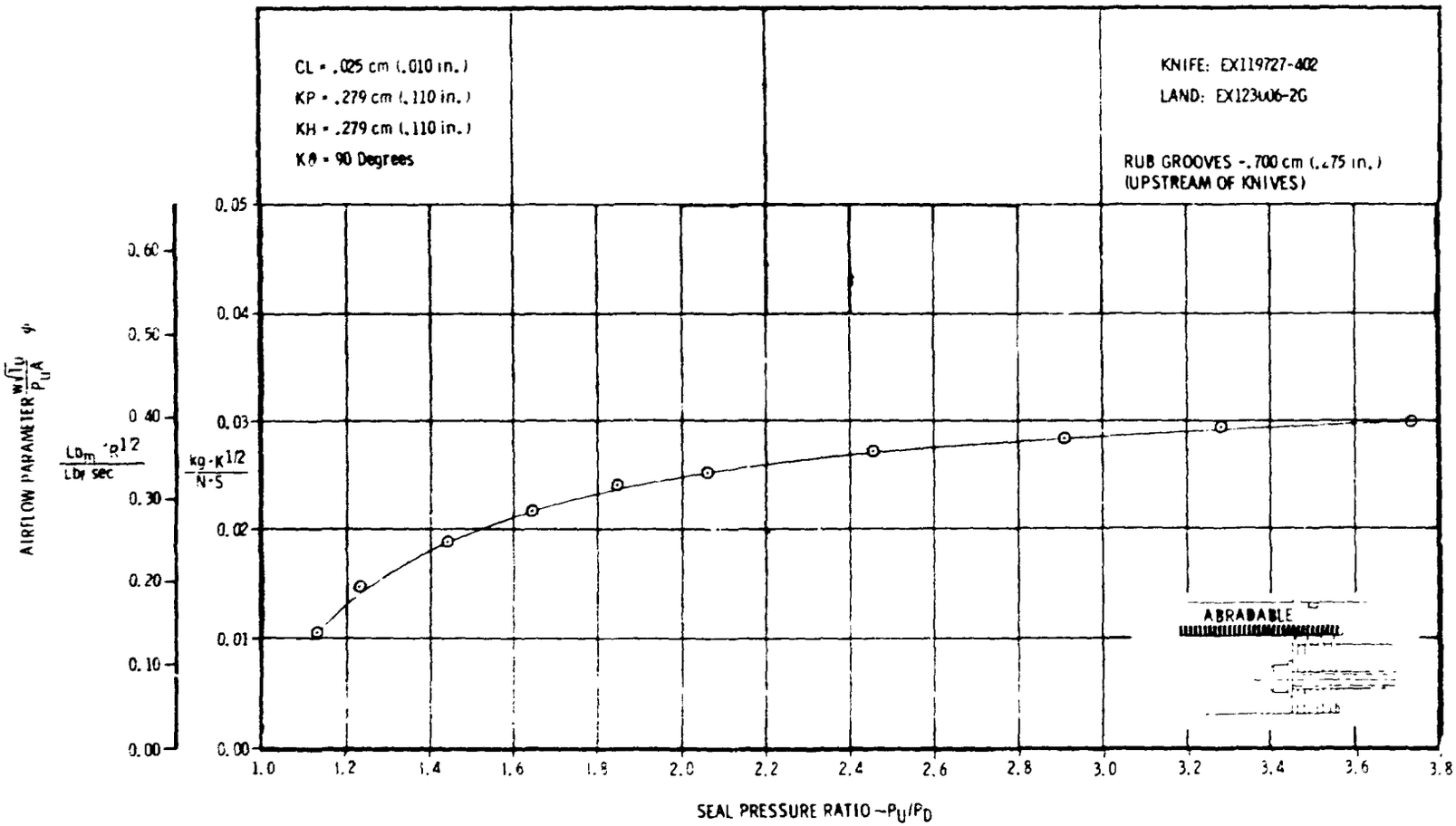

FIGURE C-11. 2D RIG TEST RESULTS OF A 4 KNIFE STRAIGHT-THROUGH SEAL WITH A RUB GROOVED "ABRADABLE A" LAND

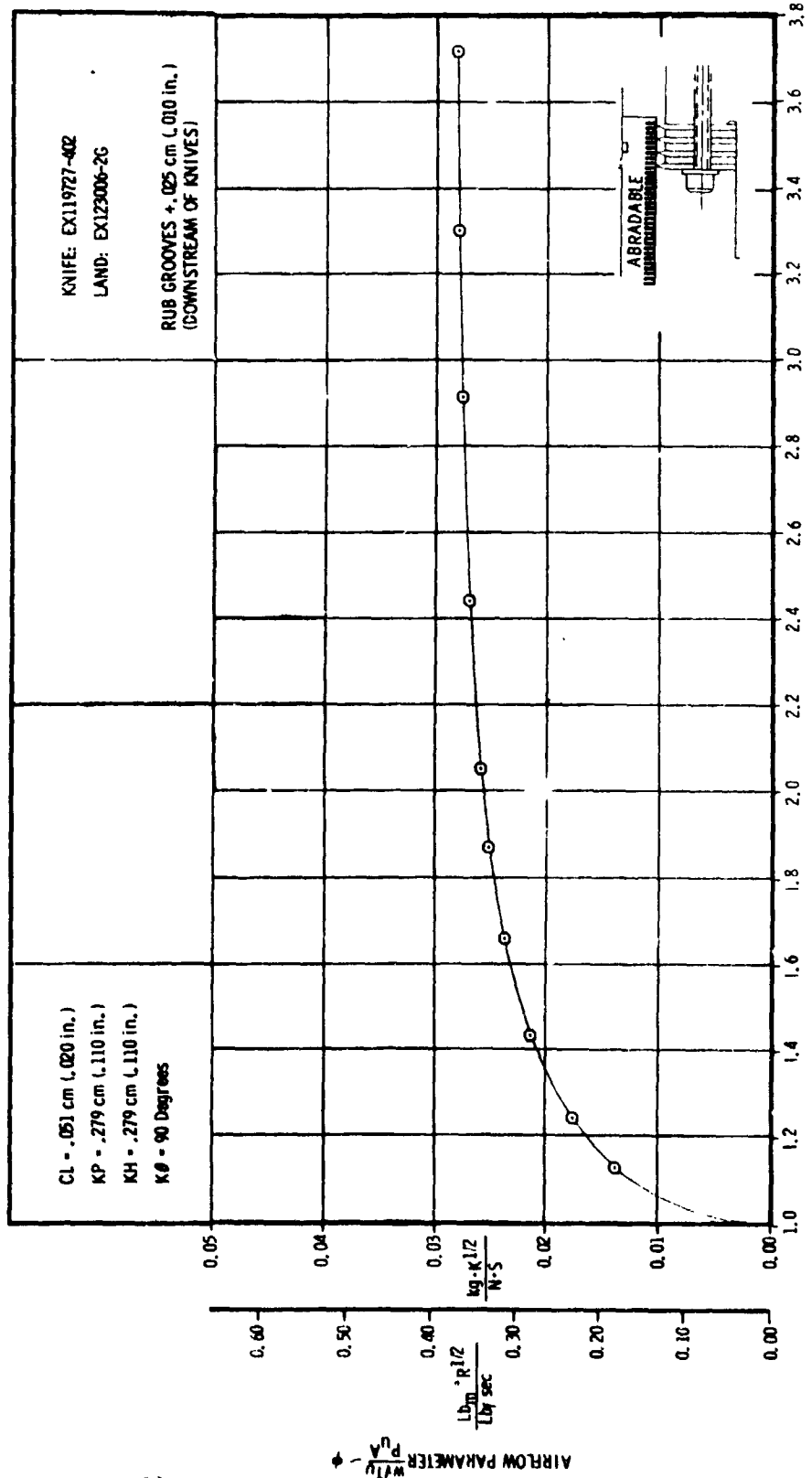

FIGURE C-12. 2D RIG TEST RESULTS OF A 4 KNIFE STRAIGHT-THROUGH SEAL WITH A RUB GROOVED "ABRADABLE A" LAND

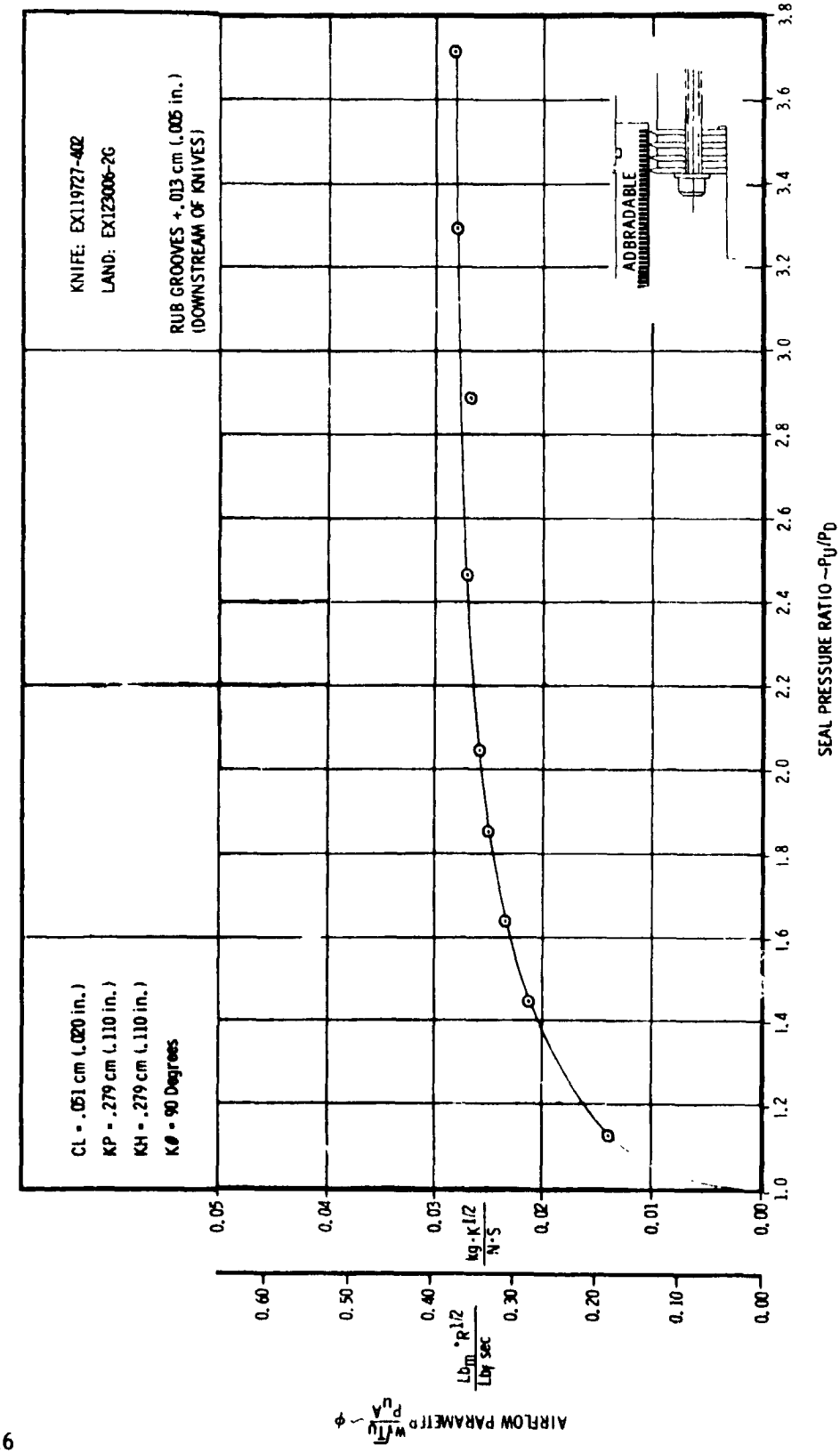

FIGURE C-13. 2D RIG TEST RESULTS OF A 4 KNIFE STRAIGHT-THROUGH SEAL WITH A RUB GROOVED "ABRADABLE A" LAND

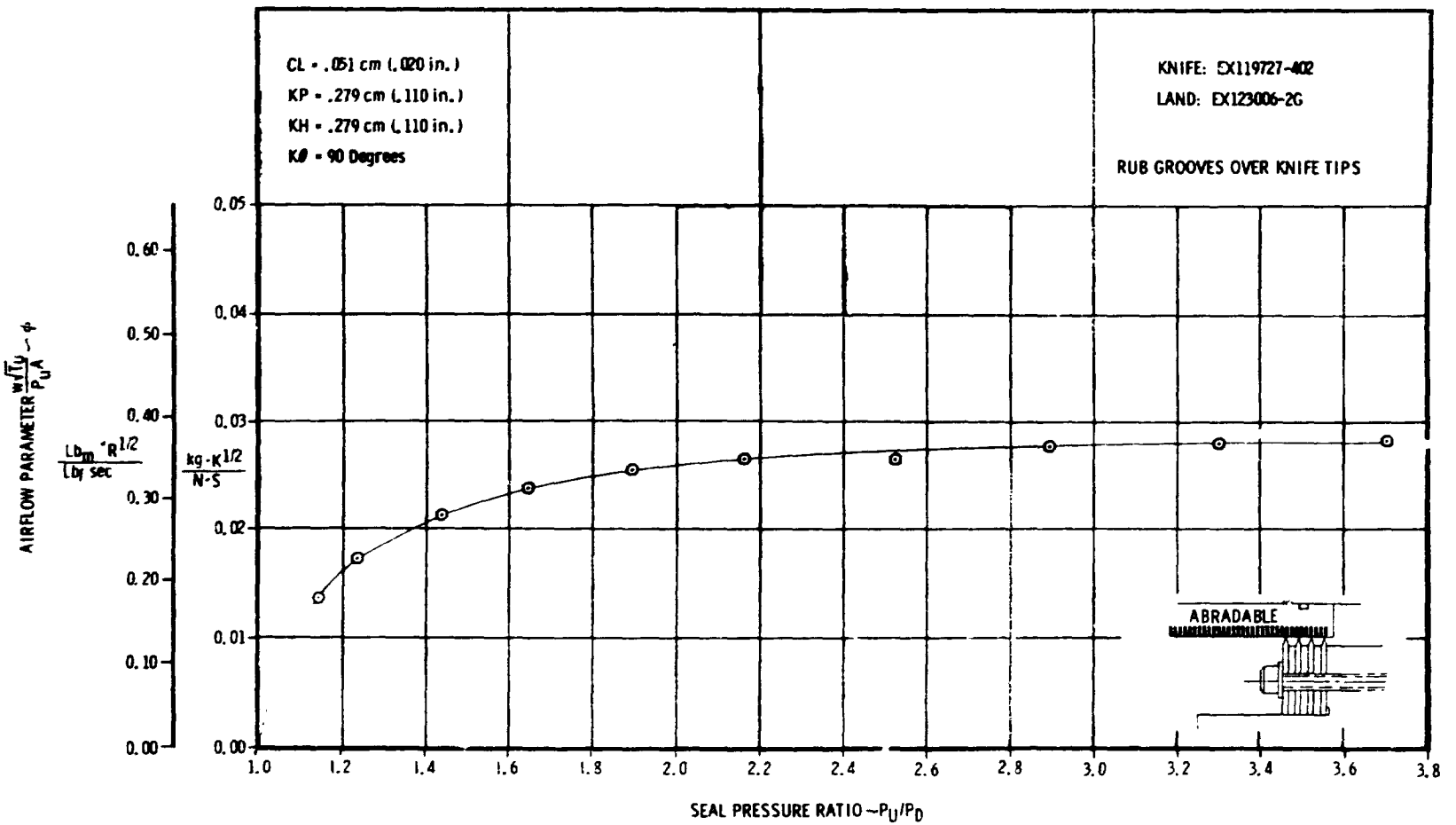

FIGURE C-14. 2D RIG TEST RESULTS OF A 4 KNIFE STRAIGHT-THROUGH SEAL WITH A RUB GROOVED "ABRADABLE A" LAND

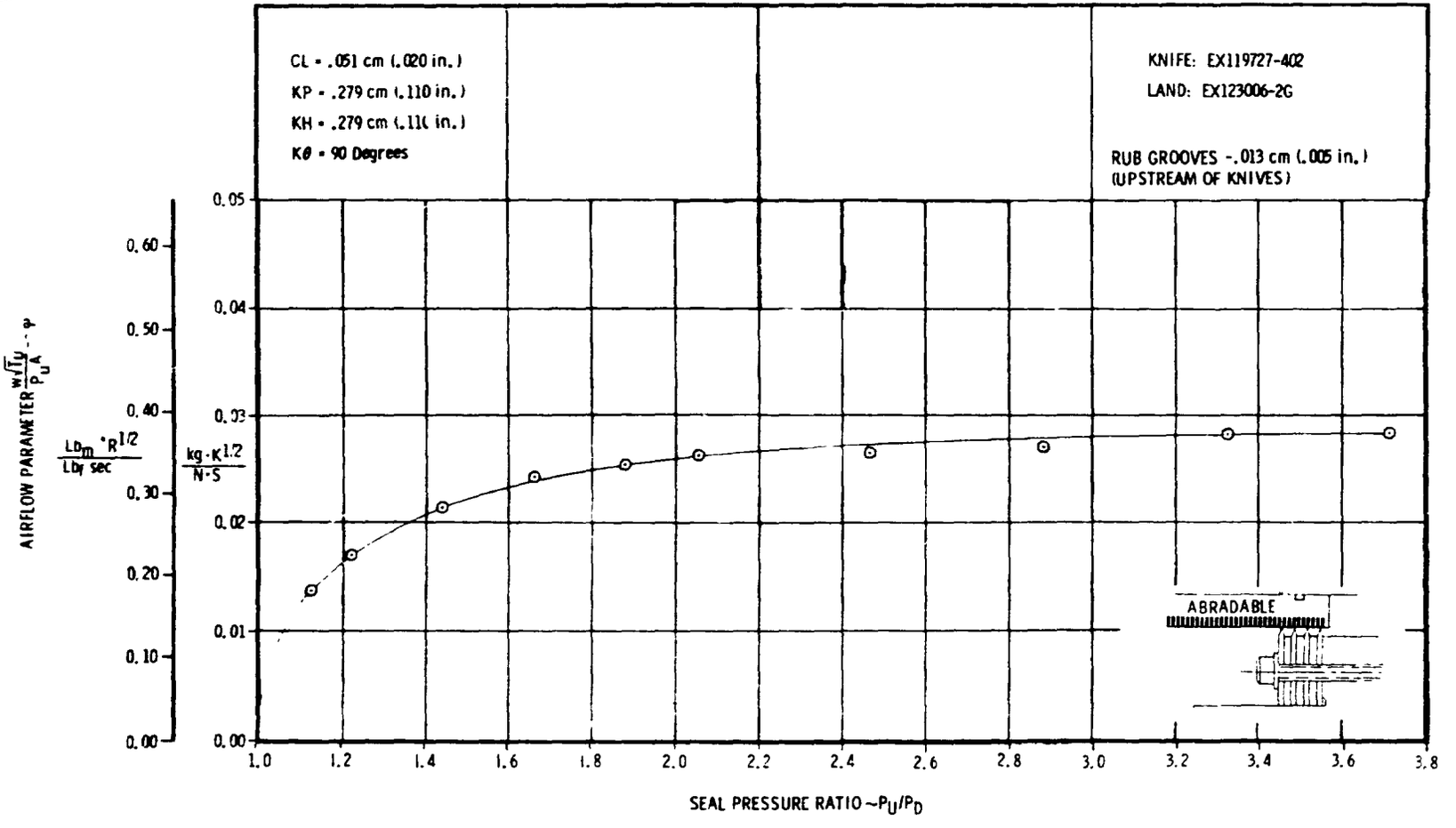

FIGURE C-15. 2D RIG TEST RESULTS OF A 4 KNIFE STRAIGHT-THROUGH SEAL WITH A RUB GROOVED "ABRADABLE A" LAND

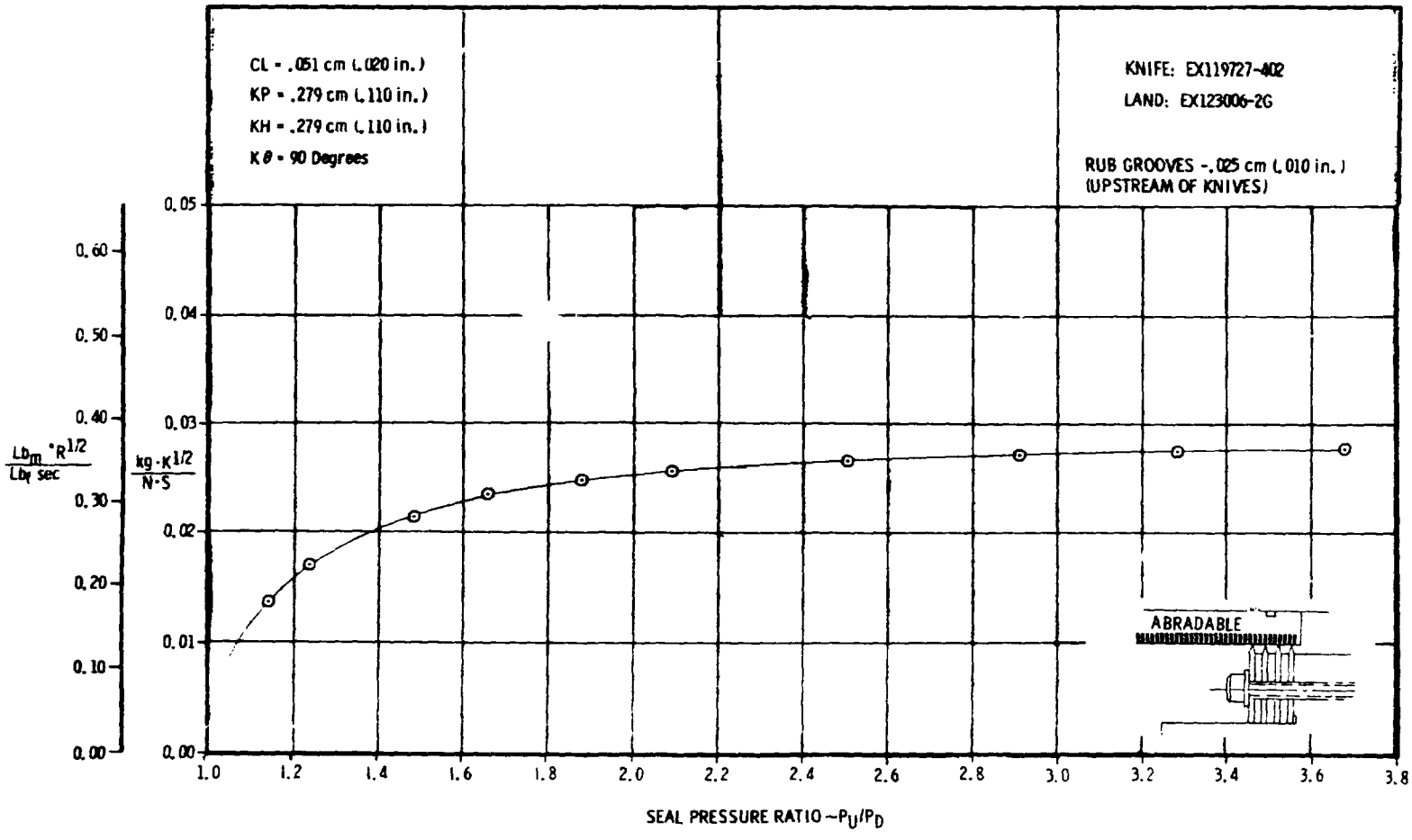

FIGURE C-16. 2D RIG TEST RESULTS OF A 4 KNIFE STRAIGHT-THROUGH SEAL WITH A RUB GROOVED "ABRADABLE A" LAND

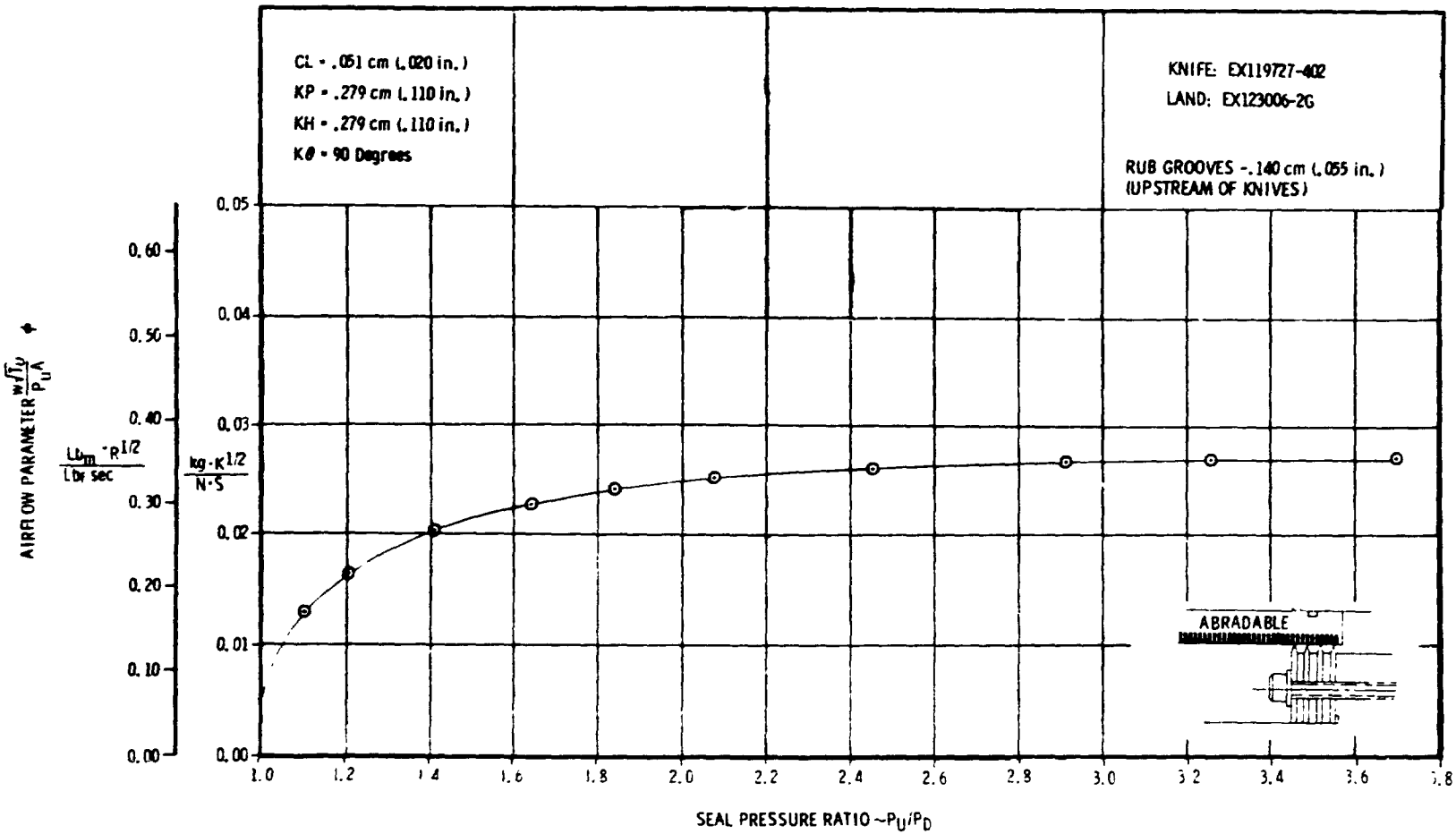

FIGURE C-17. 2D RIG TEST RESULTS OF A 4 KNIFE STRAIGHT-THROUGH SEAL WITH A RUB GROOVED "ABRADABLE A" LAND

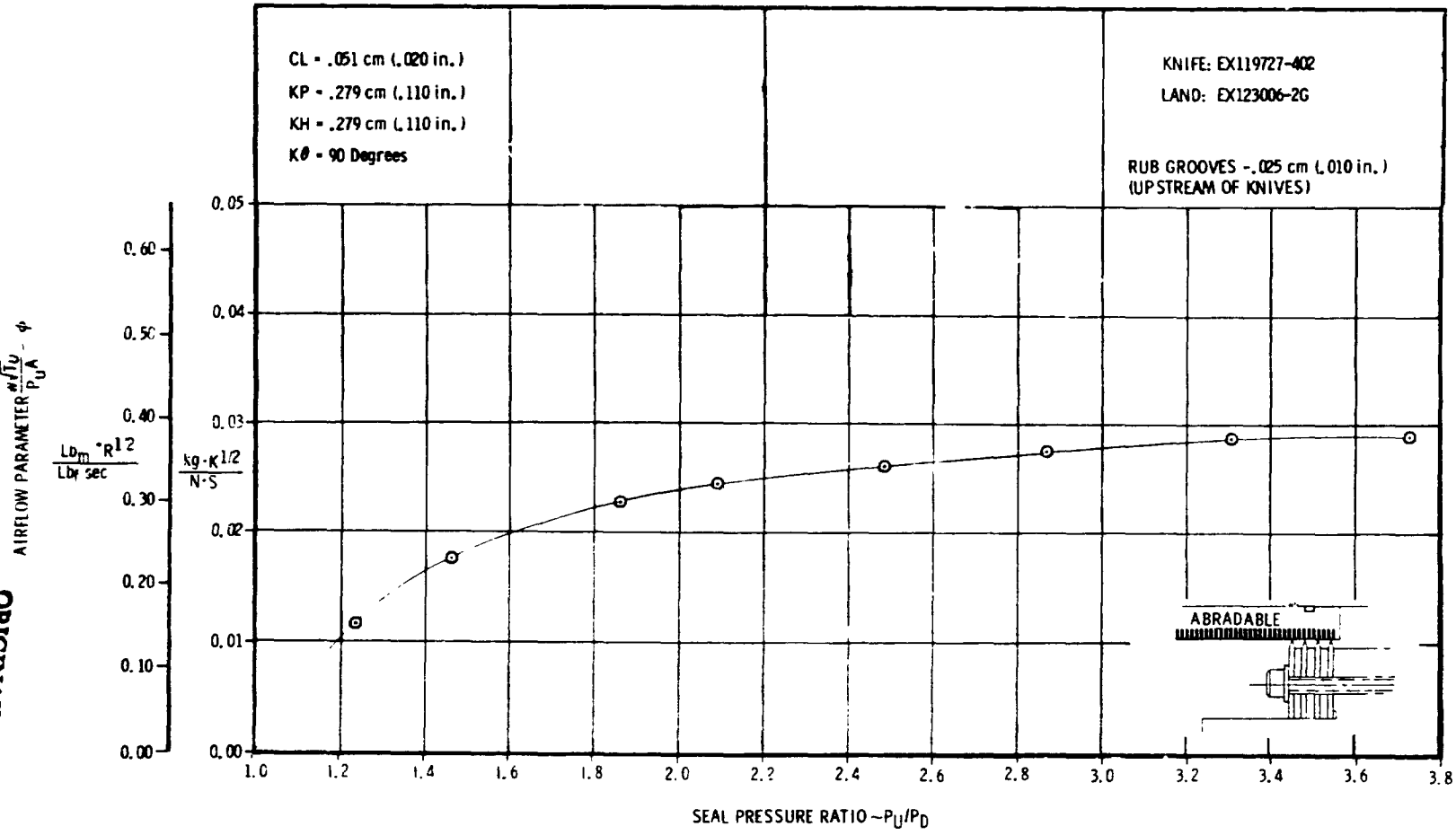

FIGURE C-18. 2D RIG TEST RESULTS OF A 4 KNIFF STRAIGHT-THROUGH SEAL WITH A RUB GROOVED "ABRADABLE A" LAND

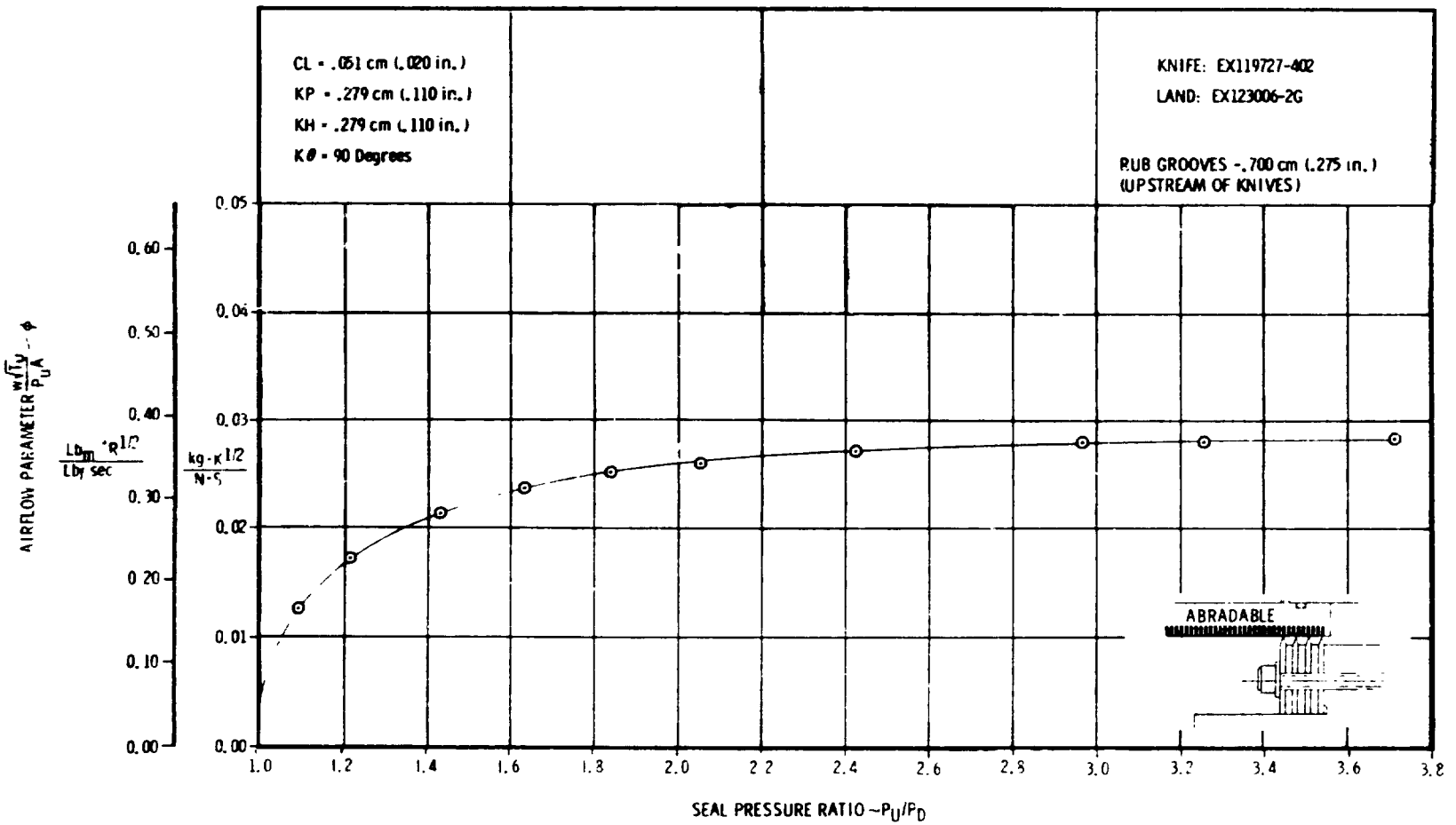

FIGURE C-19. 2D RIG TEST RESULTS OF A 4 KNIFE STRAIGHT-THROUGH SEAL WITH A RUB GROOVED "ABRADABLE A" LAND

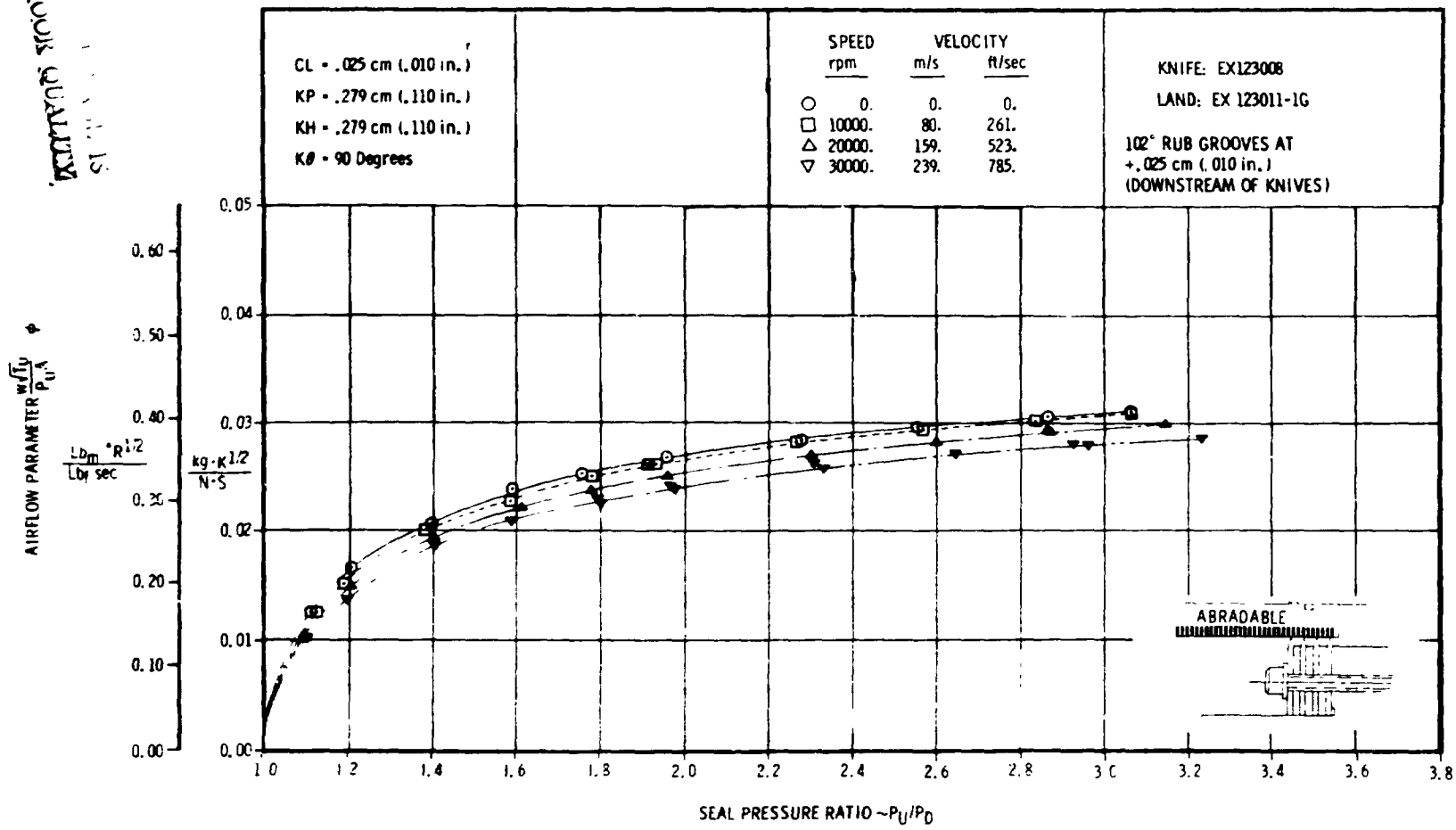

FIGURE C-20. 3D RIG TEST RESULTS OF A 4 KNIFE STRAIGHT-THROUGH SEAL WITH A RUB GROOVED "ABRADABLE A" LAND

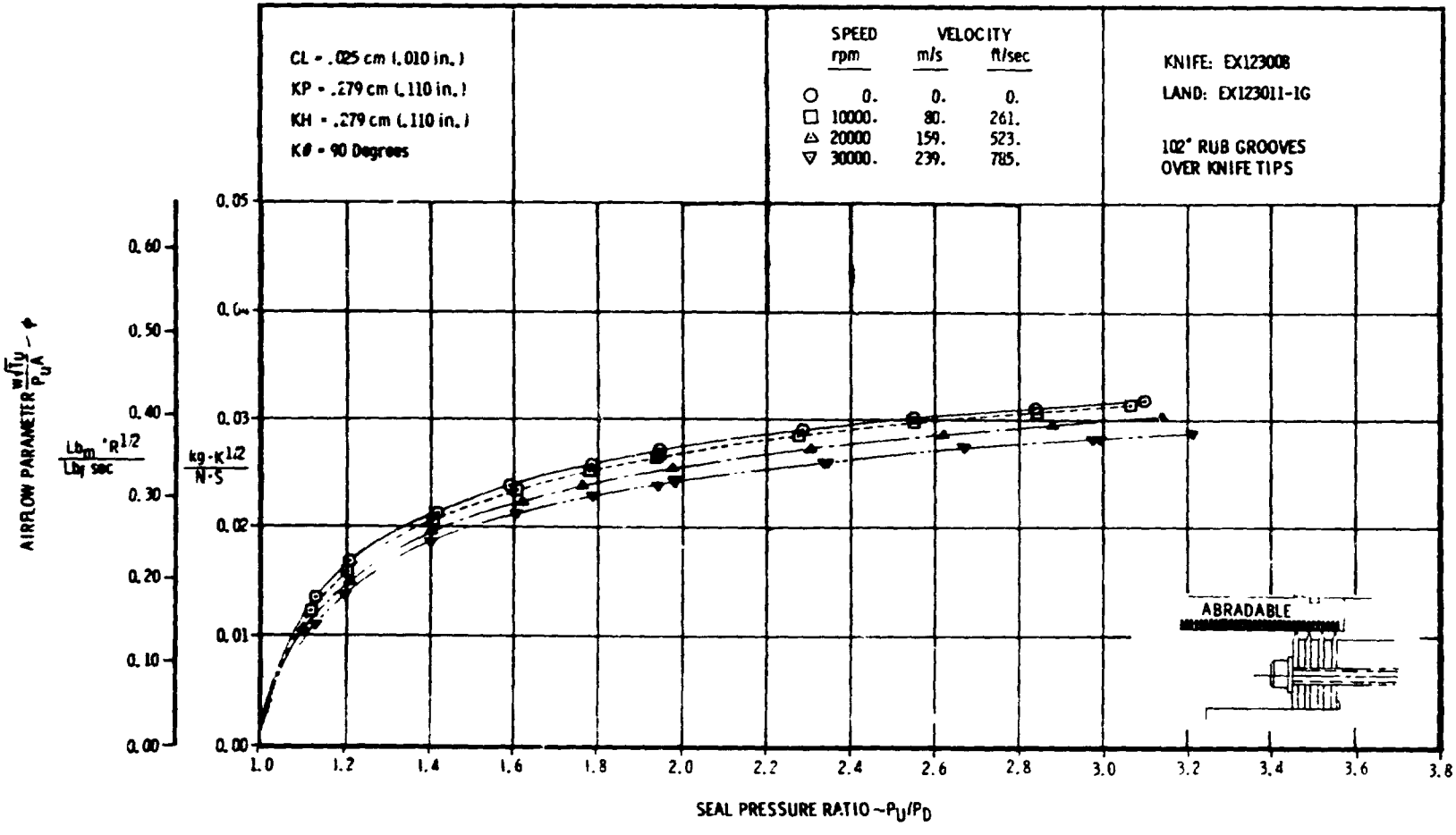

FIGURE C-21. 3D RIG TEST RESULTS OF A 4 KNIFE STRAIGHT-THROUGH SEAL WITH A RUB GROOVED "ABRADABLE A" LAND

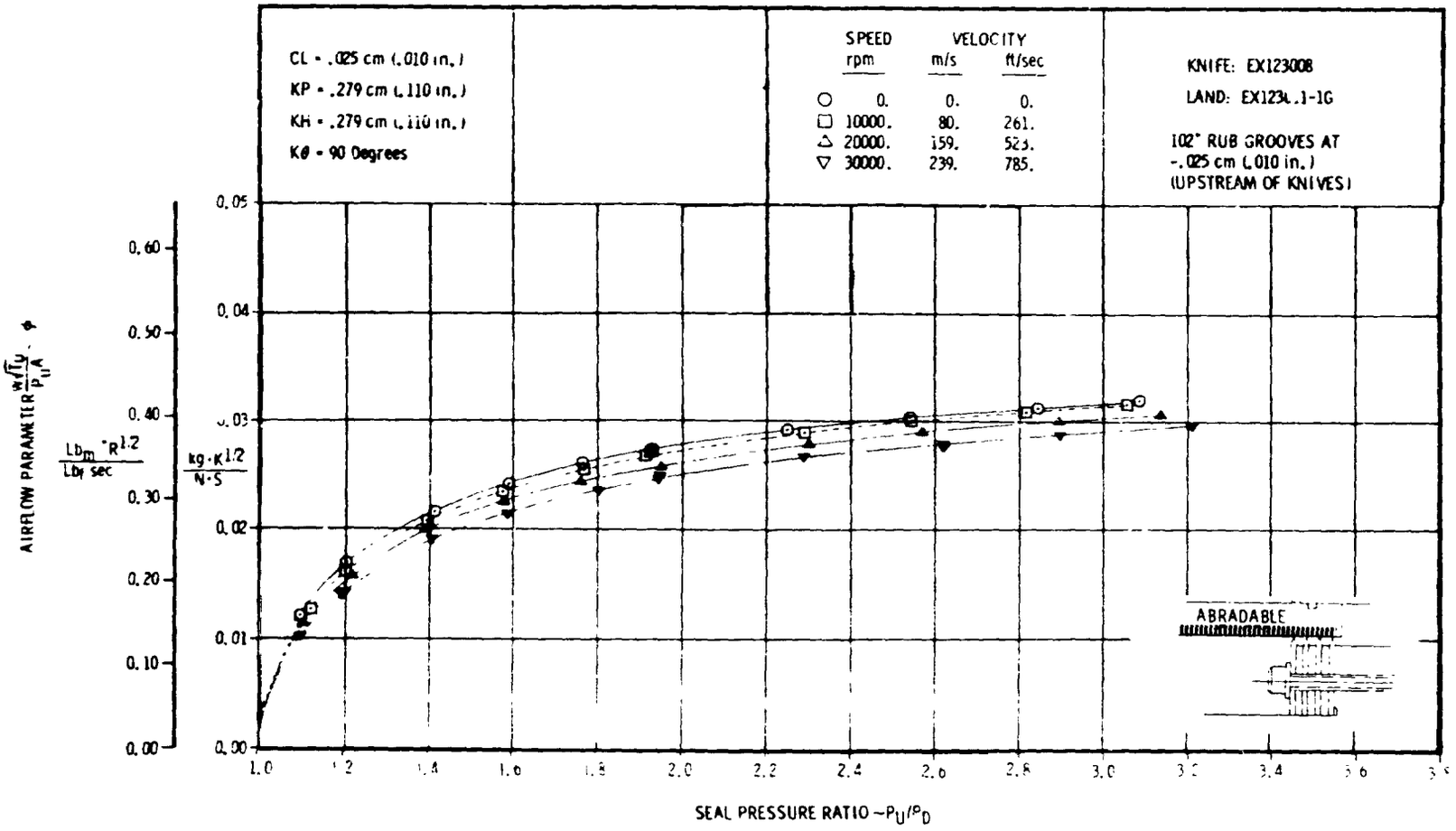

FIGURE C-22. 3D RIG TEST RESULTS OF A 4 KNIFE STRAIGHT-THROUGH SEAL WITH A RUB GROOVED "ABRADABLE A" LAND

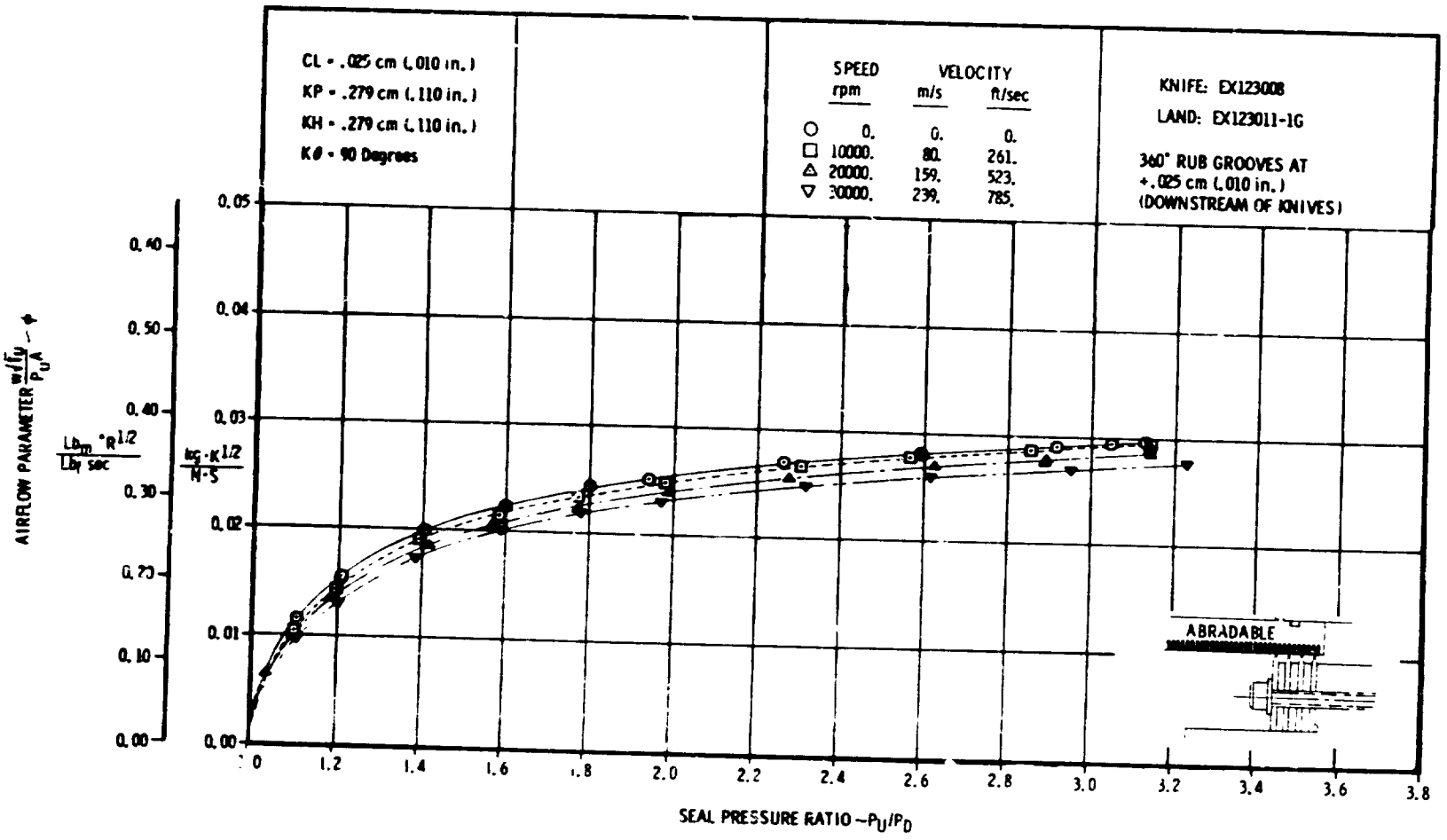

FIGURE C-23. 3D RIG TEST RESULTS OF A 4 KNIFE STRAIGHT-THROUGH SEAL WITH A RUB GROOVED "ABRADABLE A" LAND

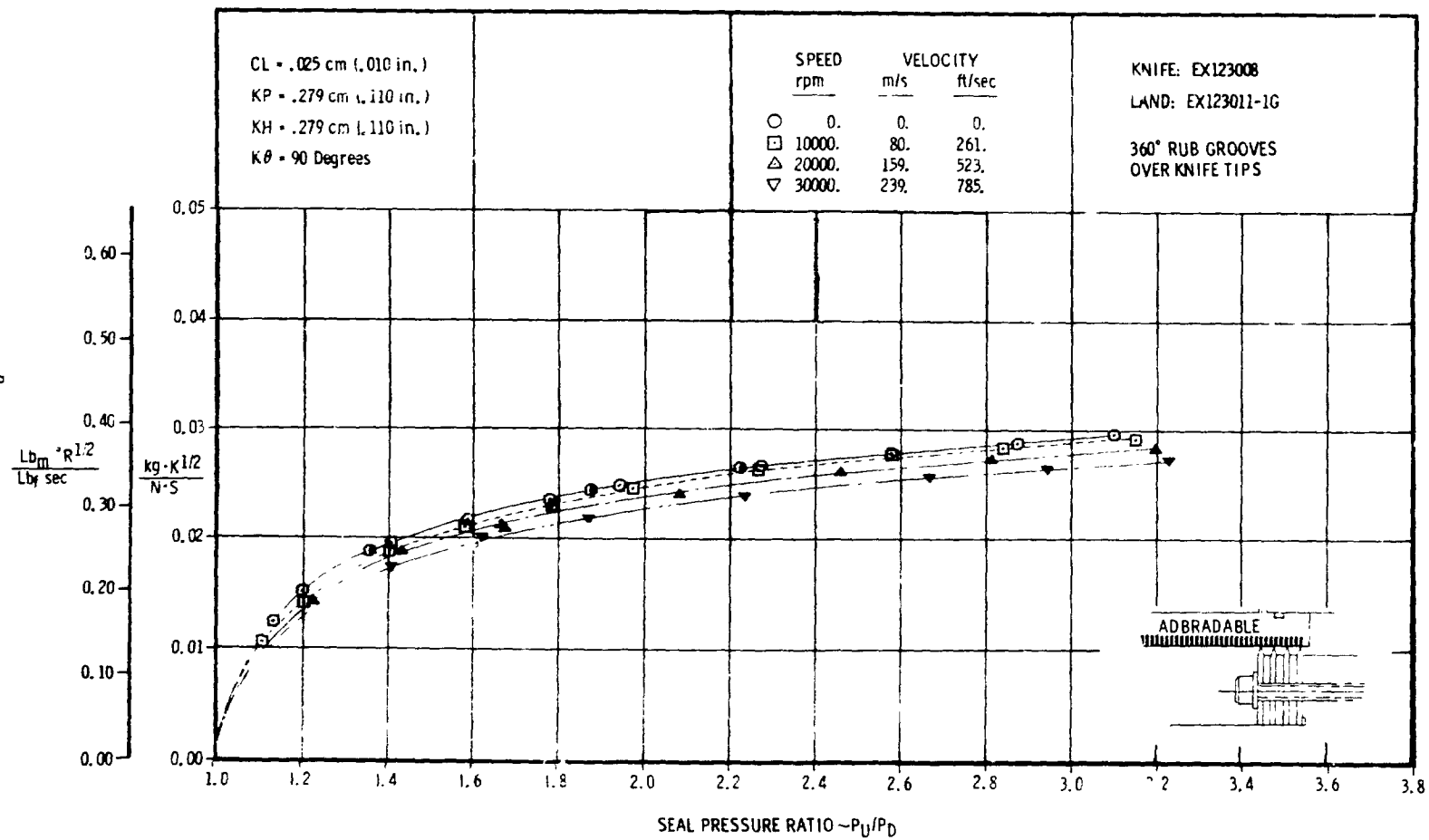

FIGURE C-24. 3D RIG TEST RESULTS OF A 4 KNIFE STRAIGHT-THROUGH SEAL WITH A RUB GROOVED "ABRADABLE A" LAND

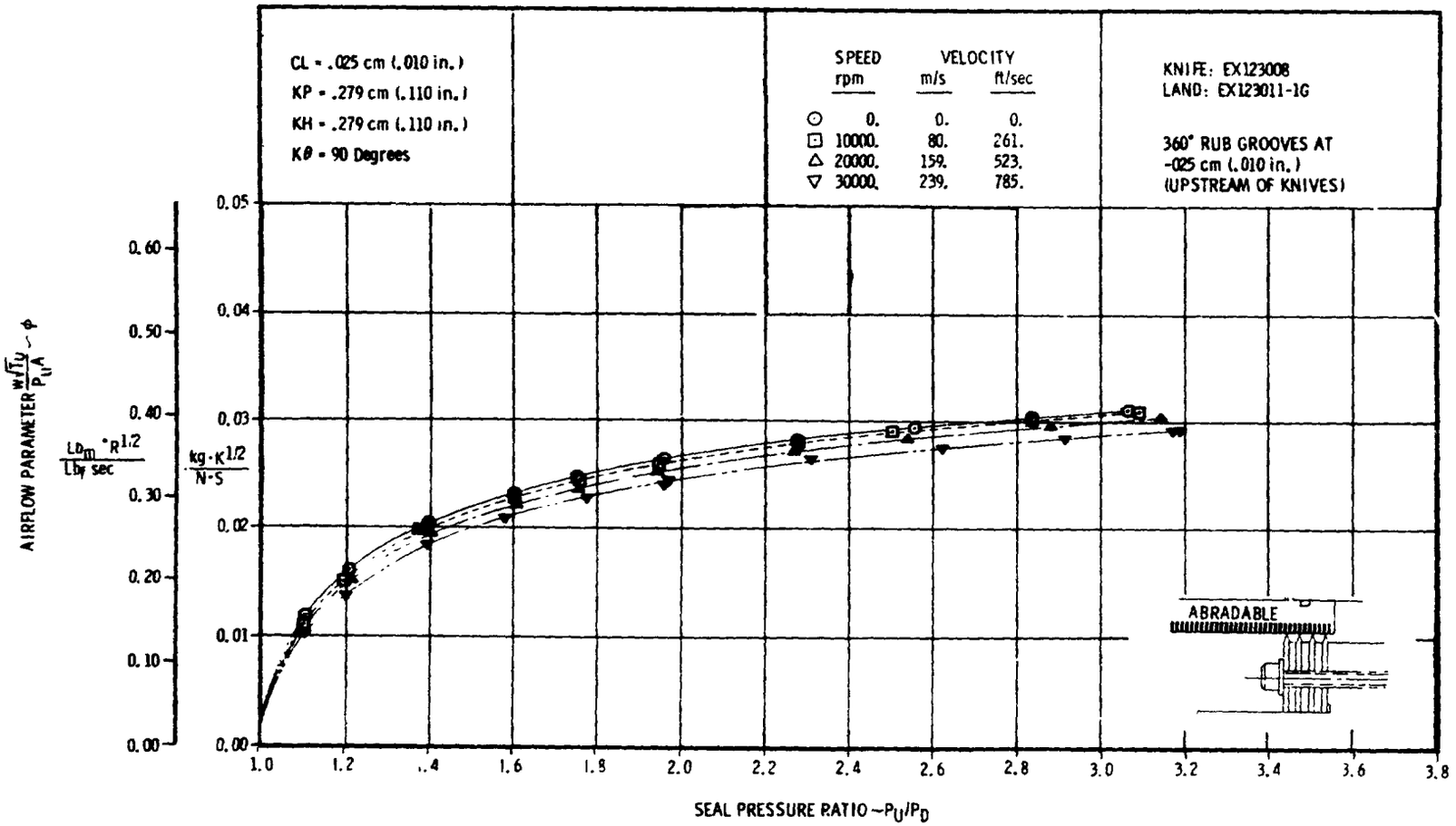

FIGURE C-25. 3D RIG TEST RESULTS OF A 4 KNIFE STRAIGHT-THROUGH SEAL WITH A RUB GROOVED "ABRADABLE A" LAND

APPENDIX D

Test Data Correlation for the 2D and 3D Seal Rigs.

The agreement between test results from the 2D rig and the 3D rig was generally good. Figures D-1 through D-4 show the rig correlation obtained for four knife straight seals with a solid-smooth land and a representative honeycomb land at .025 cm (.010 in.) and .051 cm (.020 in.) clearances. The correlation data for these straight seals are summarized in Table D-1. The honeycomb land displays an unusual sensitivity to clearance and may be sensitive to the relation between the knife tip and honeycomb cell edge orientation.

Figure D-5 illustrates the 2D rig to 3D rig correlation for the advanced seal, which was developed on the 2D rig. This comparison shows good agreement at pressure ratios less than about 1.3 and only a slight further deterioration beyond about a pressure ratio of 2.0 to 6.5% variation at a pressure ratio of 3. The correlation data for the advanced seal geometry in 2D rig and 3D rig tests are summarized in Table D-1, also.

FIGURE D-1. PERFORMANCE COMPARISON FOR 2D RIG AND 3D RIG AT STATIC CONDITIONS
4 KNIFE STRAIGHT SEAL WITH SOLID-SMOOTH LAND CLEARANCE = .025 cm (.010 in.)

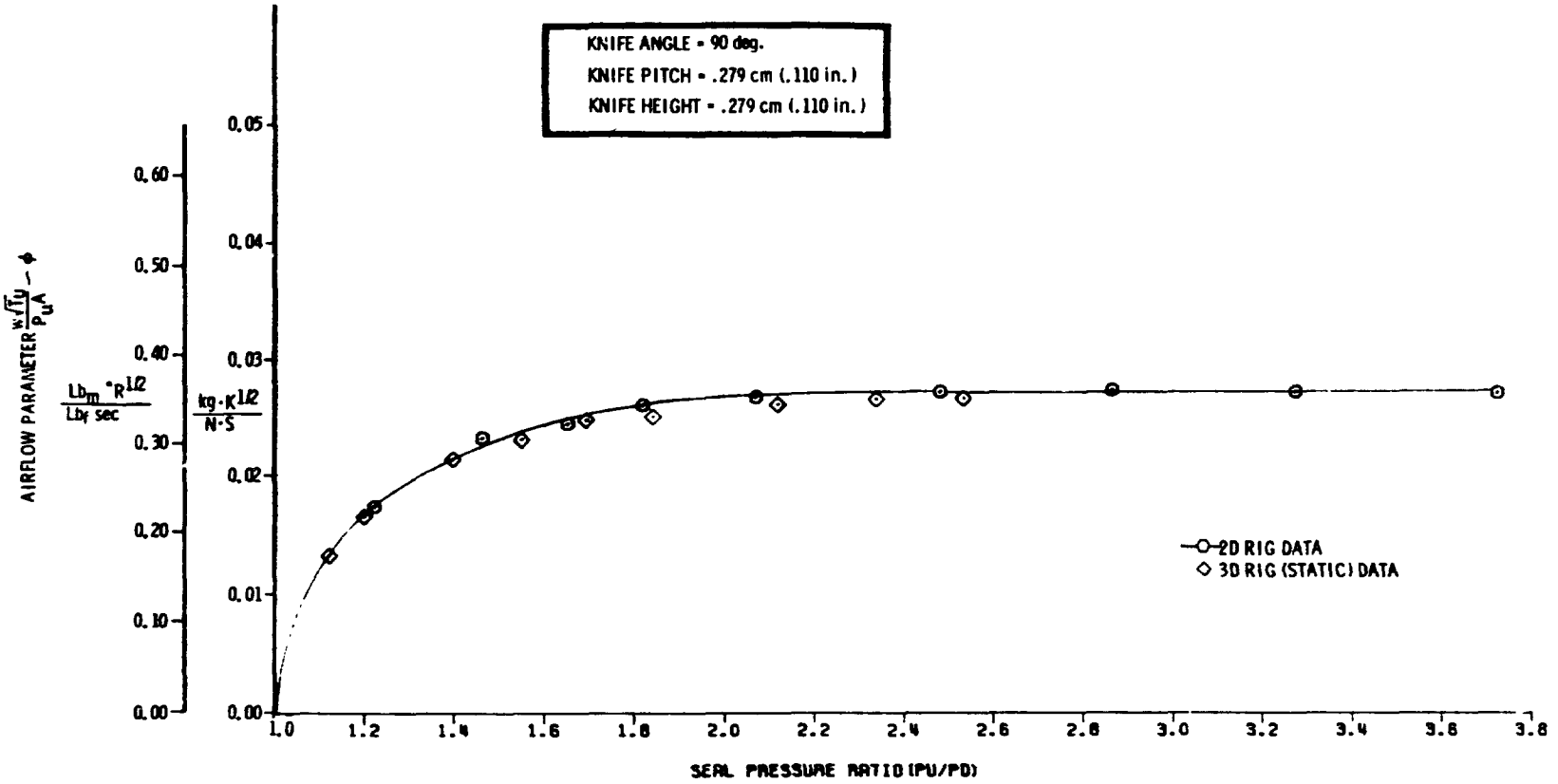

FIGURE D-2. PERFORMANCE COMPARISON FOR 2D RIG AND 3D RIG AT STATIC CONDITIONS
4 KNIFE STRAIGHT SEAL WITH SOLID-SMOOTH LAND CLEARANCE = .051 cm (.020 in.)

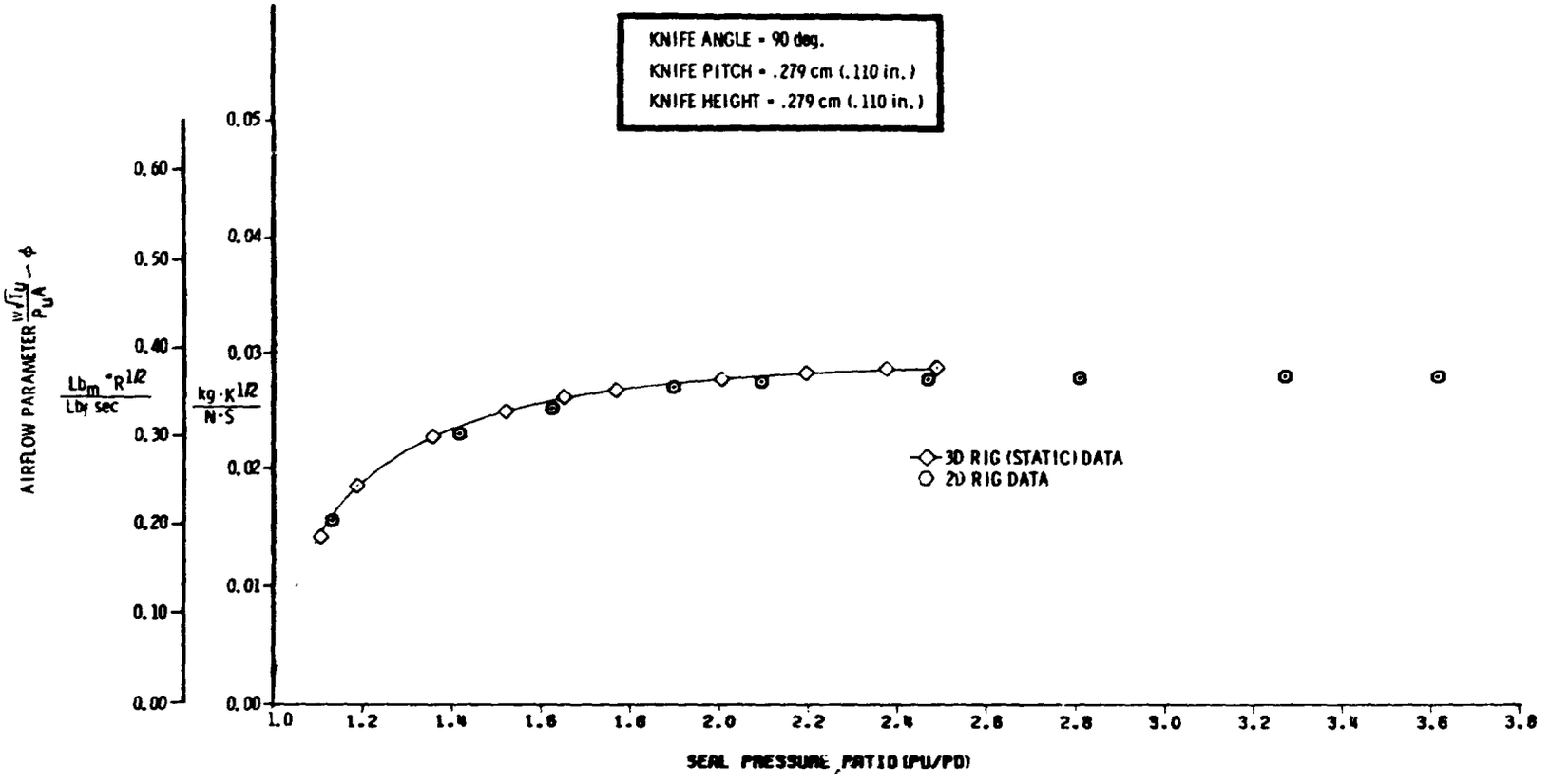

FIGURE D-3. PERFORMANCE COMPARISON FOR 2D RIG AND 3D RIG AT STATIC CONDITIONS
4 KNIFE STRAIGHT SEAL WITH .062 CELL HONEYCOMB LAND CLEARANCE = .025 cm (.010 in.)

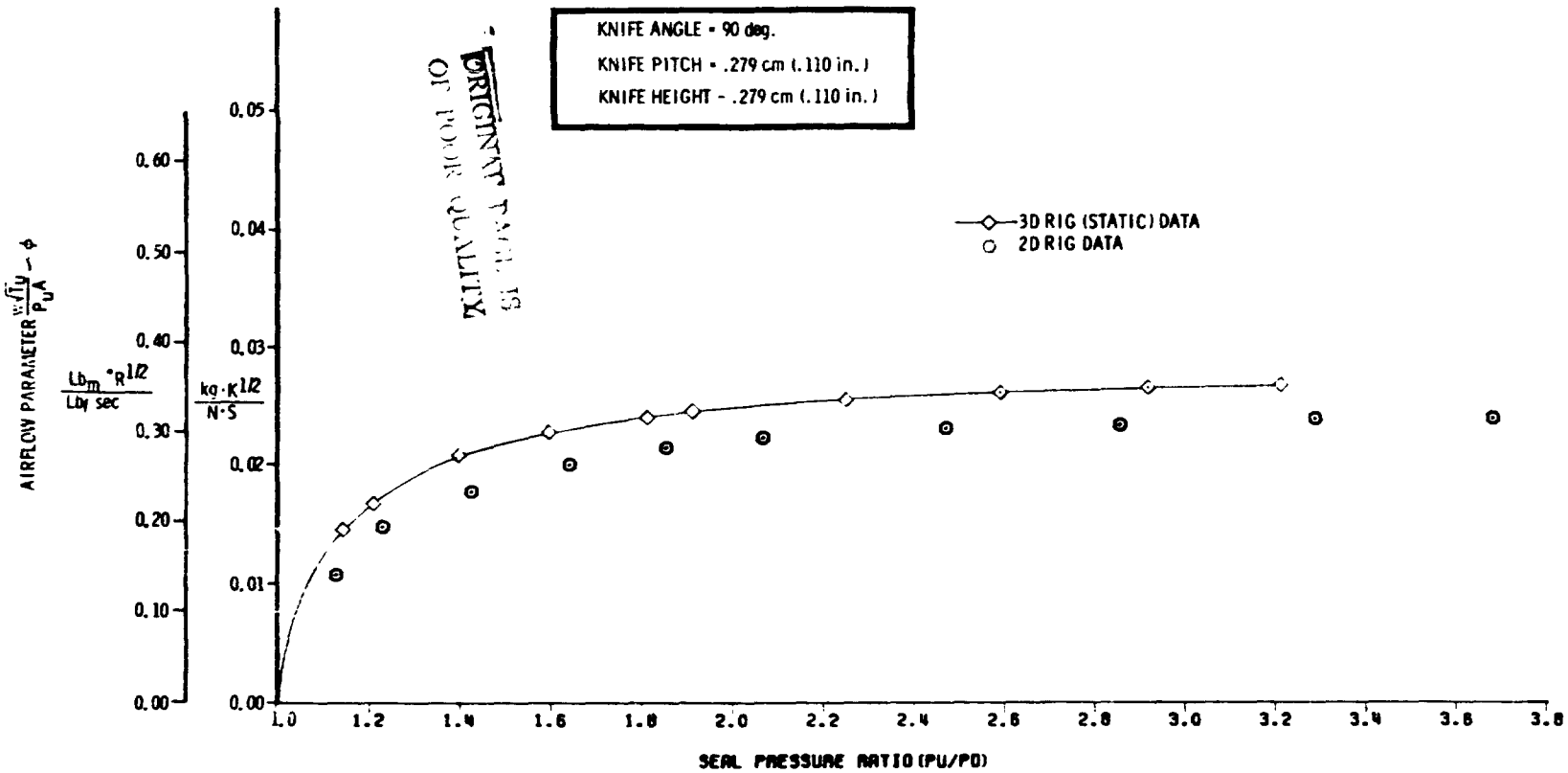

FIGURE D-4. PERFORMANCE COMPARISON FOR 2D RIG AND 3D RIG AT STATIC CONDITIONS
4 KNIFE STRAIGHT SEAL WITH .062 CELL HONEYCOMB LAND CLEARANCE = .051 cm (.020 in.)

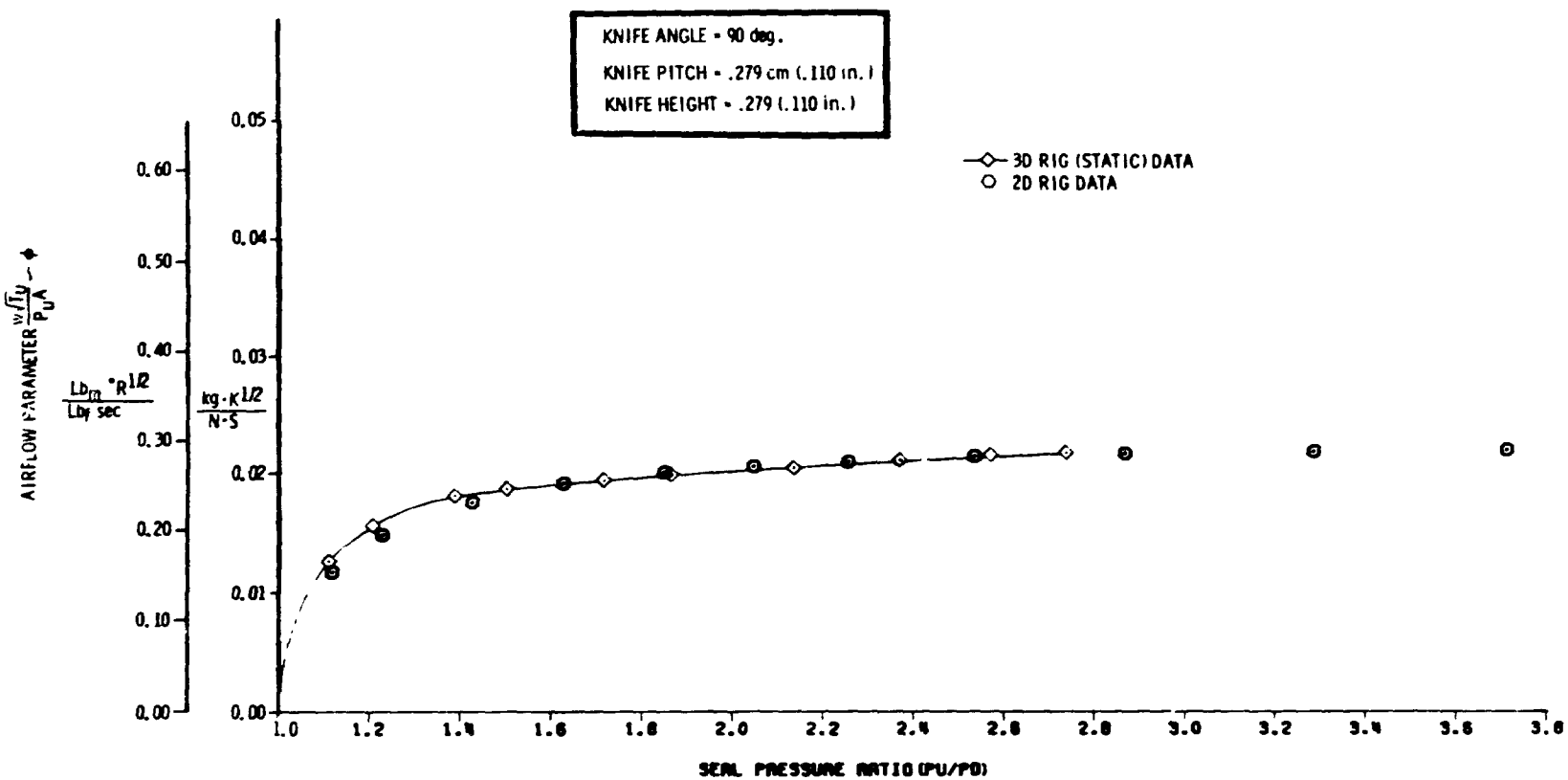

FIGURE D-5. PERFORMANCE COMPARISON FOR 2D RIG AND 3D RIG AT STATIC CONDITIONS
LTSD 4 KNIFE ADVANCED SEAL WITH SOLID SMOOTH LAND CLEARANCE = .051 cm (.020 in.)

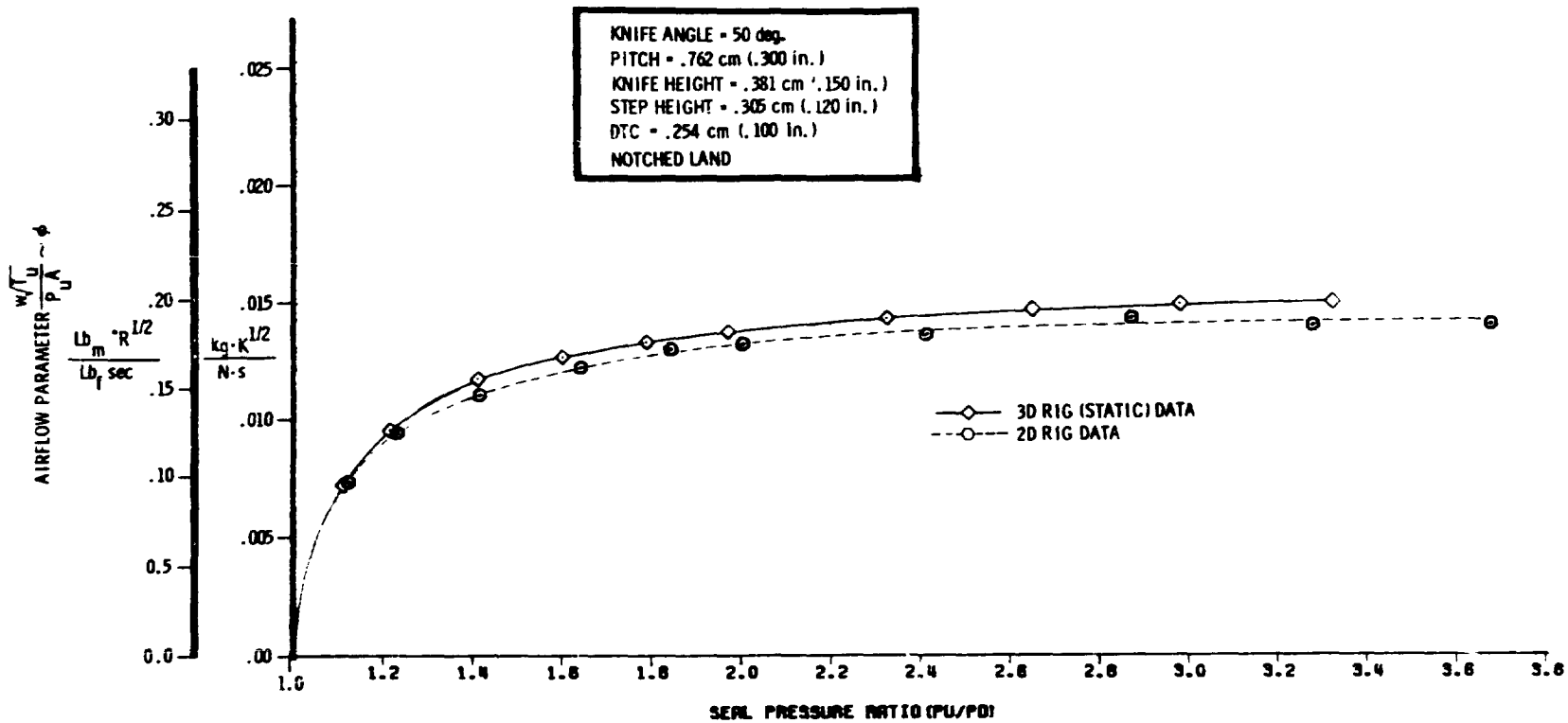

TABLE D-1. COMPARISON OF FOUR KNIFE SEAL PERFORMANCE ON THE 2D RIG AND THE 3D RIG AT A PRESSURE RATIO OF 2.0

Rig	Seal Type	Kθ, Knife Angle deg	KP, Knife Pitch cm	KP, Knife Pitch in.	KH, Knife Height cm	KH, Knife Height in.	SH, Step Height cm	SH, Step Height in.	CL, Clearance cm	CL, Clearance in.	Test Condition	Φ, Flow Parameter $\frac{kg \cdot K^{1/2}}{N \cdot s}$	Φ, Flow Parameter $\frac{lb_m R^{1/2}}{lbf\ sec}$	ΔΦ/Φ From Baseline %
	STRAIGHT													
2D	Solid-Smooth	90	.279	.110	.279	.110			.025	.010		.0272	.358	+2.3
3D	Land	90	.279	.110	.279	.110			.025	.010	Static	.0266	.350	
2D	Solid-Smooth	90	.279	.110	.279	.110			.051	.020		.0277	.365	-1.9
3D	Land	90	.279	.110	.279	.110			.051	.020	Static	.0283	.372	
2D	.159 cm(.062 in)	90	.279	.110	.279	.110			.025	.010		.0226	.298	-10.2
3D	Honeycomb	90	.279	.110	.279	.110			.025	.010	Static	.0252	.332	
2D	.159 cm(.062 in)	90	.279	.110	.279	.110			.051	.020		.0209	.275	+1.9
3D	Honeycomb	90	.279	.110	.279	.110			.051	.020	Static	.0205	.270	
	ADVANCED													
2D	LTSD	50	.762	.300	.381	.150	.305	.120	.051	.020		.0134	.176	-4.3
3D	Solid-Smooth Land	50	.762	.300	.381	.150	.305	.120	.051	.020	Static	.0140	.184	

$$\Delta\Phi/\Phi = \frac{\Phi_{2D} - \Phi_{3D}}{\Phi_{3D}}$$

APPENDIX E

Power Absorption Curves from 3D Air Seal Rig Tests on Four Knife Straight-Through Seals and an Optimized Advanced Seal Including an Application Procedure.

The labyrinth seal power absorption curves contained in Appendix E were derived from testing accomplished in the Detroit Diesel Allison 15.24 cm (6.00 in.) diameter, dynamic air seal test rig (3D rig).

Rotational power absorption was measured for:

1. Four knife straight-through seal configurations with rotor pitch values of .203 cm (.080 in.), .279 cm (.110 in.), and .356 cm (.140 in.) tested with solid-smooth, abradable, and honeycomb lands. The "Abradable A" porous material was used in the abradable land. The honeycomb land cell size was .159 cm (.062 in.), and the cell depth was .254 cm (.100 in.).

   All configurations were tested at .025 cm (.010 in.) and .051 cm (.020 in.) radial clearances.

2. An optimized advanced seal configuration was tested with solid-smooth, abradable, and honeycomb lands at a radial clearance of .051 cm (.020 in.). The materials used in the stepped land were the same three which were used in the straight-through seal configurations.

   Rotor Geometry:
   - 4 Slanted Knives
   - Knife Angle = 50°
   - Pitch = .762 cm (.300 in.)
   - Step Height = .305 cm (.120 in.)
   - Knife Height = .381 cm (.150 in.)

Calculation Procedure for Applying Rotational Seal Power Absorption Data to Engine Environmental Conditions

Sample Problem

Calculate the relative rotational power absorption difference between two potential land surfaces for a typical seal application in a high bypass ratio turbofan engine with an overall compressor pressure ratio, R_{COA} = 38.

Design Assumptions

Seal Location: First Stage, High Pressure Turbine Wheel, Inlet Face.

Seal Type: Optimized Advanced Seal.

Potential Land Surfaces:

- o Solid-Smooth Land
- o "Abradable A" Land

Seal Geometry:

Flow Direction = STLD

Seal Diameter, D_S = 61.5 cm (24.2 in.)

Clearance, CL = .051 cm (.020 in.)

Number of Knives, KN = 4

Pitch, KP = .762 cm (.300 in.)

Knife Angle, Kθ = 50°

Knife Height, KH = .381 cm (.150 in.)

Step Height, SH = .305 cm (.120 in.)

Seal Operating Environment:

Seal Inlet Temperature T_U = 940 K (1692°R)

Seal Inlet Pressure, p_U = 3723 kPa (540 psia)

Seal Pressure Ratio, p_U/p_D = 1.7

Seal Rotational Speed, RPM = 9000 rpm

Procedure

Calculate the seal dynamic operating conditions.

Seal Knife Tip Velocity,

$$V = \frac{\pi}{60000} D_S \cdot RPM$$

$$= 290. \frac{m}{s} \left(950. \frac{ft}{sec} \right)$$

Seal Knife Tip Corrected Velocity,

$$\frac{V}{\sqrt{\theta}} = \frac{290.}{\sqrt{\frac{940.}{288.16}}}$$

$$= 161. \frac{m}{s} \left(526. \frac{ft}{sec} \right)$$

From Figure E-7 for the STLD optimized advanced seal with a clearance of .051 cm (.020 in.) at $p_U/p_D = 1.7$ on the abcissa and parametric curves for a corrected knife tip speed of $V/\sqrt{\theta} = 159 \frac{m}{s} \left(523 \frac{ft}{sec} \right)$, read the seal rig rotor corrected power on the ordinate:

Land Material	$\frac{P}{\delta\sqrt{\theta}} \left(\frac{D_{std}}{D_S} \right)^*$
"Abradable A"	.373 kw (.500 hp)
Solid-Smooth	.343 kw (.460 hp)

*The diameter ratio scales the corrected power parameter to generalize the performance between the engine seal, D_S, and the reference 3D rig seal, D_{std}. The reference seal diameter for the 3D test rig is D_{std} = 15.24 cm (6.00 in.).

Therefore, the additional corrected power absorbed by an "Abradable A" land relative to a solid-smooth land is

$$\frac{\Delta P}{\delta\sqrt{\theta}} \left(\frac{D_{std}}{D_S}\right) = .030 \text{ kw } (.040 \text{ hp})$$

The additional actual power absorbed by an "Abradable A" land in the engine seal relative to a solid-smooth land is

$$\Delta P = \left[\frac{\Delta P}{\delta\sqrt{\theta}} \left(\frac{D_{std}}{D_S}\right)\right] \delta\sqrt{\theta} \left(\frac{D_S}{D_{std}}\right)$$

$$= \left[.030\right] \frac{3723.}{101.3} \sqrt{\frac{940.}{288.16}} \left(\frac{61.5}{15.24}\right) = 8.0 \text{ kw } (10.7 \text{ hp})$$

Therefore, the application of "Abradable A" material to the first stage, high pressure turbine wheel front seal will absorb 8.0 kw (10.7 hp) more than a solid-smooth land at the design conditions.

It should be noted that to determine the net system performance, the effect of leakage change must also be included.

FIGURE E-1. CORRECTED SEAL ROTOR POWER VERSUS SEAL PRESSURE RATIO FOR A FOUR KNIFE STRAIGHT SEAL

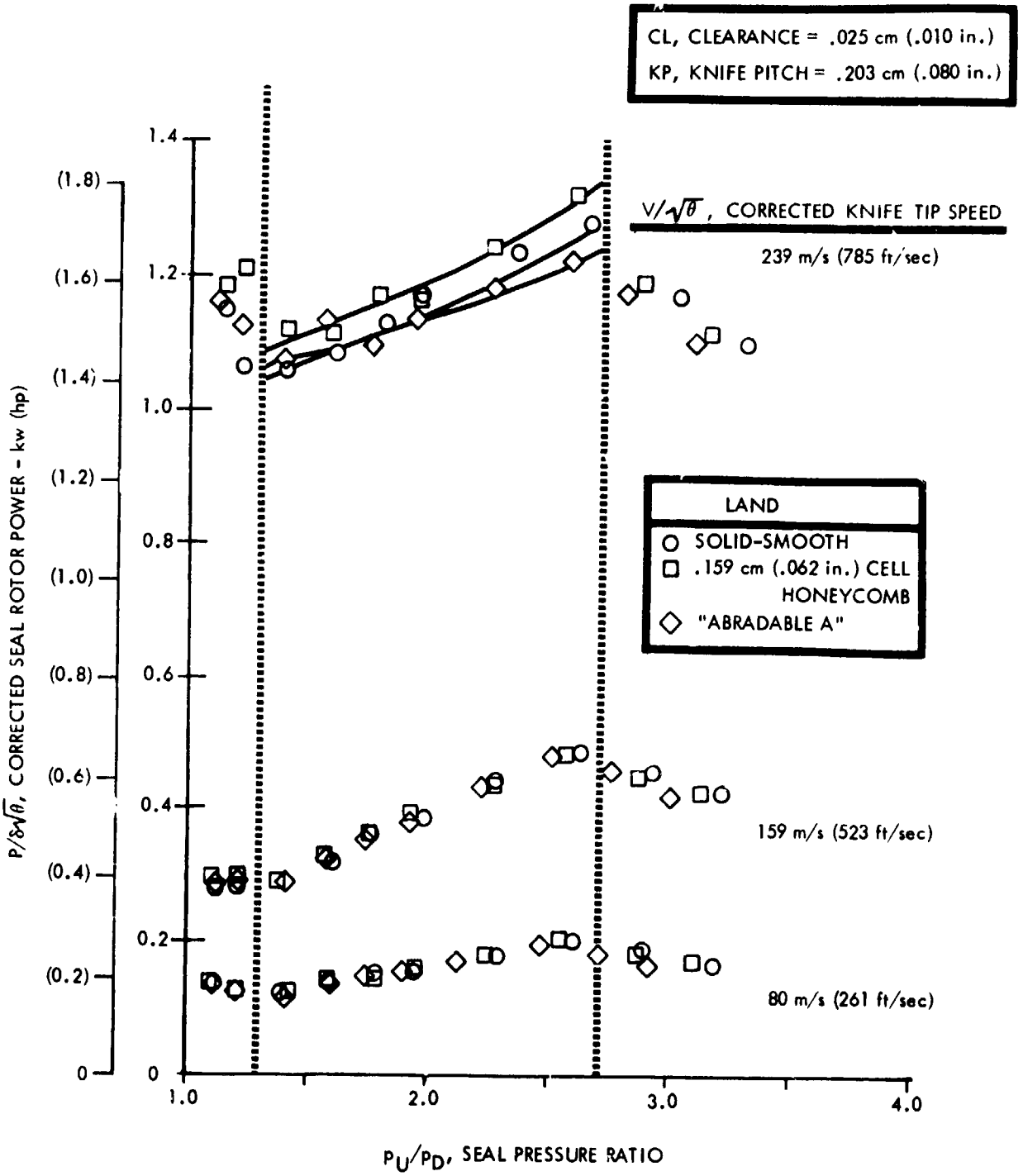

FIGURE E-2. CORRECTED SEAL ROTOR POWER VERSUS SEAL PRESSURE RATIO FOR A FOUR KNIFE STRAIGHT SEAL

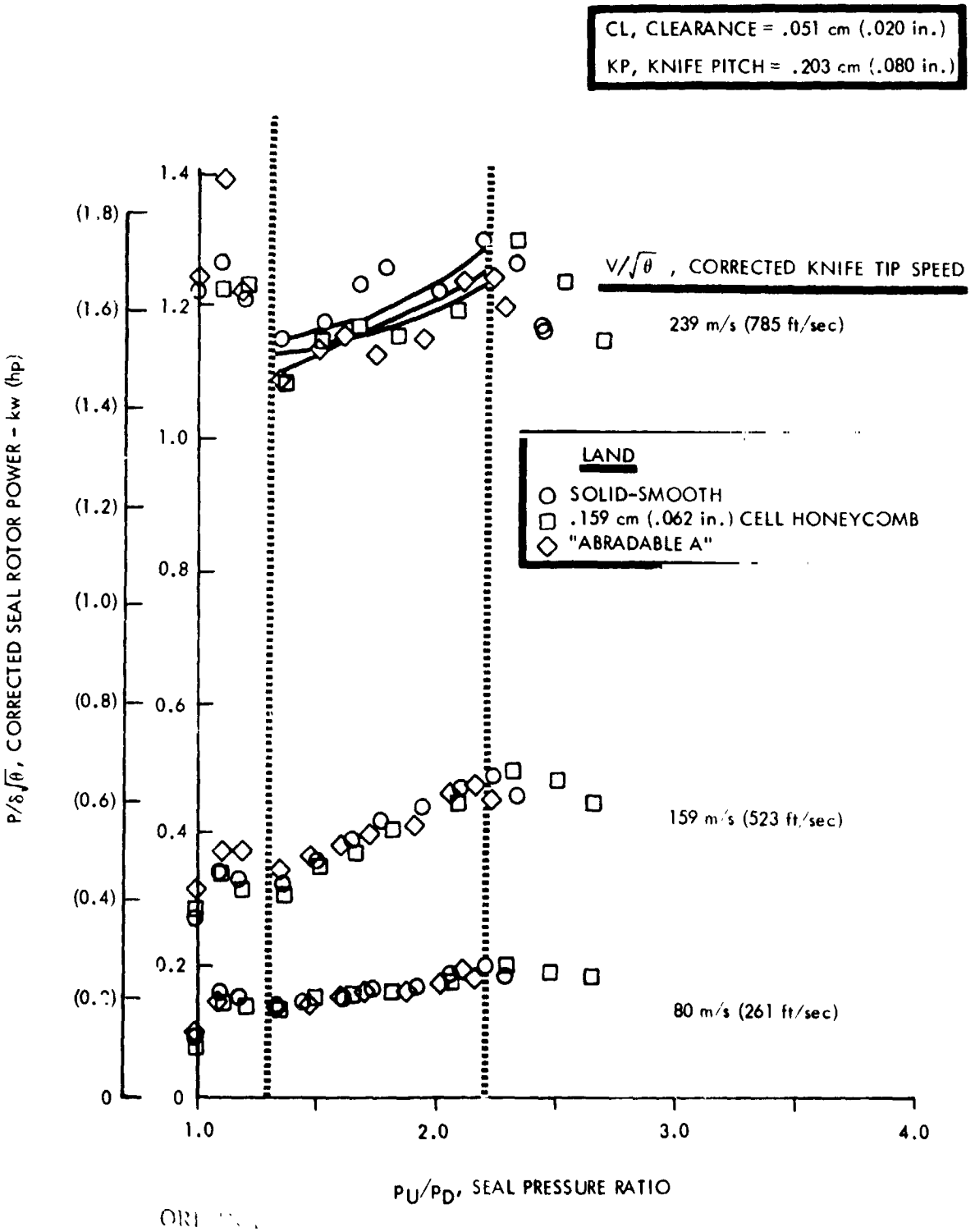

FIGURE E-3. CORRECTED SEAL ROTOR POWER VERSUS SEAL PRESSURE RATIO FOR A FOUR KNIFE STRAIGHT SEAL

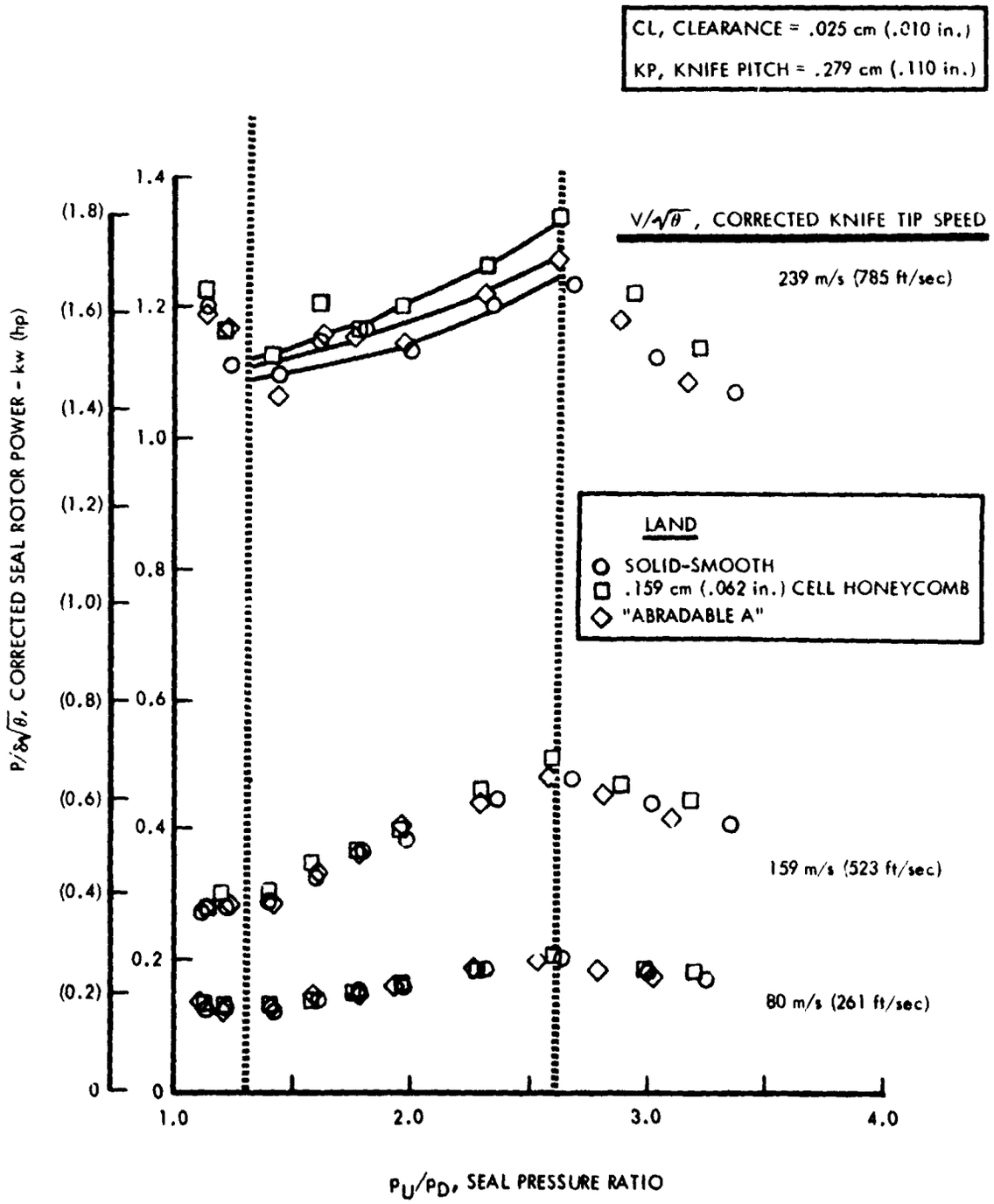

FIGURE E-4. CORRECTED SEAL ROTOR POWER VERSUS SEAL PRESSURE RATIO FOR A FOUR KNIFE STRAIGHT SEAL

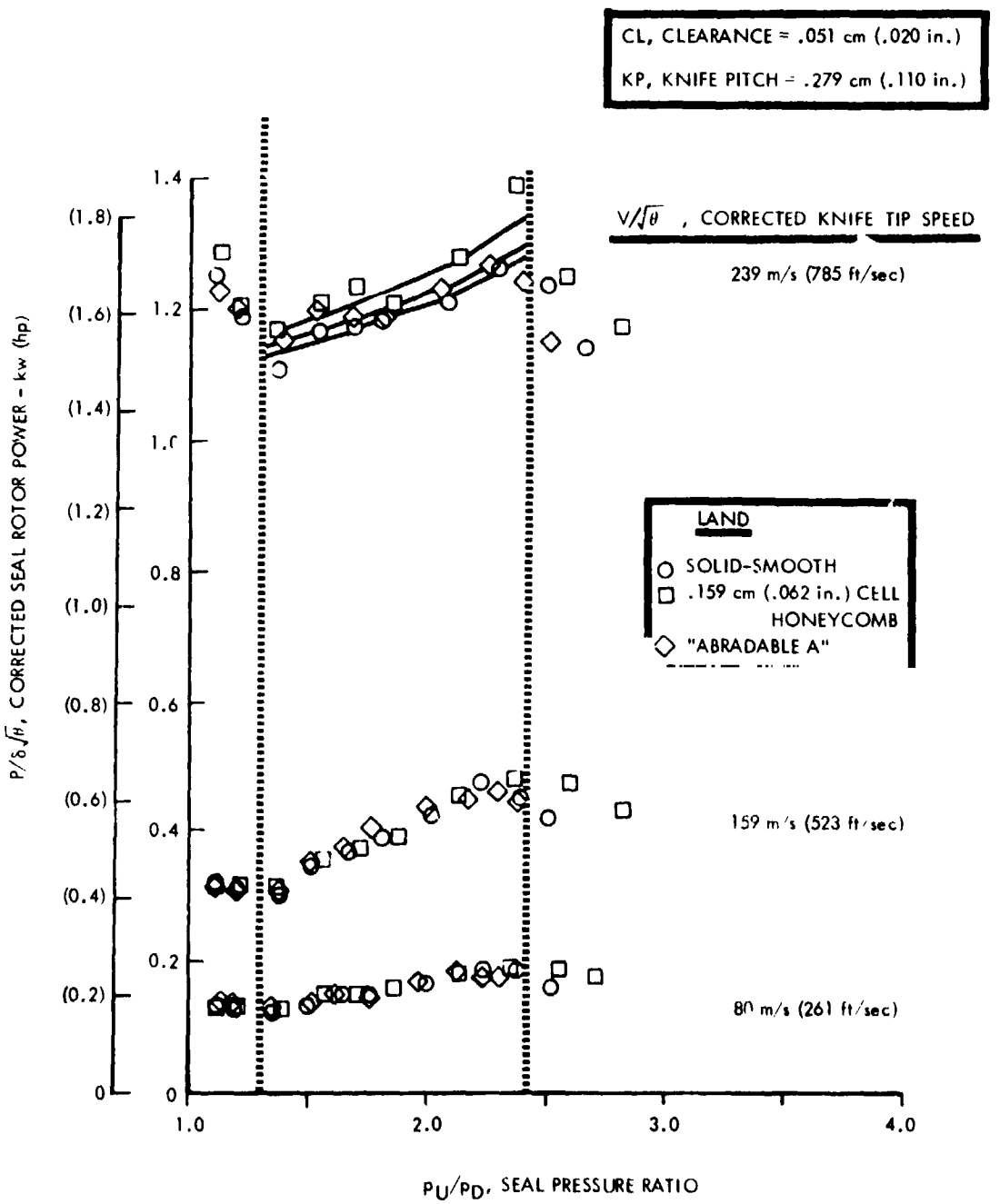

FIGURE E-5. CORRECTED SEAL ROTOR POWER VERSUS SEAL PRESSURE RATIO FOR A FOUR KNIFE STRAIGHT SEAL

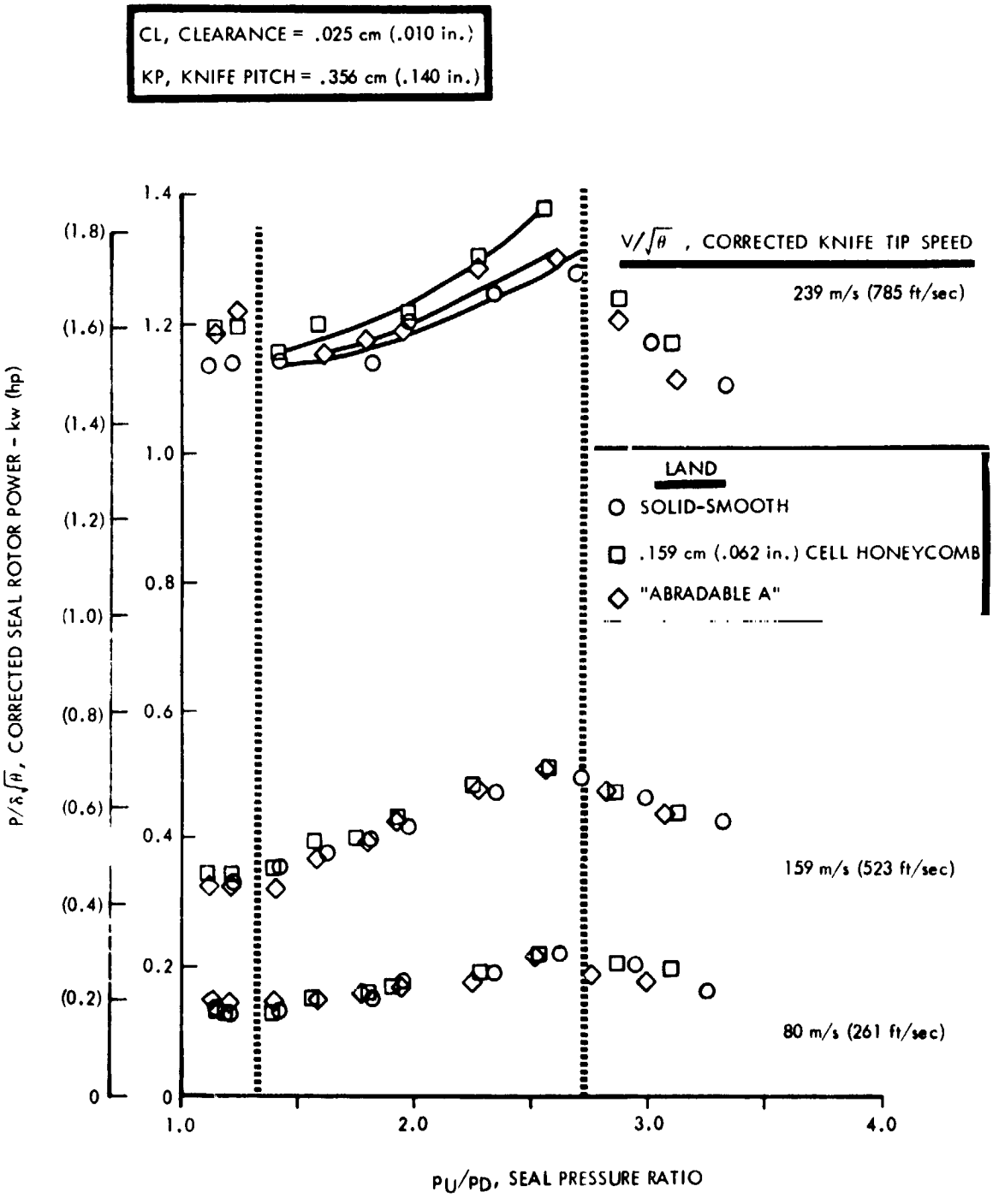

FIGURE E-6. CORRECTED SEAL ROTOR POWER VERSUS SEAL PRESSURE RAT'O FOR A FOUR KNIFE STRAIGHT SEAL

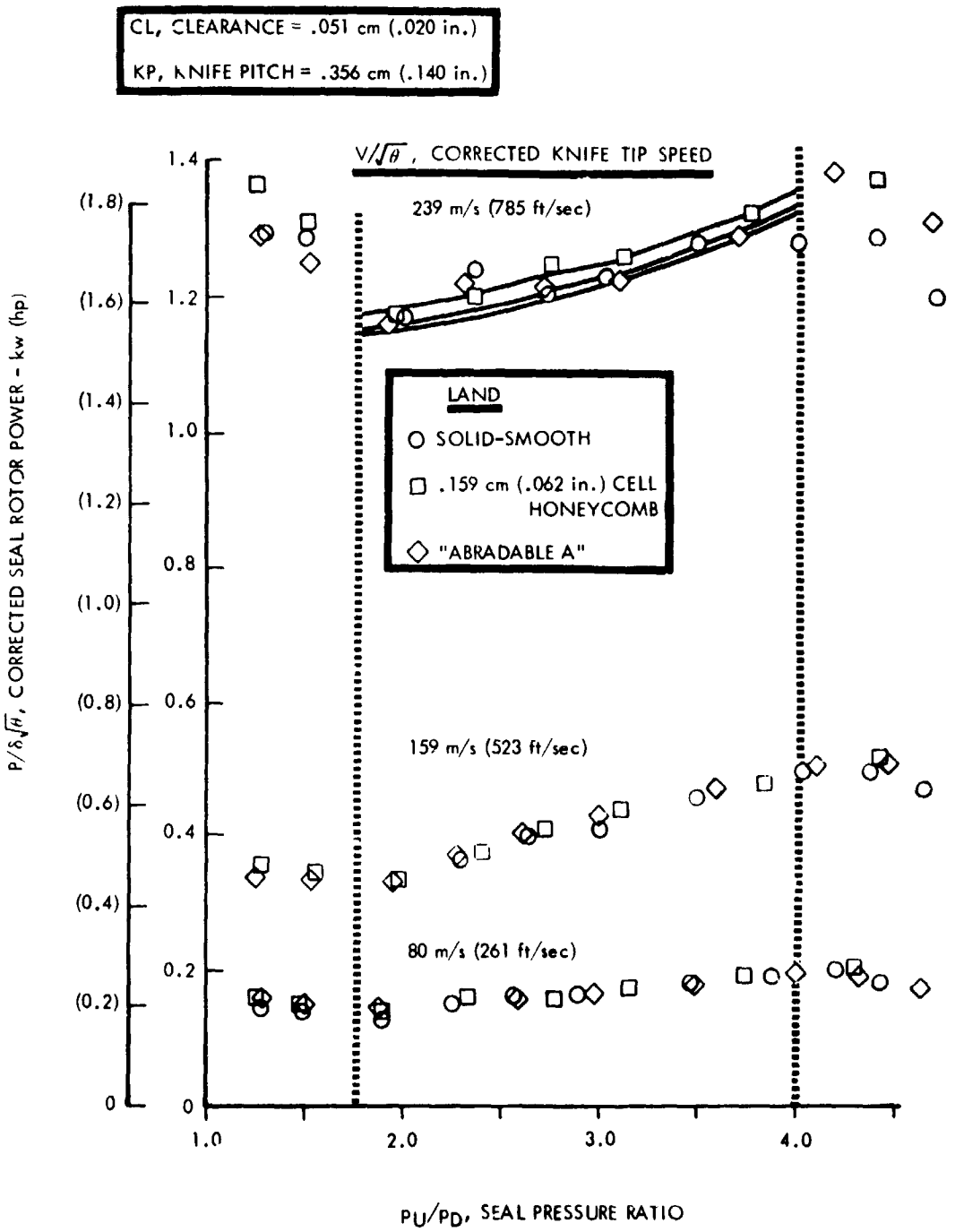

FIGURE E-7. CORRECTED SEAL ROTOR POWER VERSUS SEAL PRESSURE RATIO FOR THE OPTIMUM ADVANCED SEAL

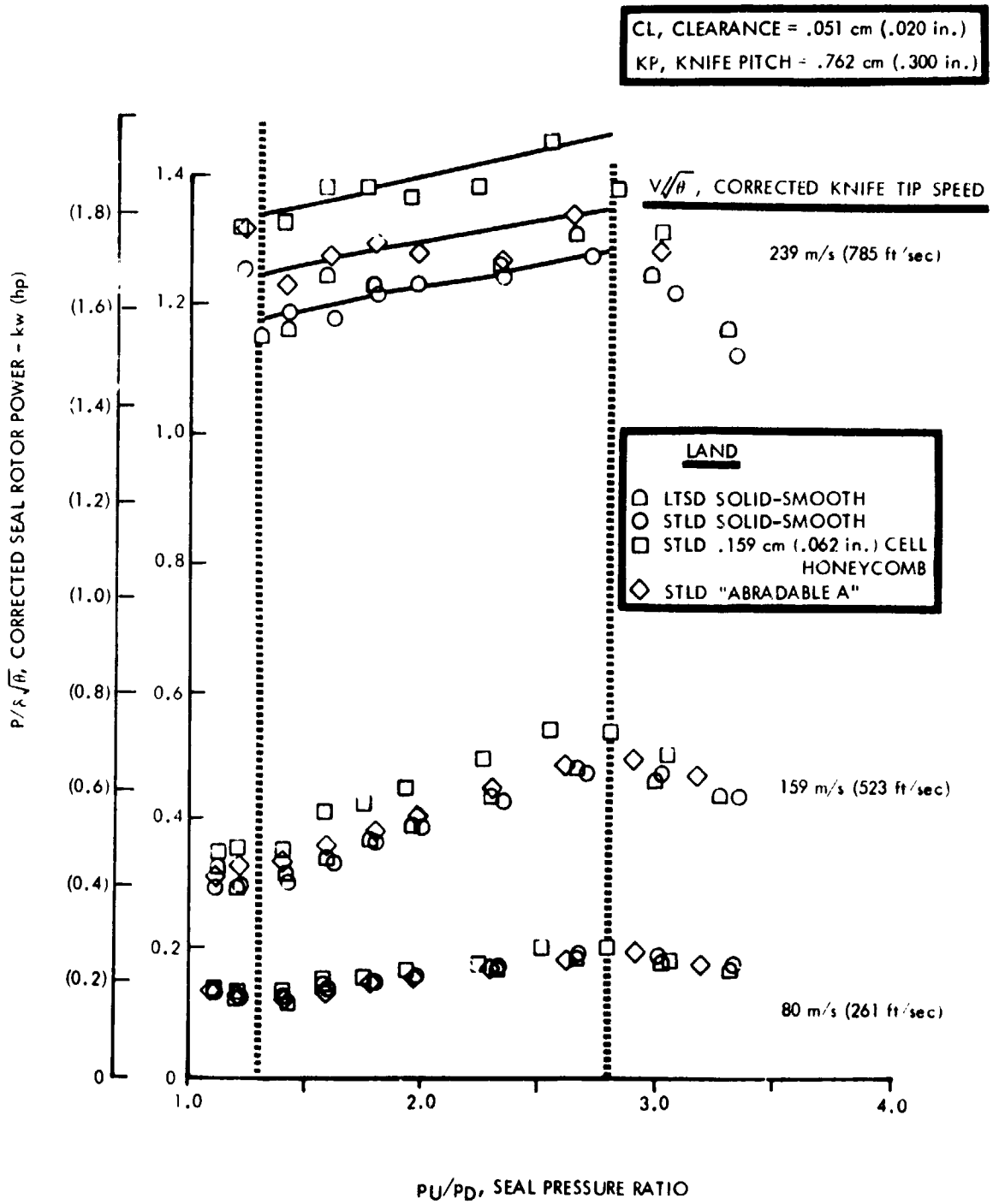

APPENDIX F

Raw Data Test Sheets

Examples of the computer program outputs from both the 2D rig and the 3D rig tests are presented for representative seal configurations and test conditions. The outputs of the programs are organized in the following groups:

(1) instrumentation readings in analog units.

(2) test data in standard working units.

(3) seal leakage performance in parametric form.

(4) seal power absorption performance test data and parameters (for the 3D rig only).

The raw data from 2D rig testing are in Figures F-1 and F-2. Figures F-3 and F-4 are examples of 3D rig data at static and dynamic test conditions.

2-D SEAL RIG DATA

SEAL CONF. [illegible] 4 KNIFE STRAIGHT SEAL [illegible] [illegible]110727-41[illegible] [illegible] [illegible]
CL=.005,K= 0,P=.110,KP=.110,SH=.[illegible],[illegible]=[illegible], T[illegible]=.0[illegible] [illegible]=[illegible] DATE: 11/[illegible]/7[illegible]

INPUT DATA

TEST RECORD NO.----------------------	21[illegible]
ORIFICE INLET PRESSURE---------------	54.[illegible]0 IN HG ABS
ORIFICE OUTLET PRESSURE--------------	[illegible]5.[illegible]0 IN HG ABS
SEAL INLET PRESSURE------------------	[illegible]6.10 IN HG ABS
SEAL OUTLET PRESSURE-----------------	29.40 IN HG ABS
ORIFICE INLET TEMPERATURE------------	75.00 DEGREES F
SEAL INLET TEMPERATURE---------------	74.00 DEGREES F
DIAMETER OF ORIFICE------------------	0.300 INCHES
CASE DEFLECTION----------------------	0.00065 IN.
SEAL LENGTH--------------------------	0.2[illegible]0 INCHES
AVERAGE CLEARANCE--------------------	0.006 INCHES

RIGHT SIDE CLEARANCES	0.005	0.006	0.005	0.006
LEFT SIDE CLEARANCES	0.006	0.006	0.005	0.006

OUTPUT DATA

ORIFICE INLET PRESSURE---------------	[illegible]6.17 PSIA
ORIFICE OUTLET PRESSURE--------------	41.75 PSIA
ORIFICE DELTA PRESSURE---------------	[illegible].42 PSIA
SEAL INLET PRESSURE------------------	42.29 PSIA
SEAL OUTLET PRESSURE-----------------	14.44 PSIA
SEAL DELTA PRESSURE------------------	27.85 PSI
ORIFICE INLET TEMPERATURE------------	534.69 DEGREES R
SEAL INLET TEMPERATURE---------------	533.69 DEGREES R
ORIFICE AREA-------------------------	0.071 SQ IN
ORIFICE FLOW-------------------------	0.0276 LB/SEC
SEAL PRESSURE RATIO------------------	2.92[illegible]

RIGHT SIDE CL. INCHES	LEFT SIDE CL. INCHES	AVG. KNIFE CLEARANCE INCHES	SEAL AREA SQ IN	FLOW PARAMETER RT/PA	FLOW PARAMETER [illegible]RT/P	DISCHARGE COEFF.
0.0050	0.0070	0.0[illegible]	0.0411	0.36[illegible]	0.015[illegible]	
0.0065	0.0065	0.0065	0.0411	0.36[illegible]17	0.01[illegible]0[illegible]	0.4112[illegible]
0.0050	0.0060	0.1060	0.0380	0.397133	0.0150[illegible]	0.4112[illegible]
0.0065	0.0070	0.0[illegible]	0.0427	0.353[illegible]	0.015[illegible]	0.445[illegible]13
						0.396109

VALUES CALCULATED USING AVERAGE CLEARANCES

0.0063	0.0067	0.1065	0.0417	0.370351	0.015069	0.[illegible]

FIGURE F-1. 2D SEAL RIG DATA FOR THE 4 KNIFE STRAIGHT SEAL WITH A SOLID-SMOOTH LAND AT .013 cm (.005 In.) CLEARANCE

ORIGINAL PAGE IS
OF POOR QUALITY

2-D SEAL RIG DATA

SEAL CODE: 7A 4 KNIFE STRAIGHT SEAL RIVE E+1[illegible] LWDS E+1[illegible]
CL=.020,KE= 4,P=.110,RHE=.110,SHE=.000,ANG=90.LTC=.000,LIN=.51 DATE: 11/22/74

INPUT DATA

TEST RECORD NO.----------	244			
ORIFICE INLET PRESSURE----------	144.20 IN HG ABS			
ORIFICE OUTLET PRESSURE----------	80.60 IN HG ABS			
SEAL INLET PRESSURE----------	82.60 IN HG ABS			
SEAL OUTLET PRESSURE----------	29.40 IN HG ABS			
ORIFICE INLET TEMPERATURE----------	75.00 DEGREES F			
SEAL INLET TEMPERATURE----------	75.00 DEGREES F			
DIAMETER OF ORIFICE----------	0.300 INCHES			
CASE DEFLECTION----------	0.00050 IN.			
SEAL LENGTH----------	6.250 INCHES			
AVERAGE CLEARANCE----------	0.020 INCHES			
RIGHT SIDE CLEARANCES	0.019	0.021	0.019	0.019
LEFT SIDE CLEARANCES	0.020	0.020	0.019	0.020

OUTPUT DATA

ORIFICE INLET PRESSURE----------	71.41 PSIA
ORIFICE OUTLET PRESSURE----------	39.59 PSIA
ORIFICE DELTA PRESSURE----------	31.82 PSIA
SEAL INLET PRESSURE----------	40.57 PSIA
SEAL OUTLET PRESSURE----------	14.44 PSIA
SEAL DELTA PRESSURE----------	26.13 PSI
ORIFICE INLET TEMPERATURE----------	534.69 DEGREES R
SEAL INLET TEMPERATURE----------	534.69 DEGREES R
ORIFICE AREA----------	0.071 SQ IN
ORIFICE FLO[illegible]----------	0.0834 LB/SEC
SEAL PRESSURE RATIO----------	2.6095

RIGHT SIDE CL. INCHES	LEFT SIDE CL. INCHES	AVG. KNIFE CLEARANCE INCHES	SEAL AREA SQ. IN	FLOW PARAMETER WRT/PA	FLOW PARAMETER WRT/P	DISCHARGE COEFF.
0.0200	0.0205	0.0202	0.1272	0.373460	0.047555	0.423E06
0.0210	0.0205	0.0207	0.1303	0.364935	0.047555	0.413E42
0.0195	0.0200	0.0197	0.1240	0.383417	0.047555	0.434E38
0.0200	0.0205	0.0202	0.1272	0.373460	0.047555	0.423E06

VALUES CALCULATED USING AVERAGE CLEARANCES

0.0201	0.0204	0.0202	0.1272	0.373460	0.047555	0.423E06

FIGURE F-2. 2D SEAL RIG DATA FOR THE 4 KNIFE STRAIGHT SEAL WITH A SOLID-SMOOTH LAND AT .051 cm (.020 in.) CLEARANCE

3-D SEAL RIG DATA

SEAL CONF. 182A FOUR KNIFE STRAIGHT SEAL - SMOOTH LAND
ROTOR EX12300A LANDS T819266 DATE: 08/05/77
CL=.010,K=04,P=.110,KH=.110,SH=0 ,ANG=90,DTC=0 ,DIR.=01

INPUT DATA

TEST SEQUENCE NO.----------	81 THRU	90
BAROMETRIC PRESSURE----------	29.42	IN HG
ORIFICE INLET PRESSURE----------	32.48	MV GAGE
ORIFICE OUTLET PRESSURE----------	23.69	MV GAGE
SEAL INLET PRESSURE----------	24.37	MV GAGE
SEAL OUTLET PRESSURE----------	3.22	MV GAGE
ORIFICE INLET TEMPERATURE----------	73.00	DEGREES F
SEAL INLET TEMPERATURE----------	72.00	DEGREES F
DIAMETER OF ORIFICE----------	0.500	INCHES
SEAL ROTOR ROTATIONAL SPEED----------	0.	RPM
AVERAGE KNIFE DIAMETER (ROTATING)----	6.003	INCHES
AVERAGE STATOR DIAMETER----------	6.023	INCHES

KNIFE DIAMETERS (ROTATING)	6.003	6.003	6.003	6.003
KNIFE DIAMETERS (STATIC)	6.003	6.003	6.003	6.003
CLEARANCE	6.023	6.023	6.023	6.023

OUTPUT DATA

BAROMETRIC PRESSURE----------	14.40	PSIA
ORIFICE INLET PRESSURE----------	56.65	PSIA
ORIFICE OUTLET PRESSURE----------	46.68	PSIA
ORIFICE DELTA PRESSURE----------	11.97	PSI
SEAL INLET PRESSURE----------	47.50	PSIA
SEAL OUTLET PRESSURE----------	18.79	PSIA
SEAL DELTA PRESSURE----------	28.81	PSI
ORIFICE INLET TEMPERATURE----------	532.69	DEGREES R
SEAL INLET TEMPERATURE----------	531.69	DEGREES R
ORIFICE AREA----------	0.196	SQ IN
ORIFICE FLOW----------	0.1395	LB/SEC
SEAL PRESSURE RATIO----------	2.5334	
AVG. KNIFE VELOCITY----------	0.0	FT/SEC

ROTATING KNIFE DIA., INCHES	STATOR DIA., INCHES	SEAL CLEARANCE INCHES	SEAL AREA SQ IN	FLOW PARAMETER WRT/PA	FLOW PARAMETER WRT/P	DISCHARGE COEFF.
6.0030	6.0230	0.0100	0.1389	0.357620	0.067553	0.456164
6.0030	6.0230	0.0100	0.1389	0.357620	0.067553	0.581599
6.0030	6.0230	0.0100	0.1389	0.357620	0.067553	0.655277
6.0030	6.0230	0.0100	0.1389	0.357620	0.067553	0.695546
VALUES CALCULATED USING AVERAGE DIAMETERS						
6.0030	6.0230	0.0100	0.1389	0.357597	0.067553	0.716553

FIGURE F-3. 3D SEAL RIG DATA FOR THE 4 KNIFE STRAIGHT SEAL WITH A SOLID-SMOOTH LAND AT .025 cm (.010 in.) CLEARANCE
(a). STATIC CONDITIONS

3-D SEAL RIG DATA

SEAL CONF. 182A FOUR KNIFE STAIGHT SEAL - SMOOTH LAND
ROTOR EX12300A LANDS T819266 DATE: 08/05/77
CL=.010,K=04,P=.110,KH=.110,SH=0 ,ANG=90,DTC=0 ,DIR.=BI

INPUT DATA

TEST SEQUENCE NO.----------	331 THRU 340	
BAROMETRIC PRESSURE----------	29.32	PSIA
ORIFICE INLET PRESSURE----------	25.94	PSIG
ORIFICE OUTLET PRESSURE----------	19.95	PSIG
SEAL INLET PRESSURE----------	20.43	PSIG
SEAL OUTLET PRESSURE----------	2.18	PSIG
ORIFICE INLET TEMPERATURE----------	77.00	DEGREES F
SEAL INLET TEMPERATURE----------	81.00	DEGREES F
DIAMETER OF ORIFICE----------	0.500	INCHES
SEAL ROTOR ROTATIONAL SPEED----------	30255.	RPM
AVERAGE KNIFE DIAMETER (ROTATING)----	6.004	INCHES
AVERAGE STATOR DIAMETER----------	6.023	INCHES

KNIFE DIAMETERS (ROTATING)	6.004	6.004	6.004	6.004
KNIFE DIAMETERS (STATIC)	6.003	6.003	6.003	6.003
CLEARANCE	0.023	0.023	0.025	0.023

OUTPUT DATA

BAROMETRIC PRESSURE----------	14.40	PSIA
ORIFICE INLET PRESSURE----------	49.74	PSIA
ORIFICE OUTLET PRESSURE----------	41.58	PSIA
ORIFICE DELTA PRESSURE----------	8.16	PSI
SEAL INLET PRESSURE----------	42.24	PSIA
SEAL OUTLET PRESSURE----------	17.37	PSIA
SEAL DELTA PRESSURE----------	24.86	PSI
ORIFICE INLET TEMPERATURE----------	536.69	DEGREES R
SEAL INLET TEMPERATURE----------	540.69	DEGREES R
ORIFICE AREA----------	0.196	SQ IN
ORIFICE FLOW----------	0.1074	LB/SEC
SEAL PRESSURE RATIO----------	2.4310	
AVG. KNIFE VELOCITY----------	792.6	FT/SEC

ROTATING KNIFE DIA. INCHES	STATOR DIA. INCHES	SEAL CLEARANCE INCHES	SEAL AREA SQ IN	FLOW PARAMETER WRT/PA	FLOW PARAMETER WRT/P	DISCHARGE COEFF.
6.0041	6.0230	0.0095	0.1790	0.330469	0.059145	0.441905
6.0041	6.0230	0.0095	0.1790	0.330469	0.059145	0.515029
6.0041	6.0230	0.0095	0.1790	0.330469	0.059145	0.556011
6.0041	6.0230	0.0095	0.1790	0.330469	0.059145	0.577708

VALUES CALCULATED USING AVERAGE DIAMETERS

6.0040	6.0230	0.0095	0.1790	0.330469	0.059145	0.568872

3-D DYNAMIC RIG SEAL ROTOR HORSEPOWER ABSORPTION DATA

INPUT DATA

TURB ORF INLET PRESSURE----------	58.91	PSIA
TURB ORF OUTLET PRESSURE----------	52.49	PSIA
TURB ORF INLET TEMPERATURE----------	78.50	DEG.F
TURB NOZZLE INLET PRESSURE(1)----------	42.19	PSIA
TURB NOZZLE INLET PRESSURE(2)----------	43.08	PSIA
TURB NOZZLE INLET TEMPERATURE----------	78.00	DEG.F
TURB EXIT PRESSURE(1)----------	14.54	PSIA
TURB EXIT PRESSURE(2)----------	14.51	PSIA
TURB EXIT TEMPERATURE----------	68.75	DEG.F
TURBINE ROTATIONAL SPEED----------	30370.	RPM

OUTPUT DATA

TURB ORF DELTA P / P----------	0.109	
TURB ORF FLOW----------	0.805	LB/SEC
TURB PRESSURE RATIO----------	2.935	
TURB BLADE SPEED - U----------	831.64	FT/SEC
TURB NOZZLE JET SPEED - Co----------	1309.40	FT/SEC
BLADE-JET SPEED RATIO----------	0.635	
TORQUE COEFFICIENT----------	0.049	
TURBINE EFFICIENCY----------	0.12	PERCENT
HORSEPOWER ABSORPTION----------	4.818	HP
CORR. HP ABSORPTION - HP/(DELTA*R(T))	1.642	HP
CORR. HP PER UNIT SEAL CIRCUMFERENCE-	0.087	HP/I...

FIGURE F-3 (b). DYNAMIC CONDITIONS, 30000 RPM

3-D SEAL RIG DATA

SEAL CONF. 2068 FOUR KNIFE STEPPED SEAL - SMOOTH LAND
ROTOR EX124180 LANDS EX124181 DATE: 11/ 4/77
CL=.020,K=04,P-.300,KH=.150,SH=.120,ANG=50,DTC=.102,DIR.=LTSD

INPUT DATA

TEST SEQUENCE NO.	101 THRU 110			
BAROMETRIC PRESSURE	29.45 IN HG			
ORIFICE INLET PRESSURE	38.23 MV GAGE			
ORIFICE OUTLET PRESSURE	27.78 MV GAGE			
SEAL INLET PRESSURE	28.67 MV GAGE			
SEAL OUTLET PRESSURE	1.21 MV GAGE			
ORIFICE INLET TEMPERATURE	72.00 DEGREES F			
SEAL INLET TEMPERATURE	71.00 DEGREES F			
DIAMETER OF ORIFICE	0.500 INCHES			
SEAL ROTOR ROTATIONAL SPEED	0. RPM			
AVERAGE KNIFE DIAMETER (ROTATING)	5.644 INCHES			
AVERAGE STATOR DIAMETER	5.683 INCHES			
KNIFE DIAMETERS (ROTATING)	6.005	5.764	5.524	5.284
KNIFE DIAMETERS (STATIC)	6.005	5.764	5.524	5.284
CLEARANCE	5.042	5.803	5.564	5.323

OUTPUT DATA

BAROMETRIC PRESSURE	14.46	PSIA
ORIFICE INLET PRESSURE	66.54	PSIA
ORIFICE OUTLET PRESSURE	52.31	PSIA
ORIFICE DELTA PRESSURE	14.24	PSI
SEAL INLET PRESSURE	53.52	PSIA
SEAL OUTLET PRESSURE	16.11	PSIA
SEAL DELTA PRESSURE	37.41	PSI
ORIFICE INLET TEMPERATURE	531.69	DEGREES R
SEAL INLET TEMPERATURE	530.69	DEGREES R
ORIFICE AREA	0.196	SQ IN
ORIFICE FLOW	0.1617	LB/SEC
SEAL PRESSURE RATIO	3.3217	
AVG. KNIFE VELOCITY	0.0	FT/SEC

ROTATING KNIFE DIA. INCHES	STATOR DIA. INCHES	SEAL CLEARANCE INCHES	SEAL AREA SQ. IN	FLOW PARAMETER WRT/PA	FLOW PARAMETER WRT/P	DISCHARGE COEFF.
6.0048	6.0425	0.0188	0.3567	0.195154	0.069613	0.212362
5.7638	5.8032	0.0197	0.3579	0.194481	0.069613	0.211629
5.5242	5.5638	0.0198	0.3448	0.201868	0.069613	0.219668
5.2841	5.3225	0.0192	0.3199	0.217622	0.069613	0.236810
VALUES CALCULATED USING AVERAGE DIAMETERS						
5.6442	5.6830	0.0194	0.3450	0.201798	0.069613	0.219591

FIGURE F-4. 3D SEAL RIG DATA FOR THE 4 KNIFE ADVANCED SEAL WITH A SOLID-SMOOTH LAND AT .051 cm (.020 in.) CLEARANCE

(a). STATIC CONDITIONS

3-D SEAL RIG DATA

SEAL CONF. 2068 FOUR KNIFE STEPPED SEAL - SMOOTH LAND
ROTOR EX124180 LANDS EX124181 DATE: 11/ 4/77
CL=.020,K=04,P=.300,KH=.150,SH=.120,ANG=50,DTC=.102,DIR.=LTSD

INPUT DATA

TEST SEQUENCE NO.	401 THRU 410	
BAROMETRIC PRESSURE	29.45	IN HG
ORIFICE INLET PRESSURE	36.85	MV GAGE
ORIFICE OUTLET PRESSURE	27.37	MV GAGE
SEAL INLET PRESSURE	28.14	MV GAGE
SEAL OUTLET PRESSURE	1.14	MV GAGE
ORIFICE INLET TEMPERATURE	73.50	DEGREES F
SEAL INLET TEMPERATURE	76.00	DEGREES F
DIAMETER OF ORIFICE	0.500	INCHES
SEAL ROTOR ROTATIONAL SPEED	29841.	RPM
AVERAGE KNIFE DIAMETER (ROTATING)	5.645	INCHES
AVERAGE STATOR DIAMETER	5.683	INCHES

KNIFE DIAMETERS (ROTATING)	6.006	5.765	5.525	5.285
KNIFE DIAMETERS (STATIC)	6.005	5.764	5.524	5.284
CLEARANCE	6.042	5.803	5.564	5.323

OUTPUT DATA

BAROMETRIC PRESSURE	14.46	PSIA
ORIFICE INLET PRESSURE	64.66	PSIA
ORIFICE OUTLET PRESSURE	51.75	PSIA
ORIFICE DELTA PRESSURE	12.91	PSI
SEAL INLET PRESSURE	52.80	PSIA
SEAL OUTLET PRESSURE	16.02	PSIA
SEAL DELTA PRESSURE	36.78	PSI
ORIFICE INLET TEMPERATURE	533.19	DEGREES R
SEAL INLET TEMPERATURE	535.69	DEGREES R
ORIFICE AREA	0.196	SQ IN
ORIFICE FLOW	0.1522	LB/SEC
SEAL PRESSURE RATIO	3.2964	
AVG. KNIFE VELOCITY	735.0	FT/SEC

ROTATING KNIFE DIA. INCHES	STATOR DIA. INCHES	SEAL CLEARANCE INCHES	SEAL AREA SQ IN	FLOW PARAMETER WRT/PA	FLOW PARAMETER WRT/P	DISCHARGE COEFF.
6.0058	6.0425	0.0183	0.3470	0.192223	0.066709	0.209519
5.7647	5.8032	0.0192	0.3497	0.190748	0.066709	0.207910
5.5250	5.5638	0.0194	0.3379	0.197411	0.066709	0.215173
5.2848	5.3225	0.0189	0.3141	0.212393	0.066709	0.231503
VALUES CALCULATED USING AVERAGE DIAMETERS						
5.6451	5.6830	0.0190	0.3374	0.197741	0.066709	0.215533

3-D DYNAMIC RIG SEAL ROTOR HORSEPOWER ABSORPTION DATA

INPUT DATA

TURB ORF INLET PRESSURE	61.33	PSIA
TURB ORF OUTLET PRESSURE	54.52	PSIA
TURB ORF INLET TEMPERATURE	74.00	DEG.F
TURB NOZZLE INLET PRESSURE(1)	43.92	PSIA
TURB NOZZLE INLET PRESSURE(2)	44.88	PSIA
TURB NOZZLE INLET TEMPERATURE	74.00	DEG.F
TURB EXIT PRESSURE(1)	14.61	PSIA
TURB EXIT PRESSURE(2)	14.60	PSIA
TURB EXIT TEMPERATURE	64.00	DEG.F
TURBINE ROTATIONAL SPEED	29878.	RPM

OUTPUT DATA

TURB ORF DELTA P / P	0.111	
TURB ORF FLOW	0.849	LB/SEC
TURB PRESSURE RATIO	3.040	
TURB BLADE SPEED - U	818.17	FT/SEC
TURB NOZZLE JET SPEED - C*	1322.70	FT/SEC
BLADE-JET SPEED RATIO	0.619	
TORQUE COEFFICIENT	0.055	
TURBINE EFFICIENCY	0.14	PERCENT
HORSEPOWER ABSORPTION	5.704	HP
CORR. HP ABSORPTION - HP/(DELTA*R(I))	1.562	HP
CORR. HP PER UNIT SEAL CIRCUMFERENCE	0.088	HP/IN

FIGURE F-4 (b). DYNAMIC CONDITIONS, 30000 RPM

APPENDIX G

Notes from the Test Log on the Subject of Acoustical Noise Generated by Specific Labyrinth Seals

The testing of certain four knife straight seals in the 2D rig produced acoustic phenomena.

During testing of the "Abradable A" and "Abradable B" lands, a step change in the sound intensity of the leakage air was noticed as seal pressure ratio was increased beyond a characteristic value. The point at which the sound step change occurred was a function of the clearance, pressure ratio, and land material. No change in the seal leakage (flow parameter characteristic) was detected. After the sound step (upward) occurred, it remained at the higher level to the maximum pressure ratio tested. When these acoustic phenomena were encountered during a test, several check points of data were taken as the pressure ratio was reduced. As the seal inlet pressure decreased, the leakage air acoustics experienced a step down in level but not necessarily at the same pressure ratio for which the sound stepped up. The phenomena were repeatable. The solid-smooth, nickel-graphite, and aluminum-polyester lands did not demonstrate the sound step change. A summary of the acoustic step observations is presented in Table G-1.

The honeycomb land tests produced an acoustic phenomenon of different characteristics. Unlike the acoustics associated with the abradable tests in which a step change in noise level occurred, the .079 cm (.031 in.) cell honeycomb land produced a continuous increase to a high noise intensity with increasing pressure ratio. Although sound measurements were not taken, the .079 cm (.031 in.) honeycomb at .051 cm (.020 in.) clearance produced a noise level which was several times the nominal loudness experienced at .013 cm (.005 in.) and .025 cm (.010 in.) clearances. The sound levels associated with the .159 cm (.062 in.) and .318 cm (.125 in.) cell honeycombs were of the same order as the typical sound levels experienced with the .079 cm (.031 in.) cell honeycomb at .013 cm (.005 in.) and .025 cm (.010 in.) clearances. Cursory analysis of the .381 cm (.150 in.) deep honeycomb test results indicated a possible correlation of the phenomenon with a 1/4 wave resonance tube effect. However, when cell depth was reduced by wax filling the honeycomb lands for subsequent tests, no acoustical noise of equivalent sound intensity was noticed during these runs. The possible effects of wax meniscus and compliance in the honeycomb cell is not known.

None of these acoustical phenomena were noted during similar tests on the 3D rig. Background noise level is considerably higher on the 3D rig and could have obscured the seal leakage acoustics.

Acoustic phenomena are of concern relative to engine applications since fatigue failure of the seal knives could result from aerodynamically induced vibration.

TABLE G-1. SUMMARY OF ABRADABLE LAND NOISE LEVEL VARIATIONS NOTED DURING TEST CALIBRATIONS

TYPE LAND	SEAL CLEARANCE cm	SEAL CLEARANCE (in.)	OPERATING MODE OF SEAL INLET PRESS, p_U	CHANGE NOTED IN NOISE LEVEL	SEAL INLET PRESSURE @ NOISE LEVEL SHIFT kPa	SEAL INLET PRESSURE @ NOISE LEVEL SHIFT (psia)	SEAL PRESSURE RATIO @ NOISE LEVEL SHIFT
"Abradable A"	.013	(0.005)	p_U Increasing	Step Change to Higher Noise Level	440.1	(63.83)	4.41
	.013	(0.005)	p_U Decreasing	Step Change to Lower Noise Level	250.5	(36.33)	2.51
"Abradable B"	.025	(0.010	p_U Increasing	Step Change to Higher Noise Level	557.6	(80.87)	5.61
	.025	(0.010)	p_U Decreasing	Step Change to Lower Noise Level	142.2	(20.62)	1.43
"Abradable B"	.013	(0.005)	p_U Increasing	Step Change to Higher Noise Level	303.0	(43.94)	3.03
	.013	(0.005)	p_U Decreasing	Step Change to Lower Noise Level	140.2	(20.33)	1.40

APPENDIX H

Symbols and Seal Nomenclature

Symbols

SYMBOL	DEFINITION	UNITS SI Metric	UNITS English
A	Flow area between the seal knives and land	cm^2	$in.^2$
C_d	Seal discharge coefficient	-	-
CL	Clearance between seal knives and land	cm	in.
c_p	Specific heat at constant pressure	J/kg · K	btu/lb_m °I
C*	Maximum jet (spouting) velocity	m/s	ft/sec
D_T	Turbine tip diameter	cm	in.
DTC	Distance-to-contact:axial clearance between knife and land, undefined for constant height straight-through seals	cm	in.
g	Standard gravitational acceleration mass conversion factor	$kg \cdot m/N \cdot s^2$	$lb_m ft/lb_f sec^2$
KH	Knife height	cm	in.
KN	Number of knives	--	--
KP	Knife pitch	cm	in.
KT	Knife tip thickness	cm	in.
Kθ	Knife angle	deg,°	deg,°
LTSD	Leakage flow direction from the large-to-small seal diameter	--	--
P	Seal rotor power absorption	kw	hp
P_D	Seal plenum downstream pressure	kPa	psia
P_U	Seal plenum upstream pressure	kPa	psia
P_{SOD}	Seal orifice downstream pressure	kPa	psia
P_{SOU}	Seal orifice upstream pressure	kPa	psia
P_{TD}	Seal drive turbine exit plenum pressure	kPa	psia
P_{TU}	Seal drive turbine inlet plenum pressure	kPa	psia
P_{TOD}	Seal drive turbine orifice downstream pressure	kPa	psia

SYMBOL	DEFINITION	UNITS SI Metric	UNITS English
P_{TOU}	Seal drive turbine orifice upstream pressure	kPa	psia
R	Gas constant	kJ/kg · K	$\frac{lb_f \cdot ft}{lb_m \cdot °R}$
RMS	Root mean square		
RPM	Rotational speed, angular velocity	rpm	rpm
SH	Step height	cm	in.
SFC	Engine thrust specific fuel consumption	$\frac{kg}{N \cdot s}$	$\frac{lb_m}{lb_f sec}$
STLD	Leakage flow direction from the small-to-large seal diameter	--	--
t	Turbine rotor stall torque	N · cm	in lb_f
$\sqrt{T}$	Square root of temperature	$K^{\frac{1}{2}}$	$°R^{\frac{1}{2}}$
T_U	Seal upstream plenum temperature	K	°R
T_{TD}	Seal drive turbine exit plenum temperature	K	°R
T_{TU}	Seal drive turbine inlet plenum temperature	K	°R
T_{SOU}	Seal orifice tube upstream temperature	K	°R
T_{TOU}	Turbine orifice tube upstream temperature	K	°R
U	Turbine blade tip speed	m/s	ft/sec
V	Seal knife tip speed	m/s	ft/sec
w	Seal airflow rate	kg/s	lb_m/sec
w_T	Turbine airflow rate	kg/s	lb_m/sec
γ	Specific heat ratio	--	--
δ	Pressure/base (std) pressure	--	--
η_T	Turbine adiabatic efficiency	--	--
θ	Temperature/base (std) temperature	--	--
π	Conventional transcendental number, ratio of circular circumference to diameter	--	--
τ	Turbine torque coefficient	--	--
$\phi = \frac{w\sqrt{T_U}}{p_U A}$	Airflow parameter	$\frac{kg \cdot K^{\frac{1}{2}}}{N \cdot s}$	$\frac{lb_m \cdot °R^{\frac{1}{2}}}{lb_f \cdot sec}$

SEAL NOMENCLATURE